THE EFFECT OF ABNORMAL METABOLISM ON GERM CELL GROWTH, MATURATION, AND FERTILIZATION IN MAMMALS

EDITED BY: Yi Fang, Qi-En Yang, Xiangwei Fu, Cecilia Dall'Aglio, Shou-Long Deng and Xianlong Wang

PUBLISHED IN: Frontiers in Veterinary Science

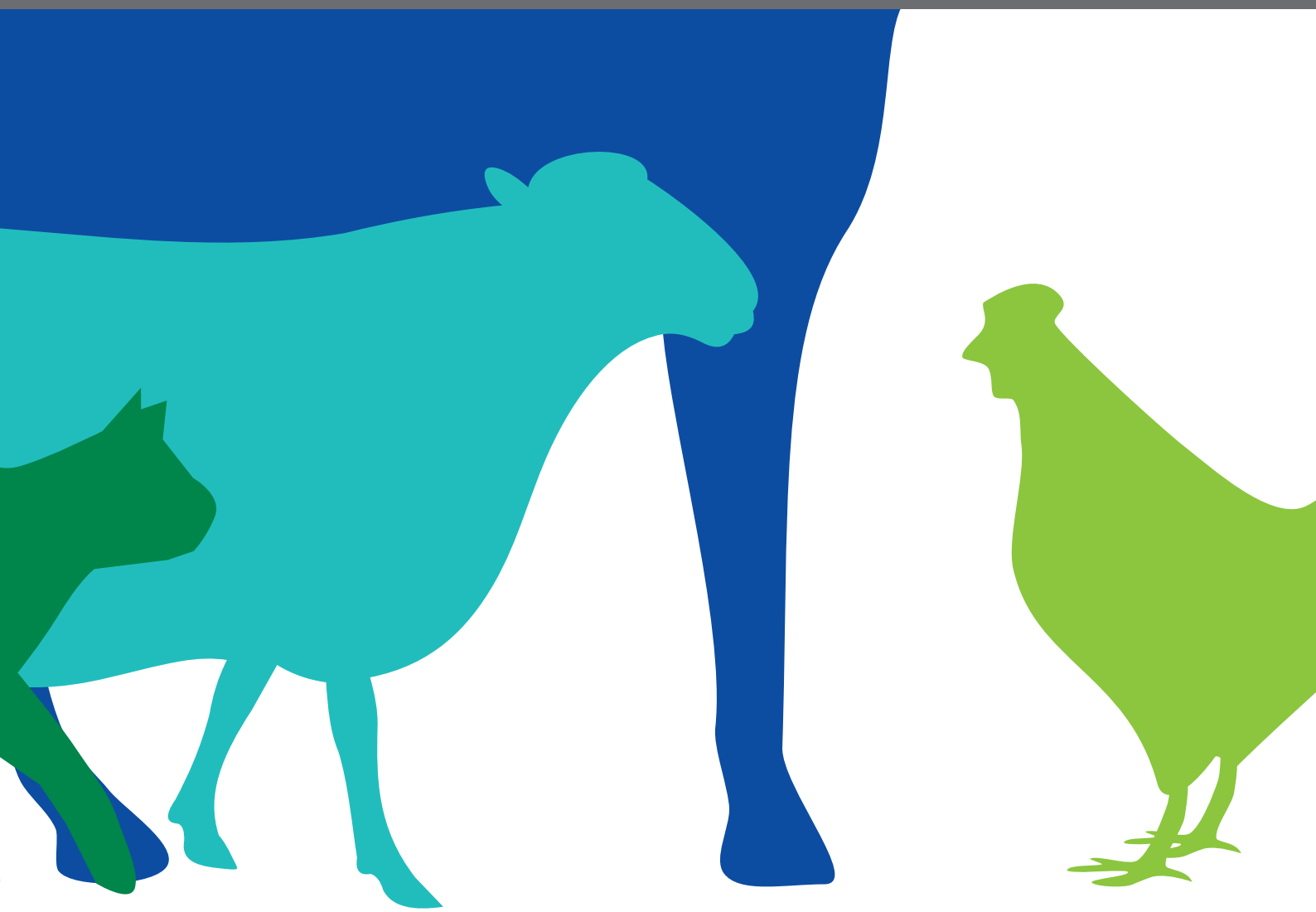

frontiers Research Topics

frontiers

ISSN 1664-8714
ISBN 978-2-88976-687-1
DOI 10.3389/978-2-88976-687-1

About Frontiers

Frontiers is more than just an open-access publisher of scholarly articles: it is a pioneering approach to the world of academia, radically improving the way scholarly research is managed. The grand vision of Frontiers is a world where all people have an equal opportunity to seek, share and generate knowledge. Frontiers provides immediate and permanent online open access to all its publications, but this alone is not enough to realize our grand goals.

Frontiers Journal Series

The Frontiers Journal Series is a multi-tier and interdisciplinary set of open-access, online journals, promising a paradigm shift from the current review, selection and dissemination processes in academic publishing. All Frontiers journals are driven by researchers for researchers; therefore, they constitute a service to the scholarly community. At the same time, the Frontiers Journal Series operates on a revolutionary invention, the tiered publishing system, initially addressing specific communities of scholars, and gradually climbing up to broader public understanding, thus serving the interests of the lay society, too.

Dedication to Quality

Each Frontiers article is a landmark of the highest quality, thanks to genuinely collaborative interactions between authors and review editors, who include some of the world's best academicians. Research must be certified by peers before entering a stream of knowledge that may eventually reach the public - and shape society; therefore, Frontiers only applies the most rigorous and unbiased reviews.
Frontiers revolutionizes research publishing by freely delivering the most outstanding research, evaluated with no bias from both the academic and social point of view. By applying the most advanced information technologies, Frontiers is catapulting scholarly publishing into a new generation.

What are Frontiers Research Topics?

Frontiers Research Topics are very popular trademarks of the Frontiers Journals Series: they are collections of at least ten articles, all centered on a particular subject. With their unique mix of varied contributions from Original Research to Review Articles, Frontiers Research Topics unify the most influential researchers, the latest key findings and historical advances in a hot research area! Find out more on how to host your own Frontiers Research Topic or contribute to one as an author by contacting the Frontiers Editorial Office: frontiersin.org/about/contact

THE EFFECT OF ABNORMAL METABOLISM ON GERM CELL GROWTH, MATURATION, AND FERTILIZATION IN MAMMALS

Topic Editors:
Yi Fang, Northeast Institute of Geography and Agroecology, Chinese Academy of Sciences (CAS), China
Qi-En Yang, Northwest Institute of Plateau Biology, Chinese Academy of Sciences (CAS), China
Xiangwei Fu, China Agricultural University, China
Cecilia Dall'Aglio, University of Perugia, Italy
Shou-Long Deng, Institute of Laboratory Animal Sciences, Chinese Academy of Medical Sciences and Peking Union Medical College, China
Xianlong Wang, Baylor College of Medicine, United States

Citation: Fang, Y., Yang, Q.-E., Fu, X., Dall'Aglio, C., Deng, S.-L., Wang, X., eds. (2022). The Effect of Abnormal Metabolism on Germ Cell Growth, Maturation, and Fertilization in Mammals. Lausanne: Frontiers Media SA.
doi: 10.3389/978-2-88976-687-1

Table of Contents

frontiers | Frontiers in Veterinary Science

EDITORIAL
published: 06 July 2022
doi: 10.3389/fvets.2022.962334

Editorial: Effects of Abnormal Metabolism on Germ Cell Growth and Maturation, and on Fertilization in Mammals

Yi Fang[1]*, *Xiangwei Fu*[2], *Qien Yang*[3], *Shoulong Deng*[4] and *Xianlong Wang*[5]

[1] Jilin Provincial Key Laboratory of Grassland Farming, Northeast Institute of Geography and Agoecology, Chinese Academy of Sciences, Changchun, China, [2] China Agricultural University, Beijing, China, [3] Key Laboratory of Adaptation and Evolution of Plateau Biota, Northwest Institute of Plateau Biology, Chinese Academy of Sciences, Xining, China, [4] NHC Key Laboratory of Human Disease Comparative Medicine, Peking Union Medical College, Institute of Laboratory Animal Sciences, Chinese Academy of Medical Sciences and Comparative Medicine Center, Beijing, China, [5] Baylor College of Medicine, Houston, TX, United States

Keywords: metabolism, sperm, oocyte, infertility, gene expression

Editorial on the Research Topic

Effects of Abnormal Metabolism on Germ Cell Growth and Maturation, and on Fertilization in Mammals

OPEN ACCESS

Edited and reviewed by:
Sebastián Demyda-Peyrás, Universidad Nacional de La Plata, Argentina

***Correspondence:**
Yi Fang
fangyi@iga.ac.cn

Specialty section:
This article was submitted to Animal Reproduction - Theriogenology, a section of the journal Frontiers in Veterinary Science

Received: *06 June 2022*
Accepted: *23 June 2022*
Published: *06 July 2022*

Citation:
Fang Y, Fu X, Yang Q, Deng S and Wang X (2022) Editorial: Effects of Abnormal Metabolism on Germ Cell Growth and Maturation, and on Fertilization in Mammals. Front. Vet. Sci. 9:962334. doi: 10.3389/fvets.2022.962334

Dynamic regulation of metabolism is critical for germ cell development and fertilization. Each process and key event in germ cell maturation and fertilization potentially requires a unique substrate and metabolic pathway, depending on the species. These pathways are particularly sensitive to changes in nutritional, chemical and endocrine environments, as well as metabolite concentrations and enzyme activities. Specifically, decreased concentrations of transport proteins and increases in glucose/lipid contents and reactive oxygen species have been implicated in meiotic defects, mitochondrial dysfunction, and epigenetic alterations, affecting germ cell maturation and development. Therefore, this special issue focuses on research highlights and challenges in metabolic events affecting mammalian germ cell growth, protection, and preservation, as well as reproductive diseases, etc. Furthermore, it also provides new insights regarding treatment of infertility caused by metabolic diseases.

It is well established that sustaining metabolism of post-thaw sperm is important for acceptable fertility following AI. High (153 mM) glucose concentrations during cooling promoted glycolysis and increased lactate concentrations in boar sperm, and resulted in sperm with circular movements. In contrast, reduced glucose concentrations suppressed sperm glycolysis and increased the activity of key enzymes in oxidative phosphorylation, as well as increased ATP concentrations. Based on those observations, a low glucose concentration (30.6 mM) was deemed suitable for cryopreservation of boar semen (Zhu et al.).

Metabolic dysfunction and obstacles to communications between an oocyte and its surroundings due to aging, heat stress (HS), disease, etc., are associated with oocyte defects and infertility. Subclinical endometritis reduced oocyte nuclear maturation and fertilization in repeat breeder (RB) cows and inhibited expressions of GDF9, StAR and FSHr, resulting in a poor microenvironment for the final stages of oocyte development in pre-ovulatory follicles of RB cows (Kafi et al.). Testicular HS can influence testicular concentrations of amino acids, fatty acids, minerals, and antioxidants and enzyme activities. Turpan black sheep had substantial resistance to HS, whereas Suffolk sheep were much more susceptible to HS, with acrosome damage, a high

proportion of sperm with DNA fragmentation, and many spermatogenic cells blocked in the zygotene and pachytene stages, followed by increased apoptosis. The PI3K-Akt-mTOR pathway is a main signaling pathway regulating spermatogonia proliferation, protein synthesis and energy metabolism by regulating expression of p70S6K and 4EBP1 in testis (Song et al.). In mice, cortical tension-related proteins pERM and pMRLC were aberrantly expressed in aged oocytes, causing decreased cortical tension. However, 5 μg/mL procyanidins (PCB2) antagonized aging-induced decreased cortical tension and protected oocytes. In addition, abnormal spindle formation and chromosome arrangement induced by cortical tension and oxidative stress in aged oocytes were also corrected by PCB2. By improving viability in vitrified-thawed oocytes, PCB2 may contribute to maintain mitochondrial function and ATP concentrations in aged oocytes (Zhuan et al.).

Endometriosis (EMs), an estrogen-dependent disease, is characterized by the appearance of the endometrium outside the uterus. The Meorangered1 module was most significantly related to infertile women with EMs. Whereas 40% of the pathways involve metabolism, intersection genes were mostly enriched in various amino acids and in the cGMP-PKG and cAMP signaling pathway. In addition, 13 miRNAs and 2 lncRNAs linked to infertility were identified to create a ceRNA regulatory network linked to infertile EMs. A strong correlation between nutrition and reproduction indicated that dietary amino acid intake influenced key molecules involved in a range of biological processes during conception (Li et al.). Therefore, clarifying associations between EMs and recurrent pregnancy loss (RPL) is a key to solving infertility, as abnormal energy metabolism may be a common pathogenic mechanism. RAB8B, GNAQ, H2AFZ, SUGT1 and LEO1 could be therapeutic candidates for RPL and EMs. The PI3K-Akt signaling pathway and platelet activation were potentially involved in EMs-induced RPL (Ye et al.).

Large-scale nuclear and cytoplasmic reorganizations require a massive amount of energy, potentially derived from a variety of substrates such as carbohydrates, amino acids, and lipids. Since these physiological processes are inherently multicellular and multi-stage, regulatory mechanisms, especially in germ cells at special stages of development, are still largely unknown. Through the proteomic profiles of porcine immature and *in vitro* mature oocytes, 237 of 763 differential proteins were classified in "metabolic process," and assigned to the following: "energy production and conversion;" "carbohydrate transport and metabolism;" "amino acid transport and metabolism;" and "lipid transport and metabolism," etc. Many proteins (e.g., methylsterol monooxygenase 1 and phosphatidate phosphatase) were implicated in in the signaling pathway of lipid metabolism during oocyte maturation (Jia et al.). Spermiogenesis is regulated by nutrients or cellular metabolism. Sugp2, selected as a spermatogenesis regulation-related protein, was enriched in the nucleus of male germ cells, acted as a chromatin-associated protein, and participated in regulation of complexed alternative splicing during gametogenesis. However, Sugp2 had limited effects on meiotic progression and fertility (Zhan et al.). There are indications that microRNA has important roles in male reproductive organ function. Changes in miRNA and mRNA profiles in the testes of juvenile, adolescent, adult, and aged sika deer were evaluated. Differentially expressed mRNA (IGF1R, ALKBH5, Piwil, etc) and miRNA (miR-140, miR-145, etc,) had important roles in regulating proliferation of spermatogonia and glycolysis through MAPK, p53, PI3K-Akt, and Hippo signaling pathways, etc. Furthermore, glycerophospholipid metabolism was only overlapping pathway throughout the life cycle. In addition, miR-140 was confirmed to directly target mutant IGF1R-3'UTR by Luciferase reporter assays (Jia et al.).

In summary, the above-mentioned studies collectively represent an enormous amount of new data on metabolic mechanisms of spermatogenesis, sperm cryopreservation, oocyte aging, and endometriosis in various species. Although this e-book cannot account for all metabolic disorders and characteristics of germ cells, they provide valuable information for understanding these special cells. In the context of the current focus on molecular mechanisms of key biological processes or events at gene and protein levels, it is hoped that this e-book will broaden research perspectives, and try to identify metabolism-based solutions for infertility.

AUTHOR CONTRIBUTIONS

YF wrote the Introduction and the Conclusion. XF, SD, QY, and XW wrote the central part with comments to the cited papers. All authors contributed to the article and approved the submitted version.

FUNDING

This topic was supported by the Strategic Priority Research Program of the Chinese Academy of Sciences (XDA27040302).

Conflict of Interest: The authors declare that the research was conducted in the absence of any commercial or financial relationships that could be construed as a potential conflict of interest.

Publisher's Note: All claims expressed in this article are solely those of the authors and do not necessarily represent those of their affiliated organizations, or those of the publisher, the editors and the reviewers. Any product that may be evaluated in this article, or claim that may be made by its manufacturer, is not guaranteed or endorsed by the publisher.

frontiers in Veterinary Science

ORIGINAL RESEARCH
published: 23 April 2021
doi: 10.3389/fvets.2021.670121

Effects of Pre-ovulatory Follicular Fluid of Repeat Breeder Dairy Cows on Bovine Fertility Transcriptomic Markers and Oocytes Maturation and Fertilization Capacity

Mojtaba Kafi[1†], *Mehran Ghaemi*[2], *Mehdi Azari*[1*], *Abdolah Mirzaei*[1], *Samad Azarkaman*[1] *and Yusof Torfi*[1]

[1] Department of Clinical Sciences, School of Veterinary Medicine, Shiraz University, Shiraz, Iran, [2] Department of Pathobiology, School of Veterinary Medicine, Shiraz University, Shiraz, Iran

OPEN ACCESS

Edited by:
Xianlong Wang,
Baylor College of Medicine,
United States

Reviewed by:
Harald Pothmann,
University of Veterinary Medicine
Vienna, Austria
Nazli Akin,
Vrije University Brussel, Belgium
Satoshi Sugimura,
Tokyo University of Agriculture and
Technology, Japan

***Correspondence:**
Mehdi Azari
mehdiazari@shirazu.ac.ir
orcid.org/0000-0001-5730-9891

†ORCID:
Mojtaba Kafi
orcid.org/0000-0002-7215-483X

Specialty section:
This article was submitted to
Animal Reproduction -
Theriogenology,
a section of the journal
Frontiers in Veterinary Science

Received: 20 February 2021
Accepted: 22 March 2021
Published: 23 April 2021

Citation:
Kafi M, Ghaemi M, Azari M, Mirzaei A, Azarkaman S and Torfi Y (2021) Effects of Pre-ovulatory Follicular Fluid of Repeat Breeder Dairy Cows on Bovine Fertility Transcriptomic Markers and Oocytes Maturation and Fertilization Capacity. Front. Vet. Sci. 8:670121. doi: 10.3389/fvets.2021.670121

The current study aimed to determine the effects of the preovulatory follicular fluid (FF) of normal heifer (NH) and repeat breeder cows with subclinical endometritis (SCE) or without (nSCE) on oocyte maturation (Experiment 1) and fertilization rates (Experiment 2). Moreover, the pattern of gene expression of cumulus oocyte-complexes was evaluated in Experiment 1. In Experiment 1, nuclear maturation in the nSCE group was higher, compared to that in the SCE group ($P = 0.05$). In addition, the oocyte nuclear maturation in the normal heifer was significantly higher, in comparison to that of SCE groups ($P < 0.05$). Furthermore, the mean percentage of normal oocyte fertilization was higher in the nSCE group, compared to that in the SCE group ($P < 0.05$). The expressions of growth differentiation factor, *GDF9;* steroidogenic acute regulatory, *StAR* and follicle-stimulating hormone receptor, *FSHr* in the NH group were significantly higher, compared to those in SCE and nSCE groups ($P < 0.05$). Moreover, the expressions of all genes in the nSCE group were not significant, in comparison to those in the SCE group ($P > 0.05$). The supplementation of oocyte maturation medium with FF from pre-ovulatory follicles of repeat breeder cows resulted in less oocyte maturation and cumulus cell expansion. In conclusion, the lower fertility in RB cows could be ascribed to the lower oocyte maturation rate and less expression of *GDF9, StAR,* and *FSHr* in the cumulus-oocyte complexes.

Keywords: endometritis, follicular fluid, gene expression, lipopolysaccharide, repeat breeder cow

INTRODUCTION

Repeat breeder (RB) cows are described as subfertile cows that do not become pregnant at least after three consecutive services. Different factors, including uterine infections, hormonal imbalances, mismanagement in the artificial insemination, nutritional factors, and genetic disorders may result in the occurrence of RB syndrome in dairy cows (1). A related study reported subclinical endometritis (SCE) in 52.7% of RB cows (2). In addition, researchers denoted that SCE is a major risk factor for reproductive failure resulting in lower reproductively of dairy cows (3, 4). On the contrary, it was found that SCE is not the cause of RB syndrome in dairy cows (5).

Follicular fluid (FF) provides an ideal microenvironment for the growth and development of the ovulatory follicle and the oocyte. Poor FF quality in ovulatory follicles has been frequently linked to low pregnancy rates in lactating cows. Metabolic dysfunctions and uterine infections are two main causes of low FF quality in ovulatory follicles (6–8). Furthermore, it was observed that the addition of ovulatory FF of RB Holstein heifers to oocyte maturation media disturbs oocyte maturation (9). The examination of the pre-ovulatory FF proteome showed differences in protein contents of less fertile cows, compared to those of more fertile ones (10). In addition, another study demonstrated that changes in FF composition in cows with liver problems lead to an impairment in the nuclear maturation of oocytes and the development of blastocyst (11).

Communication between the oocyte and its surrounding cumulus cells is an important event for development of a competent oocyte (12). Growth differentiation factor (*GDF9*) and steroidogenic acute regulatory (*StAR*) proteins play a major role in oocyte developmental competence (13, 14). In addition, the expression of follicle-stimulating hormone receptor (*FSHr*) has an important role in the cumulus cells expansion and the final maturation of COCs (15). Oocyte development, follicular growth, and estrous cyclicity were adversely affected in lactating cows with infections of the uterus or mammary gland (16, 17). Furthermore, it was reported that even though the clinical signs of uterine infection were disappeared, reduced fertility may persist in the infected cows for a variable length of time (18). Lipopolysaccharide (LPS) which is a major part of the outer leaflet of Gram-negative bacteria is emanated from the bacterial infections of the uterus and transported to the FF of ovulatory follicles. The higher levels of LPS in FF were associated with lower fertility in cows (19, 20). In a study, experimentally induced mastitis by Escherichia coli decreased the quality of pre-ovulatory FF, which this in turn, resulted in reduced oocyte developmental competence (21). Moreover, Shimizu et al. (22) indicated that uterine LPS may contribute to ovarian cyst development in cows. Moreover, the FF collected from pre-ovulatory follicles of cows with mastitis and endometritis was showed to contain LPS (20, 21). Very recently, it was observed that the FF LPS concentration of pre-ovulatory follicles in cows with SCE was significantly higher, compared to that of cows without SCE (23). No data is available on the effects of FF obtained from the preovulatory follicle of RB dairy cows with SCE on oocyte maturation and fertilization. With this background in mind, the current study aimed to assess the effects of FF obtained from the preovulatory follicle of RB cows with SCE on oocyte maturation, fertilization, and the expression of genes related to fertility in cultured cumulus-oocyte complexes (COCs).

MATERIALS AND METHODS

Experiment 1

Animals

The present study was approved by the Ethical and Research Committee of Veterinary Faculty, Shiraz University (97GCU1M1251), Iran. RB cows entered the study from a commercial Holstein dairy farm in Alborz, Iran (35° 82' N, 50° 97' E). Free-stall barns were used for the maintaining of cows and mixed feed staffs containing 40% fodder (corn silage and alfalfa) and 60% concentrated meal (soybean meal, corn, wheat bran, barley, trace minerals, and vitamins) were fed. The examination of the reproductive system of RB cows did not show any reproductive clinical signs. Means ± SD of parity, milking days, and the artificial insemination number of repeat breeder cows entered to this study were 3.3 ± 1.7, 277.9 ± 82.8, and 5.2 ± 1.6, respectively. Virgin heifers ($n = 5$) in good body condition score and 14–15 months aged were also selected as control. All heifers became pregnant in the next estrous cycle after sampling. This group of normal virgin heifers was used as the control due the presence of the maximum elements of fertility in the FF in the preovulatory follicles of these animals. The experimental design of the present study is shown in **Figure 1**.

Diagnosis of Subclinical Endometritis and Follicular Fluid Sampling

All the procedures including the diagnosis of subclinically endometriotic cows, ovulation synchronization protocol, follicular fluid sampling were conducted as described in a study by Heidari et al. (23). In brief, the estrus time of the heifers and cows were synchronized using either a two injection of PGF2α (500 μg Cloprostenol sodium, Estroplan Parnel Living Science) with 11 days interval in heifers or an Ovsynch program in RB cows. Using a cytobrush (Heinz Herenz, Hamburg, Germany), uterine secretions were collected from RB cows. For cytology, the uterine samples were spread on a slide, immersed 1 min in 90% alcohol for fixation and stained with Giemsa. RB cows with more than cut-off point of ≥3% PMNs were categorized into RBs with SCE ($n = 10$) (2, 24) and those with <3% PMNs were considered as RBs without subclinical endometritis (nSCE, $n = 13$). Six to twelve hours after detecting standing estrus in synchronized animals, transrectal ultrasonography was performed to confirm the presence of the preovulatory follicle 14–17 mm in diameter (SIUI CTS-900 Ultrasound, Shantou Institute of Ultrasonic Instruments Co., Ltd., China). The FF was aspirated as described previously by Kafi et al. (9). Briefly FF was aspirated trans-rectally using a long fine-needle covered by a hard plastic tube under the caudal epidural anesthesia. Uterine cytology showed out of 23 RB cows, 10 (43.5%) cases exhibited cytological signs of SCE whereas 13 (56.5%) cows did not.

LPS Assay of FF

The amount of LPS in the FF of pre-ovulatory follicles of each group was measured using an ELISA Kit (Hangzhou East biopharm CO., LTD, China). The intra-assay coefficient of variation (intra assay CV) and the inter-assay CV was obtained at <10 and <12%, respectively. Assay range and assay sensitivity were reported as 10-3000 EU/ml and 3.8 EU/ml, respectively. The Follicular fluid used in the present study was basically the same as what we used in our previous study (23). The LPS concentration in pooled FF of the preovulatory follicles of

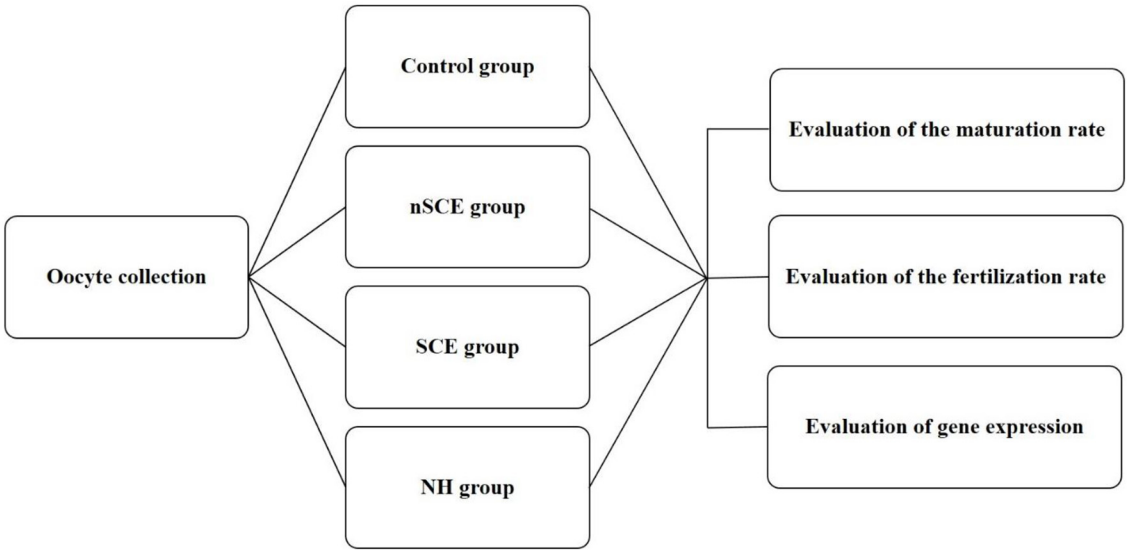

FIGURE 1 | Experimental design. Control: COCs were cultured in TCM-199 medium supplemented with 10% FCS, 5 IU/mL hCG, 10 ng/ml EGF and 0.1 IU/ml human FSH for 24 h; nSCE: COCs were cultured in the TCM-199 medium supplemented with 10% filtered FF of the nSCE for 24 h; SCE: COCs were cultured in the TCM-199 medium supplemented with 10% filtered FF of the SCE for 24 h; NH: COCs were cultured in the TCM-199 medium supplemented with 10% filtered FF of the NH for 24 h.

animals in NH, nSCE, and SCE groups was 410, 862, and 1063 EU/ml, respectively.

In vitro Maturation of Oocytes

The FF collected from five RB cows with a greater percentage of PMNs (SCE; PMNs $\geq$ 3%, $n = 5$), and the FF from five RB cows with a less percentage of PMNs (nSCE; PMNs $<$ 3%, $n = 5$) and, in addition, the FF of five normal heifers (NH, $n = 5$) were pooled separately to be substitute with serum supplement in the oocyte maturation media. Fetal calf serum (FCS) was used for serum supplement in the control group of *in vitro* maturation in Experiment 1.

For oocyte collection, the ovaries of slaughtered cows were collected and transferred to the laboratory within 2 h at 32–35°C in phosphate-buffered saline (PBS). The ovaries were washed in sterile PBS (37°C) for three times; thereafter, the cumulus-oocyte complexes (COCs) were aspirated with a 20 G hypodermic needle attached to a 10 ml disposable syringe. COCs with more than three layers of cumulus cells and a finely granulated homogenous ooplasm were selected and entered the *in vitro* maturation (25). Medium HEPES- buffered TCM-199 (Sigma, USA) supplemented with 10% FCS was used for washings of the selected COCs. In total, 735 good quality COCs were assigned to four groups. In technical control group, COCs ($n = 204$) were cultured in TCM-199 medium supplemented with 10% FCS, 5 IU/mL hCG (Karma, Germany), 10 ng/ml EGF (Sigma, USA), and 0.1 IU/ml human FSH (Follitrope, South Korea). On the other hand, in the NH group, COCs ($n = 141$) were cultured in the TCM-199 medium supplemented with 10% filtered FF of the normal heifer. In addition, in the nSCE group, COCs ($n = 217$) were cultured in TCM-199 medium supplemented with 10% filtered FF of nSCE cows. Also, in the SCE group, COCs ($n = 173$) were matured in the TCM-199 medium supplemented with 10% filtered FF of SCE cows. All cultures were carried out in four well-culture dishes (NuncTM, Denmark). In all maturation media, 50 μg/ml Gentamicin (Sigma, USA) was also added. Groups of 30–50 COCs were cultured for 24 h in a 500 μl culture media at 38.5°C in 5% CO_2.

Evaluation of Nuclear Maturation of Oocytes

After 24 h, the COCs were evaluated for nuclear maturation using the aceto-orcein staining method. Cumulus expansion degree was also graded using a stereo microscope from 0 (no expansion), 1 (partial expansion) to 2 (complete expansion). Also, for the evaluation of nuclear maturation of the oocytes, matured COCs were pipetted frequently to denude the oocytes which were then fixed using acetic alcohol under coverslips for 24 h. The oocytes were then stained using 1% aceto-orcein. Oocytes which did not reach to the metaphase were classified as "immature," oocytes that chromosomes arranged in metaphase plate and peripherally located in the ooplasm were classified as 'metaphase I (MI), oocytes with a polar body and the metaphase II plate were classified as "mature" and oocytes showed chromosomal abnormality categorized at "abnormals."

RNA Extraction

RNA was extracted from 50 COCs of each group using the RNeasy micro RNA extraction kit (Qiagen, Germany) as instructed by the manufacturer. In each group, four independent replicates were performed for extraction. Then, extracted RNA of

all samples was quantified by Nanodrop spectrometer in order to adjust the amount of starting material in the next step.

Real-Time Polymerase Chain Reaction

After oocyte maturation in 24 h, the expression levels of *GDF9, StAR,* and *FSHr* in COCs of NH, SCE, and nSCE groups were determined using real-time RT-PCR. For relative quantification, *GAPDH* housekeeping gene was used as the normalizer gene, and the NH group was assumed as the calibrator group.

cDNA Synthesis

Five hundred nanogram of each extracted RNA was entered to cDNA synthesis. REVERT-L RT kit (AmpliSens biotechnologies, Korea) was used to synthesize cDNA from extracted RNA according to the manufacturer's instruction. One No-RT control for each group was included in cDNA synthesis by the omitting of reverse transcriptase enzyme from cDNA synthesis. No-RT control is a control for DNA digestion in RNA extraction step and it must be negative in the Real-time PCR test to ensure that positive results were not due to genomic DNA remnants.

Real Time PCR

Firstly, the efficacy of each real-time PCR test was assessed by running the test on a cDNA serial dilution. If a real-time PCR had an efficiency lower than 95% or higher than 105%, the test was optimized to improve its efficiency. Power SYBR Green PCR Master Mix (Thermo Fisher Scientific, US) was consumed for the real-time PCR tests using a Corbett 6000 instrument (Qiagen, Germany). Twenty microliter of the total volume of each PCR master mix consisted of 10 μl of Power master mix, 1 μl of each primer (5 μM), 1 μl of cDNA, and 7 μl of Distilled water. The initial denaturation step was performed at the beginning of real-time PCR for 10 min at 95°C, followed by 40 cycles of 15 s at 95°C, 30 s at annealing temperature (**Table 1**), and 30 s at 72°C. The results were analyzed using the ΔΔCt method and the expression level of each gene in different groups was calculated in relation to the calibrator group (normal heifer).

Experiment 2

In vitro Fertilization

In vitro oocyte maturation was carried out in four groups as described in Experiment 1. After *in vitro* maturation of the oocytes, groups of 35–50 COCs were transferred into four well-culture dishes containing 500 μl Tyrode's medium as fertilization medium. Frozen semen which previously tested in the laboratory for IVF was used for fertilization. Motile spermatozoa from frozen/thawed semen were obtained using the swim-up method and were then added to wells containing oocytes at a final concentration of 10^6 spermatozoa ml−1 (12). Oocytes and spermatozoa were co-incubated at 38.5°C for 18 h in 5% CO_2.

Assessment of the Fertilization Rate

After the fertilization period, surrounding cumulus cells of presumptive zygotes were removed by repeated pipetting which was mounted on glass slides under coverslips fixed in an acetic alcohol solution for at least 24 h and then were stained using 1% aceto-orcein. Presumptive zygotes with two pronuclei were classified as "fertilized," while the presumptive zygotes without pronuclear formation, absent of sperm in the ooplasm, and without second polar body were classified as "non-fertilized," presumptive zygotes with more than two pronuclei were classified as "polyspermy," and oocytes with other nuclear structures were classified as "abnormal fertilization."

Statistical Analysis

The obtained data were analyzed in SPSS software (version 23). The Shapiro-Wilk test was used to assess the normality of the distribution of data sets. Differences in the cumulus expansion, maturation and fertilization rates among groups were statistically analyzed using an ANOVA test (*Post Hoc* LSD). Moreover, One Way ANOVA was applied for the statistical analysis of Real-time RT-PCR results. A $p < 0.05$ was considered statistically significant. Experiments 1 and 2 were performed in five independent replicates.

RESULTS

Experiment 1

Percentage of Cumulus Expansion and Oocyte Nuclear Maturation

The mean (±SD) percentage of COCs demonstrated that fully expanded cumulus cells were significantly lower in SCE group than the control, nSCE and NH groups (30.4 ± 8.3 vs. 65.7 ± 12.1, 46.0 ± 12.9, and 48.8 ± 11.9, respectively; $P < 0.05$). Furthermore, the percentage of fully expanded cumulus cells between nSCE and NH was not significantly different ($P > 0.05$). The mean (±SD) percentage of nuclear maturation (M II stage) of the SCE, nSCE, NH, and control groups is shown in **Table 2**. The percentage of oocyte nuclear maturation in the control group was significantly higher compared to that in other groups ($P < 0.05$). Further, the mean (±SD) percentage of nuclear maturation in the nSCE group was higher than that of the SCE group (69.4 ± 10.6 vs. 61.1 ± 8.0; $P = 0.05$). Also, the percentage of oocyte nuclear maturation in the NH group was significantly higher than that in the SCE group (72.9 ± 4.9 vs. 61.1 ± 8.03; $P < 0.05$).

Real Time RT-PCR

The mRNA expression of *GDF9, StAR*, and *FSHr* in the NH group was significantly higher than those of SCE and nSCE groups ($P < 0.05$). The mRNA expressions of *GDF9, StAR*, and *FSHr* in nSCE in comparison to those of SCE were not significantly different ($P > 0.05$). The results in detail are presented in **Figure 2**.

Experiment 2

The results in detail are presented in **Table 3**. The mean (±SD) percentage of normal oocyte fertilization was higher in the nSCE than the SCE group (58.0 ± 9.8 vs. 40.2 ± 4.5; $P < 0.05$). Furthermore, the mean (±SD) percentage of normal oocyte fertilization in the nSCE group, in comparison with the NH group was not significant (58.0 ± 9.8 vs. 48.1 ± 10.7; $P > 0.05$).

TABLE 1 | Primers used for real time RT PCR of different genes.

Gene	Primer sequences (5′ to 3′)	Annealing temperature (°C)	Accession number
GDF9	For: TGAAGATATGATAGCCACTAAG Rev: CTCCTCCTTACACAACAC	58	NM_174681.2
FSHr	For: GAATGATGTCTTGGAAGTGATAG Rev: CGATGTATAGCAGGTTGTTG	58	NM_174061.1
StAR	For: TGCCGAAGACCATCATCAAC Rev: GAGCCCTCAAACCCATTCAG	62	NC_037330.1
GAPDH	For: ATCTCGCTCCTGGAAGATG Rev: TCGGAGTGAACGGATTCG	60	NM_001034034

Primer sequences, annealing temperatures, and accession numbers. All primers designed in this study using Beacon Designer (Primier Biosoft) software.

TABLE 2 | Mean (±SD) percentages of normally mature oocytes following addition of follicular fluid collected from cows with no subclinical endometritis (nSCE), subclinical endometritis (SCE) and normal heifer (NH) to the maturation media.

Group name	Number	MII oocytes, *n* (%)	Immature oocytes, *n* (%)	MI oocytes, *n* (%)	Degraded oocytes, *n* (%)
Control	204	177 (86.7 ± 1.9)^{a}	8 (3.7 ± 3.7)	15 (7.8 ± 3.3)^{a}	4 (1.7 ± 2.9)
nSCE	217	149 (69.4 ± 10.6)^{b}	24 (9.5 ± 12.8)	41 (19.6 ± 7.3)^{b}	3 (1.3 ± 2.4)
SCE	173	105 (61.1 ± 8.0)^{c}	24 (12.7 ± 16.8)	39 (22.9 ± 13.8)^{b}	5 (3.1 ± 5.0)
NH	141	103 (72.9 ± 4.9)^{bd}	2 (1.06 ± 2.6)	33 (24.2 ± 6)^{b}	3 (1.7 ± 2.8)

In control group, oocytes are cultured with FCS.
Different letters within a column showed statistically significant difference ($P \leq 0.05$).
MII (metaphase II), MI (metaphase I).

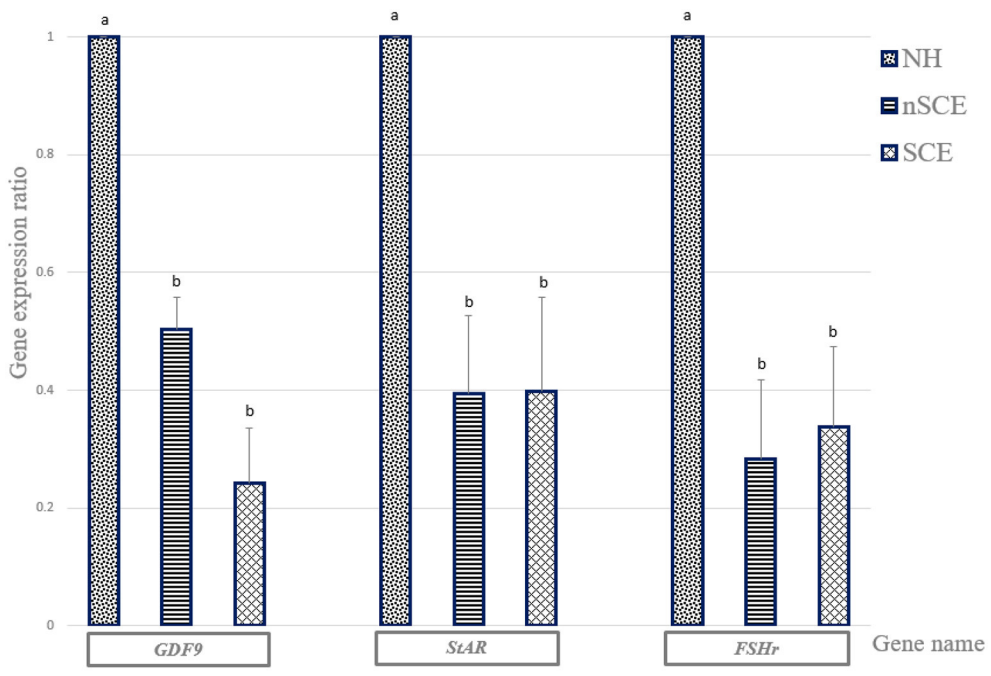

FIGURE 2 | The expression ratio of *GDF9, StAR,* and *FSHr* genes. Bar charts (with standard errors) shows the expression ratio of genes in COCs cultured in the media containing pre-ovulatory FF of normal heifer (NH) and cows with subclinical endometritis (SCE), and without subclinical endometritis (nSCE). In each gene, different letters indicates statistically significant difference ($P < 0.05$).

TABLE 3 | Mean (±SD) percentages of normally fertilized oocytes following addition of follicular fluid collected from cows with no subclinical endometritis (nSCE), subclinical endometritis (SCE) and normal heifer (NH) to the maturation media.

Group name	Number	Fertilization, *n* (%)	Non fertilized, *n* (%)	Polyspermy, *n* (%)	Abnormal fertilization, *n* (%)
Control	132	85 (66.1 ± 12.8)^{a}	39 (26.5 ± 17.5)^{a}	3 (2.6 ± 2.8)	5 (4.5 ± 5.5)
nSCE	161	94 (58.0 ± 9.8)^{ab}	63 (39.6 ± 8.1)^{ab}	10 (0.5 ± 1.2)	3 (1.7 ± 3.2)
SCE	173	70 (40.2 ± 4.5)^{c}	100 (57.8 ± 5.5)^{c}	-	3 (1.8 ± 2.1)
NH	120	58 (48.1 ± 10.7)^{bc}	54 (44.9 ± 9.8)^{bc}	1 (0.8 ± 1.9)	7 (5.9 ± 6.9)

Different letters within a column showed statistically significant difference ($P < 0.05$).

DISCUSSION

The present study strived to apply an *in vitro* model that could simulate an intra-follicular condition which occurs in the final stages of oocyte maturation in the pre-ovulatory follicles of RB cows and animals with the highest level of fertility, virgin heifers. Using FF as a component of oocyte maturation media has previously been used as a model to examine the oocyte competence in either mastitic or healthy cows (21). The results of experiment 1 showed that cumulus expansion and nuclear maturation of oocytes decreased when they were cultured *in vitro* using FF of pre-ovulatory follicles of RB cows with SCE, compared to nSCE and NH groups. The lower nuclear maturation rate in the SCE group could be due to the fact that the LPS level in the FF of pre-ovulatory follicles in RB cows with SCE was higher than that of the other groups in the present study. Similarly, Magata and Shimizu (26) using a dose-response approach found a deleterious effect of LPS on *in vitro* oocyte development in cattle. Zhao et al. (27) further showed that the LPS disrupted meiotic spindle structure and induced oxidative stress in bovine oocytes resulting in low nuclear maturation. The lower nuclear maturation rate in the SCE group in the present study explains the results of our previous study in which a lower blastocyst yield was observed when the bovine oocytes matured *in vitro* using FF of pre-ovulatory follicles of RB cows with SCE (23). One more significant finding in the present study (Experiment 2) was the lower percentage of normally *in vitro* fertilized oocytes observed in the SCE group compared to the nSCE group. The proper fertilization fundamentally depends on normal nuclear maturation and cumulus expansion to perform numerous functions required for fertilization support (28, 29).

In Experiment 1, the expression levels of *GDF9, StAR,* and *FSHr* mRNA in COCs were determined using RT-PCR. Recent researches have shown that *GDF9* protein plays a major role in oocyte developmental competence (13, 30), follicular growth, and luteinization in mammals (31). The higher oocyte nuclear maturation rates in the NH than the SCE group can be explained by the fact the *GDF9* expression level in the matured COCs in the NH group was significantly higher than those of the SCE groups in the present study. Although the nuclear maturation rate was higher in the nSCE group than that of the SCE group, however, no difference was observed in the expression level of *GDF9* in the matured COCs between the nSCE and SCE groups.

StAR mRNA expression in the COCs was significantly reduced in both nSCE and SCE groups in comparison with that of the NH group. This could be ascribed to the higher levels of LPS in the pre-ovulatory follicles of repeat breeder cows comparing to that of the virgin heifers. Steroidogenic acute regulatory protein is encoded by the *StAR* mRNA. *StAR* in COCs has been reported to be involved in the developmental competence of the oocyte and the embryo in bovine (32), and sheep (14). Magata et al. (33) found that a greater amount of LPS in the FF disrupted the function of theca and granulosa cells in the follicle leading to less steroid production. Also, SCE (34), and particularly LPS (35), can cause inflammation in bovine granulosa cells, which disrupts Steroidogenesis in follicles. Similarly, we observed a significant lower nuclear maturation rates in SCE groups than those of the NH group. The higher LPS level in the FF of the preovulatory follicles in the RB cows in the present study could be responsible for the lower expression of *StAR* mRNA in the matured COCs in the nSCE and SCE groups in the present study. Also, our result was in agreement with those of Campos et al. (36), Herzog et al. (37), Shimizu et al. (22), and Magata et al. (33). They observed that LPS reduced the *StAR* mRNA expression which could result in the reduction of steroid production. Our recent study (23) and others (20, 38) showed a lower concentration of 17-β estradiol associated with a high LPS in the FF of the pre-ovulatory follicles of SCE cows.

FSH has an important role in the cumulus cells expansion and the final maturation of COCs in cows and other mammals (15). The results of the present study showed a significant reduction in *FSHr* mRNA expression of the matured COCs in SCE group in comparison with that of the NH group. This could be explained by the presence of higher amount of LPS in FF of the pre-ovulatory follicles in SCE group. Although the LPS concentration was higher in the FF of preovulatory follicles of the RB cows with SCE than that of the nSCE cows in the present study, however, the pattern of expression of *GDF9, StAR,* and *FSHr* in the *in vitro* matured COCs did not explain the observed differences in the maturation and fertilization rates between the nSCE and SCE groups. Although it is difficult to explain this finding, however we assume that the effect on *GDF9, StAR*, and *FSHr* expression is associated with clinical endometritis rather than the sub-clinical endometritis. Alternatively, the bacterial type (G^+ and G^-) may have influenced the mRNA expression of our candidate genes as shown by Asaf et al. (21). It is important to note that significantly higher level of the expression of *GDF9, StAR,* and *FSHr* in the

matured COCs of the NH group as compared to those of the RB groups suggest the presence of a disturbance in the normal function and expression of the genes involved in the fertility in RB cows. The cumulus cells surrounding the immature oocyte play a critical role in the development of the oocyte. Expansion of the cumulus cells is one of the first morphological predictive criteria of the successful completion of oocyte maturation (29). In addition, results of different researches have shown that gene expression patterns in the cumulus cells are an acceptable marker for oocyte quality (39, 40). Results of the present study showed that the mean percentage of fully expanded cumulus cells were significantly lower in SCE group than the other experimental groups. This can explain the lower nuclear oocyte maturation and fertilization rates in the SCE group comparing with that of the nSCE group in the preset study.

CONCLUSIONS

In conclusion, the low oocyte maturation and fertilization rates could explain the disturbed fertility in RB cows specifically with subclinical endometritis. This implies the presence of poor quality of microenvironment for the final stages of oocyte development in the pre-ovulatory follicle of RB cows. Additionally, the lower fertility in RB cows could be ascribed to the lower oocyte developmental competence and less expression of *GDF9, StAR*, and *FSHr* in the cumulus-oocyte complexes.

DATA AVAILABILITY STATEMENT

The data that support the findings of this study are available from the corresponding author upon reasonable request.

ETHICS STATEMENT

The animal study was reviewed and approved by Ethical and Research Committee of Veterinary Faculty, Shiraz University (97GCU1M1251).

AUTHOR CONTRIBUTIONS

MK designed this study and involved in the lab works and writing this paper. MG performed Real time RT-PCR and contributed to writing paper. MA performed the laboratory work and revised the manuscript. AM performed the follicular fluid collection. SA and YT, DVM students, were involved in the laboratory work.

ACKNOWLEDGMENTS

The authors thank the farm staff at the Mallard dairy farm, Alborz, for their kind cooperation. They are also grateful to Dr. Mehdi Heidari for their technical help to follicular fluid collection. This study was financially supported by grant No. 97GCU2M1251 of the Shiraz University and the Center of Excellence for Research on High-Producing Dairy Cows.

REFERENCES

1. Perez-Marin CC, Molina Moreno L, Vizuete CG. Clinical approach to the repeat breeder cow syndrome. In: *A Bird's-Eye View of Veterinary Medicine*, *1st, Edn*. London: IntechOpen Press (2012). p. 337–362. doi: 10.5772/31374
2. Salasel B, Mokhtari A, Taktaz T. Prevalence, risk factors for and impact of subclinical endometritis in repeat breeder dairy cows. *Theriogenology*. (2010) 74:1271–8. doi: 10.1016/j.theriogenology.2010.05.033
3. Gilbert RO. The effects of endometritis on the establishment of pregnancy in cattle. *Reprod Fertil Dev*. (2011) 24:252–7. doi: 10.1071/RD11915
4. López-Helguera I, López-Gatius F, Garcia-Ispierto I. The influence of genital tract status in postpartum period on the subsequent reproductive performance in high producing dairy cows. *Theriogenology*. (2012) 77:1334–42. doi: 10.1016/j.theriogenology.2011.10.038
5. Pothmann, H., Prunner, I., Wagener, K., Jaureguiberry, M., de la Sota, R.L., Erber, R., et al. The prevalence of subclinical endometritis and intrauterine infections in repeat breeder cows. *Theriogenology*. (2015) 83:1249–53. doi: 10.1016/j.theriogenology.2015.01.013
6. Leroy J, Van Soom A, Opsomer G, Goovaerts I, Bols P. Reduced fertility in high yielding dairy cows: are the oocyte and embryo in danger? Part II mechanisms linking nutrition and reduced oocyte and embryo quality in high yielding dairy cows. *Reprod Domest Anim*. (2008) 43:623–32. doi: 10.1111/j.1439-0531.2007.00961.x
7. Williams EJ, Fischer DP, Noakes DE, England GCW, Rycroft A, Dobson H, et al. The relationship between uterine pathogen growth density and ovarian function in the postpartum dairy cow. *Theriogenology*. (2007) 68:549–59. doi: 10.1016/j.theriogenology.2007.04.056
8. Cheong SH, Filho OJ, Absalon-Medina VA, Schneider A, Butler WA, Gilbert RO. Uterine and systemic inflammation influences ovarian follicular function in postpartum dairy cows. *PLoS ONE*. (2017) 12:e0177356. doi: 10.1371/journal.pone.0177356
9. Kafi M, Azari M, Chashnigir O, Gharibzadeh S, Aghabozorgi Z, Asaadi A, et al. Inherent inferior quality of follicular fluid in repeat breeder heifers as evidenced by low rates of in vitro production of bovine embryos. *Theriogenology*. (2017) 102:29–34. doi: 10.1016/j.theriogenology.2017.07.011
10. Zachut M, Sood P, Levin Y, Moallem U. Proteomic analysis of preovulatory follicular fluid reveals differentially abundant proteins in less fertile dairy cows. *J Proteom*. (2016) 139:122–9. doi: 10.1016/j.jprot.2016.03.027
11. Tanaka H, Shibano K, Monji Y, Kuwayama T, Iwata H. Liver condition affects bovine oocyte qualities by changing the characteristics of follicular fluid and plasma. *Reprod Domest Anim*. (2013) 48:619–26. doi: 10.1111/rda.12135
12. Azari M, Kafi M, Ebrahimi B, Fatehi R, Jamalzadeh M. Oocyte maturation, embryo development and gene expression following two different methods of bovine cumulus-oocyte complexes vitrification. *Vet Res Commun*. (2017) 41:49–56. doi: 10.1007/s11259-016-9671-8
13. Ferreira RM, Chiaratti MR, Macabelli CH, Rodrigues CA, Ferraz ML, Watanabe YF, et al. The infertility of repeat-breeder cows during summer is associated with decreased mitochondrial DNA and increased expression of mitochondrial and apoptotic genes in oocytes. *Biol Reprod*. (2016) 94:66–71. doi: 10.1095/biolreprod.115.133017
14. Valiollahpoor Amiri M, Deldar H, Ansari Pirsaraei Z. Impact of supplementary royal jelly on *in vitro* maturation of sheep oocytes: genes involved in apoptosis and embryonic development. *Syst Biol Reprod Med*. (2016) 62:31–8. doi: 10.3109/19396368.2015.1088102
15. Ongaratto FL, Andrés V Cedeño AV, Rodriguez-Villamil P, Tríbulo A, Bó G A. Effect of FSH treatment on cumulus oocyte complex recovery by ovum pick up and *in vitro* embryo production in beef donor cows. *Anim Reprod Sci*. (2020) 214:106274. doi: 10.1016/j.anireprosci.2020.106274
16. Sheldon IM, Noakes DE, Rycroft AN, Pfeiffer DU, Dobson H. Influence of uterine bacterial contamination after parturition on ovarian dominant follicle selection and follicle growth and function in cattle. *Reproduction*. (2002) 123:837–45. doi: 10.1530/rep.0.1230837

17. Lavon Y, Leitner G, Moallem U, Klipper E, Voet H, Jacoby S, et al. Immediate and carryover effects of Gram-negative and Gram- positive toxin-induced mastitis on follicular function in dairy cows. *Theriogenology*. (2011) 76:942–53. doi: 10.1016/j.theriogenology.2011.05.001
18. Bromfield JJ, Santos JEP, Block J, Williams RS, Sheldon IM. Physiology and endocrinology symposium: uterine infection: linking infection and innate immunity with infertility in the high-producing dairy cow. *J Anim Sci*. (2015) 93:2021–33. doi: 10.2527/jas.2014-8496
19. Mateus L, Lopes da Costa L, Diniz P, Ziecik AJ. Relationship between endotoxin and prostaglandin (PGE2 and PGFM) concentrations and ovarian function in dairy cows with puerperal endometritis. *Anim Reprod Sci*. (2003) 76:143–54. doi: 10.1016/S0378-4320(02)00248-8
20. Herath S, Williams EJ, Lilly ST, Gilbert RO, Dobson H, Bryant CE, et al. Ovarian follicular cells have innate immune capabilities that modulate their endocrine function. *Reproduction*. (2007) 134:683–93. doi: 10.1530/REP-07-0229
21. Asaf S, Leitner G, Furman O, Lavon Y, Kalo D, Wolfenson D, et al. Effects of *Escherichia coli*-and *Staphylococcus aureus*-induced mastitis in lactating cows on oocyte developmental competence. *Reproduction*. (2014) 147:33–43. doi: 10.1530/REP-13-0383
22. Shimizu T, Ishizawa S, Magata F, Kobayashi M, Fricke P, Miyamoto A. Involvement of lipopolysaccharide in ovarian cystic follicles in dairy cow: expressions of LPS receptors and steroidogenesis-related genes in follicular cells of cystic follicles. *Anim Reprod Sci*. (2018) 195:89–95. doi: 10.1016/j.anireprosci.2018.05.010
23. Heidari M, Kafi M, Mirzaei A, Asaadi A, Mokhtari A. Effects of follicular fluid of preovulatory follicles of repeat breeder dairy cows with subclinical endometritis on oocyte developmental competence. *Anim Reprod Sci*. (2019) 205:62–9. doi: 10.1016/j.anireprosci.2019.04.004
24. Pascottini OB, Hostens M, Sys P, Vercauteren P, Opsomer G. Cytological endometritis at artificial insemination in dairy cows: prevalence and effect on pregnancy outcome. *J Dairy Sci*. (2017) 100:588–97. doi: 10.3168/jds.2016-11529
25. Lorenzo PL, Illera MJ, Illera JC, Illera M. Enhancement of cumulus expansion and nuclear maturation during bovine oocyte maturation *in vitro* by the addition of epidermal growth factor and insulin-like growth factor I. *Reproduction*. (1994) 101:697–701. doi: 10.1530/jrf.0.1010697
26. Magata F, Shimizu T. Effect of lipopolysaccharide on developmental competence of oocytes. *Reprod Toxicol*. (2017) 71:1–7. doi: 10.1016/j.reprotox.2017.04.001
27. Zhao SJ, Pang YW, Zhao XM, Du WH, Hao HS, Zhu HB. Effects of lipopolysaccharide on maturation of bovine oocyte *in vitro* and its possible mechanisms. *Oncotarget*. (2017) 8:4656–67. doi: 10.18632/oncotarget.13965
28. Dey SR, Deb GK, Ha AN, Lee JI, Bang JI, Lee K.L. Coculturing denuded oocytes during the *in vitro* maturation of bovine cumulus oocyte complexes exerts a synergistic effect on embryo development. *Theriogenology*. (2012) 77:e1077. doi: 10.1016/j.theriogenology.2011.10.009
29. Lonergan P, Fair T. Maturation of oocytes in vitro. *Annu Rev Anim Biosci*. (2016) 4:255–68. doi: 10.1146/annurev-animal-022114-110822
30. Regassa A, Rings F, Hoelker M. Transcriptome dynamics and molecular cross-talk between bovine oocyte and its companion cumulus cells. *BMC Genomics*. (2011) 12:57. doi: 10.1186/1471-2164-12-57
31. Dalbies-Tran R, Cadoret V, Desmarchais A, Elis S, Maillard V, Monget P, et al. A comparative analysis of oocyte development in mammals. *Cells*. (2020) 9:1002. doi: 10.3390/cells9041002
32. Salhab M, Papillier P, Perreau C, Guyader-Joly C, Dupont J, Mermillod P, et al. Thymosins β-4 and β-10 are expressed in bovine ovarian follicles and upregulated in cumulus cells during meiotic maturation. *Reprod Fertil Dev*. (2010) 22:1206–21. doi: 10.1071/RD10015
33. Magata F, Horiuchi M, Echizenya R, Miura R, Chiba S, Matsui M, et al. Lipopolysaccharide in ovarian follicular fluid influences the steroid production in large follicles of dairy cows. *Anim Reprod Sci*. (2014) 144:6–13. doi: 10.1016/j.anireprosci.2013.11.005
34. Green M, Ledgard A, Beaumont S, Berg M, McNatty K, Peterson A, et al. Long-term alteration of follicular steroid concentrations in relation to subclinical endometritis in postpartum dairy cows. *J Anim Sci*. (2011) 89:3551–60. doi: 10.2527/jas.2011-3958
35. Bromfield JJ, Sheldon IM. Lipopolysaccharide initiates inflammation in bovine granulosa cells via the TLR4 pathway and perturbs oocyte meiotic progression in vitro. *Endocrinology*. (2011) 152:5029–40. doi: 10.1210/en.2011-1124
36. Campos FT, Rincon JAA, Acosta DAV. The acute effect of intravenous lipopolysaccharide injection on serum and intrafollicular HDL components and gene expression in granulosa cells of the bovine dominant follicle. *Theriogenology*. (2017) 89:244–9. doi: 10.1016/j.theriogenology.11.013
37. Herzog K, Strüve K, Kastelic JP, Piechotta M, Ulbrich SE, Pfarrer C, et al. *Escherichia coli* lipopolysaccharide administration transiently suppresses luteal structure and function in diestrous cows. *Reproduction*. (2012) 144:467–76. doi: 10.1530/REP-12-0138
38. Price JC, Bromfield JJ, Sheldon IM. Pathogen-associated molecular patterns initiate inflammation and perturb the endocrine function of bovine granulosa cells from ovarian dominant Follicles via TLR2 and TLR4 pathways. *Endocrinology*. (2013) 154:3377–86. doi: 10.1210/en.2013-1102
39. Matoba S, Bender K, Fahey AG, Mamo S, Brennan L, Lonergan P, et al. Predictive value of bovine follicular components as markers of oocyte developmental potential. *Reprod Fertil Dev*. (2014) 26:337–45. doi: 10.1071/RD13007
40. Bunel A, Jorssen EP, Merckx E, Leroy JL, Bols PE, Sirard MA. Individual bovine in vitro embryo production and cumulus cell transcriptomic analysis to distinguish cumulus-oocyte complexes with high or low developmental potential. *Theriogenology*. (2015) 83:228–37. doi: 10.1016/j.theriogenology.2014.09.019

Conflict of Interest: The authors declare that the research was conducted in the absence of any commercial or financial relationships that could be construed as a potential conflict of interest.

frontiers in Veterinary Science

ORIGINAL RESEARCH
published: 18 October 2021
doi: 10.3389/fvets.2021.754021

Chromatin-Associated Protein Sugp2 Involved in mRNA Alternative Splicing During Mouse Spermatogenesis

Junfeng Zhan[1,2,3†], *Jianbo Li*[2,3†], *Yuerong Wu*[4†], *Panfeng Wu*[2,3], *Ziqi Yu*[2,3], *Peng Cui*[2,3], *Mofan Zhou*[2], *Yumin Xu*[2,3], *Tingyu Jin*[2,3], *Ziye Du*[2,3], *Mengcheng Luo*[2,3*] *and Cong Liu*[2,3*]

[1] Department of Urology, Zhongnan Hospital of Wuhan University, Wuhan, China, [2] Department of Tissue and Embryology, School of Basic Medical Sciences, Wuhan University, Wuhan, China, [3] Hubei Provincial Key Laboratory of Developmentally Originated Disease, Wuhan, China, [4] Center for Animal Experiment, Wuhan University, Wuhan, China

OPEN ACCESS

Edited by:
Yi Fang,
Northeast Institute of Geography and Agroecology, Chinese Academy of Science, China

Reviewed by:
Ju Yuan,
*Genome Institute of Singapore (A*STAR), Singapore*
Gong-Xue Jia,
Northwest Institute of Plateau Biology (CAS), China

***Correspondence:**
Mengcheng Luo
luomengcheng@whu.edu.cn
Cong Liu
woshiziyoudeyulc@163.com

†These authors have contributed equally to this work

Specialty section:
This article was submitted to Animal Reproduction - Theriogenology, a section of the journal Frontiers in Veterinary Science

Received: *05 August 2021*
Accepted: *13 September 2021*
Published: *18 October 2021*

Citation:
Zhan J, Li J, Wu Y, Wu P, Yu Z, Cui P, Zhou M, Xu Y, Jin T, Du Z, Luo M and Liu C (2021) Chromatin-Associated Protein Sugp2 Involved in mRNA Alternative Splicing During Mouse Spermatogenesis. Front. Vet. Sci. 8:754021. doi: 10.3389/fvets.2021.754021

Mammalian spermatogenesis is a highly ordered process that is determined by chromatin-associated moderators which still remain poorly understood. Through a multi-control group proteomics strategy, we confirmed that Sugp2 was a chromatin-associated candidate protein, and its signal arose along spermatogenesis. The expression results showed that Sugp2, which is mainly expressed in the testis, had two transcripts, encoding one protein. During spermatogenesis, Sugp2 was enriched in the nucleus of male germ cells. With the depletion of Sugp2 by CRISPER-Cas9 technology, we found that Sugp2 controlled a network of genes on metal ion and ATP binding, suggesting that alternative splicing regulation by Sugp2 is involved in cellular ion and energy metabolism during spermatogenesis, while it had a little effect on meiotic progression and male fertility. Collectively, these data demonstrated that, as a chromatin-associated protein, Sugp2 mediated the alternative splicing regulatory network during spermatogenesis.

Keywords: spermatogenesis, chromatin-associated protein, SUGP2, alternative splicing, male germ cell

INTRODUCTION

Spermiogenesis is recognized as one of the most complex biological processes. This process involves two main elements: (1) the cellular extrinsic stimuli, including organic or inorganic nutrients and growth factors produced in a supportive niche, and (2) intrinsic factors, mainly related to cellular metabolism regulated by gene expression. Alternative pre-mRNA splicing (AS) is critical for gene expression, and extensive AS variants are enriched in different developmental stages of mouse spermatogenesis. This post-transcriptional regulation promotes the establishment of a regulatory mechanism for changes in both internal and external environments of the cell during spermatogenesis and also promotes male gamete production (1–4).

As an indispensable component of gamete production, meiosis is a specialized type of cell division that creates haploid cells from diploid progenitors and ensures genetic diversity through homologous recombination (5). During meiosis, recombination is initiated by programmed DNA double-strand breaks (DSBs) generated by Spo11 (6) and TOPOVIBL (7). Subsequently, meiotic DNA DSBs will cause the phosphorylation of histone variant H2ax (γH2ax) at the Ser-139 residue, which is an early cellular response to the induction (8), recruit a series of recombination proteins

to form recombination foci, and promote homologous chromosome synapsis during the zygotene stage (9, 10). Strand invasion of the 3′ single-stranded DNA, shielded by RPA protein complex, into the duplex of the homolog is mediated by recombinase Dmc1 and Rad51 (10–12). At the pachytene stage when the homologous chromosomes are fully synapsed, recombination foci continue to mature and are eventually resolved into crossover or non-crossover events, which ensure the correct separation of homologous chromosomes (5).

The biochemical mechanism of meiosis is inseparably interconnected with a chromatin structure. Most of the regulatory factors can integrate into the chromatin body and act by various mechanisms (13). Our method for the isolation of spermatogenetic chromatin-associated proteins had identified many important male reproductive factors, such as Meiob, Scml2, and Sdx, involved in meiotic recombination, histone modification, and gene transcription, respectively (14–16). Since spermatogenesis is a multicellular and multi-stage process, the regulation mechanisms, especially in special cell types or at special stages, are still largely unknown.

In this study, adapting with proteomic data on spermatogenetic chromatin-associated proteins, we focused on Sugp2 which may be involved in RNA regulation. We systematically analyzed the expression and localization of Sugp2 in mouse testes by generating Sugp2 antibody and explored its function during spermatogenesis through a Sugp2-deficient mouse model based on CRISPER-Cas9 technology. This research would help us better understand the regulation mechanism in spermatogenesis.

MATERIALS AND METHODS

Unless otherwises specified, the drugs used in the experiments are from Sigma Aldrich (United States).

Animals

All mice were housed in the pathogen-free animal facility of Wuhan University. All animal studies were reviewed and approved by the Institutional Animal Care and Use Committee of Wuhan University. The *Sugp2* knockout mice were purchased from Jiangsu GemPharmatech Company in China. The mouse genotype was identified by extracting DNA from mouse tail and combining with PCR. The primers used for genotyping are listed in **Table 1**. All the animal experiments were performed under the animal ethical guidelines of the Institutional Care and Wuhan University.

Purification and Screening of Chromatin-Associated Proteins

The purification of chromatin-associated proteins was carried out as (15) with modifications. One hundred milligrams of testis tissues from different groups was homogenized in 1 ml of lysis buffer 1 (250 mM sucrose, 10 mM Tris-HCl, pH 8.0, 10 mM $MgCl_2$, 1 mM EGTA, and 1X protease inhibitor cocktail) on ice. After centrifugation at 300 *g* for 5 min, the supernatant containing cytoplasmic components can be collected, and the pellets were homogenized in buffer 2 (buffer 1 plus 1% Triton X-100) and centrifuged at 100 *g* to remove the nuclear membrane. The supernatant that contains chromatin-associated proteins was layered over a 1.7-M sucrose cushion and centrifuged at 50,000 *g* for 1 h in a Beckman SW32Ti rotor. The resulting pellets were further purified by resuspending in Tris buffer C (10 mM Tris HCl, 0.2 mM EDTA, 0.1% Triton X-100, and 1X protease inhibitor cocktail) and centrifugation at 1,300 *g*, and the precipitate was used for screening.

TABLE 1 | Primers used in this research.

Name	Primer
GAPDH	F: CCCCAATGTGTCCGTCGTG
	R: TGCCTGCTTCACCACCTTCT
Sugp2-Transcript1	F: AAACCCAAGGACATGGAGTTT
	R: CTATTTGGCCCGCTTGT
Sugp2-Transcript2	F: AAACCCAAGGACATGGAGTTT
	R: AGGGCTGGGGCTAGTAAGCTA
Sugp2 identification	F: CACAGCGGGTAGCAGGTAAG
	R-WT: GTGGAGCATGACAAATGGTCACATA
	R-KO: CTGCCCTTATCTATGACGCTATGG
Sugp2-antibody-F	aaatcggatggttcaactagtGAGCCTGCCAAACCCTGTCC
Sugp2-antibody-R	gtggtggtggtggtgctcgagCATGCGCTGGCGGAAGACGT

The purified chromatin-associated proteins were shipped in solidified carbon dioxide and subjected to high-performance liquid chromatography followed by HRMS at the National Facility for Protein Science in Shanghai, Zhangjiang Lab, China. The proteomics analysis from different testes samples was conducted by the PEAKS software (17).

Western Blot Analysis

Tissues were lysed in RIPA buffer (Beyotime Biotechnology) with 1X protease inhibitor cocktail (Roche) on ice. After centrifuging the lysate at 12,000 *g* for 20 min, the supernatant was added with 5× SDS loading buffer (Beyotime Biotechnology) and allowed to boil for 10 min to get the protein samples. Then, the proteins in the samples were separated by SDS-PAGE and transferred onto polyvinylidene difluoride membranes. The membranes were blocked for 1–2 h in 5% skimmed milk in TBST (TBS, 0.1% Tween-20) and incubated with primary antibodies overnight at 4°C. After three times of washing in TBST, the membranes were incubated with HRP-conjugated secondary antibodies anti-mouse or anti-rabbit for 1 h at RT. The signals were developed with SuperSignal™ West Pico PLUS Chemiluminescent Substrate (Thermo Fisher Scientific) and captured with Amersham Imager 600 (GE Healthcare Life Sciences). Information on the antibodies used are shown in **Table 2**.

Phylogenetic Analysis

The sequences of Sugp2 from different species were downloaded from the NCBI database, and these sequences were used to construct a phylogenetic tree using the Molecular Evolutionary Genetic Analysis (MEGA X) software (18).

TABLE 2 | The antibody dilution ranges used in present research.

Protein	Producer	Application	Dilution
Sug2	Our Lab	Western blot	1:100
		Immunofluorescence	1:50
Sycp3	Our Lab	Western blot	1:100
		Immunofluorescence	1:50
Sycp1	Our Lab	Western blot	1:100
		Immunofluorescence	1:50
Hspa5	Abclonal	Western blot	1:100
Vdac1	Abclonal	Western blot	1:100
Ddx4	Abcam	Immunofluorescence	1:100
Plzf	Millipore	Immunofluorescence	1:50
γ-H2ax	Abclonal	Immunofluorescence	1:100
Rad51	Our Lab	Immunofluorescence	1:50
Rpa1	Our Lab	Immunofluorescence	1:100
Mlh3	Our Lab	Immunofluorescence	1:50
Gapdh	Proteintech	Western blot	1:20,000
CoraLite-488 conjugated Affinipure Goat Anti-Mouse secondary antibody	Proteintech	Immunofluorescence	1:200
CoraLite-594 conjugated Affinipure Goat Anti-Mouse secondary antibody	Proteintech	Immunofluorescence	1:200
HRP-conjugated Affinipure Goat Anti-Mouse IgG(H+L)	Proteintech	Western blot	1:10,000
HRP-conjugated Affinipure Goat Anti-Rabbit IgG(H+L)	Proteintech	Western blot	1:10,000

Generation of Sugp2 Polyclonal Antibodies

The sequence encoding aa 723–1,056 of mouse Sugp2 was amplified by PCR and ligated into the Pet42b plasmid by homologous recombination. The reconstructed Pet42b plasmid was transformed into the BL3 strain, and the GST-fused Sugp2 expression was induced by isopropylthio-β-galactoside. After the bacterial cells were lysed by sonication, the affinity of Sugp2 antigen was purified with Ni beads and purified with dialysis. Finally, Sugp2 antibody were obtained by immunizing rabbits.

Immunofluorescence, Histological, and Surface Nuclear Spread Analyses

For immunofluorescence analysis, testes were fixed in Bouin's solution at room temperature overnight, dehydrated in 30% sucrose (in 1X phosphate-buffered saline) overnight, embedded with NEG-50 (Thermo Fisher Scientific) at −80°C, and sectioned into 8-μm cryosections. After antigen-retrieval in 0.1 M sodium citrate buffer (pH 6.0), the sections were permeated in TBS (20 mM Tris, pH 7.4, 150 mM NaCl) with 1%Triton X-100 for 30 min at room temperature. Then, the sections were blocked in TBS containing 10% goat serum (Solarbio Life Sciences) and a subsequent first antibody incubation overnight. After three times of washing in TBS, the sections were incubated with CoraLite 488- or 594-conjugated Affinipure Goat Anti-mouse or Anti-rabbit secondary antibodies (Proteintech). The samples were then washed three times with TBS, counterstained with DAPI (Solarbio Life Sciences), and covered with coverslips.

For histological analysis, the fixed testes were processed with a series of dehydration, embedded with paraffin, and sectioned at 5–8 μm. The sections were stained with hematoxylin and eosin.

The surface nuclear spread adopted the method previously reported (19). Briefly, testicular tubules were extracted in a hypotonic treatment buffer (30 mM tris, 50 mM sucrose, 17 mM trisodium citrate dihydrate, 5 mM EDTA, 0.5 mM dithiothreitol, and 1 mM phenylmethylsulfonyl fluoride). The isolated cells were re-suspended in 0.1 M sucrose and then spread on a glass slide with a thin layer of paraformaldehyde solution containing Triton X-100. Then, the slides were stained by the immunofluorescence staining method described earlier. The dilution ranges of the different antibodies used in the present study are listed in **Table 2**. Histological and fluorescence images were captured with Axio Imager 2 Microscope (Zeiss).

RNA Sequencing

The testes were isolated, and 1 μg RNA per sample was used for library preparation. Sequencing libraries were generated using NEBNext® UltraTM RNA Library Prep Kit for Illumina® (New England Biolabs) following the recommendations of the manufacturer. Briefly, mRNA was purified from total RNA using magnetic beads. Fragmentation was carried out using divalent cations under elevated temperature. First-strand cDNA was synthesized using random hexamer primer and M-MuLV Reverse Transcriptase (RNase H-). A second-strand cDNA synthesis was subsequently performed using DNA Polymerase I and RNase H. The remaining overhangs were converted into blunt ends *via* exonuclease/polymerase activities. After adenylation of the 3′ ends of DNA fragments, NEBNext Adaptor with a hairpin loop structure was ligated to prepare for hybridization. The library fragments were purified with AMPure XP system (Beckman Coulter), size selected and ligated with an adaptor using 3 μl USER Enzyme (New England Biolabs) at 37°C for 15 min followed by 5 min at 95°C before the PCR. The PCR was performed with Phusion High-Fidelity DNA polymerase, Universal PCR primers, and Index (X) Primer. Finally, the PCR products were purified with AMPure XP system. After cluster generation, the library preparations were sequenced on an Illumina Novaseq platform, and 150-bp paired-end reads were generated. All RNA sequencing data have been deposited at SRA, and the BioProject ID/accession no. is PRJNA752112.

Bioinformatic Data Analysis

Raw data (raw reads) of fastq format from WT and Sugp2 KO were firstly processed through in-house perl scripts. In this step, clean data (clean reads) were obtained by removing reads containing adapter, reads containing ploy-N, and reads with low quality from raw data. All the downstream analyses were based on the clean data with high quality. Using Hisat2 v2.0.5 (20), an index of the reference genome was built, and paired-end clean reads were aligned to the reference genome. The mapped reads of each sample were assembled by StringTie v2.1.3

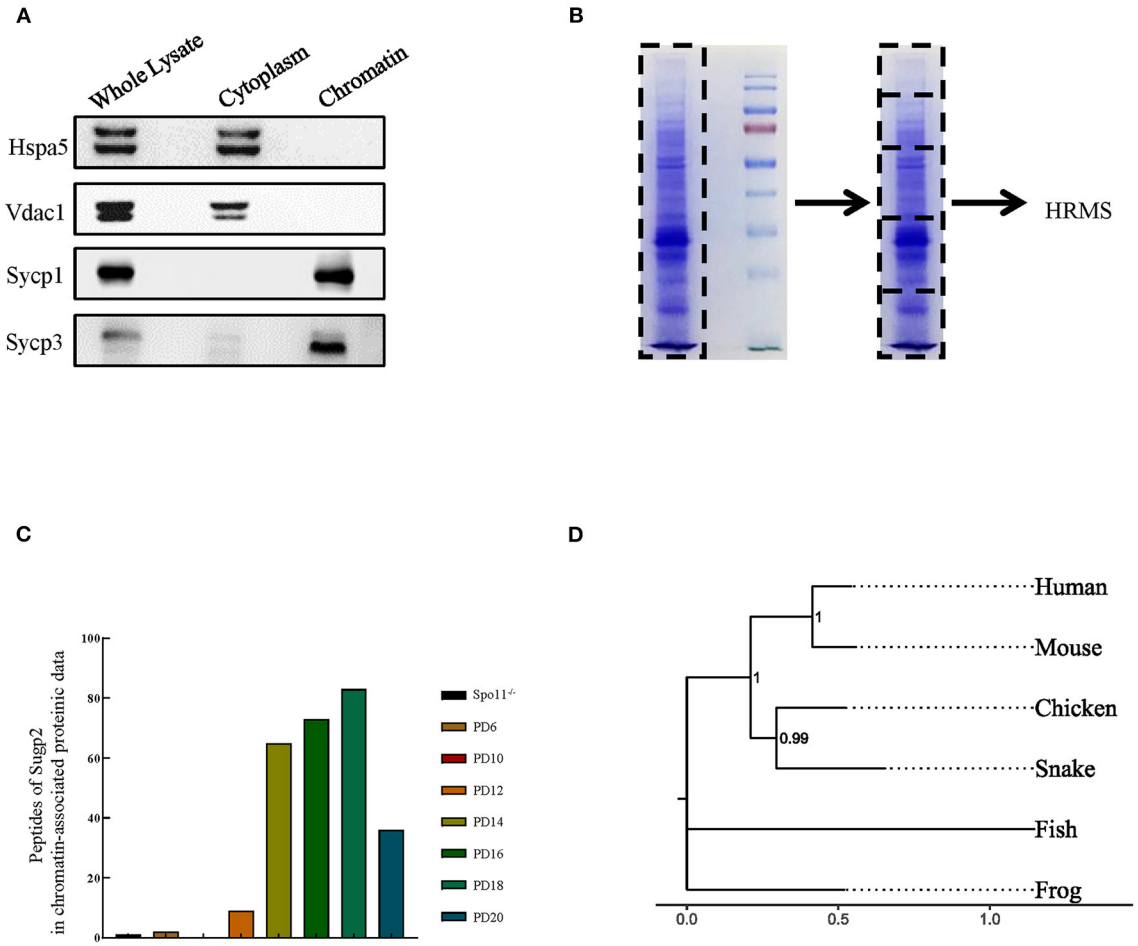

FIGURE 1 | Sugp2 was a putative spermatogenetic chromatin-associated protein by proteomic identification. **(A)** Purity assessment of isolated testis chromatin-associated proteins by western blot. Sycp1 and Sycp3 are components of meiotic synapsis complex and associated with chromatin. Hspa5 and Vdac1 are cytoplasmic protein controls. **(B)** Identification of chromatin-associated proteins by high-resolution mass spectrum. **(C)** Peptide counts of Sugp2 in testis from Spo11 knockout (Spo11$^{-/-}$) and different postnatal groups. **(D)** Phylogenetic tree for Sugp2 protein estimated by neighbor joining method. The tree was constructed by MEGA. Each name at the terminus represents the species from which the protein originated.

(21) in a reference-based approach and guided by transcriptome annotation (GRCm38, GENCODE release M25). Taking the calculated transcripts per million (TPM) as the baseline for difference expression mapping, genes with TPM <1 were excluded. The analysis of differential expression used the log2 of the calculated TPM fold change between WT and Sugp2 KO.

Statistics

Data was analyzed with one-way ANOVA followed by a Student–Newman–Keuls comparison test using SPSS 20.0 software (SPSS Inc.). Significance was set at $P < 0.05$ for all tests.

RESULTS

Sugp2 Was a Putative Spermatogenetic Chromatin-Associated Protein

Using our previously reported method for meiotic chromatin-associated protein extraction, we obtained high-purity chromatin-related proteins (**Figure 1A**). Sycp1/3, as synaptonemal complex (SC) proteins associated with meiotic chromatin, was present in the chromatin fraction, whereas Hspa5 and Vdac1 were in cytoplasmic components as marker proteins for the endoplasmic reticulum and the mitochondria, respectively. After extraction, the chromatin-associated proteins were separated by SDS–polyacrylamide gel electrophoresis (PAGE) and analyzed by high-resolution mass spectrometry (HRMS; **Figure 1B**). In the present study, we analyzed eight sets of data. Spo11$^{-/-}$ testis was used to screen for proteins involved in meiotic DNA damage repair processes since Spo11 knockout induced spermatocytes that lacked meiosis-specific DSBs and subsequent DNA damage repair processes and were arrested in the zygotene-like phase. PD6 mouse testis contains only spermatogonia but no spermatocytes, which can be used to screen meiotic spermatocyte-related proteins. While PD10, 12, 14, 16, 18, and 20 mouse testes contain spermatocytes at different developmental stages during the first wave of

spermatogenesis, they can be used to screen proteins at different meiotic stages.

By analyzing and comparing the proteomic data, we identified one putative spermatogenetic chromatin-associated protein—Sugp2, which showed high peptide abundances from PD12 to PD20 proteomic data but had a low level in Spo11$^{-/-}$ and PD10 groups (**Figure 1C**). Among different species, Sugp2 had high protein sequence conservativeness, especially between human and mice (**Figure 1D**), implying the conservation of its biological function.

Sugp2 Was Primarily Expressed in Mouse Testis

Proteomic data showed that Sugp2 was highly expressed in the process of meiosis, suggesting that it may play a role in meiosis. To obtain more information on Sugp2, we first

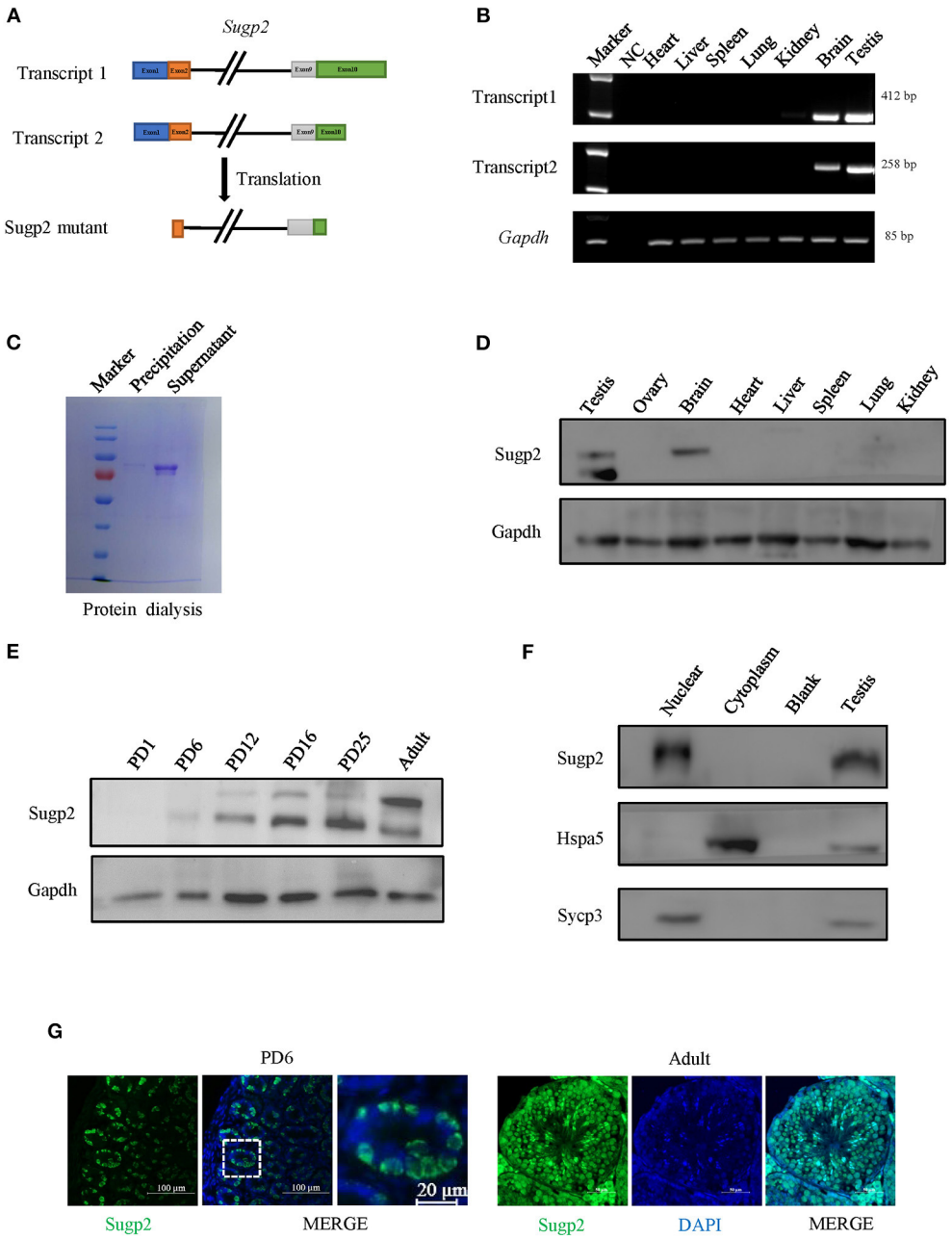

FIGURE 2 | Expression of Sugp2 during mouse spermatogenesis. **(A)** Transcription and translation information of Sugp2. **(B)** Identification of Sugp2 isoforms by RT-PCR. **(C)** Purification of Sugp2 antigen by dialysis. The expression pattern of Sugp2 in different tissues **(D)** and testes at different stages **(E)**. The expression of Sugp2 in mouse testis was confirmed by western blot **(F)** and immunofluorescence **(G)**.

verified the expression of Sugp2 in various tissues at expression and translation levels. There are two different transcripts of *Sugp2* gene according to National Center of Biotechnology (NCBI), which vary at the 5′ end but encode the same protein (**Figure 2A**). Through RT-PCR detection, both transcripts of Sugp2 existed and were primarily transcribed in adult testis and brain (**Figure 2B**). Due to the lack of effective commercial antibodies to mouse Sugp2, we made a rabbit polyclonal antibody with good effect against it by immunization with purified Sugp2-truncated protein (**Figure 2C**). Western blot analysis revealed that Sugp2 was exclusively expressed in testis and brain, and its expression increased along with the progression of the first wave of spermatogenesis (**Figures 2D,E**). What is more, the nuclear and cytoplasmic separation assay results further confirmed that Sugp2 co-localized with chromatin of the testis (**Figure 2F**). At postnatal day 6 (PD6), Sugp2 was enriched in certain cells located in the basement membrane of the seminiferous tubules, while in adult testis Sugp2 was also expressed in the spermatogenic cells located in the middle of the seminiferous tubules (**Figure 2G**).

Sugp2 Was Enriched in the Nucleus of Male Germ Cells

To further clarify the localization of Sugp2 in mouse testes during spermatogenesis, we performed double-staining with Ddx4, Plzf, and Sycp3, which indicates total germ cell, spermatogonia, and spermatocytes, respectively. By co-staining with Ddx4, we

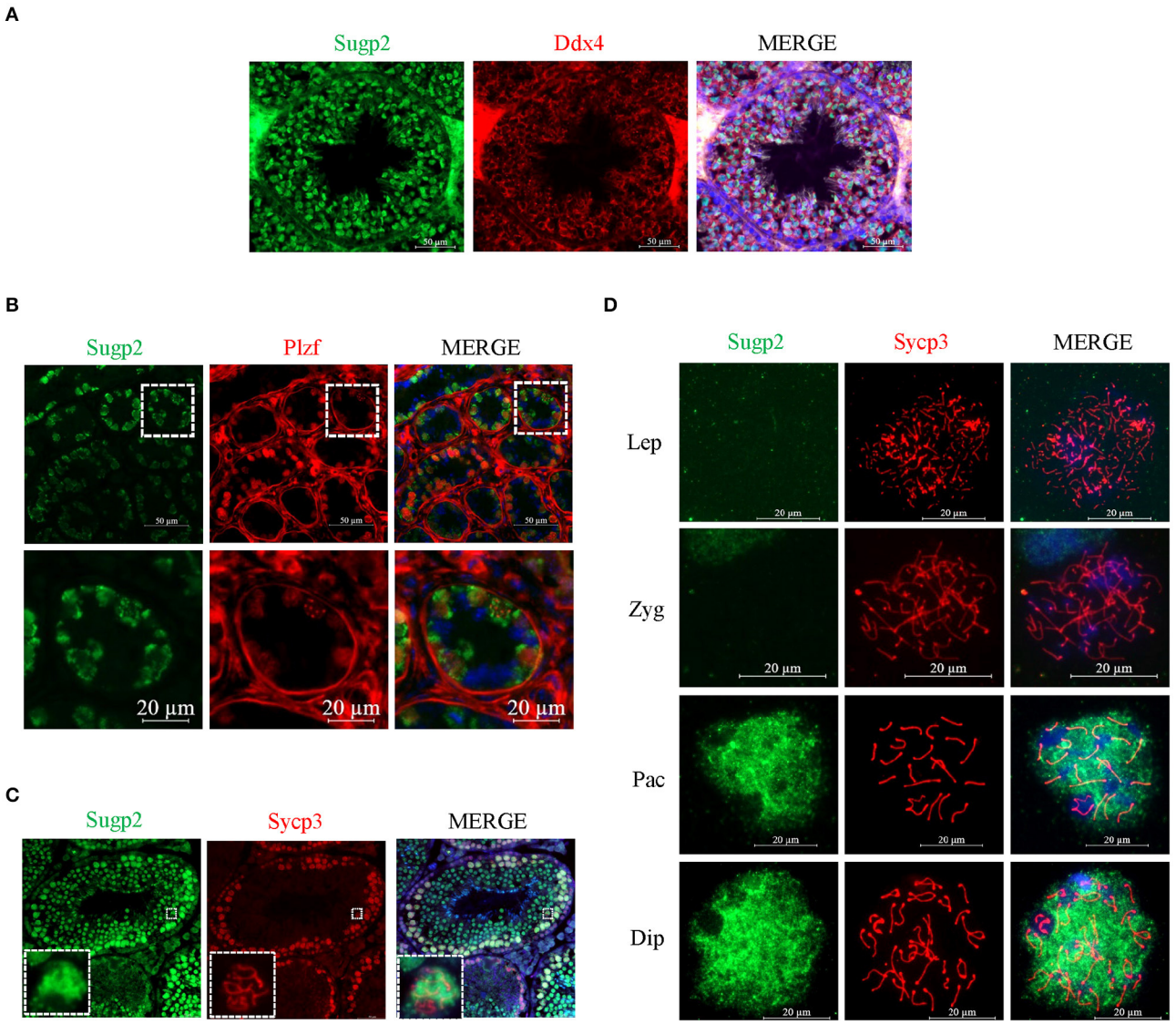

FIGURE 3 | Localization of Sugp2 in mouse testis. Frozen sections of adult **(A,C)** and PD6 **(B)** testes were co-stained with rabbit anti-Sugp2 and mouse anti-Ddx4 **(A)**, Plzf **(B)**, or Sycp3 **(C)** antibodies. Ddx4, Plzf, and Sycp3 were used as germ cells, spermatogonia, and spermatocyte markers, respectively. The DNA was stained with DAPI. Scale bar = 20 μm. **(D)** Distribution pattern of Sugp2 on the chromatin of spermatocytes from leptotene through diplotene stages.

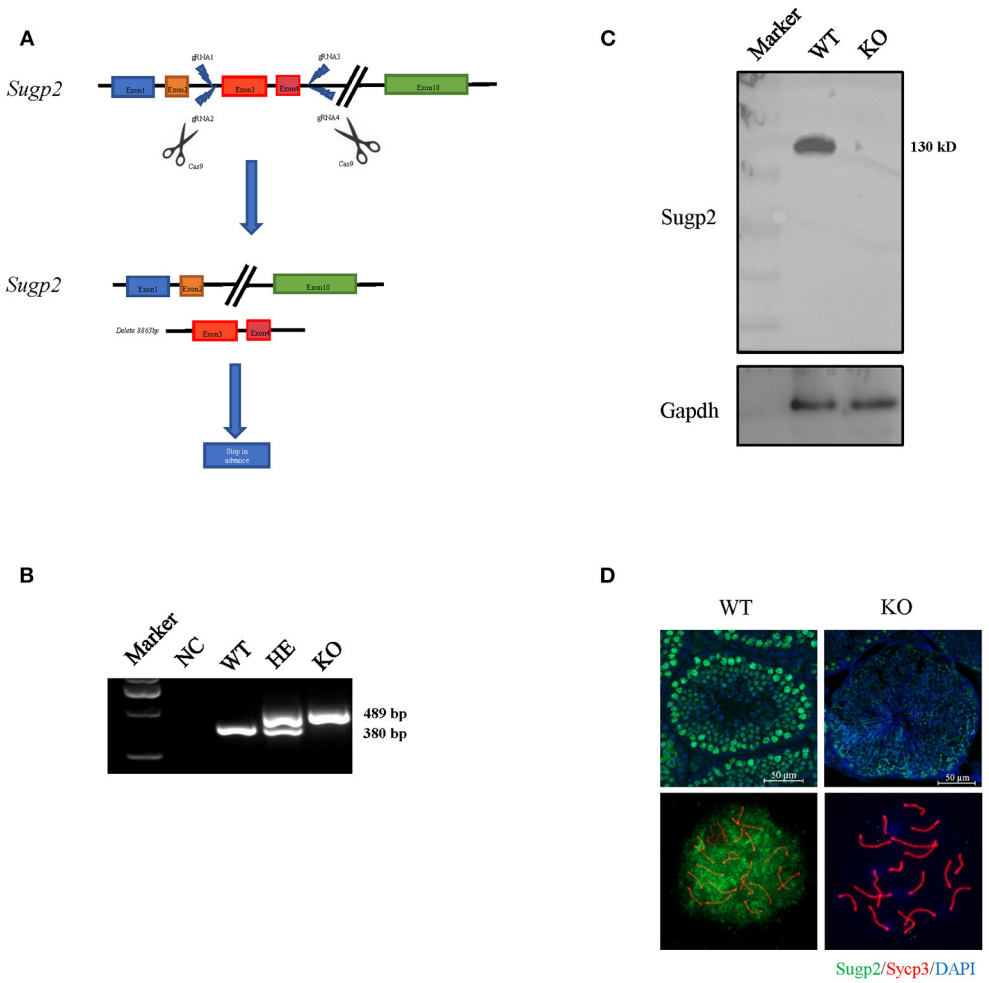

FIGURE 4 | Generation of Sugp2 knockout mouse. **(A)** Knockout strategy of Sugp2. Exons 3 and 4 were deleted by the CRISPR/Cas9 genome editing system. **(B)** Mouse genotype identification by mouse tail PCR. WT, wild type; HE, heterozygote; KO, knockout. Western blot **(C)** and immunofluorescence staining **(D)** of Sugp2 in adult WT and Sugp2 KO testes. *n*, number of samples per group.

could see the colocalization of Sugp2 and Ddx4, indicating that Sugp2 was mainly expressed in male germ cells and located in the nucleus (**Figure 3A**). Furthermore, the co-localization of Sugp2 with Plzf and Sycp3 indicated that Sugp2 was highly expressed in germ cells at different levels of maturity, including spermatogonia, spermatocytes, and haploid sperm cells. Interestingly, when co-stained with Sycp3, the Sugp2 signal was not uniform, with some blanks in certain areas (**Figures 3B,C**). In addition, immunostaining of spread spermatocyte nuclei showed diffuse Sugp2 immunofluorescent signal from the pachytene to diplotene stages, while the signal was mainly located in the autosome area but was excluded from the region of XY body (**Figure 3D**).

The Deficiency of Sugp2 Has a Little Effect on Male Fertility and Spermiogenesis

The previous expression and localization results indicated that Sugp2 may be involved in mouse spermatogenesis. To study the biological function of Sugp2, we generated Sugp2-deficient mouse ($Sugp2^{-/-}$) with the CRISPR/Cas9 genome editing system, which deleted an 8.863-kb genomic DNA fragment containing exon 3 and exon 4. The deletion induced the premature termination of translation with production of incomplete protein (**Figure 4A**). The genotyping of Sugp2 could be performed by mouse tail PCR (**Figure 4B**). Western blotting and immunofluorescence analysis confirmed the absence of the Sugp2 protein in $Sugp2^{-/-}$ testes, indicating the successful knockout of Sugp2 (**Figures 4C,D**).

Spermatogenetic problems typically resulted in sterility or reduced fertility, reduced testis weight, and/or seminiferous tubule abnormalities. The disruption of Sugp2 had a little impact on testis size (**Figure 5A**). Meanwhile, the testis weight and testis/body weight ratio of adult $Sugp2^{-/-}$ males were indistinguishable from their wild-type (WT) littermates (**Figures 5B,C**). A histological analysis showed that spermatogenesis in $Sugp2^{-/-}$ males was not grossly impaired

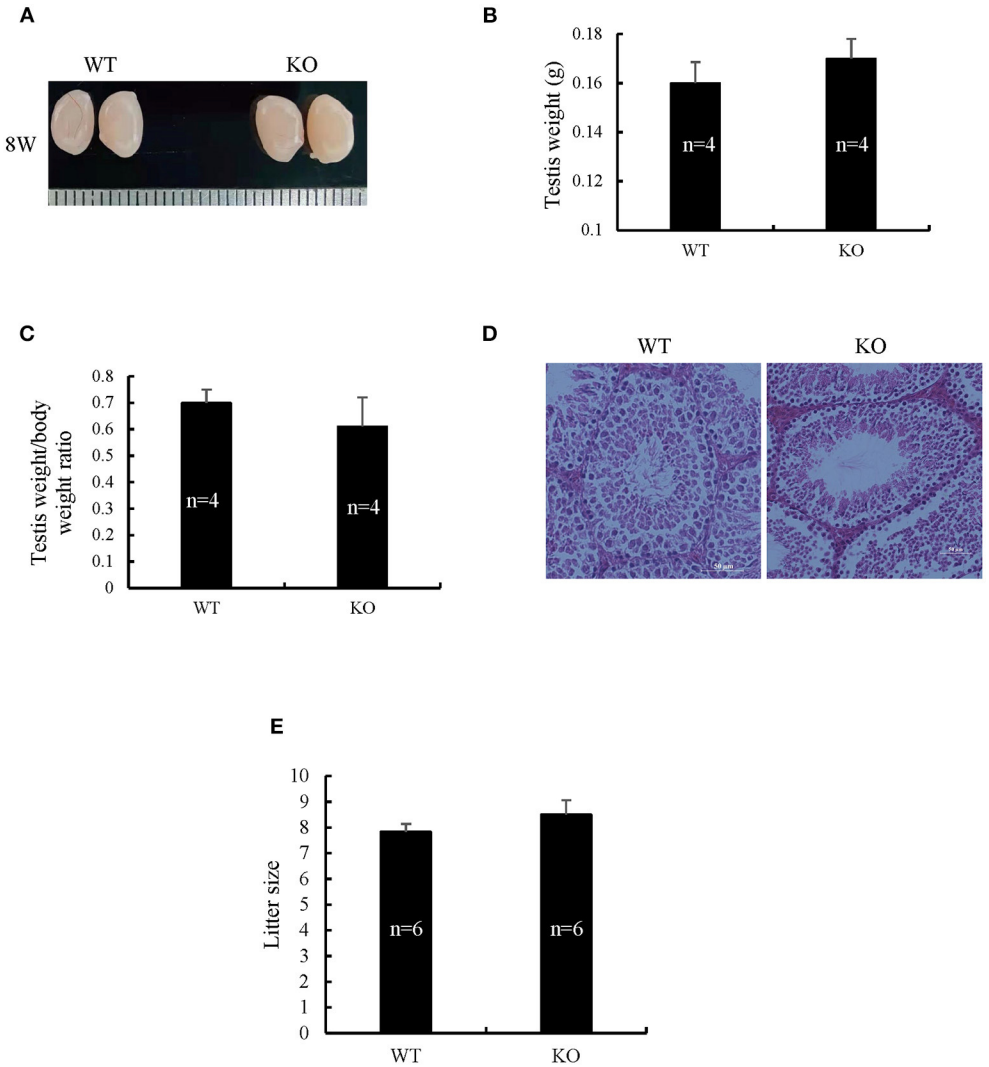

FIGURE 5 | Morphological analysis of Sugp2 knockout mouse. **(A)** Size of adult testes from wild-type (WT) and Sugp2 KO mice. Testis weight **(B)** and the ratio of testis to body **(C)** from WT and Sugp2 KO mice. Error bars represent standard error. **(D)** Hematoxylin and eosin (H&E) staining of adult testes in WT and Sugp2 KO mice. Scale bar = 50 μm. **(E)** Comparison of litter size from wild-type and Sugp2 knockout mice.

compared to WT males (**Figure 5D**). To address whether Sugp2 affected male fertility, Sugp2 knockout males were placed in cages with WT females for mating, and the litter size was recorded. The sugp2 knockout mice are fertile, and there was no significant difference in the liter size (**Figure 5E**).

Sugp2$^{-/-}$ Males Do Not Show Gross Defects in Meiotic Prophase Progression

To uncover more subtle meiotic changes in Sugp2-deficient spermatocytes, we immune-stained meiotic chromosome spreads. In meiotic prophase, germ cells can be classified into four different cytological stages—leptonema, zygonema, pachynema, and diplonema—based on the kinetic changes of the SC which consisted of central protein (Sycp1) with axial/lateral element (Sycp3). In Sugp2$^{-/-}$ spermatocytes, chromosome synapsis can process normally and SC can form and disassemble normally with no obvious defects (**Figure 6A**).

Next, we used typical markers to evaluate the formation and repair of meiotic DSBs. In WT males, γH2ax appears during leptonema and then disappears from the autosomes as DSBs are repaired, leaving its signal exclusively in the XY body during pachynema and diplonema. The appearance and disappearance of the γH2ax signal was normal in Sugp2$^{-/-}$ males, suggesting that DSB formation and repair were completed normally in the absence of Sugp2 (**Figure 6B**). We also stained the Rpa1 and Rad51 involved in meiotic recombination, whose foci are maximal at early- to mid-zygonema and then decrease as DSBs are repaired *via* homologous recombination. Rpa1 and Rad51 in Sugp2$^{-/-}$ spermatocytes displayed an overall similar progression with that of WT spermatocytes (**Figures 7A,B**). At

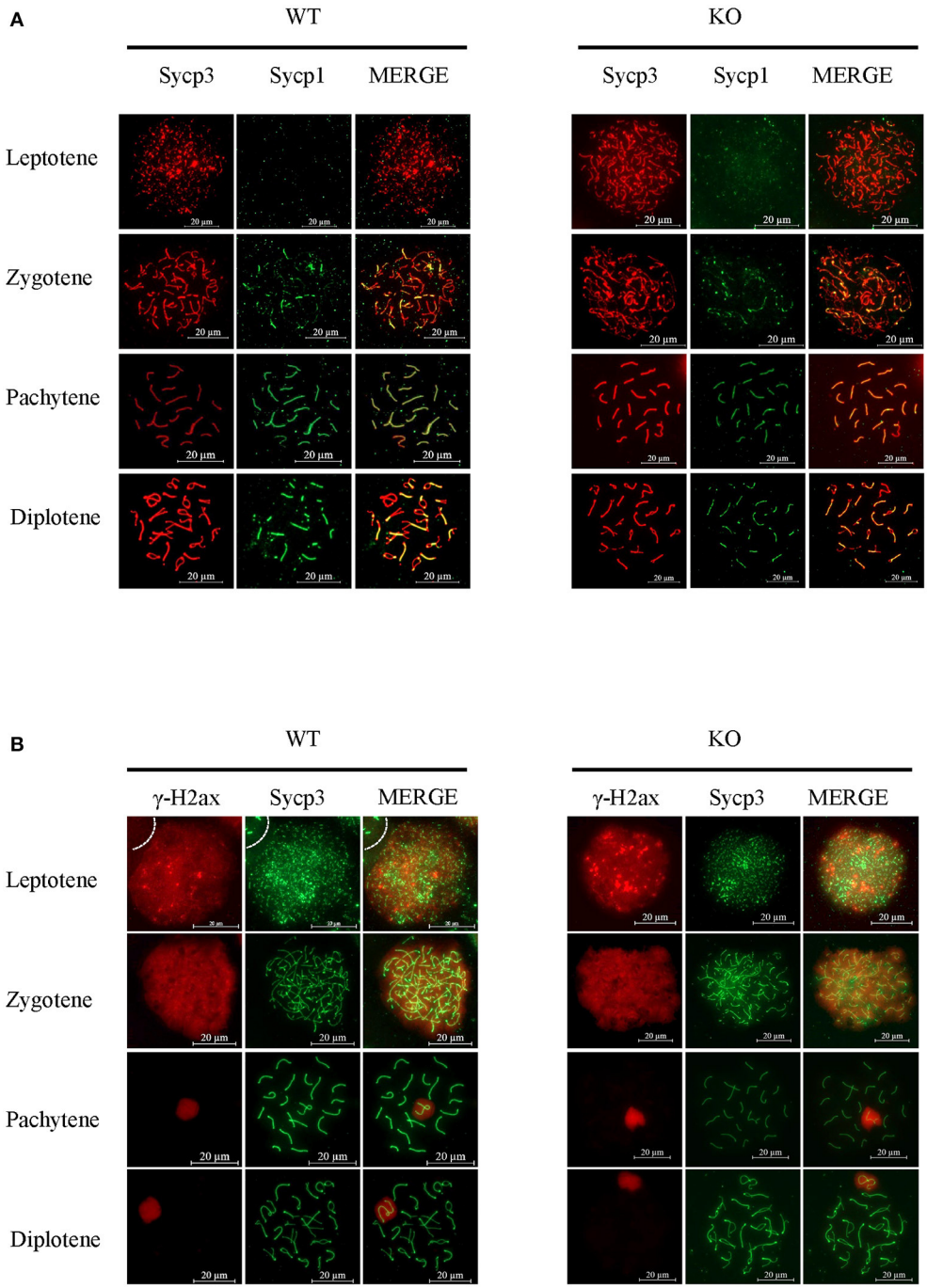

FIGURE 6 | Function of Sugp2 in chromosome synapsis and double-strand break repair in spermatocytes. **(A)** Chromosome spread from wild-type control and Sugp2 knockout testes was labeled for synaptonemal complex proteins (Sycp1 and Sycp3). **(B)** Distribution of γH2ax in wild-type and Sugp2 KO spermatocytes. Scale bar = 20 μm.

the mid-late pachytene stage, the Mlh3 foci become apparent in spermatocytes, marking sites of crossover. Compared to their WT controls, the Sugp2$^{-/-}$ males showed little difference in Mlh3 foci (**Figure 7C**). These results demonstrated that Sugp2 was dispensable for the initiation and completion of meiotic prophase progression.

Sugp2 Regulates Pre-mRNA Splicing During Spermatogenesis

Considering that Sugp2 is a potential member of the SR-related family of pre-mRNA processing factors, we isolated mRNA from adult WT control and Sugp2$^{-/-}$ testes and then performed whole-transcriptome RNA sequencing. A total of

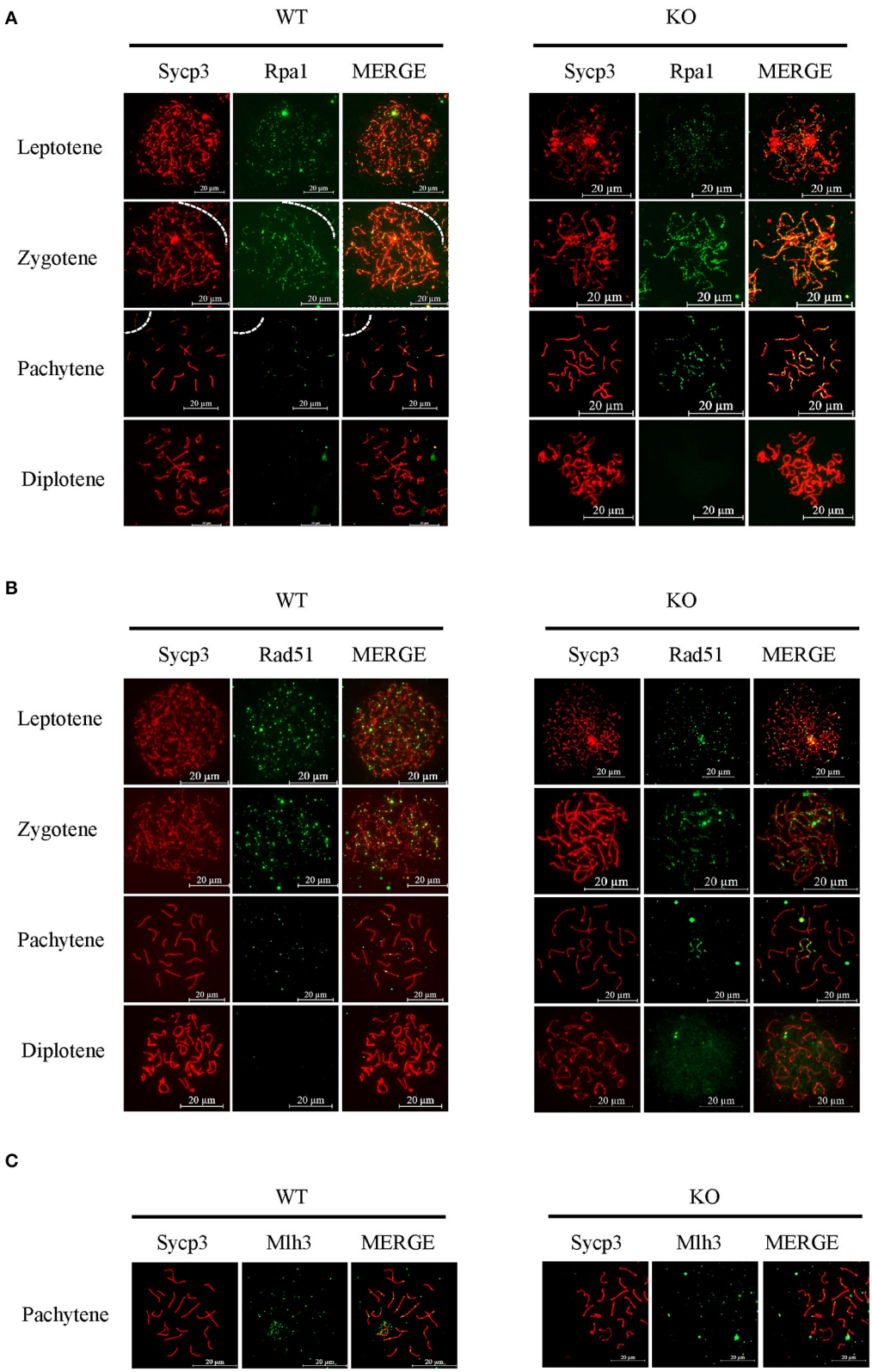

FIGURE 7 | Sugp2 is not essential for meiotic recombination. Immunolabeling for the synaptonemal complex component Sycp3 and recombination protein Rpa1 **(A)** and Rad51 **(B)**. **(C)** The crossover formation was analyzed by staining Mlh3. Scale bar = 20 μm.

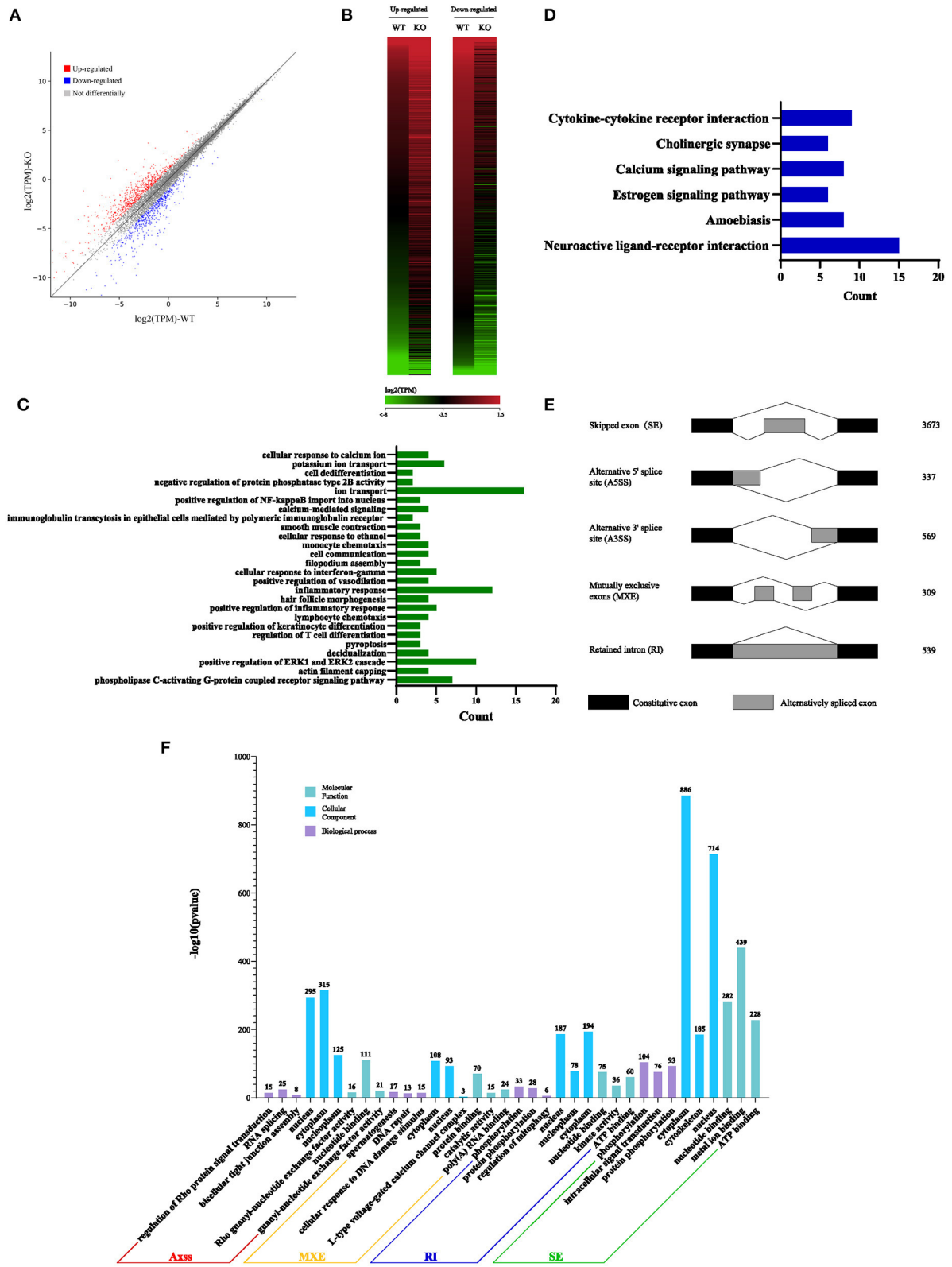

FIGURE 8 | Sugp2 is involved in RNA splicing during spermatogenesis. Volcano plot **(A)** and heat map **(B)** of differentially expressed transcripts in Sugp2 KO testis compared with WT control. Green dots represent significantly downregulated transcripts, red dots represent significantly upregulated transcripts (|log2FC| >1), and gray dots represent unchanged transcripts. Gene Ontology (GO) **(C)** and Kyoto Encyclopedia of Genes and Genomes **(D)** functional analysis of differentially expressed genes. **(E)** Five significantly affected RNA splicing events in Sugp2 KO spermatogenic cells from adult mice. **(F)** The three most significantly ($P < 0.05$) enriched GO terms in biological process, molecular function, and cellular component branches from each AS group are presented.

66,763,192 clean reads were used for downstream bioinformatics analysis for the control and Sugp2$^{-/-}$ testes, respectively. With a common parameter ($|\log_2 FC| > 1$), the total transcripts showed about 1,331 differential expressions in Sugp2-deficient testis, in which 729 genes were upregulated and 602 genes downregulated (**Figures 8A,B**). Then, we performed Gene Ontology (GO) and Kyoto Encyclopedia of Genes and Genomes (KEGG) analysis to further analyze the effect of Sugp2 knockout on cell function. The functional analysis results indicated that Sugp2 may participate in ion metabolism and neuroactive signal pathway, but all functions were only with a few changed genes (**Figures 8C,D**). Since the SURP and G-patch domain contained in Sugp2 are mainly involved in transcript alternative splicing, we analyzed the influence of Sugp2 deletion on AS. Five different AS types were compared between WT control and Sugp2$^{-/-}$ testes. Compared with control, 5,427 AS events were significantly affected (P-value < 0.01) in Sugp2$^{-/-}$ testes. Among those affected AS events, the majority (3,673/5,427) of the changed splicing events were skipped exon (SE), which indicated that Sugp2 was involved in mRNA splicing during mouse spermatogenesis (**Figure 8E**). Then, we performed GO analysis about the affected AS from five different groups to further uncover the function of alternative splicing genes. The top three most significantly ($P < 0.05$) enriched GO terms were displayed. In the SE group, Sugp2 mainly regulated the expression of genes on metal ion, ATP, and nucleotide binding, implying its function on metal ion, and energy metabolism (**Figure 8F**). All these data indicated that Sugp2 participated in mRNA alternative splicing and may be involved in cell ion and energy metabolism during mouse spermatogenesis.

DISCUSSION

Mammalian spermatogenesis is a complex process involving a variety of cell types and developmental stages in a highly collaborative order accompanied with complicated structural changes in chromatin involved in complex regulation mechanisms (13, 22). Therefore, in the present study, we developed a multiple control group proteomics strategy to systematically identify different spermatogenetic chromatin-associated proteins in different cell or meiotic stages. Sugp2, in the data, drew our attention since its expression arose along with meiotic progression, but with a few signals in Spo11$^{-/-}$ testis in which there were neither meiotic recombination events nor post-zygotene spermatocytes.

Sugp2, also known as SFRS14, contains SURP1/2 domains which are mostly presented in alternative splicing regulators as well as one G-patch domain, a region of six highly conserved glycine residues commonly found in RNA-processing proteins (23, 24). Highly differentiated tissues, such as testis and brain, have more post-transcription regulation than any other tissues (25). All of these prompted us to perform a functional study of Sugp2 in spermatogenesis.

Our results firstly evidenced that Sugp2 had two transcripts encoding some proteins in the testis, and it had been demonstrated that its transcription isoforms could be regulated during spermatogenesis (26). This also indicated that there was a complicated regulation mechanism on Sugp2 expression. Sugp2 protein was primarily expressed in mouse testis and enriched in the nucleus of male germ cells. Interestingly, Sugp2 was diffused in the autosome area but was excluded from the region of the XY body from the pachynema to diplonema. This localization pattern was similar with RNA poly II which would also be absent from the XY body because of meiotic sex chromosome inactivation, resulting in the inactivation of the asynapsed XY chromosome regions (27, 28). The chromatin localization of Sugp2 may also support its regulation in gene expression during spermatogenesis.

The knockout of sugp2 triggered some changes in the expression level of some transcripts compared with the WT control. After GO and KEGG analysis, we found that each of the most affected group only had few changed genes, which could not provide more information about Sugp2-regulated molecular functions. Then, we conducted AS analysis since the domains SURP1/2 and G-patch always participated in the AS process. Alternative splicing, by which pre-mRNA molecules can be spliced in different ways to generate multiple mRNA isoforms from a single gene, is the main mechanism of transcriptome and proteome expansion that can explain the phenotypic complexity of organisms and tissues (29–31). In the five main AS events, Sugp2 mainly regulated the skip of exons which would probably generate abnormal exon-skipped transcripts with a premature termination codon. The abnormal alternative splicing in SE was closely associated with male infertility (32, 33). The GO analysis based on AS data indicated that Sugp2 may participate in metal ion and energy metabolism. Combined with the results of KEGG, Sugp2 may be involved in calcium transport and signal transduction, which play an essential role in male germ cell development and function (34, 35).

Unexpectedly, Sugp2-deficient males were fully fertile and exhibited no gross spermatogenetic abnormalities. The deficiency of Sugp2 had no obvious effect on meiotic synapsis, DSB repair and meiotic recombination, and male fertility. Sugp2 knockout significantly altered the expression profiles compared with WT controls. Changes in the transcription level or the alternative splicing variants of these altered genes could not probably cause gross harm to mouse spermatogenesis. What is more, through analysis of the proteomics screen data, we found that Sugp1, which shares a high homology with Sugp2 and also has SURP1/2 and G patch domains, also showed a high signal during spermatogenesis, indicating that it may also have functions in the testis (36). Whether Sugp2 is a redundant gene for Sugp1 can be further verified by double-knockout experiments.

In summary, our results showed that Sugp2 was a chromatin-associated protein and enriched in the nucleus of male germ cells. Although Sugp2 was dispensable for male fertility, it indeed regulated many AS events during spermatogenesis.

DATA AVAILABILITY STATEMENT

The datasets presented in this study can be found in online repositories. The names of the repository/repositories and

accession number(s) can be found below: https://www.ncbi.nlm.nih.gov/, PRJNA752112.

ETHICS STATEMENT

The animal study was reviewed and approved by the animal ethical guidelines of the Institutional Care and Wuhan University.

AUTHOR CONTRIBUTIONS

CL, JZ, JL, and YW designed and conceived the research and performed most of the experiments. JZ, JL, and CL purified all chromatin-associated proteins and identified Sugp2. JL, PW, and CL made the antibodies. YW managed and bred the animals used in the research and analyzed the phenotype. ZY performed the bioinformatics analysis. PC, MZ, YX, TJ, and ZD analyzed the data and phenotypes. CL and JZ wrote the manuscript. ML participated in the manuscript discussion. All the authors participated in the manuscript preparation and approved the final manuscript.

FUNDING

This research was supported by National Key Research and Development Program of 363 China (Grant No. 2018YFC1003400), National Natural Science Foundation of China (Grant No. 31771588), Strategic Collaborative Research Program of the Ferring Institute of Reproductive Medicine (Grant No. FIRMC200509), and Chinese Academy of Sciences (Grant No. FIRMC200509 to ML).

ACKNOWLEDGMENTS

We thank Dr. Chao Peng and Yue Yin (Mass Spectrometry System at the National Facility for Protein Science in Shanghai, Zhangjiang Lab, SARI, China) for proteomics data collection and analysis.

REFERENCES

1. Rossi P, Dolci S. Paracrine mechanisms involved in the control of early stages of Mammalian spermatogenesis. *Front Endocrinol (Lausanne).* (2013) 4:181. doi: 10.3389/fendo.2013.00181
2. Walker WH. Regulation of mammalian spermatogenesis by miRNAs. Semin *Cell Dev Biol.* (2021) 2021:S1084-9521(21)00118-X. doi: 10.1016/j.semcdb.2021.05.009
3. Gui Y, Yuan S. Epigenetic regulations in mammalian spermatogenesis: RNA-m(6)A modification and beyond. *Cell Mol Life Sci.* (2021) 78:4893–905. doi: 10.1007/s00018-021-03823-9
4. Iwamori N, Tominaga K, Sato T, Riehle K, Iwamori T, Ohkawa Y, et al. MRG15 is required for pre-mRNA splicing and spermatogenesis. *Proc Natl Acad Sci USA.* (2016) 113:E5408–15. doi: 10.1073/pnas.1611995113
5. Handel MA, Schimenti JC. Genetics of mammalian meiosis: regulation, dynamics and impact on fertility. *Nat Rev Genet.* (2010) 11:124–36. doi: 10.1038/nrg2723
6. Keeney S, Giroux CN, Kleckner N. Meiosis-specific DNA double-strand breaks are catalyzed by Spo11, a member of a widely conserved protein family. *Cell.* (1997) 88:375–84. doi: 10.1016/s0092-8674(00)81876-0
7. Robert T, Nore A, Brun C, Maffre C, Crimi B, Bourbon HM, et al. The TopoVIB-Like protein family is required for meiotic DNA double-strand break formation. *Science.* (2016) 351:943–9. doi: 10.1126/science.aad5309
8. Mah LJ, El-Osta A, Karagiannis TC. gammah2ax: a sensitive molecular marker of DNA damage and repair. *Leukemia.* (2010) 24:679–86. doi: 10.1038/leu.2010.6
9. Hunter N, Borner GV, Lichten M, Kleckner N. Gamma-H2ax illuminates meiosis. *Nat Genet.* (2001) 27:236–8. doi: 10.1038/85781
10. Baudat F, Imai Y, de Massy B. Meiotic recombination in mammals: localization and regulation. *Nat Rev Genet.* (2013) 14:794–806. doi: 10.1038/nrg3573
11. Yoshida K, Kondoh G, Matsuda Y, Habu T, Nishimune Y, Morita T. The mouse RecA-like gene Dmc1 is required for homologous chromosome synapsis during meiosis. *Mol Cell.* (1998) 1:707–18. doi: 10.1016/S1097-2765(00)80070-2
12. Cloud V, Chan YL, Grubb J, Budke B, Bishop DK. Rad51 Is an accessory factor for Dmc1-mediated joint molecule formation during meiosis. *Science.* (2012) 337:1222–5. doi: 10.1126/science.1219379
13. Sassone-Corsi P. Unique chromatin remodeling and transcriptional regulation in spermatogenesis. *Science.* (2002) 296:2176–8. doi: 10.1126/science.1070963
14. Zhan J, Cui P, Yu Z, Qu W, Luo M. SDX on the X chromosome is required for male sex determination. *Cell Res.* (2021). doi: 10.1038/s41422-021-00539-0. [Epub ahead of print].
15. Luo M, Yang F, Leu NA, Landaiche J, Handel MA, Benavente R, et al. MEIOB exhibits single-stranded DNA-binding and exonuclease activities and is essential for meiotic recombination. *Nat Commun.* (2013) 4:2788. doi: 10.1038/ncomms3788
16. Luo M, Zhou J, Leu NA, Abreu CM, Wang J, Anguera MC, et al. Polycomb protein SCML2 associates with USP7 and counteracts histone H2A ubiquitination in the XY chromatin during male meiosis. *PLoS Genet.* (2015) 11:e1004954. doi: 10.1371/journal.pgen.1004954
17. Ma B, Zhang K, Hendrie C, Liang C, Li M, Doherty-Kirby A, et al. PEAKS: powerful software for peptide *de novo* sequencing by tandem mass spectrometry. *Rapid Commun Mass Spectrom.* (2003) 17:2337–42. doi: 10.1002/rcm.1196
18. Kumar S, Stecher G, Li M, Knyaz C, Tamura K. MEGA X: molecular evolutionary genetics analysis across computing platforms. *Mol Biol Evol.* (2018) 35:1547–9. doi: 10.1093/molbev/msy096
19. Peters AH, Plug AW, van Vugt MJ, de Boer P. A drying-down technique for the spreading of mammalian meiocytes from the male and female germline. *Chromosome Res.* (1997) 5:66–8. doi: 10.1023/a:1018445520117
20. Kim D, Paggi JM, Park C, Bennett C, Salzberg SL. Graph-based genome alignment and genotyping with HISAT2 and HISAT-genotype. *Nat Biotechnol.* (2019) 37:907–15. doi: 10.1038/s41587-019-0201-4
21. Kovaka S, Zimin AV, Pertea GM, Razaghi R, Salzberg SL, Pertea M. Transcriptome assembly from long-read RNA-seq alignments with StringTie2. *Genome Biol.* (2019) 20:278. doi: 10.1186/s13059-019-1910-1
22. La HM, Hobbs RM. Mechanisms regulating mammalian spermatogenesis and fertility recovery following germ cell depletion. *Cell Mol Life Sci.* (2019) 76:4071–102. doi: 10.1007/s00018-019-03201-6
23. Sampson ND, Hewitt JE. SF4 and SFRS14, two related putative splicing factors on human chromosome 19p13.11. *Gene.* (2003) 305:91–100. doi: 10.1016/s0378-1119(02)01230-1
24. Kuwasako K, He F, Inoue M, Tanaka A, Sugano S, Guntert P, et al. Solution structures of the SURP domains and the subunit-assembly mechanism within the splicing factor SF3a complex in 17S U2 snRNP. *Structure*. (2006). 14:1677–89. doi: 10.1016/j.str.2006.09.009
25. Mele M, Ferreira PG, Reverter F, DeLuca DS, Monlong J, Sammeth M, et al. Human genomics. The human transcriptome across tissues and individuals. *Science.* (2015) 348:660–5. doi: 10.1126/science.aaa0355

26. Hannigan MM, Zagore LL, Licatalosi DD. Ptbp2 controls an alternative splicing network required for cell communication during spermatogenesis. *Cell Rep*. (2017) 19:2598–612. doi: 10.1016/j.celrep.2017.05.089
27. Yan W, McCarrey JR. Sex chromosome inactivation in the male. *Epigenetics*. (2009) 4:452–6. doi: 10.4161/epi.4.7.9923
28. Hirota T, Blakeley P, Sangrithi MN, Mahadevaiah SK, Encheva V, Snijders AP, et al. SETDB1 links the meiotic DNA damage response to sex chromosome silencing in mice. *Dev Cell*. (2018) 47:645. doi: 10.1016/j.devcel.2018.10.004
29. Keren H, Lev-Maor G, Ast G. Alternative splicing and evolution: diversification, exon definition and function. *Nat Rev Genet*. (2010) 11:345–55. doi: 10.1038/nrg2776
30. Nilsen TW, Graveley BR. Expansion of the eukaryotic proteome by alternative splicing. *Nature*. (2010) 463:457–63. doi: 10.1038/nature08909
31. Bohnsack KE, Ficner R, Bohnsack MT, Jonas S. Regulation of DEAH-box RNA helicases by G-patch proteins. *Biol Chem*. (2021) 402:561–79. doi: 10.1515/hsz-2020-0338
32. Hellwinkel OJ, Holterhus PM, Struve D, Marschke C, Homburg N, Hiort O. A unique exonic splicing mutation in the human androgen receptor gene indicates a physiologic relevance of regular androgen receptor transcript variants. *J Clin Endocrinol Metab*. (2001) 86:2569–75. doi: 10.1210/jcem.86.6.7543
33. Song H, Wang L, Chen D, Li F. The function of Pre-mRNA alternative splicing in mammal spermatogenesis. *Int J Biol Sci*. (2020) 16:38–48. doi: 10.7150/ijbs.34422
34. Zhang X, Huang R, Zhou Y, Zhou W, Zeng X. IP3R channels in male reproduction. *Int J Mol Sci*. (2020) 21:9179. doi: 10.3390/ijms21239179
35. Zanatta AP, Goncalves R, Ourique da Silva F, Pedrosa RC, Zanatta L, Bouraima-Lelong H, et al. Estradiol and 1alpha,25(OH)2 vitamin D3 share plasma membrane downstream signal transduction through calcium influx and genomic activation in immature rat testis. *Theriogenology*. (2021) 172:36–46. doi: 10.1016/j.theriogenology.2021.05.030
36. Zhang J, Ali AM, Lieu YK, Liu Z, Gao J, Rabadan R, et al. Disease-causing mutations in SF3B1 alter splicing by disrupting interaction with SUGP1. *Mol Cell*. (2019) 76:82.e7–95.e7. doi: 10.1016/j.molcel.2019.07.017

Conflict of Interest: The authors declare that the research was conducted in the absence of any commercial or financial relationships that could be construed as a potential conflict of interest.

Publisher's Note: All claims expressed in this article are solely those of the authors and do not necessarily represent those of their affiliated organizations, or those of the publisher, the editors and the reviewers. Any product that may be evaluated in this article, or claim that may be made by its manufacturer, is not guaranteed or endorsed by the publisher.

frontiers in Veterinary Science

ORIGINAL RESEARCH
published: 07 February 2022
doi: 10.3389/fvets.2021.792869

Proteomic Exploration of Porcine Oocytes During Meiotic Maturation *in vitro* Using an Accurate TMT-Based Quantitative Approach

Baoyu Jia[1†], *Decai Xiang*[2†], *Qingyong Shao*[2], *Qionghua Hong*[2], *Guobo Quan*[2*] and *Guoquan Wu*[2*]

[1] Key Laboratory of Animal Gene Editing and Animal Cloning in Yunnan Province, College of Veterinary Medicine, Yunnan Agricultural University, Kunming, China, [2] Yunnan Provincial Genebank of Livestock and Poultry Genetic Resources, Yunnan Provincial Engineering Laboratory of Animal Genetic Resource Conservation and Germplasm Enhancement, Yunnan Animal Science and Veterinary Institute, Kunming, China

OPEN ACCESS

Edited by:
Yi Fang,
Chinese Academy of Science, China

Reviewed by:
Jasmin Walter,
University of Zurich, Switzerland
Wei Shen,
Qingdao Agricultural University, China

***Correspondence:**
Guobo Quan
waltq20020109@163.com
Guoquan Wu
wuguoquan1982@163.com

[†]These authors have contributed equally to this work

Specialty section:
This article was submitted to Animal Reproduction - Theriogenology, a section of the journal Frontiers in Veterinary Science

Received: 11 October 2021
Accepted: 20 December 2021
Published: 07 February 2022

Citation:
Jia B, Xiang D, Shao Q, Hong Q, Quan G and Wu G (2022) Proteomic Exploration of Porcine Oocytes During Meiotic Maturation in vitro Using an Accurate TMT-Based Quantitative Approach. Front. Vet. Sci. 8:792869. doi: 10.3389/fvets.2021.792869

The dynamic changes in protein expression are well known to be required for oocyte meiotic maturation. Although proteomic analysis has been performed in porcine oocytes during *in vitro* maturation, there is still no full data because of the technical limitations at that time. Here, a novel tandem mass tag (TMT)-based quantitative approach was used to compare the proteomic profiles of porcine immature and *in vitro* mature oocytes. The results of our study showed that there were 763 proteins considered with significant difference—450 over-expressed and 313 under-expressed proteins. The GO and KEGG analyses revealed multiple regulatory mechanisms of oocyte nuclear and cytoplasmic maturation such as spindle and chromosome configurations, cytoskeletal reconstruction, epigenetic modifications, energy metabolism, signal transduction and others. In addition, 12 proteins identified with high-confidence peptide and related to oocyte maturation were quantified by a parallel reaction monitoring technique to validate the reliability of TMT results. In conclusion, we provided a detailed proteomics dataset to enrich the understanding of molecular characteristics underlying porcine oocyte maturation *in vitro*.

Keywords: porcine oocytes, *in vitro* maturation, proteome, TMT, PRM

INTRODUCTION

The domestic pig, as an important livestock species, has been thought to be an ideal large animal model for health and disease research due to its similar organ sizes and physiology to humans (1, 2). It is therefore imperative to generate various types of specially designed pigs for applications in agricultural and biomedical research (3), which is dependent on the constant development of reproductive techniques. Moreover, oocytes occupy a vital position in these technical procedures and directly determine their efficiencies (4). The acquirement of high-quality oocytes through *in vitro* maturation (IVM) technique has become increasingly prominent because the potential of oocytes matured *in vitro* still remain in a compromised state due to incomplete cytoplasmic maturation (5, 6). Currently, numerous studies have been conducted to elucidate the complex regulatory mechanisms underlying oocyte maturation in order to improve the IVM efficiency (7), but the existing mechanisms are not comprehensive enough.

Oocyte maturation is the final step of mammal oogenesis during which meiotic resumption occurs as a progression from initial germinal vesicle (GV) breakdown into metaphase II (MII) arrest (8). This process is accompanied by the deposition of maternal RNAs and proteins regarded as one part of the cytoplasmic maturation for successful oocyte maturation, zygotic genome activation and early embryo development (9, 10). The transcriptome allows an overview of gene expression profile to improve our understanding toward molecular mechanisms of oocyte maturation (11). However, the transcriptional activity is minuscule during oocyte maturation (12), and mRNA and protein levels are rarely correlated well, particularly in oocytes (13). Conversely, a large number of proteins are activated or inactivated by post-translational modifications to employ in oocyte maturation such as nuclear reorganization, cytoskeleton rearrangement, organelle architecture, etc (14). These events are accurately controlled by a network of protein interactions and functions. Therefore, more in-depth proteomic research is of great significance for further elucidating the molecular processes during oocyte maturation.

During the past decade, proteomic strategies have been widely applied to explore the maturation mechanisms of mammalian oocytes including human (15), mouse (16, 17), pig (13, 18–20), cattle (21, 22) and buffalo (23, 24). However for porcine oocytes, all previous studies were conducted by two-dimensional gel electrophoresis (2-DE) to identify the protein composition. But this 2-DE technique remains very difficult to detect low molecular weight and low abundance proteins, with a disadvantage in the accurate quantitation from multiple samples (25). So, in these studies there is a maximum of no more than 1,000 proteins identified in porcine oocytes during IVM. An alternative approach with high-throughput technology is necessary to achieve the comprehensive identification and quantification of proteins for porcine oocytes.

Currently, tandem mass tag (TMT) labeling coupled with liquid chromatography tandem mass spectrometry (LC-MS/MS) is becoming a mainstream proteomic technique attracting tremendous attention in various research fields, due to its advantages of high throughput, sensitivity, accuracy, and stability (26, 27). In addition, a novel targeted method, parallel reaction monitoring (PRM) is applicable to the identification and quantification of low abundant proteins with good selectivity and sensitivity (28), and thus has been used to validate the candidate proteins. In our previously published work, these techniques have already been employed to analyze the proteomic changes of porcine oocytes after vitrification (29). Combining these data, the present study aimed to further acquire the proteomic characteristics of porcine oocytes during meiotic maturation *in vitro*, in order to better understand the potential mechanisms underpinning this process with the protein dimension.

MATERIALS AND METHODS

All chemicals and reagents used in this study were purchased from Sigma-Aldrich Chemical Company (Shanghai, China) unless otherwise specified.

Oocyte Collection and IVM

In this study, medium and procedures for oocyte collection and IVM were as described previously (30). Pre-pubertal ovaries were obtained from a local abattoir and transported to the laboratory in saline at 35–37°C within 2 h. Follicular fluid was aspirated from 3–8 mm antral follicles using a syringe with an 18-gauge needle. Cumulus-oocyte complexes (COCs) in sediments were washed two times in Tyrode's lactate-HEPES-polyvinyl alcohol medium (31), then selected under a stereomicroscope (Olympus, Tokyo, Japan). After washing three times in IVM medium, 50–70 COCs with uniform oocyte cytoplasm and over 3 layers of compact cumulus cells were cultured in each well of a 24-well plate (Costar, Corning, NY, USA) containing 500 μL IVM medium for 42–44 h at 39°C in an atmosphere of 5% CO_2 with saturated humidity. The composition of IVM medium was a tissue culture medium-199 (ThermoFisher Scientific, Grand Island, NY, USA) supplemented with 3.05 mM D-glucose, 0.57 mM cysteine, 0.91 mM sodium pyruvate, 10% (v/v) porcine follicular fluid, 10 ng/mL epidermal growth factor, 0.5 μg/mL each follicle-stimulating hormone, and luteinizing hormone.

Protein Extraction, Digestion and TMT Labeling

For collecting GV oocytes, COCs were incubated in 0.1% hyaluronidase for 10 min at 39°C and then mechanically stripped of cumulus cells by repeated aspiration with a 200-μL pipette. In addition, after 42–44 h of IVM, oocytes were also freed from cumulus cells, and those with a first polar body (a characteristic of MII stage) were used for experiments. Both GV and MII oocytes were washed three times in cold Dulbecco's phosphate buffered saline containing 0.3% (w/v) polyvinyl alcohol and stored at −80°C. Three biological replicates were carried out and about 1,500 oocytes were used for each sample.

For protein extraction, these samples were lysed on ice in 8 M urea containing 1% protease inhibitor cocktail through a high intensity ultrasonic processor and then centrifugated at 12,000 g at 4°C for 10 min to obtain the supernatant. Protein concentration was measured by a bicinchoninic acid protein assay kit (Pierce, Rockford, IL, USA) following the manufacturer's instructions. Moreover, the protein solution was reduced with 5 mM dithiothreitol at 56°C for 30 min, alkylated with 11 mM iodoacetamide at room temperature for 15 min, and diluted to ensure the urea concentration was less than 2 M. Trypsin was added at 1:50 mass ratio (trypsin: protein) at 37°C overnight for the first digestion and continuously at 1:100 mass ratio (trypsin: protein) for 4 h to complete a post-digestion. After digestion, peptides were desalted on a Strata X C18 SPE column (Phenomenex, Torrance, CA, USA), vacuum-dried, and reconstituted in 0.5 M TEAB. For TMT labeling, one unit of TMT reagent (Thermo Fisher Scientific, Waltham, MA, USA) was reconstituted in acetonitrile to mix with peptides at room temperature for 2 h. Peptides derived from MII oocyte samples were labeled TMT tags of 126, 127N and 127C, and peptides derived from GV oocyte samples were labeled with TMT tags of 128N, 129N and 129C. Finally, the labeled peptide mixtures were desalted and dried under vacuum centrifugation.

LC-MS/MS Analysis

Firstly, tryptic peptides were separated at a gradient of 8–32% acetonitrile (pH 9.0) over 60 min into 60 fractions using high pH reverse-phase high performance liquid chromatography with an Agilent 300 Extend C18 column (5 μm particles, 4.6 mm ID, 250 mm length; Agilent, Santa Clara, USA), followed by combining into 9 fractions and vacuum-drying. After dissolving in solvent A (0.1% formic acid), these peptides were directly loaded onto a home-made reversed-phase analytical column (15-cm length, 75 μm i.d.) to elute with gradient solvent B (0.1% formic acid in 98% acetonitrile). The linear gradient settings were as follows: 7–16% over 50 min, 16–30% in 35 min, 30–80% in 2 min and 80% for the last 3 min, which was performed on an EASY-nLC 1,000 ultraperformance liquid chromatography (UPLC) system (Thermo Fisher Scientific, Waltham, MA, USA) at a flow rate of 400 nL/min.

The peptides were subjected to nanospray ionization at 2.0 kV voltage and then detected with tandem mass spectrometry (MS/MS) in Q Exactive^{TM} Plus (Thermo Fisher Scientific, Waltham, MA, USA) coupled online to the UPLC system. Precursor and fragment ion spectra were acquired in the high-resolution Orbitrap with 350–1,550 m/z at a resolution of 60,000 and 100 m/z at a resolution of 30,000, respectively. A data dependent scanning mode was used to acquire a mass fragmentation date. Each full mass spectrometry (MS) scan was followed by 20 MS/MS scans (30.0 s dynamic exclusion) corresponding from the ten most abundant precursor ions of full MS for higher-energy collisional dissociation (HCD) fragmentation with 32% normalized collision energy (NCE). In addition, automatic gain control (AGC) was set at 5E4, and maximum injection time (max IT) was 70 ms.

Database Processing

The resulting MS/MS spectra were processed using Maxquant search engine (v1.5.2.8) against the Sus scrofa UniProt proteome database (40,708 sequences). Moreover, we added a reverse decoy database to reduce the false positive identification results. Trypsin/P was specified as the cleavage enzyme, allowing up to two missing cleavages. The minimum peptide length was specified as seven amino acids, with a maximum of five modifications per peptide. Precursor mass tolerance was 20 ppm and fragment mass tolerance was 5 ppm. Carbamidomethylation on cysteine was specified as fixed modification and oxidation on methionine and N-terminal acetylation as variable modification. The false discovery rate for each peptide was adjusted to <1%, and minimum score for peptides was set to >40. Student's *t*-test was used to analyze statistical significances between two samples, and *P*-value of <0.05 and fold change of ≥ 1.20 or ≤ 0.83 were set as the threshold for differentially expressed proteins (DEPs).

Bioinformatics Analysis

Gene Ontology (GO) annotation proteome was derived from the UniProt-GOA database (http://www.ebi.ac.uk/GOA/) based on biological process, cellular component and molecular function (32). Proteins were further searched with the InterProScan software (http://www.ebi.ac.uk/interpro/) if they were not annotated by the UniProt-GOA database. The online service tool KAAS4 was used to annotate the Kyoto Encyclopedia of Genes and Genomes (KEGG) description (33). Furthermore, enrichment analysis was also carried out by using the Metascape software (http://metascape.org) (34).

PRM Validation

For PRM analysis, we carried out three biological replicates with at least 1,000 oocytes used for each sample. The tryptic digested peptides were prepared according to the procedures described above. Similarly, peptides were dissolved in solvent A and then eluted with gradient solvent B (6–25% over 40 min, 25–35% in 12 min, climbing to 80% in 4 min, and holding at 80% for the last 4 min), at a flow rate of 500 nL/min. Subsequently, the eluted peptides were subjected to a nanospray ionization source (2.2 kV electrospray voltage) followed by Q Exactive^{TM} Plus coupled online to the UPLC. A data-independent acquisition was conducted on an Orbitrap as follows: full MS scan at a resolution of 70,000 with 350–1,060 m/z (AGC, 3E6; max IT, 50 ms) followed by 20 MS/MS scans at a resolution of 17,500 (AGC, 1E5; max IT, 120 ms; isolation window, 1.6 m/z). In addition, 27% NCE with HCD was used to fragment precursor ions. Acquired PRM data were processed through a Skyline software (version 3.6, MacCoss Lab, University of Washington, USA) (35). The target proteins were quantified according to the fragment ion peak area for confirming the TMT results. We selected 12 proteins according to high-confidence peptide and functional importance, including wee1-like protein kinase 2 (WEE2), kinesin-like protein (KIF20A), ubiquitin conjugating enzyme E2 C (UBE2C), DNA (cytosine-5)-methyltransferase (DNMT1), proliferating cell nuclear antigen (PCNA), CD59 glycoprotein (CD59), growth differentiation factor 9 (GDF9), coronin (CORO1C), tudor and KH domain-containing protein (TDRKH), tropomyosin

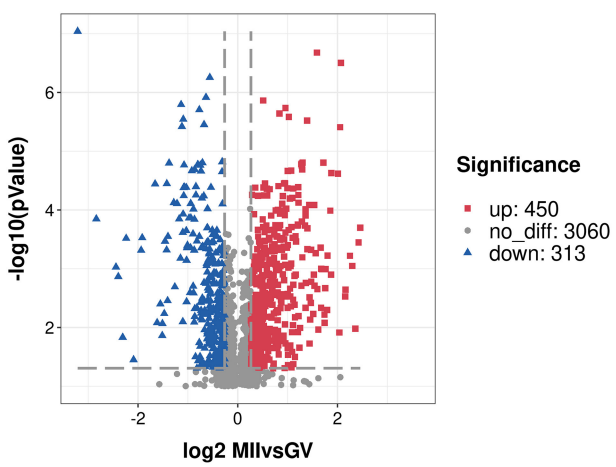

FIGURE 1 | A volcano plot of differentially expressed proteins. Proteins with fold change of ≥ 1.20 or ≤ 0.83 and $P < 0.05$ were considered statistically significant. Red blocks indicate significant over-expressed proteins, blue triangles indicate significant under-expressed proteins, while gray circles indicate proteins without differences. The X-axis represents fold change, Y-axis means *P*-value.

alpha-4 chain (TPM4), annexin (ANXA1) and cytoplasmic polyadenylation element-binding protein 1 (CPEB1).

RESULTS

Protein Identification

After a stringent criteria for quality control (TMT labeling efficiency of 98.42%, peptide mass error within 5 ppm), we obtained a total of 3,823 proteins with quantitative information and the detailed description is provided in **Supplementary Table S1**. Moreover, a principal component analysis of all quantified proteins showed two completely independent clusters, indicating that the replicates from each treatment were very close to each other (**Supplementary Figure S1**). Among these proteins, 763 proteins (P-value < 0.05, fold change of ≥ 1.20 or ≤ 0.83) were considered as the DEPs, and 450 proteins were over-expressed, and 313 proteins were under-expressed in the MII oocyte (**Supplementary Table S2**). A volcano plot indicated the repartition of each protein abundance (**Figure 1**). In addition, there were 144 DEPs with fold change more than two, including 101 over-expressed and 43 under-expressed proteins.

Functional Classification Analysis

First, we performed a GO functional classification on the DEPs and showed 32 terms including 16 biological processes, 8 cellular components and 8 molecular functions (**Figure 2** and **Supplementary Table S3**). For the biological process, the top five GO terms consisted of "cellular process" (343 proteins), "single-organism process" (239 proteins), "metabolic process" (237 proteins), "biological regulation" (228 proteins) and "cellular component organization" (146 proteins). In the cellular component, the most abundant terms were "cell" and "organelle" with 349 and 304 proteins, respectively. The "binding" (536 proteins) and "catalytic activity" (186 proteins) were the largest two terms for molecular function.

In addition, functional classification based on the COG/KOG database was also used to analyze the protein function and characteristic. These DEPs were assigned to 25 COG/KOG categories (**Figure 3** and **Supplementary Table S4**). The largest category was "signal transduction mechanisms" (105 proteins),

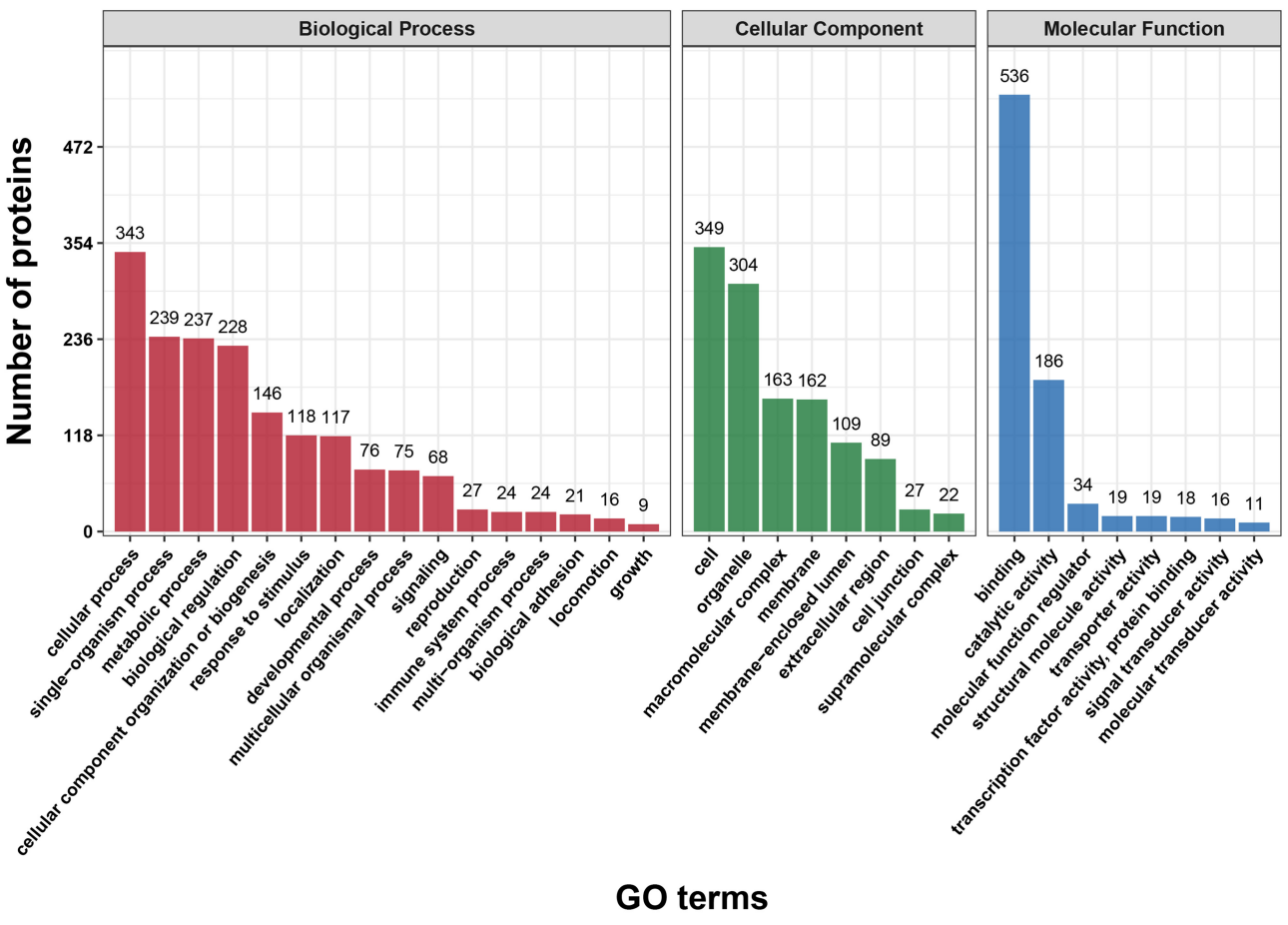

FIGURE 2 | Gene Ontology (GO) classification analysis of differentially expressed proteins (DEPs) in terms of biological process, cellular component and molecular function. Each bar represents the number of DEPs.

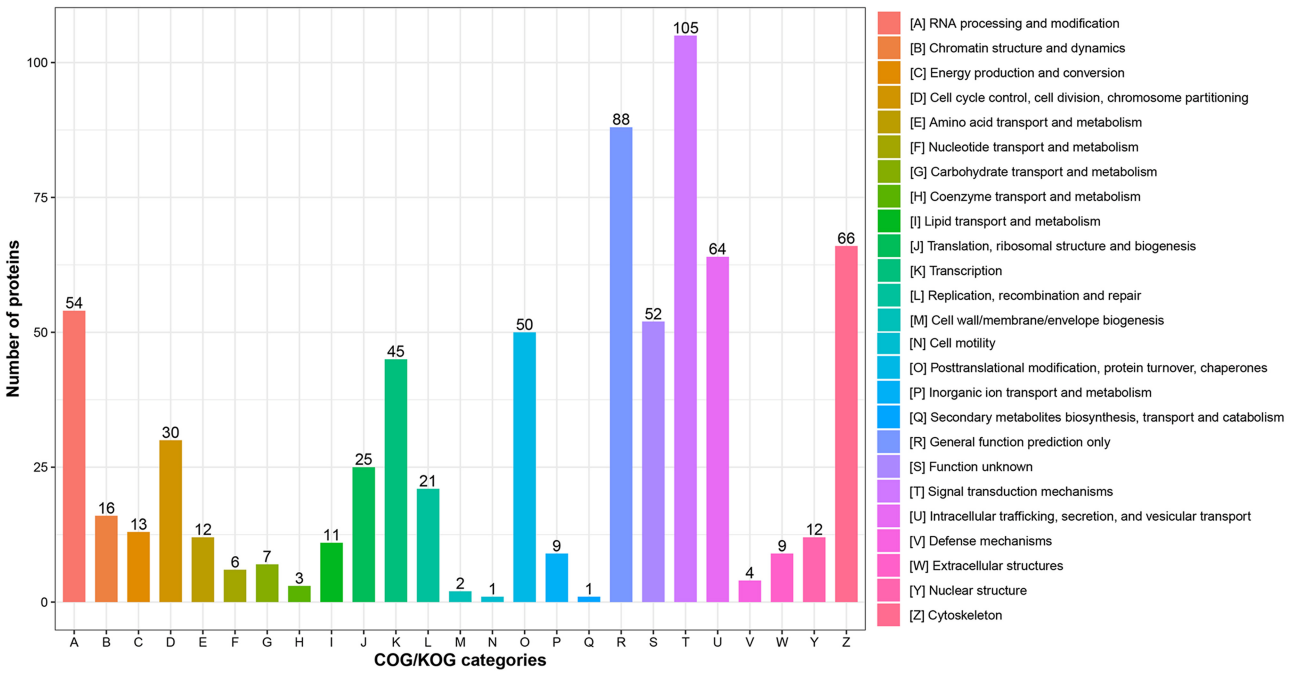

FIGURE 3 | COG/KOG functional classification analysis of differentially expressed proteins (DEPs). The DEPs were aligned to COG/KOG database and classified into 20 functional clusters. Each bar represents the number of DEPs.

followed by "general function prediction only" (88 proteins) and "cytoskeleton" (66 proteins). Moreover, some DEPs were clustered in important categories related to oocyte meiosis such as "cell cycle control, cell division, chromosome partitioning" (30 proteins), "chromatin structure and dynamics" (16 proteins) and "nuclear structure" (12 proteins).

Functional Enrichment Analysis

First of all, the detailed information of GO functional enrichment is shown in **Figure 4** and **Supplementary Table S5**. Within the molecular function, a number of over-expressed DEPs were enriched for microtubule-related terms including "microtubule binding," "microtubule motor activity" and "tubulin binding," whereas "actin filament binding" and "actin binding" terms were under-expressed. A molecular function analysis showed that most of the over-expressed DEPs were involved in the regulation of the nucleus and chromosome, and the under-expressed terms were concerned with "cell junction," "adherens junction" and "anchoring junction." Regarding the biological process from over-expressed DEPs, almost all terms related to the cell cycle networks were "mitotic cycle process," "nuclear division," "regulation of cell cycle process," "mitotic nuclear division," "chromatin organization," etc. Still there were some under-expressed DEPs associated with "actin cytoskeleton organization" and "actin filament organization" terms.

We next used KEGG pathway analysis to delineate the protein functions (**Figure 5** and **Supplementary Table S6**). Several signaling pathways related to oocyte maturation were enriched including "oocyte meiosis," "progesterone-mediated oocyte maturation," "thyroid hormone signaling pathway," "insulin signaling pathway," "MAPK signaling pathway," etc. Moreover, the under-expressed DEPs enriched the many significant pathways associated with "cell adhesion molecules," "adherens junction," "tight junction" and "regulation of actin cytoskeleton."

Based on the Metascape software, the enriched clusters for DEPs included those of "cell cycle," "mRNA processing," "cell division," "organelle localization," "actin filament-based process" and others (**Figure 6** and **Supplementary Table S7**).

PRM Validation

As shown in **Figure 7** and **Supplementary Figure S2**, the expression patterns of these proteins quantified by PRM and TMT were completely consistent, although the fold change in protein expression levels varied between the two techniques.

DISCUSSION

There is a large pool of protein composition stored in GV oocytes, which exhibits dynamic changes during the process of meiotic resumption. Accumulation of maternally derived proteins in cytoplasm is critical to oocyte maturation, fertilization and embryo development (36). Thus, an investigation of oocyte proteome variations during the GV to MII transition is of great significance to uncover regulatory proteins and related functional phenotypes of oocyte maturation. The present results showed a series of differential proteins between GV and MII oocytes. A substantial number of known proteins associated with both nuclear and cytoplasmic maturation were further

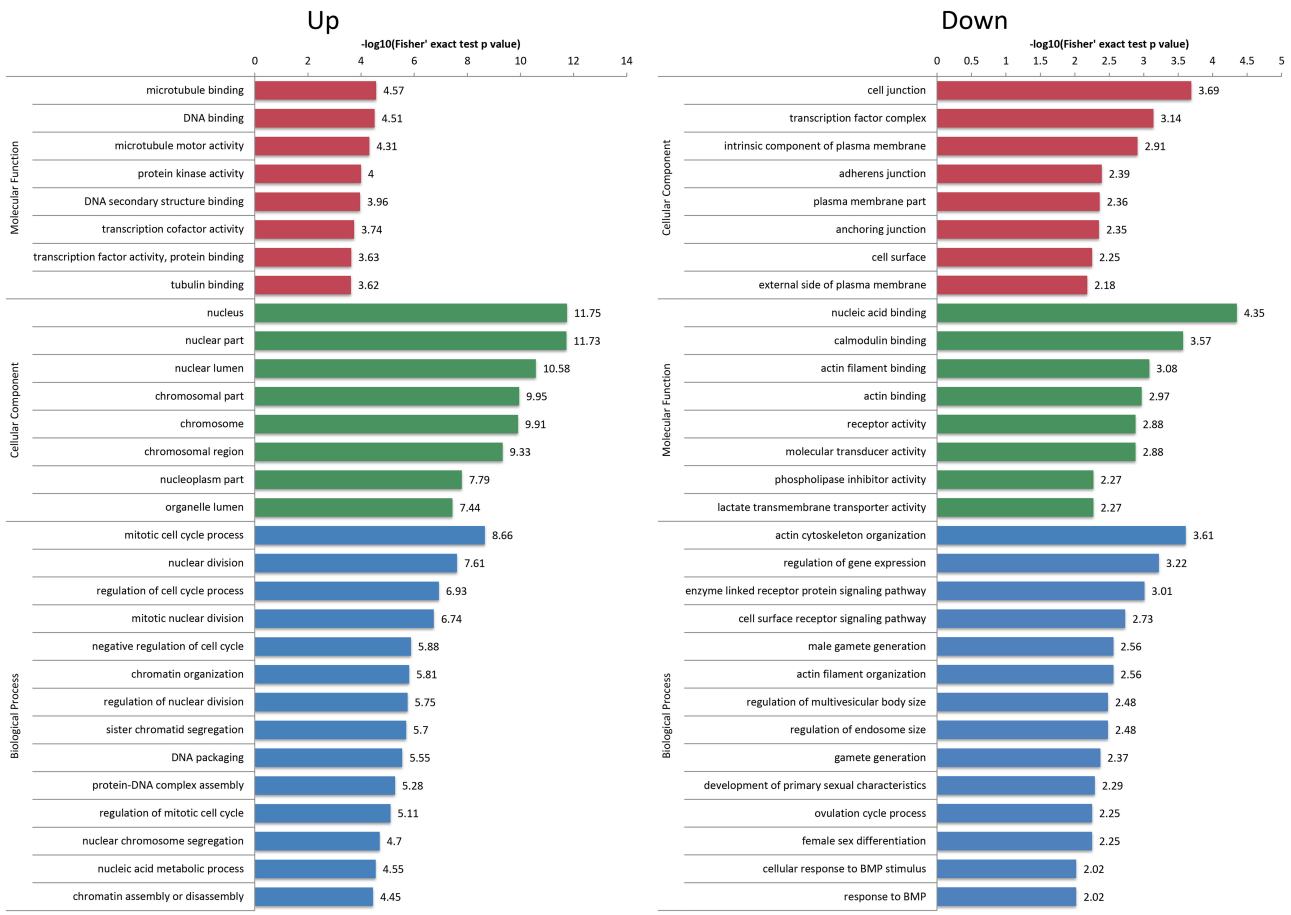

FIGURE 4 | Gene Ontology (GO) enrichment analysis of differentially expressed proteins (DEPs). The over-expressed and under-expressed DEPs were enriched into cellular component, molecular function and biological process. The bar represents the enrichment score associated with each term, and score value is shown as -log10 (Fisher's exact test *P*-value).

confirmed by the current study. We also found that some novel proteins were supposed to take part in oocyte maturation. Furthermore, bioinformatics interrogation revealed important changes in protein regulation of multiple cellular functions in porcine oocytes during IVM.

Regarding the porcine oocytes, high-throughput technology has not been used for proteome analysis. Our study obtained 763 quantified proteins considered as significant difference in the MII oocytes through TMT-based proteomic approach, which is far more than date of Kim et al. who have reported 16 over-expressed and 12 under-expressed proteins using 2-DE analysis (13). Another study also found only 16 proteins that were differentially expressed during IVM of porcine oocytes (19). Moreover, almost all of these DEPs identified in previously reported studies were not detected in the current study.

Cellular metabolism is vital for oocyte maturation because the large-scale reorganizations of nucleus and cytoplasm require a massive amount of energy from various substrates such as carbohydrates, amino acids, and lipids (37). Currently, both glucose and pyruvate are commonly added to IVM medium to support porcine oocyte maturation and subsequent early embryo development (38). In the present study, there were 237 DEPs classified in the "metabolic process," some of which were assigned to "energy production and conversion," "carbohydrate transport and metabolism," "amino acid transport and metabolism," "lipid transport and metabolism" and so on, according to COG/KOG categories. These proteins play a crucial role in the regulation of energy metabolism during oocyte maturation. For instance, monocarboxylate transporter 1 (SLC16A1) and solute carrier family 16 member 3 (SLC16A3), belonging to a family of proton-linked monocarboxylate transporters, are involved in the movement of lactate, pyruvate, acetate and ketone bodies, and their regulation and function have been confirmed in preimplantation mouse embryos (39). Thioredoxin domain containing 9 (TXNDC9), as a prominent member of thioredoxins, can maintain the redox state and regulate the folding of actin and tubulin (40). It has been reported that TXNDC9 is required for mouse oocyte maturation and shows a higher protein expression in GV stage compared to MII stage (41). However, we observed the highest level of

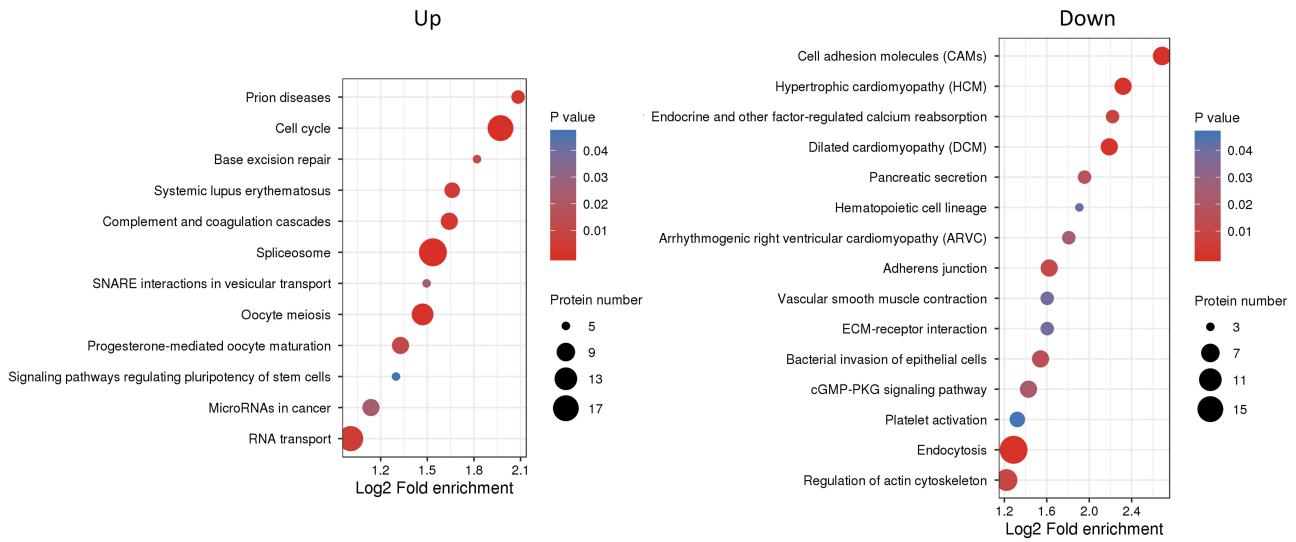

FIGURE 5 | Kyoto Encyclopedia of Genes and Genomes (KEGG) pathway enrichment analysis of differentially expressed proteins (DEPs). The *P*-value was calculated using a Fisher's exact test. The X-axis represents the log2 fold enrichment, Y-axis means KEGG pathway. Bubble size corresponds to the number of DEPs for each term.

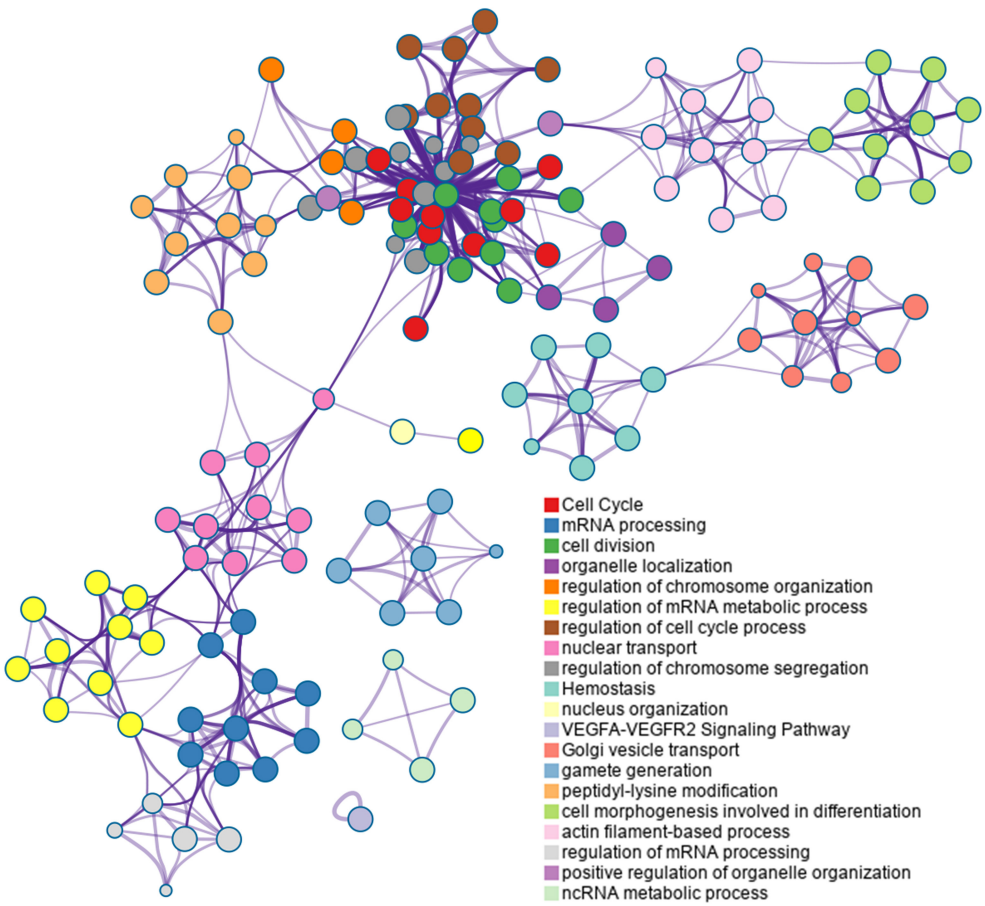

FIGURE 6 | Top 20 clusters in the enrichment network of differentially expressed proteins (DEPs). Metascape is used for annotation and enrichment visualization of DEPs. Each circle represents an enriched term and is colored according to cluster identity. Terms with a similarity score >0.3 are linked by edges.

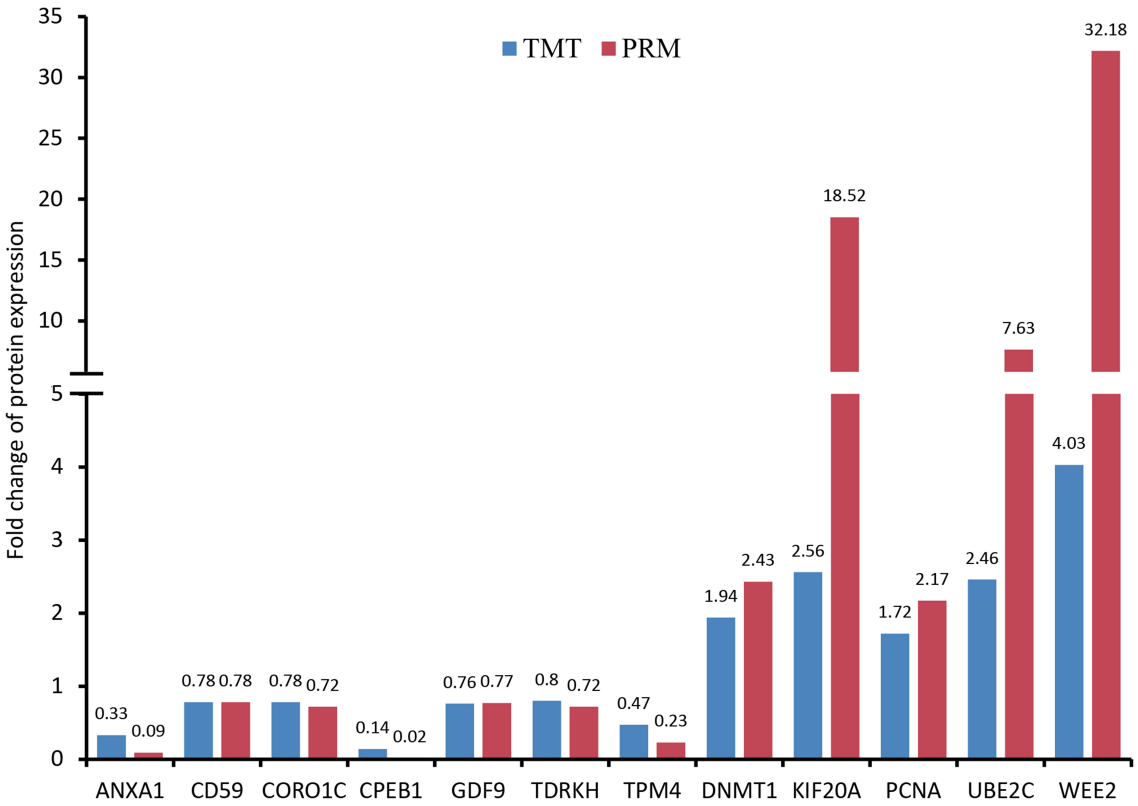

FIGURE 7 | Validation of differentially expressed proteins (DEPs) using parallel reaction monitoring (PRM) analysis. There are 12 candidate DEPs obtained to verify the tandem mass tag (TMT) results.

TXNDC9 protein in porcine oocytes after IVM. Conversely, there are a large number of lipid droplets in porcine oocyte cytoplasm, which have been demonstrated to play a fundamental role in the oocyte maturation process by providing an energy source from lipid metabolism (42, 43). Based on our results, many proteins were uncovered to participate in the signaling pathway of lipid metabolism during oocyte maturation such as methylsterol monooxygenase 1 (MSMO1), phospholipase A2 activating protein (PLAA), phosphatidate phosphatase (LPIN2), acetyl-CoA carboxylase 1 (ACACA), etc. LPIN2 promotes the accumulation of lipid droplets and its degradation is essential for lipolysis activation (44). The under-expressed expression of LPIN2 protein in MII oocytes may also suggest a marked increase in lipid metabolism during the IVM process.

In the biological process, the over-expressed proteins were mainly enriched in the GO terms associated with cell cycle regulation, indicating that they might play a key role in the meiotic progression of oocytes. The KEGG enrichment analysis also identified two pathways, "cell cycle" and "oocyte meiosis," as significantly enriched. As expected, the present study found some known proteins including CPEB1, KIF20A, kinetochore complex component (NDC80), mitotic checkpoint protein BUB3 (BUB3), UBE2C and others. Previous studies have showed that these proteins mentioned above are essential for meiotic resumption of porcine oocytes such as regulating spindle formation and chromosome alignment (45–49). Incidentally, we observed that securing (PTTG1) expression was over-expressed 4.1-fold in MII oocytes, which may participate in the processes of oocyte maturation and zygotic genome activation as a maternal protein (50). Conversely, several proteins that have not yet been studied in porcine oocytes were also identified to be involved in the cell cycle. For example, WEE2 protein is an oocyte specific tyrosine kinase and is critical for exit from MII arrest and promotes pronuclear formation (51). Structural maintenance of chromosomes protein (SMC1B), a meiosis specific component of cohesin complex, is considered essential for meiotic chromosomal segregation (52). CHEK1 is an uncharacterized protein in pigs whose function may be associated with cell cycle arrest (53). In a word, all of these proteins contained in the above terms and pathways may play their respective roles in order to assure normal nuclear maturation of porcine oocytes.

The dynamic remodeling of cytoskeleton plays crucial roles in spindle assembly, chromosome segregation and organelle reorganization, ensuing proper nuclear and cytoplasmic maturation of mammalian oocytes (54). Based on the molecular function analysis, the terms related to microtubule regulation mainly enriched the over-expressed proteins and the majority

of them belong to kinesin motor family of proteins (KIF11, KIF14, KIF15, KIF23, KIF4A, KIF18A, KIF20A, KIF20B, KIF2C, KIFC1). These proteins are essential for the functional mechanisms of macromolecule transport, microtubule dynamics, cell cycle progression and cytokinesis (55). It has been well known that dynamic changes in actin filaments are implicated in various events during oocyte meiotic maturation (56). In this study, we found that the enriched GO terms and KEGG pathways for under-expressed proteins contained actin-based functions. Among the proteins, myosin IB (MYO1B), myosin IE (MYO1E) and myosin VB (MYO5B) need specific attention, because they are numbers of the myosin family of motor proteins and also may have important roles in actin cytoskeleton remodeling during oocyte maturation.

It is established that the increase in progesterone induced by a luteinizing hormone is associated with meiotic resumption of porcine oocytes (57). As we expected, the KEGG pathways analysis showed that a total of 8 over-expressed proteins were involved in the "progesterone-mediated oocyte maturation" pathway, indicating their function in regulation of oocyte maturation. These proteins have been well elucidated as maternal proteins necessary for oogenesis. For instance, cyclin B1 (CCNB1) and proto-oncogene serine/threonine-protein kinase mos (MOS) are required for maturation promoting factor activation and mitogen-activated protein kinase cascade (58). The spindle checkpoint signaling depends on (BUB1) and serine/threonine-protein kinase PLK (PLK1) (59). Conversely, we found that the "cGMP-PKG signaling pathway" was significantly under-expressed in MII compared to GV oocytes, suggesting that this pathway was an important part of the regulatory mechanism related to meiotic maturation. Notable among these was the protein phosphatase 3 regulatory subunit B, alpha (PPP3R1) acting as the regulatory subunit of calcineurin B. It has been reported that calcineurin is present in porcine oocytes (60), and may modulate the meiotic maturation of mouse oocytes (61). Finally, another significantly enriched pathway was the Hippo signaling pathway, which has been speculated to be involved during oocyte maturation (62).

In this study, we also identified a series of DEPs related to epigenetic modifications including DNA methylation, histone acetylation and methylation. Among them, DNMT1, lymphoid specific helicase (HELLS), tudor domain containing 1 (TDRD1), tudor and TDRKH were enriched in the "DNA methylation or demethylation" term. It is worth mentioning that the expression of HELLS was elevated by 2.7-fold in MII oocytes, which as a DNA helicase is essential for genome-wide DNA methylation (63). In addition, GO enrichment analysis revealed the following enriched terms: "histone acetylation," "histone H3 acetylation," "H4 histone acetyltransferase complex," and "histone acetyltransferase complex." Both down-regulator of transcription 1 (DR1) and transcriptional adapter 3 (TADA3) were found to be involved in these terms, indicating that they might have a function during meiotic maturation in porcine oocytes through the modulation of histone deacetylation. However, the two proteins have hardly been studied previously in mammalian oocytes. The present study also showed that the retinoblastoma-binding family of proteins (RBBP4, RBBP5 and RBBP7) were linked to the formation of "histone methyltransferase complex" based on cellular component analysis. It has been reported that RBBP4 and RBBP7 can regulate histone deacetylation and chromosome segregation during mouse oocyte maturation (64, 65).

Conversely, our proteomic data were confirmed to be entirely reliable through PRM target validation for the selected 12 proteins. In the discussion above, WEE2, KIF20A, UBE2C, DNMT1, TDRKH and CPEB1 have been described to exert important roles in oocyte meiotic maturation. Moreover, GDF9, ANXA1 and PCNA are considered as oocyte-specific proteins and also identified in human oocytes through single-cell proteomics (15). It has been reported that CORO1C as an actin-binding protein is associated with cytogenesis in oocytes and embryos (66). According to a previous report (67), TPM4 might also be involved in the formation of microtubule structure in porcine oocyte maturation. Finally, our study found several cell surface glycoproteins with different expression including CD59, CD61, CD99 and CD276, suggesting that these proteins likely play important roles in porcine oocyte fertilization.

CONCLUSION

In conclusion, we found 763 significantly altered proteins in GV and MII oocytes, suggesting that they might closely be related to oocyte maturation. Moreover, the functional classification and enrichment analysis revealed that these proteins were involved in multiple regulatory mechanisms of meiotic resumption and cytoplasmic maturation, such as spindle and chromosome configurations, cytoskeletal reconstruction, epigenetic modifications, energy metabolism, signal transduction and so on. All of these findings provide a deeper insight into the molecular characteristics of proteome in regulation of porcine oocyte maturation following IVM process.

DATA AVAILABILITY STATEMENT

The datasets presented in this study can be found in online repositories. The names of the repository/repositories and accession number(s) can be found at: http://www.proteomexchange.org/, PXD023107.

ETHICS STATEMENT

Ethical review and approval was not required because live animals were not used in this study. Experiments carried out were according to institutional ethical guidelines and safety procedures.

AUTHOR CONTRIBUTIONS

BJ, DX, and GW conceived the experiments. BJ, DX, QS, QH, GQ, and GW conducted the experiments. BJ,

DX, and GQ performed statistical analysis and figure generation. BJ, DX, and GW wrote the manuscript. GQ and GW reviewed the manuscript. All authors have read and agreed to the published version of the manuscript.

FUNDING

This work was supported by National Natural Science Foundation of China (Nos. 31660661, 32160793, and 31960663), Yunnan Applied Basic Research Projects (Nos. 202001AS070001 and 202101AT070213), and Yunnan Young Academic Leader Program (No. 202005AC160004).

ACKNOWLEDGMENTS

The authors are grateful to PTM Biolab, Inc (Hangzhou, China) for carrying out the MS analysis.

SUPPLEMENTARY MATERIAL

The Supplementary Material for this article can be found online at: https://www.frontiersin.org/articles/10.3389/fvets.2021.792869/full#supplementary-material

Supplementary Figure S1 | A principal component analysis of all quantified proteins.

Supplementary Figure S2 | The fragment ion peak area distribution of identified peptides.

Supplementary Table S1 | Annotation of quantified proteins.

Supplementary Table S2 | Differentially expressed proteins.

Supplementary Table S3 | GO classification analysis.

Supplementary Table S4 | COG/KOG classification analysis.

Supplementary Table S5 | GO enrichment analysis.

Supplementary Table S6 | KEGG pathway enrichment analysis.

Supplementary Table S7 | Cluster analysis of enriched GO terms.

REFERENCES

1. Tang Z, Li Y, Wan P, Li X, Zhao S, Liu B, et al. LongSAGE analysis of skeletal muscle at three prenatal stages in Tongcheng and Landrace pigs. *Genome Biol.* (2007) 8:R115. doi: 10.1186/gb-2007-8-6-r115
2. Wilkinson S, Lu ZH, Megens HJ, Archibald AL, Haley C, Jackson IJ, et al. Signatures of diversifying selection in European pig breeds. *PLoS Genet.* (2013) 9:e1003453. doi: 10.1371/journal.pgen.1003453
3. Yang H, Wu Z. Genome editing of pigs for agriculture and biomedicine. *Front Genet.* (2018) 9:360. doi: 10.3389/fgene.2018.00360
4. Hashimoto S. Application of *in vitro* maturation to assisted reproductive technology. *J Reprod Dev.* (2009) 55:1–10. doi: 10.1262/jrd.20127
5. Zhang M, Zhang C, Pan L, Gong S, Cui W, Yuan H, et al. Meiotic arrest with roscovitine and follicular fluid improves cytoplasmic maturation of porcine oocytes by promoting chromatin de-condensation and gene transcription. *Sci Rep.* (2017) 7:11515–74. doi: 10.1038/s41598-017-11970-y
6. Lee S, Kang H, Jeong P, Nanjidsuren T, Song B, Jin YB, et al. Effect of oocyte quality assessed by brilliant cresyl blue (BCB) staining on cumulus cell expansion and sonic hedgehog signaling in porcine during *in vitro* maturation. *Int J Mol Sci.* (2020) 21:4423. doi: 10.3390/ijms21124423
7. Gilchrist RB. Recent insights into oocyte-follicle cell interactions provide opportunities for the development of new approaches to *in vitro* maturation. *Reprod Fertil Dev.* (2011) 23:23–31. doi: 10.1071/RD10225
8. Li R, Albertini DF. The road to maturation: somatic cell interaction and self-organization of the mammalian oocyte. *Nat Rev Mol Cell Biol.* (2013) 14:141–52. doi: 10.1038/nrm3531
9. Watson AJ. Oocyte cytoplasmic maturation: a key mediator of oocyte and embryo developmental competence. *J Anim Sci.* (2007) 85:E1–3. doi: 10.2527/jas.2006-432
10. Conti M, Franciosi F. Acquisition of oocyte competence to develop as an embryo: integrated nuclear and cytoplasmic events. *Hum Reprod Update.* (2018) 24:245–66. doi: 10.1093/humupd/dmx040
11. Luong XG, Daldello EM, Rajkovic G, Yang CR, Conti M. Genome-wide analysis reveals a switch in the translational program upon oocyte meiotic resumption. *Nucleic Acids Res.* (2020) 48:3257–76. doi: 10.1093/nar/gkaa010
12. De La Fuente R, Eppig JJ. Transcriptional activity of the mouse oocyte genome: companion granulosa cells modulate transcription and chromatin remodeling. *Dev Biol.* (2001) 229:224–36. doi: 10.1006/dbio.2000.9947
13. Kim J, Kim J, Jeon Y, Kim D, Yang T, Soh Y, et al. Identification of maturation and protein synthesis related proteins from porcine oocytes during *in vitro* maturation. *Proteome Sci.* (2011) 9:28. doi: 10.1186/1477-5956-9-28
14. Budna J, Bryja A, Celichowski P, Kahan R, Kranc W, Ciesiółka S, et al. Genes of cellular components of morphogenesis in porcine oocytes before and after IVM. *Reproduction.* (2017) 154:535–45. doi: 10.1530/REP-17-0367
15. Virant-Klun I, Leicht S, Hughes C, Krijgsveld J. Identification of maturation-specific proteins by single-cell proteomics of human oocytes. *Mol Cell Proteomics.* (2016) 15:2616–27. doi: 10.1074/mcp.M115.056887
16. Vitale AM, Calvert ME, Mallavarapu M, Yurttas P, Perlin J, Herr J, et al. Proteomic profiling of murine oocyte maturation. *Mol Reprod Dev.* (2007) 74:608–16. doi: 10.1002/mrd.20648
17. Wang S, Kou Z, Jing Z, Zhang Y, Guo X, Dong M, et al. Proteome of mouse oocytes at different developmental stages. *Proc Natl Acad Sci U S A.* (2010) 107:17639–44. doi: 10.1073/pnas.1013185107
18. Ellederova Z, Halada P, Man P, Kubelka M, Motlik J, Kovarova H. Protein patterns of pig oocytes during *in vitro* maturation. *Biol Reprod.* (2004) 71:1533–9. doi: 10.1095/biolreprod.104.030304
19. Susor A, Ellederova Z, Jelinkova L, Halada P, Kavan D, Kubelka M, et al. Proteomic analysis of porcine oocytes during *in vitro* maturation reveals essential role for the ubiquitin C-terminal hydrolase-L1. *Reproduction.* (2007) 134:559–68. doi: 10.1530/REP-07-0079
20. Zhao Q, Guo Z, Piao S, Wang C, An T. Discovery of porcine maternal factors related to nuclear reprogramming and early embryo development by proteomic analysis. *Proteome Sci.* (2015) 13:18. doi: 10.1186/s12953-015-0074-5
21. Labas V, Teixeira-Gomes A, Bouguereau L, Gargaros A, Spina L, Marestaing A, et al. Intact cell MALDI-TOF mass spectrometry on single bovine oocyte and follicular cells combined with top-down proteomics: a novel approach to characterise markers of oocyte maturation. *J Proteomics.* (2018) 175:56–74. doi: 10.1016/j.jprot.2017.03.027
22. Marei W, Van Raemdonck G, Baggerman G, Bols P, Leroy J. Proteomic changes in oocytes after *in vitro* maturation in lipotoxic conditions are different from those in cumulus cells. *Sci Rep.* (2019) 9:3673. doi: 10.1038/s41598-019-40122-7
23. Chen L, Zhai L, Qu C, Zhang C, Li S, Wu F, et al. Comparative proteomic analysis of buffalo oocytes matured *in vitro* using iTRAQ technique. *Sci Rep-Uk.* (2016) 6:31795. doi: 10.1038/srep31795
24. Fu Q, Liu Z, Huang Y, Lu Y, Zhang M. Comparative proteomic analysis of mature and immature oocytes of the swamp buffalo (Bubalus bubalis). *Int J Mol Sci.* (2016) 17:94. doi: 10.3390/ijms17010094
25. Gygi SP, Corthals GL, Zhang Y, Rochon Y, Aebersold R. Evaluation of two-dimensional gel electrophoresis-based proteome analysis technology. *Proc Natl Acad Sci U S A.* (2000) 97:9390–5. doi: 10.1073/pnas.160270797
26. Thompson A, Schafer J, Kuhn K, Kienle S, Schwarz J, Schmidt G, et al. Tandem mass tags: a novel quantification strategy for comparative analysis of complex protein mixtures by MS/MS. *Anal Chem.* (2003) 75:1895–904. doi: 10.1021/ac030267r
27. Pagel O, Loroch S, Sickmann A, Zahedi RP. Current strategies and findings in clinically relevant post-translational modification-specific proteomics.

Expert Rev Proteomic. (2015) 12:235–53. doi: 10.1586/14789450.2015.1042867
28. Peterson AC, Russell JD, Bailey DJ, Westphall MS, Coon JJ. Parallel reaction monitoring for high resolution and high mass accuracy quantitative, targeted proteomics. *Mol Cell Proteomics.* (2012) 11:1475–88. doi: 10.1074/mcp.O112.020131
29. Jia B, Xiang D, Fu X, Shao Q, Hong Q, Quan G, et al. Proteomic changes of porcine oocytes after vitrification and subsequent *in vitro* maturation: a tandem mass tag-based quantitative analysis. *Front Cell Dev Biol.* (2020) 8:614577. doi: 10.3389/fcell.2020.614577
30. Jia BY, Xiang DC, Zhang B, Quan GB, Shao QY, Hong QH, et al. Quality of vitrified porcine immature oocytes is improved by coculture with fresh oocytes during *in vitro* maturation. *Mol Reprod Dev.* (2019) 86:1615–27. doi: 10.1002/mrd.23249
31. Funahashi H, Cantley TC, Day BN. Synchronization of meiosis in porcine oocytes by exposure to dibutyryl cyclic adenosine monophosphate improves developmental competence following *in vitro* fertilization. *Biol Reprod.* (1997) 57:49–53. doi: 10.1095/biolreprod57.1.49
32. Barrell D, Dimmer E, Huntley RP, Binns D, O'Donovan C, Apweiler R. The GOA database in 2009–an integrated gene ontology annotation resource. *Nucleic Acids Res.* (2009) 37:D396–403. doi: 10.1093/nar/gkn803
33. Kanehisa M, Furumichi M, Tanabe M, Sato Y, Morishima K. KEGG new perspectives on genomes, pathways, diseases and drugs. *Nucleic Acids Res.* (2017) 45:D353–61. doi: 10.1093/nar/gkw1092
34. Zhou Y, Zhou B, Pache L, Chang M, Khodabakhshi AH, Tanaseichuk O, et al. Metascape provides a biologist-oriented resource for the analysis of systems-level datasets. *Nat Commun.* (2019) 10:1523. doi: 10.1038/s41467-019-09234-6
35. MacLean B, Tomazela DM, Shulman N, Chambers M, Finney GL, Frewen B, et al. Skyline: an open source document editor for creating and analyzing targeted proteomics experiments. *Bioinformatics.* (2010) 26:966–8. doi: 10.1093/bioinformatics/btq054
36. Ge C, Lu W, Chen A. Quantitative proteomic reveals the dynamic of protein profile during final oocyte maturation in zebrafish. *Biochem Biophys Res Commun.* (2017) 490:657–63. doi: 10.1016/j.bbrc.2017.06.093
37. Xie H, Wang Y, Jiao G, Kong D, Li Q, Li H, et al. Effects of glucose metabolism during *in vitro* maturation on cytoplasmic maturation of mouse oocytes. *Sci Rep.* (2016) 6:20764. doi: 10.1038/srep20764
38. Yuan B, Liang S, Kwon J, Jin Y, Park S, Wang H, et al. The role of glucose metabolism on porcine oocyte cytoplasmic maturation and its possible mechanisms. *PLoS ONE.* (2016) 11:e168329. doi: 10.1371/journal.pone.0168329
39. Jansen S, Pantaleon M, Kaye PL. Characterization and regulation of monocarboxylate cotransporters slc16a7 and slc16a3 in preimplantation mouse embryos. *Biol Reprod.* (2008) 79:84–92. doi: 10.1095/biolreprod.107.066811
40. Chen D, Zou J, Zhao Z, Tang X, Deng Z, Jia J, et al. TXNDC9 promotes hepatocellular carcinoma progression by positive regulation of MYC-mediated transcriptional network. *Cell Death Dis.* (2018) 9:1110. doi: 10.1038/s41419-018-1150-4
41. Ma F, Hou L, Yang L. Txndc9 is required for meiotic maturation of mouse oocytes. *Biomed Res Int.* (2017) 2017:6265890. doi: 10.1155/2017/6265890
42. Kajdasz A, Warzych E, Derebecka N, Madeja ZE, Lechniak D, Wesoly J, et al. Lipid stores and lipid metabolism associated gene expression in porcine and bovine parthenogenetic embryos revealed by fluorescent staining and RNA-seq. *Int J Mol Sci.* (2020) 21:6488. doi: 10.3390/ijms21186488
43. Kim EH, Kim GA, Taweechaipaisankul A, Ridlo MR, Lee SH, Ra K, et al. Phytanic acid-derived peroxisomal lipid metabolism in porcine oocytes. *Theriogenology.* (2020) 157:276–85. doi: 10.1016/j.theriogenology.2020.07.007
44. Kaushik S, Cuervo AM. Degradation of lipid droplet-associated proteins by chaperone-mediated autophagy facilitates lipolysis. *Nat Cell Biol.* (2015) 17:759–70. doi: 10.1038/ncb3166
45. Nishimura Y, Kano K, Naito K. Porcine CPEB1 is involved in Cyclin B translation and meiotic resumption in porcine oocytes. *Anim Sci J.* (2010) 81:444–52. doi: 10.1111/j.1740-0929.2010.00755.x
46. Wei X, Gao C, Luo J, Zhang W, Qi S, Liang W, et al. Hec1 inhibition alters spindle morphology and chromosome alignment in porcine oocytes. *Mol Biol Rep.* (2014) 41:5089–95. doi: 10.1007/s11033-014-3374-4
47. Zhang Y, Liu J, Peng X, Zhu C, Han J, Luo J, et al. KIF20A regulates porcine oocyte maturation and early embryo development. *PLoS ONE.* (2014) 9:e102898. doi: 10.1371/journal.pone.0102898
48. Choi JW, Zhou W, Nie ZW, Niu YJ, Shin KT, Cui XS. Spindlin1 alters the metaphase to anaphase transition in meiosis I through regulation of BUB3 expression in porcine oocytes. *J Cell Physiol.* (2018) 234:8963–74. doi: 10.1002/jcp.27566
49. Fujioka YA, Onuma A, Fujii W, Sugiura K, Naito K. Contributions of UBE2C and UBE2S to meiotic progression of porcine oocytes. *J Reprod Dev.* (2018) 64:253–9. doi: 10.1262/jrd.2018-006
50. Xie B, Qin Z, Liu S, Nong S, Ma Q, Chen B, et al. Cloning of porcine pituitary tumor transforming gene 1 and its expression in porcine oocytes and embryos. *PLoS ONE.* (2016) 11:e153189. doi: 10.1371/journal.pone.0153189
51. Hanna CB, Mudaliar D, John K, Allen CL, Sun L, Hawkinson JE, et al. Development of WEE2 kinase inhibitors as novel non-hormonal female contraceptives that target meiosis. *Biol Reprod.* (2020) 103:368–77. doi: 10.1093/biolre/ioaa097
52. Kawai K, Harada T, Ishikawa T, Sugiyama R, Kawamura T, Yoshida A, et al. Parental age and gene expression profiles in individual human blastocysts. *Sci Rep.* (2018) 8:2380. doi: 10.1038/s41598-018-20614-8
53. Anger M, Stein P, Schultz RM. CDC6 Requirement for spindle formation during maturation of mouse oocytes1. *Biol Reprod.* (2005) 72:188–94. doi: 10.1095/biolreprod.104.035451
54. Ferrer-Vaquer A, Barragan M, Rodriguez A, Vassena R. Altered cytoplasmic maturation in rescued *in vitro* matured oocytes. *Hum Reprod.* (2019) 34:1095–105. doi: 10.1093/humrep/dez052
55. Camlin NJ, McLaughlin EA, Holt JE. Motoring through: the role of kinesin superfamily proteins in female meiosis. *Hum Reprod Update.* (2017) 23:409–20. doi: 10.1093/humupd/dmx010
56. Sun Q, Schatten H. Regulation of dynamic events by microfilaments during oocyte maturation and fertilization. *Reproduction.* (2006) 131:193–205. doi: 10.1530/rep.1.00847
57. Shimada M, Nishibori M, Yamashita Y. Effects of adding luteinizing hormone to a medium containing follicle stimulating hormone on progesterone-induced differentiation of cumulus cells during meiotic resumption of porcine oocytes. *Anim Sci J.* (2004) 75:515–23. doi: 10.1111/j.1740-0929.2004.00222.x
58. Cao L, Jiang J, Fan H. Positive feedback stimulation of Ccnb1 and Mos mRNA translation by mapk cascade during mouse oocyte maturation. *Front Cell Dev Biol.* (2020) 8:609430. doi: 10.3389/fcell.2020.609430
59. Jia L, Li B, Yu H. The Bub1–Plk1 kinase complex promotes spindle checkpoint signalling through Cdc20 phosphorylation. *Nat Commun.* (2016) 7:10818. doi: 10.1038/ncomms10818
60. Tumová L, Petr J, Žalmanová T, Chmelíková E, Kott T, Tichovská H, et al. Calcineurin expression and localisation during porcine oocyte growth and meiotic maturation. *Anim Reprod Sci.* (2013) 141:154–63. doi: 10.1016/j.anireprosci.2013.07.011
61. Wang L, Zhen Y, Liu X, Cao J, Wang Y, Huo L. Inhibition of calcineurin by FK506 stimulates germinal vesicle breakdown of mouse oocytes in hypoxanthine-supplemented medium. *PeerJ.* (2017) 5:e3032. doi: 10.7717/peerj.3032
62. Pennarossa G, Gandolfi F, Brevini TAL. Biomechanical signaling in oocytes and parthenogenetic cells. *Front Cell Dev Biol.* (2021) 9:646945. doi: 10.3389/fcell.2021.646945
63. Baumann C, Ma W, Wang X, Kandasamy MK, Viveiros MM, De La Fuente R. Helicase LSH/Hells regulates kinetochore function, histone H3/Thr3 phosphorylation and centromere transcription during oocyte meiosis. *Nat Commun.* (2020) 11:4486. doi: 10.1038/s41467-020-18009-3
64. Balboula AZ, Stein P, Schultz RM, Schindler K. Knockdown of RBBP7 unveils a requirement of histone deacetylation for CPC function in mouse oocytes. *Cell Cycle.* (2014) 13:600–11. doi: 10.4161/cc.27410
65. Balboula AZ, Stein P, Schultz RM, Schindler K. RBBP4 regulates histone deacetylation and bipolar spindle assembly during oocyte maturation in the mouse. *Biol Reprod.* (2015) 92:105. doi: 10.1095/biolreprod.115.128298
66. Kleppe L, Karlsen Ø, Edvardsen RB, Norberg B, Andersson E, Taranger GL, et al. Cortisol treatment of prespawning female cod affects cytogenesis related factors in eggs and embryos. *Gen Comp Endocr.* (2013) 189:84–95. doi: 10.1016/j.ygcen.2013.04.028

67. Chermuła B, Brazert M, Jeseta M, Ozegowska K, Sujka-Kordowska P, Konwerska A, et al. The unique mechanisms of cellular proliferation, migration and apoptosis are regulated through oocyte maturational development—a complete transcriptomic and histochemical study. *Int J Mol Sci.* (2019) 20:84. doi: 10.3390/ijms20010084

Conflict of Interest: The authors declare that the research was conducted in the absence of any commercial or financial relationships that could be construed as a potential conflict of interest.

Publisher's Note: All claims expressed in this article are solely those of the authors and do not necessarily represent those of their affiliated organizations, or those of the publisher, the editors and the reviewers. Any product that may be evaluated in this article, or claim that may be made by its manufacturer, is not guaranteed or endorsed by the publisher.

frontiers in Veterinary Science

ORIGINAL RESEARCH
published: 28 March 2022
doi: 10.3389/fvets.2022.845709

Identification of Potential Molecular Mechanism Related to Infertile Endometriosis

Xiushen Li[1,2,3†], *Li Guo*[4†], *Weiwen Zhang*[1], *Junli He*[5], *Lisha Ai*[6], *Chengwei Yu*[7,8*], *Hao Wang*[1,2,3*] *and Weizheng Liang*[5*]

[1] Department of Obstetrics and Gynecology, Shenzhen University General Hospital, Shenzhen, China, [2] Guangdong Key Laboratory for Biomedical Measurements and Ultrasound Imaging, School of Biomedical Engineering, Shenzhen University Health Science Center, Shenzhen, China, [3] Shenzhen Key Laboratory, Shenzhen University General Hospital, Shenzhen, China, [4] School of Pharmaceutical Sciences, Health Science Center, Shenzhen University, Shenzhen, China, [5] Department of Pediatrics, Shenzhen University General Hospital, Shenzhen, China, [6] Department of Teaching and Research, Shenzhen University General Hospital, Shenzhen, China, [7] School of Future Technology, University of Chinese Academy of Sciences, Beijing, China, [8] Chinese Academy of Sciences (CAS) Key Laboratory of Genome Sciences and Information, Beijing Institute of Genomics, Chinese Academy of Sciences, Beijing, China

OPEN ACCESS

Edited by:
Yi Fang,
Northeast Institute of Geography and Agroecology (CAS), China

Reviewed by:
Songjie Feng,
University of Vienna, Austria
Xiaofei Guo,
Tianjin Academy of Agricultural Sciences, China

***Correspondence:**
Weizheng Liang
jmbb1203@126.com
Hao Wang
haowang0806@gmail.com
Chengwei Yu
yuchengwei2019d@big.ac.cn

†These authors have contributed equally to this work and share first authorship

Specialty section:
This article was submitted to Animal Reproduction - Theriogenology, a section of the journal Frontiers in Veterinary Science

Received: *30 December 2021*
Accepted: *28 February 2022*
Published: *28 March 2022*

Citation:
Li X, Guo L, Zhang W, He J, Ai L, Yu C, Wang H and Liang W (2022) Identification of Potential Molecular Mechanism Related to Infertile Endometriosis. Front. Vet. Sci. 9:845709. doi: 10.3389/fvets.2022.845709

Objectives: In this research, we aim to explore the bioinformatic mechanism of infertile endometriosis in order to identify new treatment targets and molecular mechanism.

Methods: The Gene Expression Omnibus (GEO) database was used to download MRNA sequencing data from infertile endometriosis patients. The "limma" package in R software was used to find differentially expressed genes (DEGs). Weighted gene co-expression network analysis (WGCNA) was used to classify genes into modules, further obtained the correlation coefficient between the modules and infertility endometriosis. The intersection genes of the most disease-related modular genes and DEGs are called gene set 1. To clarify the molecular mechanisms and potential therapeutic targets for infertile endometriosis, we used Gene Ontology (GO), Kyoto Gene and Genome Encyclopedia (KEGG) enrichment, Protein-Protein Interaction (PPI) networks, and Gene Set Enrichment Analysis (GSEA) on these intersecting genes. We identified lncRNAs and miRNAs linked with infertility and created competing endogenous RNAs (ceRNA) regulation networks using the Human MicroRNA Disease Database (HMDD), mirTarBase database, and LncRNA Disease database.

Results: Firstly, WGCNA enrichment analysis was used to examine the infertile endometriosis dataset GSE120103, and we discovered that the Meorangered1 module was the most significantly related with infertile endometriosis. The intersection genes were mostly enriched in the metabolism of different amino acids, the cGMP-PKG signaling pathway, and the cAMP signaling pathway according to KEGG enrichment analysis. The Meorangered1 module genes and DEGs were then subjected to bioinformatic analysis. The hub genes in the PPI network were performed KEGG enrichment analysis, and the results were consistent with the intersection gene analysis. Finally, we used the database to identify 13 miRNAs and two lncRNAs linked to infertility in order to create the ceRNA regulatory network linked to infertile endometriosis.

Conclusion: In this study, we used a bioinformatics approach for the first time to identify amino acid metabolism as a possible major cause of infertility in patients with endometriosis and to provide potential targets for the diagnosis and treatment of these patients.

Keywords: infertile endometriosis, molecular mechanism, GEO, bioinformatics, ceRNA

INTRODUCTION

Endometriosis, an estrogen-dependent disease, is characterized by the appearance of the endometrium outside the uterus (1). Laparoscopy is the most common approach for diagnosing endometriosis (2). Treatment methods include surgery and oral hormonal drugs, but both of which are usually accompanied by side effects. Although the theories of implantation, somatic epithelial metaplasia, and induction help to explain the pathophysiology of endometriosis to some extent, the mechanism of endometriosis formation remains unknown. Endometriosis can induce symptoms such as dysmenorrhea, dysuria, fatigue, deep intercourse pain, and infertility, which can seriously affect the patient's body, work, life, and psychology (3–5). About 30–50% of patients with endometriosis will be accompanied by infertility (6). However, the mechanism of infertile endometriosis is still unclear. Despite the fact that infertile endometriosis has a significant impact on patients, our knowledge of the condition is still restricted.

As a system biology tool, Weighted Gene Co-expression Network Analysis (WGCNA) can be used to analyze the gene expression patterns of multiple samples and cluster genes with similar expression patterns. WGCNA can explore the relationship between diseases and gene modules, which act as significant markers and signaling pathways in the occurrence and development of diseases (7, 8). Therefore, WGCNA is frequently employed to investigate the molecular mechanisms of various diseases including coronary artery disease, neuropathic pain, colon adenocarcinoma, and acute myocardial infarction (9–12).

Therefore, in this research, we employed WGCNA to investigate the gene modules that caused infertile endometriosis and further explored the signaling pathways and competing endogenous RNA (ceRNA) regulatory networks involved in pathogenesis through bioinformatics. Our findings may provide new molecular mechanisms and therapeutic targets for the therapy of infertile endometriosis.

MATERIALS AND METHODS

Data Filtered and Download

We used the keywords "endometriosis" and "infertility" to search the Gene Expression Omnibus (GEO) database (http://ncbi.nlm.nih.gov/geo/). The following conditions were used as screening criteria for this study: (1) The data set must include both fertile and infertile endometriosis patients, with a minimum of 5 patients in each group; (2) The type of tissue used for sequencing should be consistent; (3) The data set included in this study must contain the original sequencing data. Finally, the GSE120103 data set was screened out for further investigation.

DEGs Identification and Bioinformatics Analysis

Only genes with adjusted $p < 0.001$ and $|\log2FC| > 2$ were considered DEGs in this investigation, we searched the GSE120103 data set by the "limma" package in R software. The "clusterProfiler" package in R software was used for Gene Ontology. (GO) enrichment analysis and Kyoto Encyclopedia of Genes and Genomes (KEGG) enrichment analysis of DEGs. We displayed the results of the enrichment analysis through the "ggplot2" package in R software. We used the STRING database (https://cn.string-db.org/) to generate the protein-protein interaction (PPI) network where the gene interaction score was more than 0.9.

WGCEA

WGCNA can integrate the results of sequencing into biologically significant co-expressed gene modules and analyze the correlation between these gene modules and diseases (12). Therefore, we used WGCNA to explore modules related to infertile endometriosis. We used the "WGCNA" package in R software to perform WGCNA analysis on the GSE120103 data set. we utilized the "pickSoftThreshold" function to filter the soft powers in this study. The topological overlap matrix (TOM) and the accompanying dissimilarity matrix (1-TOM) were then obtained based on the adjacency matrix's construction. The "cutreeDynamic" function in R software was used to identify different gene modules. Furthermore, the "moduleEigengenes" function and the "mergeCloseModules" function in R software were used to cluster and merge gene modules, respectively. Finally, the correlation coefficient between the modular characteristic gene and the disease was calculated.

Identification the Shared Gene and Bioinformatics Analysis

We chose the MEorangered1 module because it had the strongest association with infertile endometriosis. DEGs and the genes in MEorangered1 were intersected. The Venn diagram was used to represent these intersecting genes, which were referred to as gene set 1. GO enrichment analysis and KEGG enrichment analysis were performed on gene set 1 by using R software. PPI networks

Abbreviations: GEO, Gene Expression Omnibus; WGCNA, Weighted Gene Co-Expression Network Analysis; DEGs, differentially expressed genes; GO, Gene Ontology; KEGG, Kyoto Encyclopedia of Genes and Genomes; PPI, protein protein interaction; GSEA, Gene Set Enrichment Analysis; miRNA, microRNA; ceRNA, competing endogenous RNAs; HMDD, Human MicroRNA Disease Database; TOM, topological overlap matrix; ncRNAs, Non-coding RNAs.

were constructed though the STRING database. Cytoscape is a professional biological data analysis program often used to visualize PPI networks. In this study, we used the "CytoNCA" plug-in in Cytoscape software to calculate the Betweenness, Closeness, Degree, Eigenvector, Network, and Local Average Connectivity between nodes. Hub genes were defined as nodes with values above the median of these features. The PPI network between Hub genes was visualized using Cytoscape software.

Identify of microRNA and lncRNA

MicroRNA(miRNA) has the ability to promote or inhibit mRNA degradation and translation. We searched for infertility-related miRNAs through the Human MicroRNA Disease Database (HMDD) (http://www.cuilab.cn/hmdd/) and the MiRTarBase database (https://mirtarbase.cuhk.edu.cn/~miRTarBase/miRTarBase_2022/php/index.php) and the online tool LncBase Experimental v.2 (http://diana.imis.athena-innovation.gr/DianaTools/index.php?r=site/page&view=software) to find mRNAs and lncRNAs associated with these miRNAs. To search for lncRNAs associated with infertility, We used the LncRNADisease database (http://www.cuilab.cn/lncrnadisease) constructed by Peking University.

Construction of ceRNA Regulate Network

We took intersections of target genes for each miRNA, DEGs and genes in the MEorangered1 module, respectively. The Degree value of each node in the ceRNA network was calculated using the cytoHubba plug-in in the cytoscape software. The ceRNA regulate network was visualized using Cytoscape software.

RESULTS

Information of the GEO Dataset

We identified 18 datasets in the GEO database using the keywords "endometriosis" and "infertility." According to our selection criteria, only the GSE120103 dataset, based on the GPL6480 sequencing platform, was retrieved. We used endometrial tissue sequencing data from 9 infertile and 9 fertile patients with endometriosis for bioinformatic analysis in this study.

Identification of DEGs

Using the "limma" package in R software, we discovered 3,149 differentially expressed genes (**Supplementary Table 1**, **Figure 1A**). Low-expressed genes were represented by green dots on the left and high-expressed genes were represented by red dots on the right. We generated the heat map to show the 50 most significantly up-regulated and down-regulated genes in each sample, as shown in **Figure 1B**. The level of gene expression was linked to color. Low-level expression was represented by green, whereas high-level genes were represented by red. We discovered 8 pathways using GSEA (only showed signaling pathways with $p < 0.05$), including arachidonic acid and selenium amino acid metabolism, calcium signaling pathway, steroid hormone biosynthesis, and JAK-STAT signaling pathway (**Figure 1C**).

Results of the WGCNA

WGCNA constructs the weighted co-expression network based on all genes' expression levels obtained by sequencing to indicate the association between gene modules and diseases, as well as the strength of the relationship. 22 co-expressed gene modules were discovered by WGCNA analysis (**Figure 2A**). As shown in **Figure 2B**, the MEorangered1 module (**Supplementary Table 2**) had the strongest relationship with infertile endometriosis ($R = 0.93$, $p = 2e\text{-}8$). As shown in **Figure 2C**, we integrated the genes in the MEorangered1 module with the DEG to yield 1857 overlapping genes, which we termed gene set 1 (**Supplementary Table 3**).

Bioinformatics Analysis of Gene Set 1

The results of the GO enrichment analysis for gene set 1 were shown in **Figure 3A** (**Supplementary Table 4**). In terms of Biological Process, results closely related to infertility include single fertilization, fertilization, and cellular process involved in reproduction in multicellular organisms. In terms of Cellular Component, it was mainly related to postsynaptic, transporter complex, ion channel complex, and transmembrane transporter complex. In terms of Molecular Function, it was mainly related to neurotransmitter receptor activity, ion channel activity, gated channel activity and substrate-specific channel activity. Infertile endometriosis might be linked to amino acid metabolism (Glycine, Serine, Tryptophan, Tyrosine, Phenylalanine, and Threonine), Gastric acid secretion, Bile secretion, Collecting duct acid secretion, cGMP–PKG signaling pathway, cAMP signaling pathway, Calcium signaling pathway, and so on, according to the results of KEGG enrichment analysis (**Supplementary Table 5**).

Identification of Hub Genes

Though the STRING database, we generated the PPI network for Gene set 1 with 342 nodes and 397 edges (**Figure 3C**, **Supplementary Table 6**). Only non-isolated nodes (linked to at least one node) and edges with gene interaction values > 0.9 are shown in the PPI network. The more genes related with a node, the redder it is. We used cytoscape software to identify nodes with values greater than the median based on mediator, proximity, degree, eigenvector, network, and local average connectivity in order to construct the PPI network (**Figure 3D**, **Supplementary Tables 7**, **8**). The circle's diameter is proportional to the node's degree.

Bioinformatics Analysis of Hub Genes

We performed GO enrichment analysis on the hub genes retrieved (**Figure 3E**, **Supplementary Table 9**). In terms of biological processes, the findings were mainly related to the metabolic processes of the human body, including serotonin, indole-containing compound, catechol-containing compound, catecholamine, amine, and neurotransmitter etc. In terms of cell components, it was mainly related to cytosolic ribosome, cell leading edge, actomyosin, pseudopodium, etc. In terms of Molecular Function, the results mainly related to oxidoreductase activity, monooxygenase activity, steroid

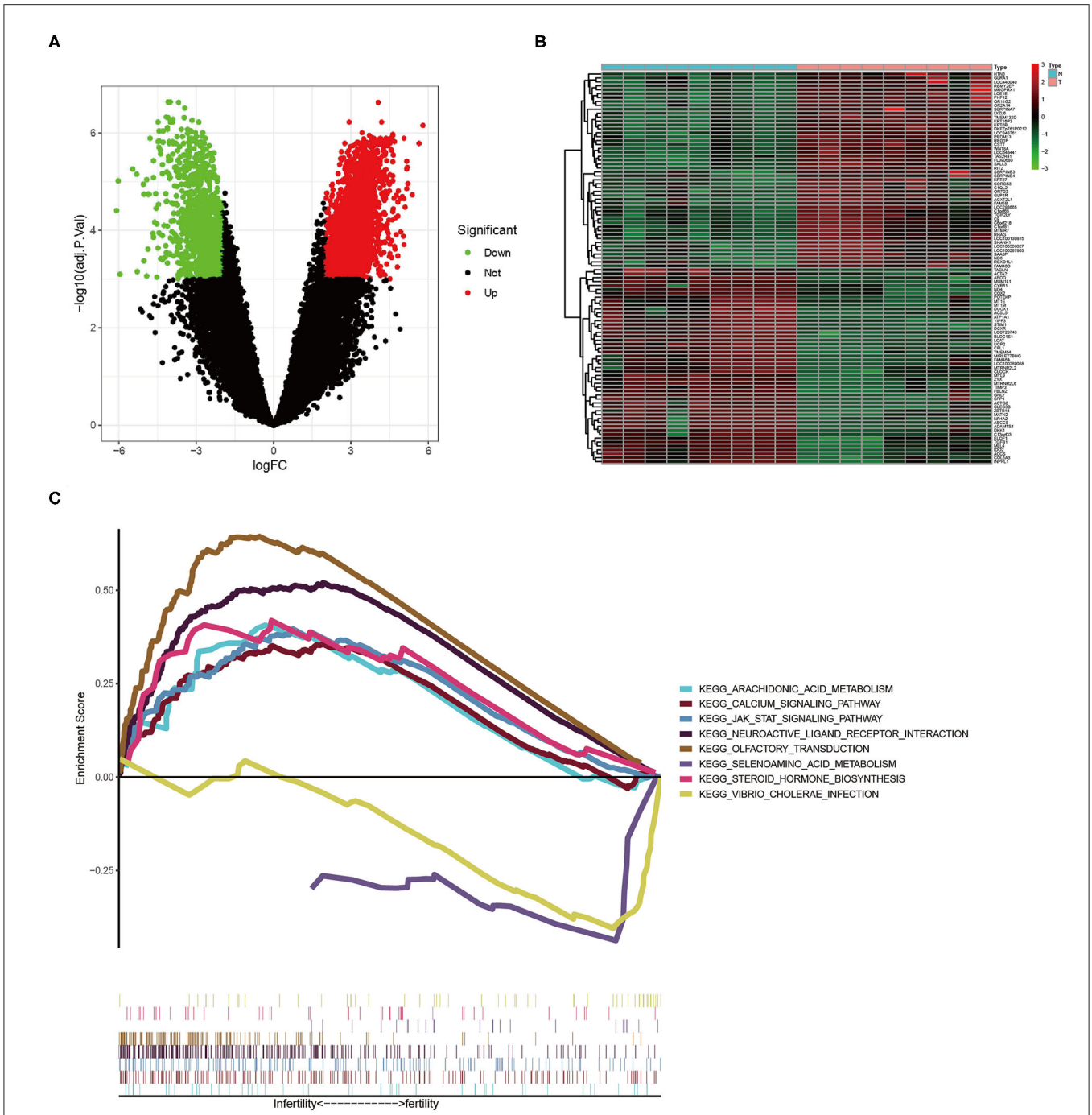

FIGURE 1 | (A) The volcano plot of DEGs. **(B)** The heat map of DEGs (only the 50 most up-regulated and down-regulated genes are shown, respectively). **(C)** The results of GSEA enrichment analysis.

hydroxylase activity, heme binding, oxygen binding. The results of KEGG enrichment analysis found that the cause of infertility in endometriosis may be related to the metabolism of a variety of amino acids (tyrosine, phenylalanine, tryptophan, arginine, proline, etc.), Ras signaling pathway, cAMP signaling pathway, Ovarian steroidogenesis, and so on (**Figure 3F**, **Supplementary Table 10**).

Potential Mechanism of Infertile Endometriosis

We intersected the pathways in the KEGG enrichment analysis results of hub genes and gene set 1, and found a total of 10 overlapping pathways (**Figure 4A**, **Supplementary Table 11**). The "enrichplot" package in R software was used to identify and illustrate the relationships between these 10 pathways. As

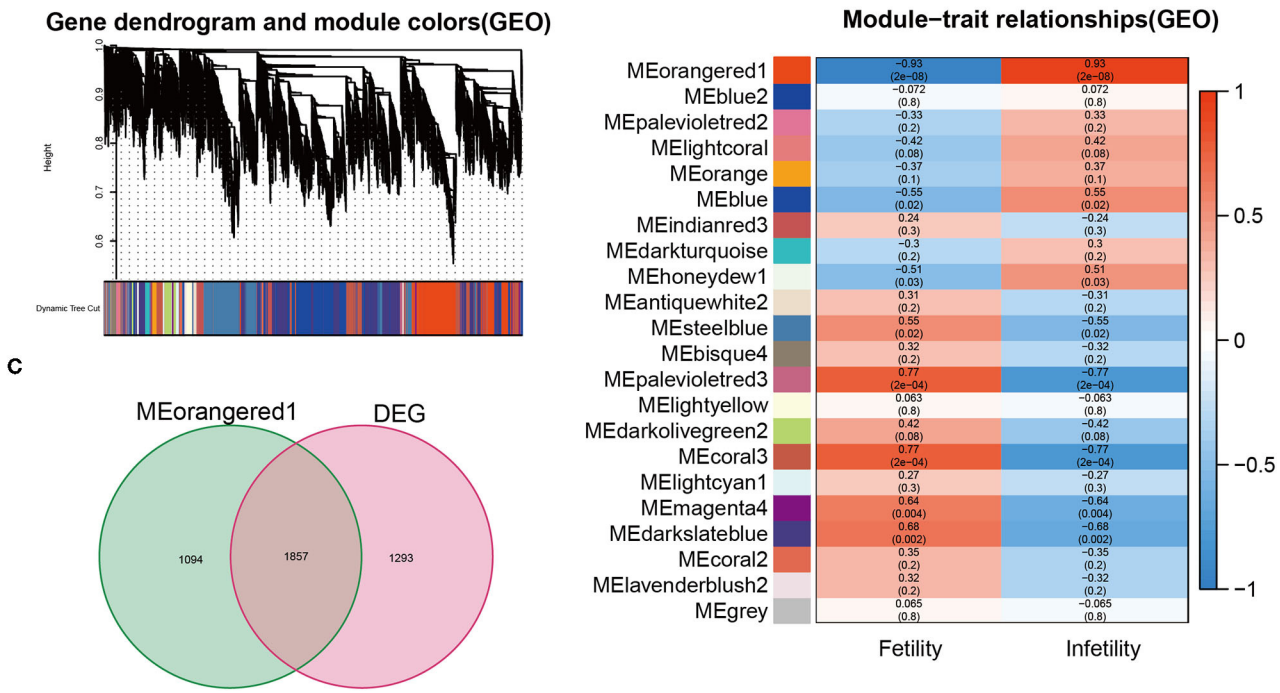

FIGURE 2 | (A) The cluster dendrogram of co-expression genes in infertile endometriosis. **(B)** Module–trait relationships in infertile endometriosis. **(C)** The intersection genes between DEG and the orangered1 modules.

shown in **Figure 4B**, the mechanism of infertile endometriosis might be related to the metabolism of multiple amino acids (Tryptophan, Tyrosine, Phenylalanine, Glycine, serine and threonine), and chemical addiction (Nicotine, Cocaine, Amphetamine), Serotonergic synapse, cAMP signaling pathway, Long-term potentiation.

Construction of ceRNA Network

Through using HMDD database, we discovered 13 miRNAs related to infertility, including hsa-let-7b, hsa-mir-122, hsa-mir-1302, hsa-mir-133b, hsa-mir-17, and others (**Supplementary Table 12**). Through the mirTarBase database, the mRNAs controlled by these 13 miRNAs were predicted (**Supplementary Table 13**). Following that, we crossed each miRNA target gene with gene set 1 (**Supplementary Table 14**). We discovered two lncRNAs associated to infertility in the LncRNADisease database: H19 and NEAT1. We used the online tool LncBase Experimental v.2 to search for the relationship between infertility-related lncRNAs and miRNAs. Finally, we used Cytoscape software to create the ceRNA regulatory network (**Figure 5**). mRNA, miRNA, and lncRNA are represented by yellow circle nodes, red triangle nodes, and blue diamond nodes, respectively. The darker the color, the more nodes are connected to the node.

DISCUSSION

Endometriosis is a non-malignant gynecological disease whose pathophysiology is currently unknown. For the diagnosis of endometriosis, laparoscopy remains the gold standard, and no specific biomarkers or therapeutic targets have been identified (13, 14). It is estimated that about 10% of women of childbearing age suffer from endometriosis. Short menstrual cycles, night work, and short breastfeeding time are high risk factors for endometriosis (13–15). Infertility is one of the most prevalent endometriosis complications, and it has the significant impact on patients' lives. However, the molecular mechanisms by which endometriosis causes infertility are unclear. In this study, we download the patient's transcriptome data and used bioinformatics methods to explore the molecular mechanism and regulatory network between infertility and endometriosis. The results of this study may provide a new research direction for infertility endometriosis and provide help for the clinical treatment of patients.

Through KEGG enrichment analysis of genes set 1, we identified multiple pathways closely associated with infertile endometriosis, including toxic substance addiction (Nicotine, Morphine, Cocaine), estrogen signaling pathways, calcium signaling pathways and metabolism of multiple amino acids (Phenylalanine, Glycine, serine, threonine, Tryptophan, Tyrosine). Smoking during pregnancy has been associated with the development of endometriosis by the mechanism related to smoking-induced changes in maternal estrogen levels (16–18). Nicotine, which is found in cigarette smoke, is one of the chemicals known to be detrimental to human health. Nicotine affects the female reproductive system by suppressing the expression of receptors for steroid hormones in endometrial cells (19). Morphine, a member of the opium alkaloids family,

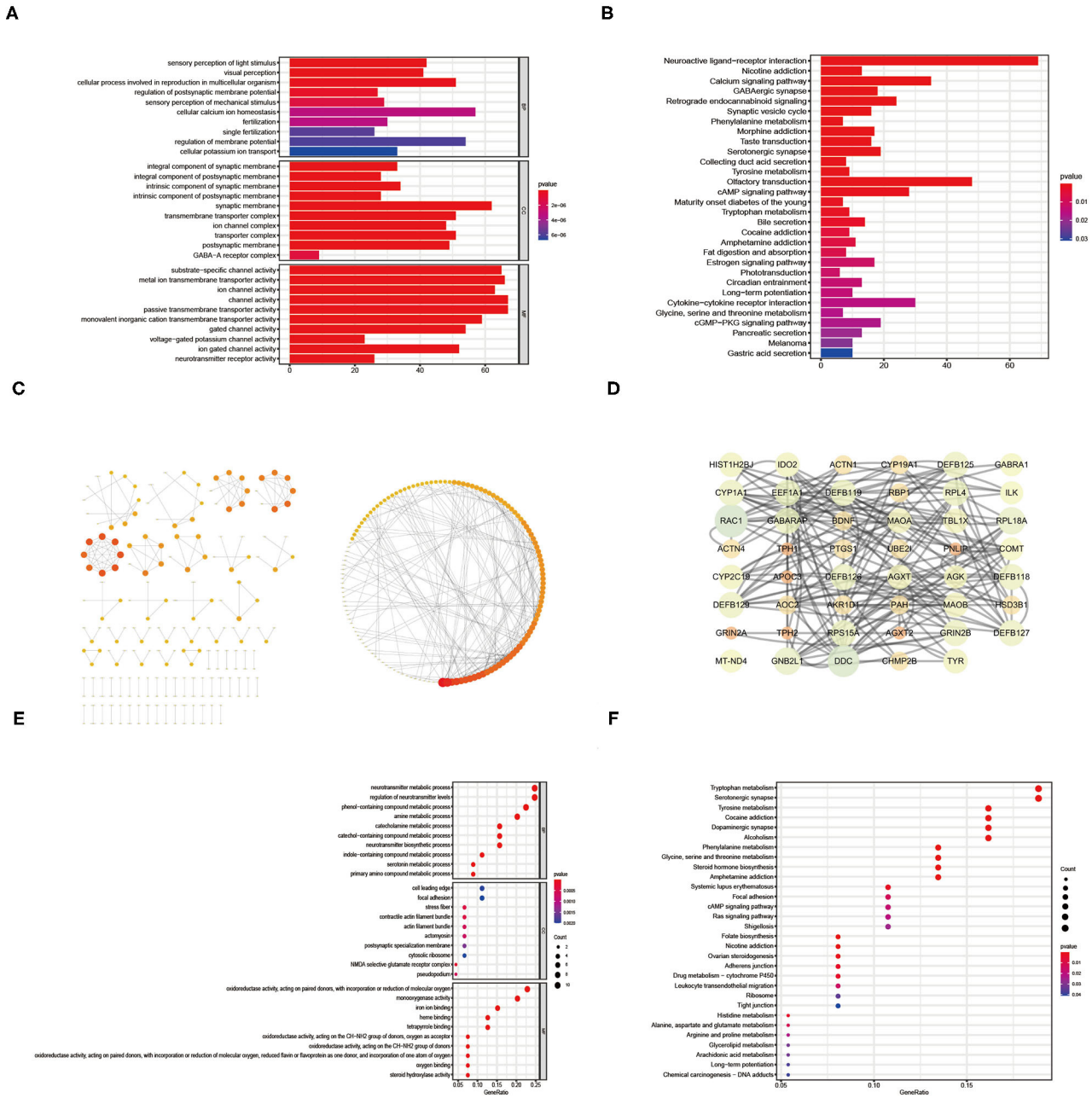

FIGURE 3 | The GO enrichment analysis, KEGG enrichment analysis and PPI network results of intersection genes between DEG and the Meorangered1 modules **(A–C)**. The GO enrichment analysis, KEGG enrichment analysis and PPI network results of hub genes from intersection genes between DEG and the Meorangered1 modules **(D–F)**.

is associated with female reproductive system. The ovaries of rats treated with morphine may develop cystic changes that lead to the development of anovulatory infertility (20). Cocaine may be a risk factor for primary infertility. Women who use cocaine have a considerably higher risk of infertility linked to malformed fallopian tubes than women who do not use cocaine (21). When endometrial tissue forms over other tissues, the body's estrogen signaling pathways are disrupted, leading to pelvic pain and reducing the likelihood of pregnancy (22). One of estrogen's effectors, brain-derived neurotrophic factor, can be utilized as a biomarker to measure female infertility. Brain-derived neurotrophic factor is associated with the proliferation of endometrial tissue and is considered a potential target for infertile patients with endometriosis (23). The calcium signaling pathway is considered to be an important component of human reproduction as it influences the biological processes of cell

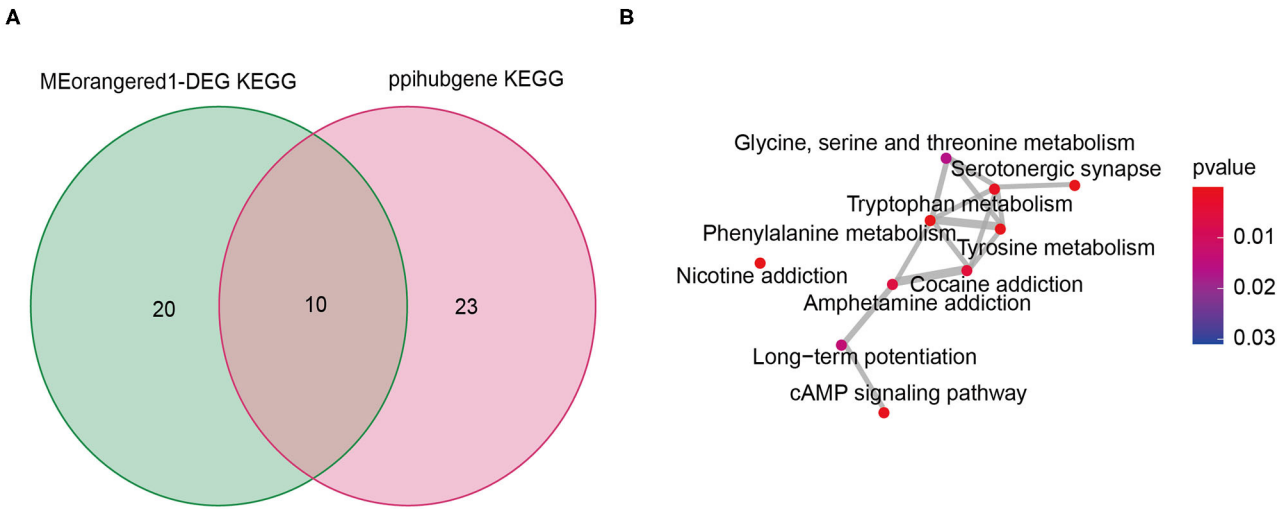

FIGURE 4 | The shared signaling pathway of KEGG enrichment analysis from intersection genes between DEG and the Meorangered1 modules and hub genes **(A)**. Crosstalk analysis of the shared signaling pathway **(B)**.

division, differentiation and death (24, 25). By regulating downstream effectors, the calcium signaling system integrates and decodes information from the cellular microenvironment to mediate biological processes like egg activation and embryonic development (26). There is a strong correlation between enteral nutrition and reproduction. Amino acids in the diet influence key molecules involved in a range of biological processes during conception, such as oocyte fertilization and embryo implantation (27).

PPI network was used to screen the hub genes in gene set 1. To further clarify the molecular mechanisms associated with the development of infertile endometriosis, we intersected the KEGG enrichment results of the hub genes and the genes in gene set 1 to obtain a total of 10 pathways. We believe that these ten pathways are highly relevant to the molecular mechanisms that lead to the onset of infertility in endometriosis. Of these, nicotine addiction and cocaine addiction are recognized risk factors for the emergence of infertility in women (28, 29). Two-fifths of the pathway involves amino acid metabolism and therefore we believe that abnormal amino acid metabolism leads to infertility in patients with endometriosis.

To find potential biomarkers and therapeutic targets for infertile endometriosis patients, the degree values of each node in the PPI network were calculated. The four genes with the highest degree values, DDC, RAC1, GNB2L1, and RPL18A, were identified as possible targets for the identification and therapy of infertile endometriosis. DDC catalyzes the manufacture of dopamine and serotonin, which helps govern neural function. Although DDC is implicated in apoptosis and has been linked to a number of human neurodegenerative illnesses, the mechanisms underpinning its link to infertility are unknown (30, 31). Down-regulation of RAC1 expression in mouse endometrium leads to embryo implantation failure (32). Through the AKT/NF-kappaB pathway, RAC1 is involved in inflammatory changes in endometrial tissue, which is a common cause of female infertility (33).

Endometriosis is a benign disease, but it has the ability to invade and maintain the survival function of ectopic tissue, similar to cancer. RPL18A is involved in the cycle arrest process of non-small cell lung cancer A549 cells by affecting the expression of several cell cycle-related proteins, including Cyclin A2 and Cyclin B1 (34). The expression of GNB2L1 was higher in ectopic endometrial tissue from patients with endometriosis than in normal patients, regardless of whether they were in the proliferative or secretory phase of the menstrual cycle. GNB2L1 is associated with the progression of endometriosis and contributes to the removal of ectopic endometrium by reducing cell proliferation and angiogenesis (35). Therefore, GNB2L1 has the potential to act as a biomarker and therapeutic target for endometriosis. These four genes may provide assistance in the clinical detection and treatment of infertility in patients with endometriosis.

Non-coding RNAs (ncRNAs) are not directly involved in protein translation, but they are involved in many biological processes in the body (36). ncRNAs are associated with the development of many diseases and can be divided into small RNAs and lncRNAs depending on their length. LncRNAs have functions as molecular scaffolds for chromatin and miRNA sponges, translating and degrading RNAs that are involved in the development of most diseases (37). As a type of small ncRNA, miRNA regulates gene expression mainly by silencing mRNA translation and degrading mRNA. LncRNA control gene expression by binding to miRNAs in a competitive manner. As a result, the ceRNA network connects the mRNAs, miRNAs, and lncRNAs, contributing to our understanding of the gene regulatory network and molecular mechanisms that lead to infertility in endometriosis patients. We searched the HMDD, mirTarBase database, and LncRNADisease database for miRNAs and lncRNAs linked to infertility, and then used

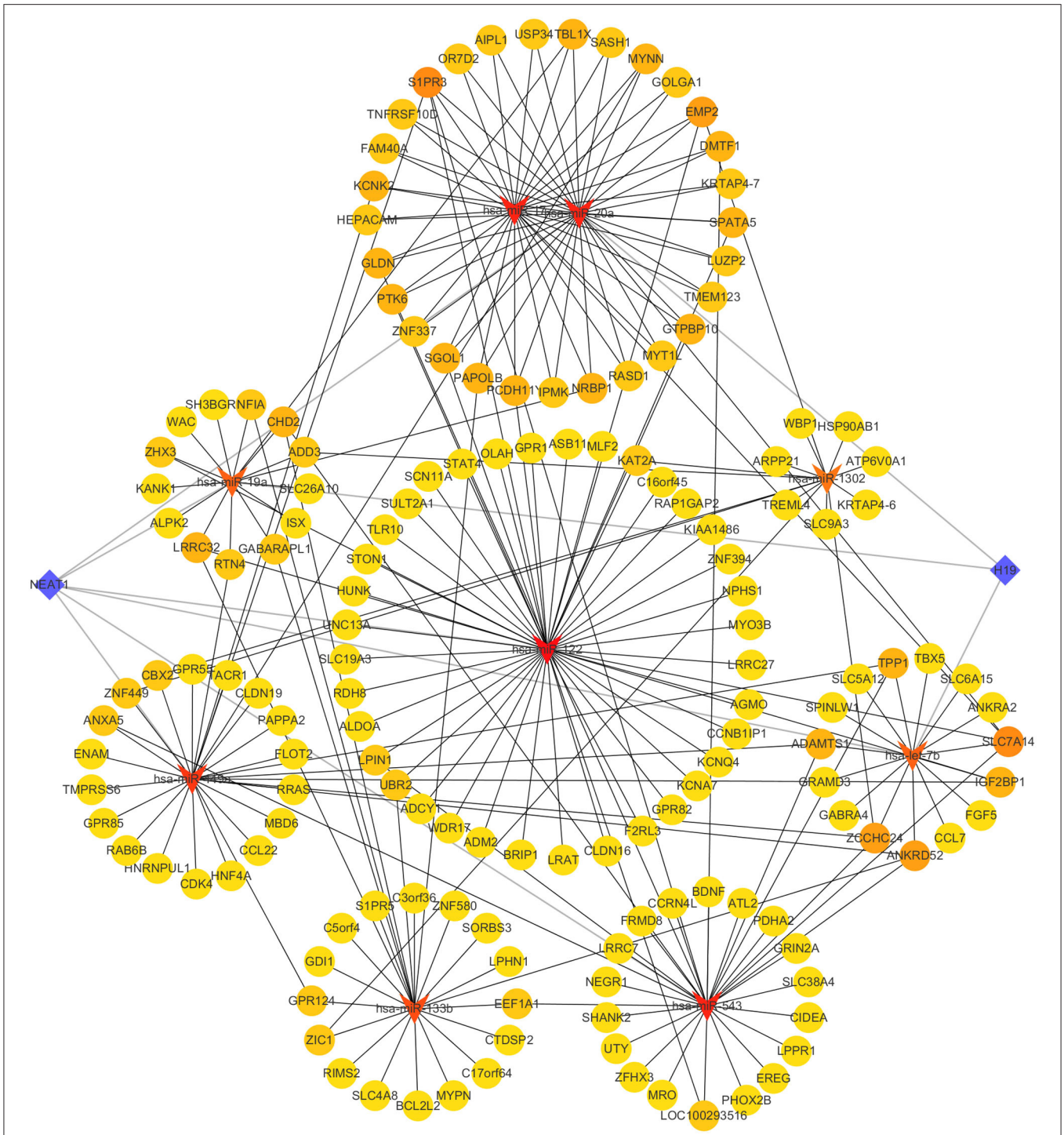

FIGURE 5 | The ceRNA regulatory network. Red triangles, yellow circles, and blue diamonds correspond to miRNAs, hub genes, and lncRNAs, respectively.

Cytoscape software to build a ceRNA regulatory network linked to infertile endometriosis. This ceRNA network can reveal the regulatory links between genes linked to infertility, as well as biomarkers and targets for the diagnosis and therapy of infertile endometriosis.

CONCLUSION

In this study, we included sequencing results of endometrial tissue from fertile and infertile patients with endometriosis. We discovered that the mechanism of

infertile endometriosis patients may be linked to amino acid metabolism by bioinformatics analysis. We also constructed the ceRNA regulatory network that could be linked to infertility in women with endometriosis. These findings could aid in the clinical treatment of patients.

DATA AVAILABILITY STATEMENT

The original contributions presented in the study are included in the article/**Supplementary Materials**, further inquiries can be directed to the corresponding authors.

AUTHOR CONTRIBUTIONS

WL, HW, XL, and CY developed the concept of the project and wrote the manuscript. XL and LG collected and analyzed the data with the help of WZ, JH, and LA. All authors reviewed and discussed the results and contributed to the paper preparation. All authors have read and approved the manuscript.

FUNDING

This study was supported by Shenzhen Key Laboratory Foundation (ZDSYS20200811143757022) and Shenzhen Science and Technology Innovation Commission Project (Grant No. JCYJ20180302174235893).

SUPPLEMENTARY MATERIAL

The Supplementary Material for this article can be found online at: https://www.frontiersin.org/articles/10.3389/fvets.2022.845709/full#supplementary-material

Supplementary Table 1 | DEGs.

Supplementary Table 2 | The genes in MEorangered1 module.

Supplementary Table 3 | The genes in gene set 1.

Supplementary Table 4 | The GO enrichment analysis results of gene set 1.

Supplementary Table 5 | The KEGG enrichment analysis results of gene set 1.

Supplementary Table 6 | The PPI network of gene set 1.

Supplementary Table 7 | Calculation results of betweenness, closeness, degree, eigenvector, network and local average connectivity-based method.

Supplementary Table 8 | The hub genes.

Supplementary Table 9 | The GO enrichment analysis results of hub genes.

Supplementary Table 10 | The KEGG enrichment analysis results of hub genes.

Supplementary Table 11 | Intersection of KEGG enrichment analysis results of hub genes and gene set 1.

Supplementary Table 12 | MiRNA related to infertility.

Supplementary Table 13 | Intersection of predicted miRNA target gene and gene set 1.

Supplementary Table 14 | MiRNA-mRNA network.

REFERENCES

1. Zondervan KT, Becker CM, Koga K, Missmer SA, Primers PVJNRD. Endometriosis. *Nat Rev Dis Primers.* (2018) 4:9. doi: 10.1038/s41572-018-0008-5
2. Zondervan KT, Becker CM, Missmer SA. Endometriosis. *N Engl J Med.* (2020) 382:1244–56. doi: 10.1056/NEJMra1810764
3. Gallagher JS, DiVasta AD, Vitonis AF, Sarda V, Laufer MR, Missmer SA. The impact of endometriosis on quality of life in adolescents. *J Adolescent Health.* (2018) 63:766–72. doi: 10.1016/j.jadohealth.2018.06.027
4. Rush G, Misajon R, Hunter JA, Gardner J, O'Brien KS. The relationship between endometriosis-related pelvic pain and symptom frequency, and subjective wellbeing. *Health Qual Life Outcomes.* (2019) 17:123. doi: 10.1186/s12955-019-1185-y
5. Nnoaham KE, Hummelshoj L, Webster P, d'Hooghe T, de Cicco Nardone F, de Cicco Nardone C, et al. Impact of endometriosis on quality of life and work productivity: a multicenter study across ten countries. *Fertility Sterility.* (2011) 96:366–73.e8. doi: 10.1016/j.fertnstert.2011.05.090
6. Giudice LC, Kao LC. Endometriosis. *Lancet.* (2004) 364:1789–99. doi: 10.1016/S0140-6736(04)17403-5
7. Langfelder P, Horvath S. Wgcna: an R package for weighted correlation network analysis. *BMC Bioinformatics.* (2008) 9:559. doi: 10.1186/1471-2105-9-559
8. Presson AP, Sobel EM, Papp JC, Suarez CJ, Whistler T, Rajeevan MS, et al. Integrated weighted gene co-expression network analysis with an application to chronic fatigue syndrome. *BMC Syst Biol.* (2008) 2:95. doi: 10.1186/1752-0509-2-95
9. Peng XY, Wang Y, Hu H, Zhang XJ, Li Q. Identification of the molecular subgroups in coronary artery disease by gene expression profiles. *J Cell Physiol.* (2019) 23, 16540–8. doi: 10.1002/jcp.28324
10. Cobos EJ, Nickerson CA, Gao F, Chandran V, Bravo-Caparrós I, González-Cano R, et al. Mechanistic differences in neuropathic pain modalities revealed by correlating behavior with global expression profiling. *Cell Rep.* (2018) 22:1301–12. doi: 10.1016/j.celrep.2018.01.006
11. Jiang C, Liu Y, Wen S, Xu C, Gu L. *In silico* development and clinical validation of novel 8 gene signature based on lipid metabolism related genes in colon adenocarcinoma. *Pharmacol Res.* (2021) 169:105644. doi: 10.1016/j.phrs.2021.105644
12. Wang Y, Zhang X, Duan M, Zhang C, Wang K, Feng L, et al. Identification of potential biomarkers associated with acute myocardial infarction by weighted gene coexpression network analysis. *Oxidative Med Cell Longevity.* (2021) 2021:5553811. doi: 10.1155/2021/5553811
13. Matalliotakis IM, Cakmak H, Fragouli YG, Goumenou AG, Mahutte NG, Arici A. Epidemiological characteristics in women with and without endometriosis in the yale series. *Arch Gynecol Obstetrics.* (2008) 277:389–93. doi: 10.1007/s00404-007-0479-1
14. Farland LV, Eliassen AH, Tamimi RM, Spiegelman D, Michels KB, Missmer SA. History of breast feeding and risk of incident endometriosis: prospective cohort study. *BMJ.* (2017) 358:j3778. doi: 10.1136/bmj.j3778
15. Schernhammer ES, Vitonis AF, Rich-Edwards J, Missmer SA. Rotating nightshift work and the risk of endometriosis in premenopausal women. *Am J Obstetrics Gynecol.* (2011) 205:476.e1–8. doi: 10.1016/j.ajog.2011.06.002
16. Buck Louis GM, Hediger ML, Peña JB. Intrauterine exposures and risk of endometriosis. *Hum Reprod.* (2007) 22:3232–6. doi: 10.1093/humrep/dem338
17. Hughes EG, Brennan BG. Does cigarette smoking impair natural or assisted fecundity? *Fertility Sterility.* (1996) 66:679–89. doi: 10.1016/S0015-0282(16)58618-X
18. Augood C, Duckitt K, Templeton AA. Smoking and female infertility: a systematic review and meta-analysis. *Human Reprod.* (1998) 13:1532–9. doi: 10.1093/humrep/13.6.1532

19. Totonchi H, Miladpour B, Mostafavi-Pour Z, Khademi F, Kasraeian M, Zal F. Quantitative analysis of expression level of estrogen and progesterone receptors and Vegf genes in human endometrial stromal cells after treatment with nicotine. *Toxicol Mech Methods*. (2016) 26:595–600. doi: 10.1080/15376516.2016.1218578
20. Karimi R, Karami M, Nadoushan MJ. Rat's polycystic ovary due to intraventromedial hypothalamus morphine injection. *Reprod Sci*. (2018) 25:867–72. doi: 10.1177/1933719117698581
21. Mueller BA, Daling JR, Weiss NS, Moore DE. Recreational drug use and the risk of primary infertility. *Epidemiology*. (1990) 1:195–200. doi: 10.1097/00001648-199005000-00003
22. Marquardt RM, Kim TH, Shin JH, Jeong JW. Progesterone and estrogen signaling in the endometrium: what goes wrong in endometriosis? *Int J Mol Sci*. (2019) 20:3822. doi: 10.3390/ijms20153822
23. Dong F, Zhang Q, Kong W, Chen J, Ma J, Wang L, et al. Regulation of endometrial cell proliferation by estrogen-induced Bdnf signaling pathway. *Gynecol Endocrinol*. (2017) 33:485–9. doi: 10.1080/09513590.2017.1295439
24. Stewart TA, Davis FM. An element for development: calcium signaling in mammalian reproduction and development. *Biochim Biophys Acta Mol Cell Res*. (2019) 1866:1230–8. doi: 10.1016/j.bbamcr.2019.02.016
25. Berridge MJ, Bootman MD, Lipp P. Calcium–a life and death signal. *Nature*. (1998) 395:645–8. doi: 10.1038/27094
26. Miao YL, Williams CJ. Calcium signaling in mammalian egg activation and embryo development: the influence of subcellular localization. *Mol Reprod Dev*. (2012) 79:742-56. doi: 10.1002/mrd.22078
27. Dai Z, Wu Z, Hang S, Zhu W, Wu G. Amino acid metabolism in intestinal bacteria and its potential implications for mammalian reproduction. *Mol Human Reprod*. (2015) 21:389–409. doi: 10.1093/molehr/gav003
28. Wesselink AK, Hatch EE, Rothman KJ, Mikkelsen EM, Aschengrau A, Wise LA. Prospective study of cigarette smoking and fecundability. *Human Reprod*. (2019) 34:558–67. doi: 10.1093/humrep/dey372
29. Buck GM, Sever LE, Batt RE, Mendola P. Life-style factors and female infertility. *Epidemiology*. (1997) 8:435–41. doi: 10.1097/00001648-199707000-00015
30. Fischer AG, Ullsperger M. An update on the role of serotonin and its interplay with dopamine for reward. *Front Human Neurosci*. (2017) 11:484. doi: 10.3389/fnhum.2017.00484
31. Burkhard P, Dominici P, Borri-Voltattorni C, Jansonius JN, Malashkevich VN. Structural insight into Parkinson's disease treatment from drug-inhibited dopa decarboxylase. *Nat Struct Biol*. (2001) 8:963–7. doi: 10.1038/nsb1101-963
32. Ma HL, Gong F, Tang Y, Li X, Li X, Yang X, et al. Inhibition of endometrial Tiam1/Rac1 signals induced by Mir-22 up-regulation leads to the failure of embryo implantation during the implantation window in pregnant mice. *Biol Reprod*. (2015) 92:152. doi: 10.1095/biolreprod.115.128603
33. Liu J, Guo S, Jiang K, Zhang T, Zhiming W, Yaping Y, et al. Mir-488 mediates negative regulation of the Akt/Nf-Kb pathway by targeting Rac1 in Lps-induced inflammation. *J Cell Physiol*. (2020) 235:4766–77. doi: 10.1002/jcp.29354
34. Xia Y, Zhang X, Sun D, Gao Y, Zhang X, Wang L, et al. Effects of water-soluble components of atmospheric particulates from rare earth mining areas in china on lung cancer cell cycle. *Particle Fibre Toxicol*. (2021) 18:27. doi: 10.1186/s12989-021-00416-z
35. Gomes VA, Bonocher CM, Rosa ESJC, de Paz CCP, Ferriani RA, Meola J. The apoptotic, angiogenic and cell proliferation genes Cd63, S100a6 E Gnb2l1 are altered in patients with endometriosis. *Revista brasileira de ginecologia e obstetricia*. (2018) 40:606–13. doi: 10.1055/s-0038-1673364
36. Beermann J, Piccoli MT, Viereck J, Thum T. Non-coding Rnas in development and disease: background, mechanisms, and therapeutic approaches. *Physiol Rev*. (2016) 96:1297–325. doi: 10.1152/physrev.00041.2015
37. Pankiewicz K, Laudański P, Issat T. The role of noncoding RNA in the pathophysiology and treatment of premature ovarian insufficiency. *Int J Mol Sci*. (2021) 22:9336. doi: 10.3390/ijms22179336

Conflict of Interest: The authors declare that the research was conducted in the absence of any commercial or financial relationships that could be construed as a potential conflict of interest.

The handling editor YF declared a shared affiliation with the author CY at the time of the review.

frontiers in Veterinary Science

ORIGINAL RESEARCH
published: 30 March 2022
doi: 10.3389/fvets.2022.856536

Reducing the Glucose Level in Pre-treatment Solution Improves Post-thaw Boar Sperm Quality

Zhendong Zhu[1,2], *Weijing Zhang*[1], *Rongnan Li*[2] *and Wenxian Zeng*[2*]

[1] College of Animal Science and Technology, Qingdao Agricultural University, Qingdao, China, [2] College of Animal Science and Technology, Northwest A&F University, Yangling, China

Frozen–thawed boar sperm was not widely used in pig artificial insemination as the sperm quality was damaged by biochemical and physical modifications during the cryopreservation process. The aim of this study was to investigate whether reduction of the glucose level in diluted medium could protect the post-thaw boar sperm or not. Boar sperm was diluted with the pre-treatment medium with different doses of glucose (153, 122.4, 91.8, 61.2, 30.6, and 0 mM) during the cooling process. The sperm motility patterns and glycolysis were evaluated during the cooling process. Meanwhile, the post-thaw sperm quality, ATP level, mitochondrial function as well as apoptosis were also measured. It was observed that 153 mM glucose treatment showed the highest glycolysis in boar sperm as the activities of hexokinase, fructose-bisphosphate aldolase A, and lactate dehydrogenase are the highest as well as the lactate level. Reduction of the glucose level from 153 to 30.6 mM suppressed sperm glycolysis. In addition, treatment with 153 mM glucose made the sperm demonstrate a circle-like movement along with a high value of curvilinear velocity and amplitude of the lateral head, while decreasing the glucose level reduced those patterns in the cooling process. Moreover, reduction of the glucose level also significantly increased the post-thaw sperm's total motility, progressive motility, straight-linear velocity, membrane integrity, and acrosome integrity. The treatment with 30.6 mM glucose showed the highest value among the treatments. Furthermore, the post-thaw sperm's succinate dehydrogenase activity, malate dehydrogenase activity, mitochondrial membrane potential as well as ATP level were increased by reducing the glucose level from 153 to 30.6 mM. Interestingly, the treatment with 30.6 mM glucose showed the lowest apoptosis of post-thaw sperm among the treatments. Those observations suggest that reduction of the glucose level in diluted medium increased the post-thaw boar sperm quality *via* decreasing the glycolytic metabolism. These findings provide novel insights that reduction of boar sperm activity *via* decreasing sperm glycolysis during the cooling process helps to improve the post-thaw sperm quality during cryopreservation.

Keywords: boar sperm, cryopreservation, glycolysis, quality, metabolism

OPEN ACCESS

Edited by:
Yi Fang,
Northeast Institute of Geography and Agroecology (CAS), China

Reviewed by:
Guobo Quan,
Yunnan Animal Science and Veterinary Institute, China
Kampon Kaeoket,
Mahidol University, Thailand

***Correspondence:**
Wenxian Zeng
zengwenxian2015@126.com

Specialty section:
This article was submitted to Animal Reproduction - Theriogenology, a section of the journal Frontiers in Veterinary Science

Received: *17 January 2022*
Accepted: *18 February 2022*
Published: *30 March 2022*

Citation:
Zhu Z, Zhang W, Li R and Zeng W (2022) Reducing the Glucose Level in Pre-treatment Solution Improves Post-thaw Boar Sperm Quality. Front. Vet. Sci. 9:856536. doi: 10.3389/fvets.2022.856536

INTRODUCTION

Sperm cryopreservation is one of the most essential assisted reproductive techniques in the livestock industry. During the cooling, freezing, and thawing processes, the sperm suffers from lots of dramatic changes in its physical and chemical surroundings (1, 2) that cause phase transitions of the membrane lipids (3) and impair cellular metabolism homeostasis. Previous studies found that cryo-damages affect post-thaw boar sperm fertility (4, 5). In order to increase the fertilization rates of artificial insemination (AI) with the post-thaw boar sperm, several research groups modify the cryopreservation extender, cooling temperature program or develop a sperm infusion method (2, 6). Though AI with post-thaw boar sperm could achieve a high conception rate of about 70% recently (7), the frozen–thawed boar sperm has not been widely accepted by commercial pork production. Only <1% of artificial inseminations are done with boar frozen–thawed sperm (6) because the birth rate and litter size in artificial insemination with post-thaw semen could not exceed 75–80% and 9–11.5 live births (8, 9) when compared to the utilization of liquid-stored semen at 17°C which is 20–30% more efficient in birth rate and results in 2 to 3 more young born per litter (8). In addition, the lifespan of post-thaw boar sperm in the female reproductive tracts is much shorter than that of fresh semen (10), which is also a major reason for the limitation of the post-thaw boar sperm application. Hence, novel strategies to maintain post-thaw boar sperm motility and function are important for the application of AI with frozen–thawed sperm in the swine industry.

In mammalian sperm, glycolysis and mitochondrial oxidative phosphorylation (OXPHOS) are the two major metabolic pathways for generating ATP (11, 12). Glycolysis occurs along the entire length of the principal piece of the flagellum as the glycolysis-related enzymes were distributed in those regions (12–14). Meanwhile, the OXPHOS occurs on the sperm mid-piece where the mitochondrion was located (15, 16). Sperm metabolism could be altered by its surrounding environment (14). A high-glucose medium stimulates sperm glycolysis and activates boar sperm motility patterns with circle-like tracts (17). Interestingly, the glucose level in boar fresh seminal plasma was very low (18). In addition, during cryopreservation, the sperm was cooled before the freezing process to lower down the sperm activity due to the fact that activated sperm is not a good condition for freezing (19). In somatic cell or organ cryopreservation, decreasing the cellular metabolic activity is beneficial to increase the cell and organ quality after recovering from cryopreservation (20, 21). However, the Modena solution, which contained 153 mM glucose, is usually regarded as the pre-treatment medium before the boar semen was cooled to 15°C during the cryopreservation process (19). Furthermore, in our previous study, we found that the reduction of glucose level in the incubation medium led to a decrease in boar sperm glycolysis metabolism (17). Therefore, we hypothesize that decreasing the glucose level in the pre-treatment medium might enhance the post-thaw boar sperm quality *via* reducing sperm glycolysis to protect the sperm during cryopreservation.

MATERIALS AND METHODS

Chemicals and Extenders

All chemicals and reagents were purchased from Sigma unless specified otherwise.

The Modena solution was composed of 153 mM D-glucose, 26.7 mM trisodium citrate, 11.9 mM sodium hydrogen carbonate, 15.1 mM citric acid, 6.3 mM EDTA-2Na, 46.6 mM Tris, 1,000 IU/ml Penicillin G Sodium Salt, 100 μg/ml polymyxin B, and 1 mg/ml streptomycin. According to our previous study (17), lactose was used instead of glucose to make different doses of glucose pre-treatment extenders (153, 122.4, 91.8, 61.2, 30.6, and 0 mM). As described by previous studies (19, 22), the modified Niwa and Sasaki freezing extender (mNSF1) was prepared with 80% (v/v) of 0.31 M lactose monohydrate, 20% (v/v) of egg yolk, 1,000 IU/ml Penicillin G Sodium Salt, and 100 μg/ml polymyxin B. The second dilution (mNSF2) was made with mNSF1 containing 1.5% (v/v) Orvus Es Paste (Miyazaki Chemical Sales, Ltd., Tokyo, Japan) and 2% (v/v) glycerol. Modena solution was also used as thawing solution.

Semen Collection and Processing

Five mature and fertile Duroc boars (aged 2 years) were used in the present study. All animal treatments and experimental procedures were approved by the Qingdao Agricultural University Institutional Animal Care and Use Committee (QAU-1121010). A sperm-rich fraction was collected weekly from each boar using the gloved-hand technique and filtered through double gauze. Only the ejaculates containing sperm with more than 90% motility and 85% normal morphology were used in this study. The ejaculated semen was pooled to avoid individual differences.

According to our previous study (22), fresh semen was divided into 6 parts and directly diluted with the pre-treatment solution with different doses of glucose level (v:v = 1:1) for 2 h at 15°C. After that, the samples were centrifuged for 10 min at 700 × *g* to remove the pre-treatment solutions. The sperm pellets were resuspended with mNSF1 at a concentration of 2.0×10^9 sperm/ml and cooled from 15 to 5°C with 1.5 h. Subsequently, the sperm sample was mixed with mNSF2 (v/v = 1:1) and packed into 0.5-ml plastic straws. The straws were placed in liquid nitrogen vapor for 10 min, plunged into it for storage. The straws were transferred to water at 60°C for 8 s to thaw the frozen sperm and diluted with 4.5 ml of thawing solution per straw.

Evaluation of Sperm Motility, Membrane Integrity, and Acrosome Integrity

Sperm motility was measured using a computer-assisted sperm motility analysis (CASA) system (HT CASA-Ceros II; Hamilton Thome, MA, USA). Briefly, a 5-μl aliquot of semen was placed on the analyzer's Makler chamber and maintained at 37°C during the analysis. Three fields were selected for computer-assisted analysis; more than 500 sperms were evaluated (17).

Sperm membrane integrity and acrosome integrity were, respectively, evaluated using LIVE/DEAD Sperm Viability Kit (L7011; Thermo Fisher Scientific) and fluorescein isothiocyanate (FITC)–peanut agglutinin according to our previous study (23).

The stained sperm was monitored and photographed by an epifluorescence microscope (Nikon 80i; Tokyo, Japan) with a set of filters (×200).

Evaluation of Sperm Mitochondrial Membrane Potential

JC-1 Mitochondrial Membrane Potential Detection Kit (Beyotime Institute of Biotechnology, China) was used to analyze the changes of sperm mitochondrial activity ($\Delta\Psi$m) (24). The monomer and aggregates of the two types of JC-1 in stained mitochondrial plasma emit green fluorescence in low $\Delta\Psi$m and emit red fluorescence in high $\Delta\Psi$m, respectively. Briefly, sperm samples (2×10^6/ml) were stained with 1× JC-1 at 37°C for 30 min. The fluorescence intensity of both mitochondrial JC-1 monomers and aggregates was detected with a monochromator microplate reader (Safire II, Tecan, Switzerland). The $\Delta\psi$m of sperm in each treatment group was calculated as the fluorescence ratio of red (aggregates) to green (monomer). The analyses were performed in triplicate ($n = 3$).

Analysis of Hexokinase Activity

According to a previous study (25), a 2-deoxyglucose Uptake Measurement Kit was used to measure the sperm hexokinase activity (Cosmo Bio, Japan). The sperm sample pellets were mixed with the reaction mix in a 96-well microplate. The absorbance was measured with a multimode plate reader at 420 nm. The 2DG6P level was calculated using a standard curve.

Measure of Fructose-Bisphosphate Aldolase a Activity

Sperm ALDOA activity was measured with an aldolase activity colorimetric assay kit (BioVision, K665-100) (25). The sperm sample was homogenized with aldolase assay buffer and centrifuged to collect supernatant. Then, the supernatants were used to analyze ALDOA activity in a 96-well plate. The absorbance was measured with a multimode plate reader at 450 nm according to the manufacturer's instructions.

Measure of LDH Activity

Lactate dehydrogenase assay kit (Nanjing Jiancheng Bioengineering Institute, China) was used to measure the lactate dehydrogenase (LDH) activity. According to the manufacturer's instructions, sperm sample pellets were lysed ultrasonically (20 kHz, 750 W, operating at 40% power, 5 cycles of 3 s on and 5 s off) and centrifuged at 2,000 × *g* for 10 min at 4°C. The supernatants were added to a 96-well plate for the analysis of LDH activity with a microplate reader at 450 nm (26). The analyses were performed in triplicate ($n = 3$).

Detection of Lactate Level

Sperm lactate content was measured with a lactate detection kit (Nanjing Jiancheng, China) according to the manufacturer's instruction. Briefly, the level of lactate was measured by detecting the NADH formed consequently to lactate oxidation by LDH with a microplate reader at 340 nm (27).

Measure of MDH and SDH Activities

According to our previous study, Malate Dehydrogenase Assay Kit and Succinate Dehydrogenase Assay kit (Nanjing Jiancheng Bioengineering Institute, China) were used to measure the activities of malate dehydrogenase (MDH) and succinate dehydrogenase (SDH), respectively. The sperm sample pellets were lysed ultrasonically (20 kHz, 750 W, operating at 40% power, 5 cycles of 3 s on and 5 s off) and centrifuged at 2,000 × *g* for 10 min at 4°C to collect the supernatant. Then, the supernatant was added to the 96-well plate for evaluation of MDH and SDH activities with a microplate reader at 340 and 600 nm, respectively. The analyses were performed in triplicate ($n = 3$).

Measure of Sperm ATP Level

ATP Assay Kit (Beyotime Institute of Biotechnology) was used to measure the post-thaw sperm ATP level according to our previous study (26). After lysis and centrifugation, 50 μl of the sperm supernatant was mixed with 100 μl luciferin/luciferase reagent in 96-well plates. An Ascent Luminoskan luminometer (Thermo Scientific, Palm Beach, FL, United States) was used to read the luminescence at integration × 1,000 ms. The analyses were performed in triplicate ($n = 3$).

Annexin V-FITC/PI Assay

Annexin V-FITC/PI apoptosis detection kit (Sigma-Aldrich, St. Louis, MO, USA) was used to assess sperm apoptosis according to the manufacturer's instructions but with slight modifications. The post-thaw sperm was centrifuged and washed thrice with phosphate-buffered saline at 400 × *g* for 5 min. The sperm was resuspended with 1× Annexin V binding buffer at a concentration of 1×10^6 sperm/ml. A total of 5 μl Annexin V-FITC (AN) and 3 μl PI was then added to each aliquot of 100-μl sample. The tubes were mixed gently and incubated at room temperature for 10 min in dark. Different labeling patterns of stained sperm were observed and counted with a fluorescence microscope (80i; Nikon) at 400× magnification.

Statistical Analysis

Data from three replicates were compared using either Student's *t*-test or one-way analysis of variance followed by Tukey's *post-hoc* test (Statview; Abacus Concepts, Inc., Berkeley, CA). All the values are presented as mean ± standard deviation (SD). Treatments were considered statistically different from one another at $p < 0.05$.

RESULTS

High Glucose Level in the Pre-treatment Medium Activated the Glycolytic Metabolism and Decreased the Membrane Integrity and Acrosome Integrity in Boar Sperm During the Cooling Process

As shown in **Figures 1A–C**, during the cooling process, the activities of hexokinase, ALDOH, and LDH in 153 mM glucose medium pre-treatment (high glucose) showed the highest value among the treatments. It was observed

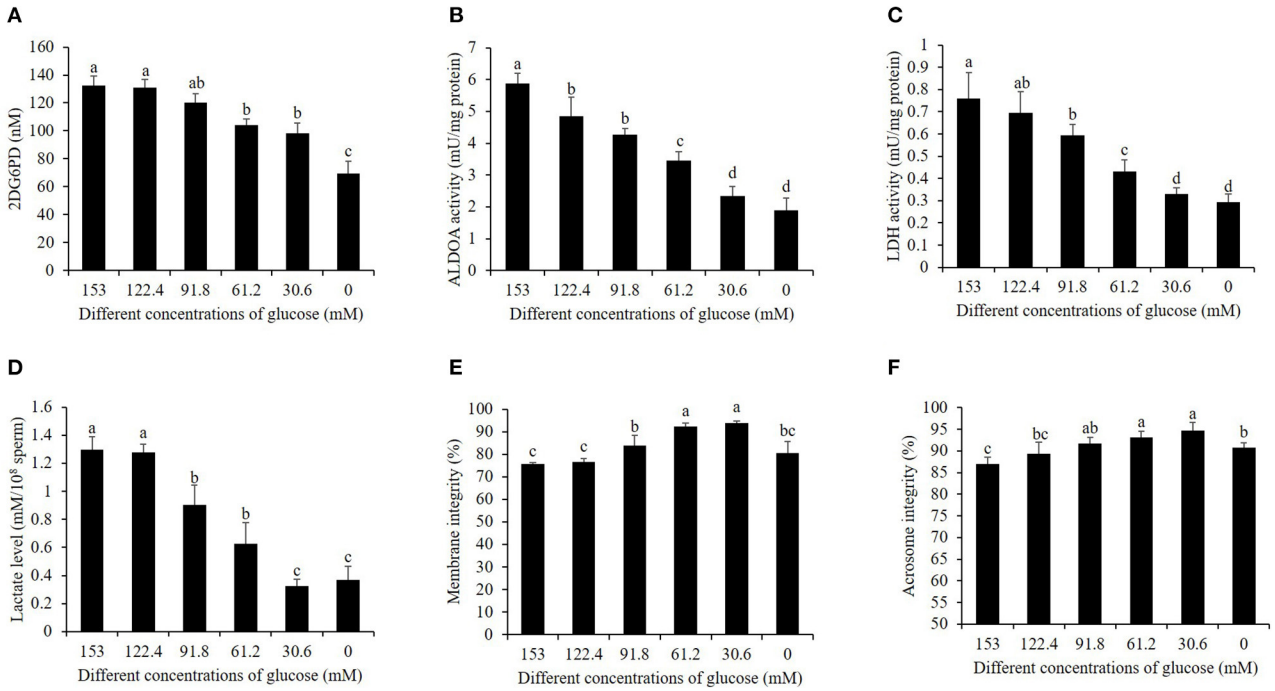

FIGURE 1 | Effects of different glucose levels in the pre-treatment solution on boar sperm hexokinase activity **(A)**, ALDOA activity **(B)**, LDH activity **(C)**, LDH level **(D)**, membrane integrity **(E)**, and acrosome integrity **(F)** during the cooling process. Values are specified as mean ± standard deviation. Columns with different lowercase letters differ significantly ($p < 0.05$). ALDOA, aldolase A; LDH, lactate dehydrogenase.

that the reduction of glucose level in the pre-treatment medium significantly decreased the hexokinase, ALDOH, and LDH activities (**Figures 1A–C**). In addition, decreasing the glucose level also reduced the value of the lactate level, considering that lactate is one of the products in the sperm's glycolytic pathway (**Figure 1D**). The values of sperm membrane integrity and acrosome integrity were also improved by a reduction of glucose level during the cooling process (**Figures 1E,F**).

High Glucose Level in the Pre-treatment Medium Increased the Ratio of Sperms With Circle-Like Track Patterns and Decreased the Sperm Membrane Integrity and Acrosome Integrity During the Cooling Process

Interestingly, when the sperm motility patterns were analyzed by CASA, the sperm motility tracks revealed that the high-glucose pre-treatment made the sperm move with circle-like tracks. Meanwhile, the reduction of the glucose level decreased the ratio of sperms with circle-like movement, and the movement changed to a linear-like track pattern during the cooling process (**Figures 2A–F**). The sperm's total motility was not changed by 153- to 30.6-mM glucose treatments, but treatment with 0 mM glucose significantly decreased it (**Figure 2G**). Besides this, the patterns of sperm VCL and ALH were also significantly decreased in the treatments where there was a reduction of the glucose level from 153 to 0 mM (**Figures 2H,I**).

Reduction of the Glucose Level in Pre-treatment Medium Increased Post-thaw Sperm Motility, Membrane Integrity, and Acrosome Integrity

When the sperm was thawing, from the sperm motility tracks generated from the CASA it was observed that the post-thaw sperm motility patterns were significantly increased by a reduction of the glucose level (**Figures 3A–F**). The values of sperm total motility, progressive motility, and straight line velocity (VSL) in the treatments with 91.8, 61.2, and 30.6 mM glucose were significantly higher than those in the treatment with 153 mM, and the treatment with 30.6 mM showed the highest value among the treatments (**Figures 3G–I**). However, the glucose pre-treatment with 0 mM did not increase those motility patterns compared to the high-glucose-medium treatment (**Figures 3G–I**).

In terms of post-thaw sperm membrane integrity and acrosome integrity, the reduction of the glucose level from 153 to 30.6 mM significantly increased them, while the treatment with 0 mM glucose did not increase the membrane integrity (**Figures 4A,B**). Moreover, the treatment with 30.6 mM glucose presented the best values of post-thaw sperm membrane integrity and acrosome integrity (**Figures 4A,B**).

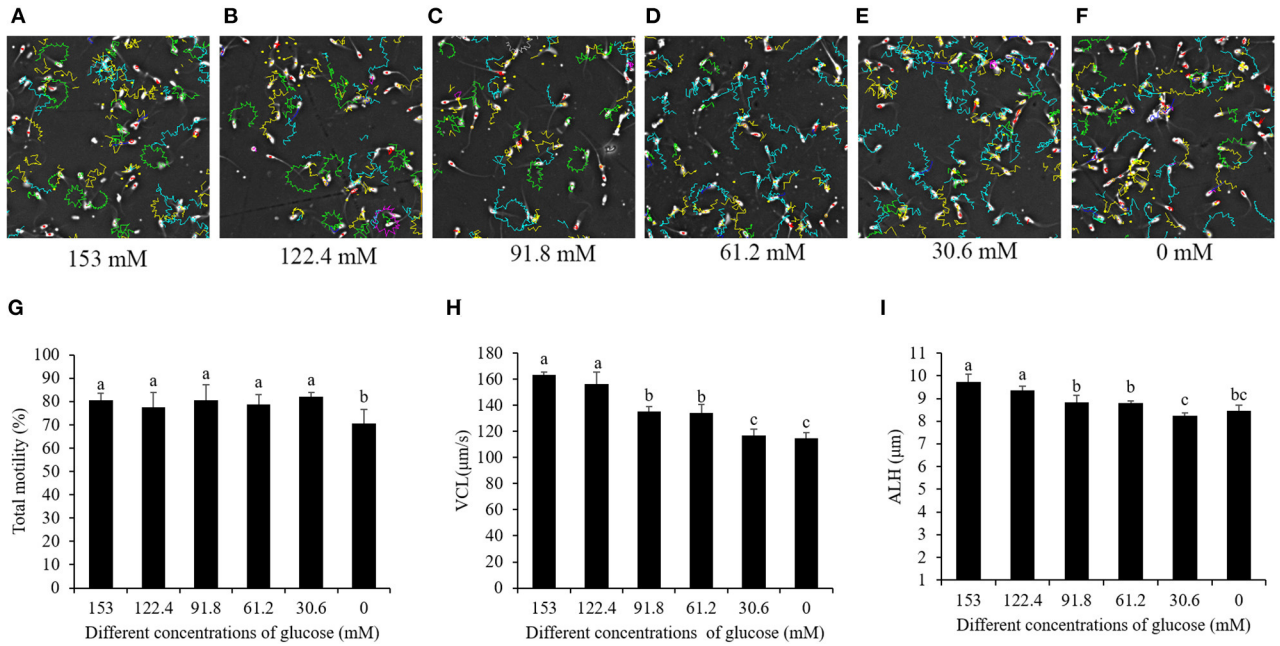

FIGURE 2 | Computer-assisted sperm motility analysis-derived changes in the sperm motility track by reducing the glucose level in the pretreatment solution from 153 to 0 mM **(A–F)**. Effects of glucose level in the pre-treatment solution on sperm total motility **(G)**, VCL **(H)**, and ALH **(I)** during the cooling process. Values are specified as mean ± standard deviation. Columns with different lowercase letters differ significantly ($p < 0.05$). VCL, curvilinear velocity; ALH, amplitude of lateral head displacement.

Reduction of the Glucose Level in Pre-treatment Medium Increased Post-thaw Sperm Mitochondrial Function for ATP Generation

Post-thaw sperm mitochondrial membrane potential was measured with JC-1 staining kit. As shown in **Figure 5**, it was observed that there are two kinds of sperm after staining with the JC-1 probe. The blue arrow showed that the post-thaw sperm emits green fluorescence with low mitochondrial membrane potential, while the black arrow showed that the post-thaw sperm emits red or orange fluorescence with high mitochondrial membrane potential. Reduction of the glucose level during the cooling process significantly increased the post-thaw sperm mitochondrial membrane potential (**Figure 4C**). Interestingly, the reduction of glucose level during the cooling process also increased the post-thaw sperm activities of MDH and SDH enzymes in which the two are key enzymes of TCA cycle for ATP generation, and the treatment with 30.6 mM glucose showed the best effects (**Figures 4D,E**). Moreover, the ATP level of the post-thaw sperm was also observed to increase by reduction of the glucose level during the cooling process (**Figure 4F**).

Reduction of the Glucose Level in Pre-treatment Medium Decreased Post-thaw Sperm With Apoptosis

As shown in **Figures 6A–D**, after the sperm samples were stained by the Annexin V-FITC/PI assay kit, four subpopulations of post-thaw sperm were observed: the black arrow indicated the live sperm (AN−/PI−), the red arrow indicated the early apoptotic sperm (AN+/PI−), the white arrow indicated the late apoptotic sperm (AN+/PI+), and the blue arrow indicated the nonviable necrotic sperm (AN−/PI+). Reduction of the glucose level in pre-treatment medium significantly decreased the post-thaw sperm with apoptosis (AN+/PI− and AN+/PI+), and the treatment with 30.6 mM glucose showed the lowest percentage of post-thaw sperm with apoptosis (**Figure 6E**).

DISCUSSION

Sperms are special cells with high differentiation that play key roles in paternal DNA delivery and oocyte activation during the fertilization process (28). Boar sperm is deposited in the pig uterus during natural mating or conventional artificial insemination (2, 29). The sperm is physically transported from the site of deposition to the fertilization site, which is located in the oviduct (30). When the sperm transport is facilitated by uterine contractions, the sperm must be with good motility to traverse the uterotubal junction prior to oviduct binding and to locate the egg following ovulation, suggesting that sperm motility is a key factor for improving the chances of fertilization (17, 30). In the present study, we found that decreasing the glucose level in the pre-treatment significantly increased the post-thaw sperm motility, and this might contribute to the improvement of fertilization using frozen boar sperm in artificial inseminations.

Sperm motility depends on ATP production by both the glycolysis in the cytoplasm and oxidative phosphorylation in the mitochondria (11, 14, 17). It is well-known that the sperm

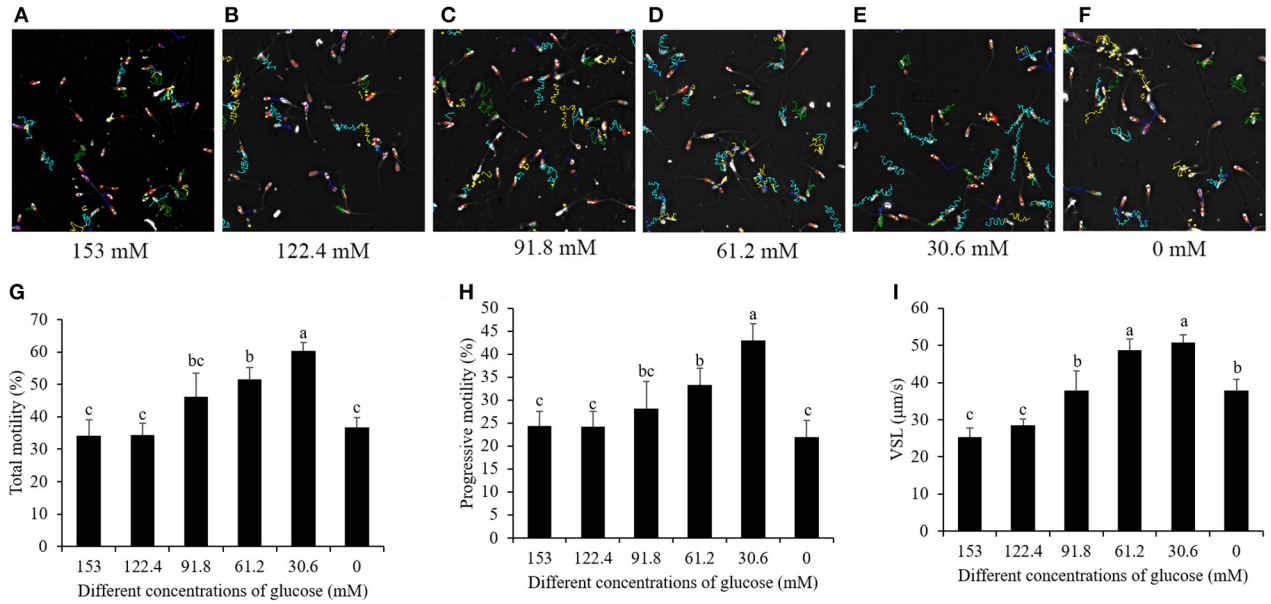

FIGURE 3 | Computer-assisted sperm motility analysis-derived changes of post-thaw sperm motility track by reducing the glucose level in the pretreatment solution from 153 to 0 mM **(A–F)**. Effects of glucose level in the pretreatment solution on post-thaw sperm total motility **(G)**, progressive motility **(H)**, and VSL **(I)**. Values are specified as mean ± standard deviation. Columns with different lowercase letters differ significantly. VSL, straight line velocity.

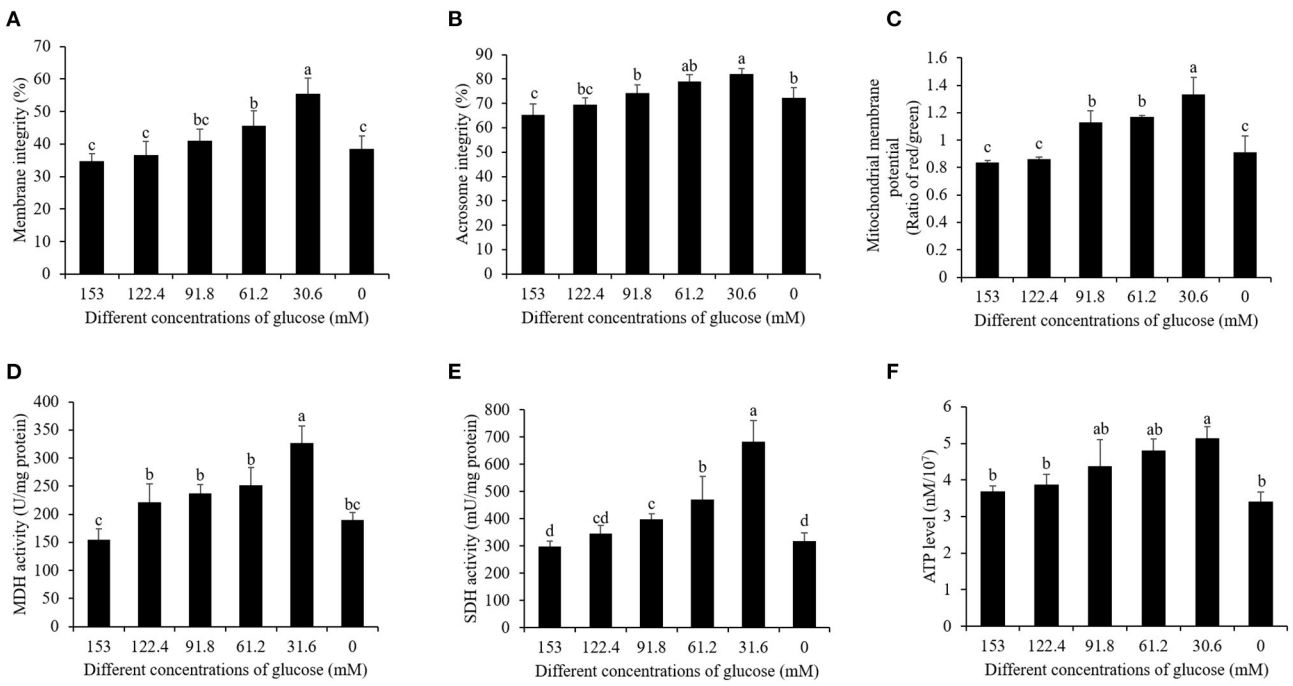

FIGURE 4 | Effects of different glucose levels in the pretreatment solution on boar post-thaw sperm membrane integrity **(A)**, acrosome integrity **(B)**, mitochondrial membrane potential **(C)**, MDH level **(D)**, SDH level **(E)**, and ATP level **(F)** after thawing. Values are specified as mean ± standard deviation. Columns with different lowercase letters differ significantly ($p < 0.05$). MDH, malate dehydrogenase; SDH, succinate dehydrogenase.

contains three distinct regions, namely, head, mid-piece, and tail. Most enzymes involved in glycolysis were located in the sperm head and tail, while those enzymes related with the oxidative phosphorylation pathway were located in the mid-piece where the mitochondria are located (13, 31). In somatic cells, ATP generation occurs by metabolic pathways, depending on oxygen

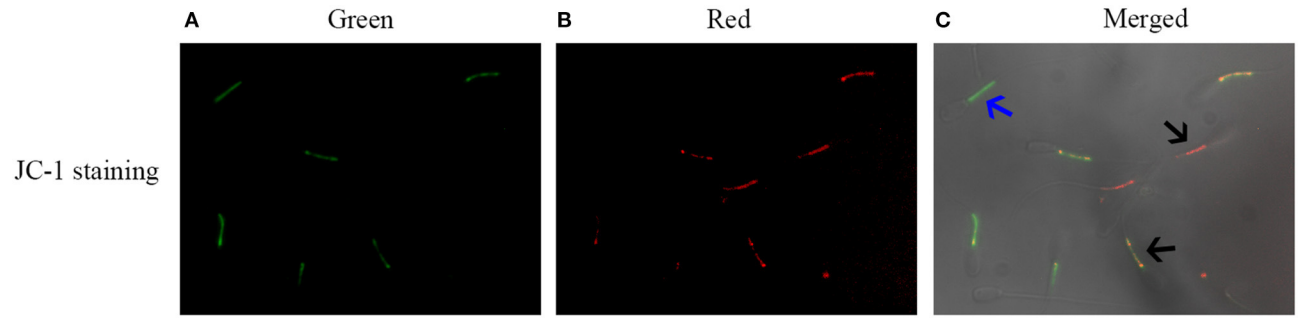

FIGURE 5 | Images of sperm stained with JC-1 probe **(A–C)**. The monomer emits green fluorescence **(A)**, while the aggregates emit red fluorescence **(C)**. The blue arrow indicated the sperm with low mitochondrial membrane potentials, while the black arrow indicated the sperm with high mitochondrial membrane potentials.

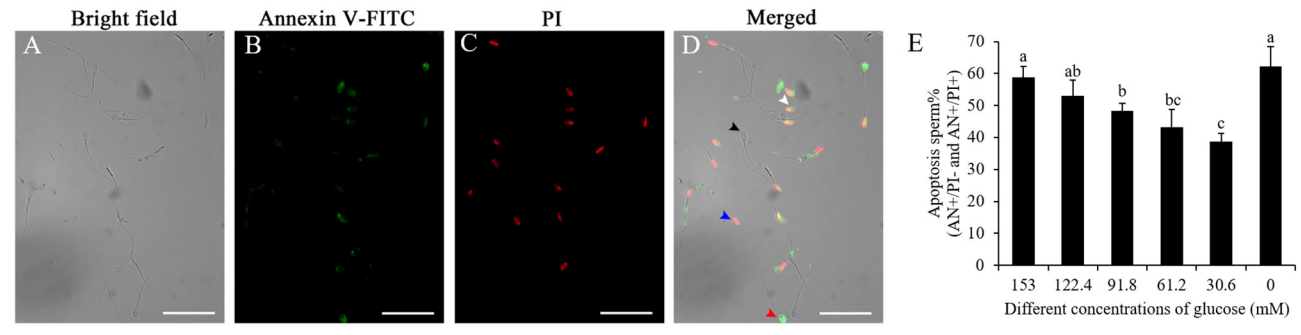

FIGURE 6 | Photos of the boar post-thaw sperm stained with the Annexin V-FITC/PI assay kit **(A–D)**: live sperm (AN-/PI-; black arrow), early apoptotic sperm (AN+/PI–; red arrow), late apoptotic sperm (AN+/PI+; white arrow), and non-viable necrotic sperm (AN–/PI+; blue arrow). Effects of different concentrations of glucose on boar post-thaw sperm apoptosis **(E)**. Values are specified as mean ± standard deviation. Columns with different lowercase letters differ significantly ($p < 0$ 05).

availability and the composition of metabolic substrates in their environment (32, 33). In our previous study (17), during the boar sperm incubation process, ATP generation from the glycolysis pathway decreased when the glucose level in the incubation medium was reduced, which suggests that boar sperm can change the metabolic pathway. Moreover, when HepG2 cells were treated with a medium containing a high level of glucose, the glycolysis pathway was highly activated, and if the glucose level in the medium was reduced, the glycolysis pathway for ATP generation would decrease (34). In the present study, it was observed that, during the cooling process before cryopreservation, the values of the activities of hexokinase, ALDOA, and LDH as well as the lactate level in the high-glucose treatment were significantly higher than those in the low-glucose treatment, suggesting that the high-glucose pre-treatment medium enhanced boar sperm glycolysis, and the reduction of glucose level helped to inactive boar sperm glycolysis during the cooling process. Those results were supported by previous studies which showed that sperm glycolysis metabolism was enhanced when they arrived at the oviduct as the oviduct fluid contained a high glucose level to induce zigzag motility for the sperm to penetrate the oocyte (35). Our previous study revealed that boar sperm energy metabolism could be changed and enhanced depending on the metabolic substrates in their environment. Moreover, the observation on the boar sperm moving with circle-like tracks in high-glucose pre-treatment medium in the present study was also consistent with high-glycolysis-induced boar sperm with high VCL and ALH motility patterns (17). Furthermore, the boar fresh semen contained very low glucose (18), which suggests that glycolysis is not active in boar sperm when just ejaculated. Thus, during the dilution process, if the boar semen was diluted with a high-glucose medium, the boar sperm might suffer from high glycolysis stress, thus causing decreased sperm quality. The sperm membrane integrity and acrosome integrity in the high-glucose pretreatment in this study were lower than those in the treatment with 30.6 mM glucose (low glucose), thus agreeing with it. Therefore, a high-glucose medium could stimulate sperms with high glycolysis that would lead to disruption of sperm cellular homeostasis and decreased sperm quality and function.

On a worldwide basis, around 99% of artificial inseminations in pigs are done with liquid semen stored at 17°C, while <1% of frozen–thawed sperm are used (29). The problems associated with cryopreservation procedures and their post-thaw results limit the use of frozen–thawed sperm. The frozen–thawed sperm still show a lower survival rate, or the surviving sperm shows a shorter lifespan *in vitro* (36) compared to liquid-stored sperm. Thus, artificial insemination with frozen–thawed sperm has obviously resulted in a low farrowing rate (70–80%). Meanwhile, >90% is achieved by conventional AI of liquid-stored semen under controlled breeding management conditions (4, 8). In addition, the artificial insemination of frozen–thawed sperm has

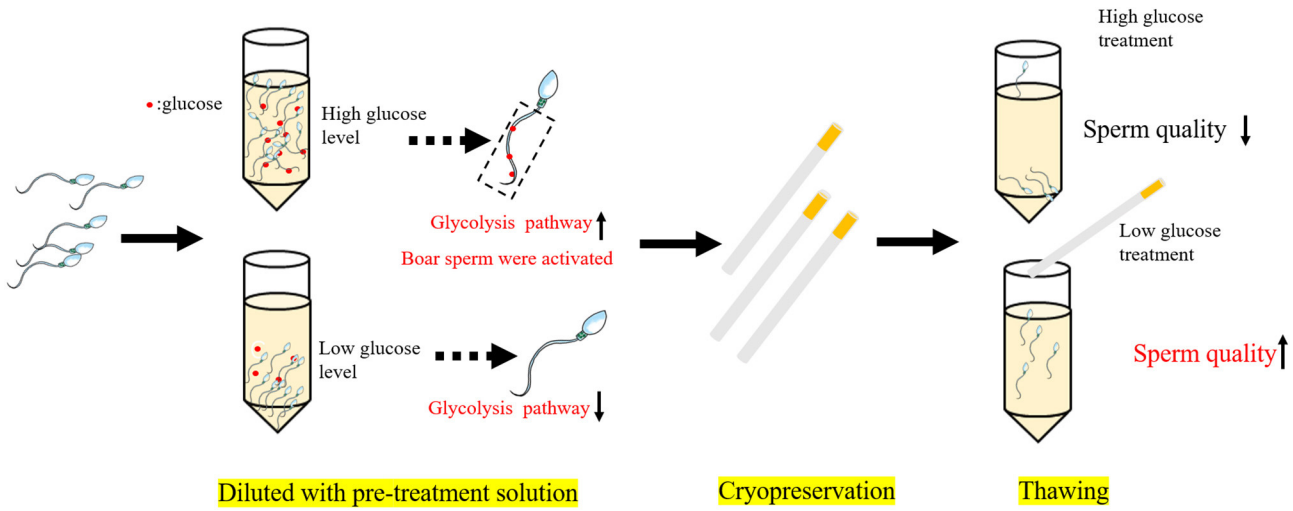

FIGURE 7 | Mechanisms of reducing the glucose level in the pre-treatment solution improve the boar post-thaw sperm quality. High glucose level in the pretreatment solution enhances the stimulation of the glycolysis pathway and led to the activation of boar sperm before cryopreservation, thus resulting in decreased boar post-thaw sperm quality, whereas reduction of the glucose level would inactivate the glycolysis pathway to increase the post-thaw sperm quality during cryopreservation.

resulted in smaller litter sizes, usually 2 to 3 piglets fewer than that when liquid-stored sperm was used (8, 9), indicating that preventing boar sperm cryo-damage during the cryopreservation process is still a critical challenge. Although several studies have tested additives and changes in the speed of cooling and thawing to improve the boar sperm quality in recent years (6, 19), the overall procedure is basically still the same, which is just a simple modification of the protocol reported by Westendorf almost 40 years ago (37). Developing a novel and effective method for boar sperm cryopreservation might help to improve the post-thaw sperm quality, and it has become vital for the use of frozen–thawed sperm in pig artificial insemination. As we all know, keeping the sperm with good function before cryopreservation is generally a benefit for improving the post-thaw sperm. If the sperm was excessively activated before cryopreservation, the post-thaw sperm quality was decreased. In the present study, we found that the post-thaw sperm quality patterns, such as the total motility, progressive motility, VSL, membrane integrity, and acrosome integrity, were significantly increased by decreasing the glucose level in the pre-treatment medium as the low-glucose pre-treatment suppressed the sperm from high glycolysis activation, while the high-glucose medium induced sperm glycolysis. Therefore, during the cooling process, using low-glucose medium diluted with freshly ejaculated semen helps to protect boar sperm function and thus improve the post-thaw sperm quality.

Interestingly, when we analyzed the activities of SDH and MDH, which are two key enzymes of OXPHOS, it was found that those enzymes' activities were increased in the low-glucose treatment compared to that in the high-glucose treatment. It might be because the sperm mitochondria were protected from cryo-damage in the low-glucose treatment. The result of the mitochondrial membrane potential was consistent with it. Besides that, in this study, the low-glucose treatment also decreased the post-thaw sperm apoptosis. It agreed with a report that sperms with high activation led to a decreased sperm lifespan during liquid storage *in vitro* (5, 38). Based on those results, before cryopreservation, dilution of the ejaculated semen with a low-glucose medium is essential to improve the post-thaw sperm mitochondrial function.

In conclusion, as shown in **Figure 7**, during the cooling process, a high glucose level in the pre-treatment solution enhances the stimulation of the glycolysis pathway and led to activation of the boar sperm before cryopreservation, thus result in decreased boar post-thaw sperm quality, whereas reducing the glucose level would inactivate the glycolysis pathway to increase the post-thaw sperm quality during cryopreservation.

DATA AVAILABILITY STATEMENT

The original contributions presented in the study are included in the article.

ETHICS STATEMENT

The animal study was reviewed and approved by Qingdao Agriculture University Institutional Animal Care and Use Committee.

AUTHOR CONTRIBUTIONS

ZZ was responsible for experimental design, sample, data analysis, and writing of the manuscript. WZh and RL were responsible for sample collection and data analysis. WZe was responsible for the discussion about the experimental design. All authors contributed to the article and approved the submitted version.

FUNDING

This work was supported in part by the Start-up Found for High-level Talents of Qingdao Agricultural University for ZZ (1121010), the Shandong Province Central Guided Local Science and Technology Development Project for ZZ (YDZX2021113), and the National Key R&D Program of China (number 2018YFD0501000) for WZe.

REFERENCES

1. Di Santo M, Tarozzi N, Nadalini M, Borini A. Human sperm cryopreservation: update on techniques, effect on DNA integrity, and implications for ART. *Adv Urol.* (2012) 2012:854837. doi: 10.1155/2012/854837
2. Rodríguez-Gil JE, Estrada E. Artificial Insemination in boar reproduction. In: Bonet S, Casas I, Holt WV, Yeste M. *Boar Reproduction: Fundamentals and New Biotechnological Trends.* Berlin; Heidelberg: Springer Berlin Heidelberg (2013). p. 589–607.
3. Woelders H. Fundamentals and recent development in cryopreservation of bull and boar semen. *Vet Q.* (1997) 19:135–8. doi: 10.1080/01652176.1997.9694758
4. Bolarin A, Roca J, Rodriguez-Martinez H, Hernandez M, Vazquez JM, Martinez EA. Dissimilarities in sows' ovarian status at the insemination time could explain differences in fertility between farms when frozen-thawed semen is used. *Theriogenology.* (2006) 65:669–80. doi: 10.1016/j.theriogenology.2005.06.006
5. Pezo F, Romero F, Zambrano F, Sanchez RS. Preservation of boar semen: an update. *Reprod Domest Anim.* (2019) 54:423–34. doi: 10.1111/rda.13389
6. Yeste M. Recent advances in boar sperm cryopreservation: state of the art and current perspectives. *Reprod Domest Anim.* (2015) 50(Suppl. 2):71–9. doi: 10.1111/rda.12569
7. Okazaki T, Mihara T, Fujita Y, Yoshida S, Teshima H, Shimada M. Polymyxin B neutralizes bacteria-released endotoxin and improves the quality of boar sperm during liquid storage and cryopreservation. *Theriogenology.* (2010) 74:1691–700. doi: 10.1016/j.theriogenology.2010.05.019
8. Eriksson BM, Petersson H, Rodriguez-Martinez H. Field fertility with exported boar semen frozen in the new flatpack container. *Theriogenology.* (2002) 58:1065–79. doi: 10.1016/S0093-691X(02)00947-0
9. Didion BA, Braun GD, Duggan MV. Field fertility of frozen boar semen: a retrospective report comprising over 2600 AI services spanning a four year period. *Anim Reprod Sci.* (2013) 137:189–96. doi: 10.1016/j.anireprosci.2013.01.001
10. Pursel VG, Schulman LL, Johnson LA. Distribution and morphology of fresh and frozen-thawed sperm in the reproductive tract of gilts after artificial insemination. *Biol Reprod.* (1978) 19:69–76. doi: 10.1095/biolreprod19.1.69
11. Storey BT. Mammalian sperm metabolism: oxygen and sugar, friend and foe. *Int J Dev Biol.* (2008) 52:427–37. doi: 10.1387/ijdb.072522bs
12. du Plessis SS, Agarwal A, Mohanty G, van der Linde M. Oxidative phosphorylation versus glycolysis: what fuel do spermatozoa use. *Asian J Androl.* (2015) 17:230–5. doi: 10.4103/1008-682X.135123
13. Cao W, Gerton GL, Moss SB. Proteomic profiling of accessory structures from the mouse sperm flagellum. *Mol Cell Proteomics.* (2006) 5:801–10. doi: 10.1074/mcp.M500322-MCP200
14. Mukai C, Travis AJ. What sperm can teach us about energy production. *Reprod Domestic Anim.* (2012) 47:164–9. doi: 10.1111/j.1439-0531.2012.02071.x
15. Amaral A, Lourenco B, Marques M, Ramalho-Santos J. Mitochondria functionality and sperm quality. *Reproduction.* (2013) 146:R163–74. doi: 10.1530/REP-13-0178
16. Moraes CR, Meyers S. The sperm mitochondrion: organelle of many functions. *Anim Reprod Sci.* (2018) 194:71–80. doi: 10.1016/j.anireprosci.2018.03.024
17. Zhu Z, Umehara T, Okazaki T, Goto M, Fujita Y, Hoque SAM, et al. Gene expression and protein synthesis in mitochondria enhance the duration of high-speed linear motility in boar sperm. *Front Physiol.* (2019) 10:252. doi: 10.3389/fphys.2019.00252
18. Mateo-Otero Y, Fernandez-Lopez P, Ribas-Maynou J, Roca J, Miro J, Yeste M, et al. Metabolite profiling of pig seminal plasma identifies potential biomarkers for sperm resilience to liquid preservation. *Front Cell Dev Biol.* (2021) 9:669974. doi: 10.3389/fcell.2021.669974
19. Okazaki T, Shimada M. New strategies of boar sperm cryopreservation: development of novel freezing and thawing methods with a focus on the roles of seminal plasma. *Anim Sci J.* (2012) 83:623–9. doi: 10.1111/j.1740-0929.2012.01034.x
20. Bakhach J. The cryopreservation of composite tissues: principles and recent advancement on cryopreservation of different type of tissues. *Organogenesis.* (2009) 5:119–26. doi: 10.4161/org.5.3.9583
21. Jang TH, Park SC, Yang JH, Kim JY, Seok JH, Park US, et al. Cryopreservation and its clinical applications. *Integr Med Res.* (2017) 6:12–18. doi: 10.1016/j.imr.2016.12.001
22. Zhu ZD, Li RN, Fan XT, Lv YH, Zheng Y, Hoque SAM, et al. Resveratrol improves boar sperm quality via 5 ' AMP-activated protein kinase activation during cryopreservation. *Oxid Med Cell Longev.* (2019) 2019:5921503 doi: 10.1155/2019/5921503
23. Zhu ZD, Fan XT, Lv YH, Zhang N, Fan CN, Zhang PF, et al. Vitamin E analogue improves rabbit sperm quality during the process of cryopreservation through its antioxidative action. *Plos ONE.* (2015) 10:e0145383. doi: 10.1371/journal.pone.0145383
24. Zhu Z, Li R, Ma G, Bai W, Fan X, Lv Y, et al. 5'-AMP-activated protein kinase regulates goat sperm functions via energy metabolism *in vitro*. *Cell Physiol Biochem.* (2018) 47:2420–31. doi: 10.1159/000491616
25. Zhu Z, Umehara T, Tsujita N, Kawai T, Goto M, Cheng B, et al. Itaconate regulates the glycolysis/pentose phosphate pathway transition to maintain boar sperm linear motility by regulating redox homeostasis. *Free Radic Biol Med.* (2020) 159:44–53. doi: 10.1016/j.freeradbiomed.2020.07.008
26. Zhu Z, Li R, Wang L, Zheng Y, Hoque SAM, Lv Y, et al. glycogen synthase kinase-3 regulates sperm motility and acrosome reaction via affecting energy metabolism in goats. *Front Physiol.* (2019) 10:968. doi: 10.3389/fphys.2019.00968
27. Li RN, Zhu ZD, Zheng Y, Lv YH, Tian XE. Wu, et al. Metformin improves boar sperm quality via 5'-AMP-activated protein kinase-mediated energy metabolism *in vitro*. *Zool Res.* (2020) 41:527–538. doi: 10.24272/j.issn.2095-8137.2020.074
28. Barroso G, Valdespin C, Vega E, Kershenovich R, Avila R, Avendano C, et al. Developmental sperm contributions: fertilization and beyond. *Fertil Steril.* (2009) 92:835–48. doi: 10.1016/j.fertnstert.2009.06.030
29. Knox RV. Artificial insemination in pigs today. *Theriogenology.* (2016) 85:83–93. doi: 10.1016/j.theriogenology.2015.07.009
30. Suarez SS, Pacey AA. Sperm transport in the female reproductive tract. *Hum Reprod Update.* (2006) 12:23–37. doi: 10.1093/humupd/dmi047
31. Piomboni P, Focarelli R, Stendardi A, Ferramosca A, Zara V. The role of mitochondria in energy production for human sperm motility. *Int J Androl.* (2012) 35:109–24. doi: 10.1111/j.1365-2605.2011.01218.x
32. Gohil VM, Sheth SA, Nilsson R, Wojtovich AP, Lee JH, Perocchi F, et al. Nutrient-sensitized screening for drugs that shift energy metabolism from mitochondrial respiration to glycolysis. *Nat Biotechnol.* (2010) 28:249–55. doi: 10.1038/nbt.1606
33. Potter M, Newport E, Morten KJ. The Warburg effect: 80 years on. *Biochem Soc Trans.* (2016) 44:1499–505. doi: 10.1042/BST20160094
34. Marroquin LD, Hynes J, Dykens JA, Jamieson JD, Will Y. Circumventing the Crabtree effect: replacing media glucose with galactose increases susceptibility of HepG2 cells to mitochondrial toxicants. *Toxicol Sci.* (2007) 97:539–47. doi: 10.1093/toxsci/kfm052
35. Umehara T, Tsujita N, Goto M, Tonai S, Nakanishi T, Yamashita Y, et al. Methyl-beta cyclodextrin and creatine work synergistically under hypoxic conditions to improve the fertilization ability of boar ejaculated sperm. *Anim Sci J.* (2020) 91:e13493. doi: 10.1111/asj.13493
36. Waberski D, Weitze KF, Gleumes T, Schwarz M, Willmen T, Petzoldt R. Effect of time of insemination relative to ovulation on fertility with liquid and frozen boar semen. *Theriogenology.* (1994) 42:831–40. doi: 10.1016/0093-691X(94)90451-N

37. Westendorf P, Richter L, Treu H, Heidecke FW, Zimmermann F. [Deep freezing of boar semen. Insemination results using the Hulsenberger pailleten procedure]. *Dtsch Tierarztl Wochenschr.* (1977) 84:41–42.
38. Yeste M. State-of-the-art of boar sperm preservation in liquid and frozen state. *Anim Reprod.* (2017) 14:69–81. doi: 10.21451/1984-3143-AR895

Conflict of Interest: The authors declare that the research was conducted in the absence of any commercial or financial relationships that could be construed as a potential conflict of interest.

Publisher's Note: All claims expressed in this article are solely those of the authors and do not necessarily represent those of their affiliated organizations, or those of the publisher, the editors and the reviewers. Any product that may be evaluated in this article, or claim that may be made by its manufacturer, is not guaranteed or endorsed by the publisher.

frontiers | Frontiers in Veterinary Science

ORIGINAL RESEARCH
published: 05 April 2022
doi: 10.3389/fvets.2022.854503

Comparison of miRNA and mRNA Expression in Sika Deer Testes With Age

Boyin Jia[1,2†], Linlin Zhang[1†], Fuquan Ma[1], Xue Wang[1], Jianming Li[2,3], Naichao Diao[1,2], Xue Leng[2,3], Kun Shi[2,3], Fanli Zeng[2,3], Ying Zong[2,3], Fei Liu[1,2], Qinglong Gong[1,2], Ruopeng Cai[1,2], Fuhe Yang[4], Rui Du[2,3] and Zhiguang Chang[5]**

[1] College of Animal Medicine/College of Animal Science and Technology, Jilin Agricultural University, Changchun, China, [2] Laboratory of Production and Product Application of Sika Deer of Jilin Province, Jilin Agricultural University, Changchun, China, [3] College of Chinese Medicine Materials, Jilin Agricultural University, Changchun, China, [4] Institute of Wild Economic Animals and Plants and State Key Laboratory for Molecular Biology of Special Economical Animals, Chinese Academy of Agricultural Sciences, Changchun, China, [5] The Seventh Affiliated Hospital, Sun Yat-sen University, Shenzhen, China

OPEN ACCESS

Edited by:
Yi Fang,
Northeast Institute of Geography and Agroecology (CAS), China

Reviewed by:
Qi-En Yang,
Northwest Institute of Plateau Biology (CAS), China
Wei Kang,
Dalian University of Technology, China

***Correspondence:**
Rui Du
duruijlau@163.com
Zhiguang Chang
changzhg@mail.sysu.edu.cn

†These authors have contributed equally to this work

Specialty section:
This article was submitted to Animal Reproduction - Theriogenology, a section of the journal Frontiers in Veterinary Science

Received: *14 January 2022*
Accepted: *22 February 2022*
Published: *05 April 2022*

Citation:
Jia B, Zhang L, Ma F, Wang X, Li J, Diao N, Leng X, Shi K, Zeng F, Zong Y, Liu F, Gong Q, Cai R, Yang F, Du R and Chang Z (2022) Comparison of miRNA and mRNA Expression in Sika Deer Testes With Age. Front. Vet. Sci. 9:854503. doi: 10.3389/fvets.2022.854503

To elucidate the complex physiological process of testis development and spermatogenesis in Sika deer, this study evaluated the changes of miRNA and mRNA profiles in the four developmental stages of testis in the juvenile (1-year-old), adolescence (3-year-old), adult (5-year-old), and aged (10-year-old) stages. The results showed that a total of 198 mature, 66 novel miRNAs, and 23,558 differentially expressed (DE) unigenes were obtained; 14,918 (8,413 up and 6,505 down), 4,988 (2,453 up and 2,535 down), and 5,681 (2,929 up and 2,752 down) DE unigenes, as well as 88 (43 up and 45 down), 102 (44 up and 58 down), and 54 (18 up and 36 down) DE miRNAs were identified in 3- vs. 1-, 5- vs. 3-, and 10- vs. 5-year-old testes, respectively. By integrating miRNA and mRNA expression profiles, we predicted 10,790 mRNA–mRNA and 69,883 miRNA–mRNA interaction sites. The target genes were enriched by GO and KEGG pathways to obtain DE mRNA (IGF1R, ALKBH5, Piwil, HIF1A, BRDT, etc.) and DE miRNA (miR-140, miR-145, miR-7, miR-26a, etc.), which play an important role in testis development and spermatogenesis. The data show that DE miRNAs could regulate testis developmental and spermatogenesis through signaling pathways, including the MAPK signaling pathway, p53 signaling pathway, PI3K-Akt signaling pathway, Hippo signaling pathway, etc. miR-140 was confirmed to directly target mutant IGF1R-3′UTR by the Luciferase reporter assays. This study provides a useful resource for future studies on the role of miRNA regulation in testis development and spermatogenesis.

Keywords: sika deer, testis development, spermatogenesis, mRNA, miRNA

INTRODUCTION

Testis development and spermatogenesis are the major processes in male reproduction. Germ cells are the direct participants in spermatogenesis, which is the key in reproduction (1). Spermatogenesis is a complex process of cellular divisions and developmental changes in testicular seminiferous tubules (2). However, there are few studies on gene regulation of testis development in Cervidae family. It was only reported that MT1, MT2, VEGF, INSL3, LGR8, aFGF, bFGF, IGF-1, IGF-2, TGF alpha genes of roe deer, and steroidogenic enzymes (P450scc, P450c17,

3betaHSD, and P450arom) of Sika Deer were involved in the regulation of testis development and spermatogenesis (3–7). In addition to mRNA encoding proteins, many ncRNAs are also involved in regulation, including miRNAs.

miRNA specifically binds to the 3′UTR sequences of mRNA to degrade target genes or inhibit the translation of target genes, thereby regulating gene expression and participating in biological processes (8). miRNA presents a major effect during the testis development and spermatogenesis (9). miRNA is involved in three distinctive phases of spermatogenesis, which include mitosis of spermatogonia, meiosis of spermatocytes, and maturation of spermatids (9). For example, miR-34c and miR-221 regulate spermatogonial stem cells self-renewal by target gene Nanos2 and c-Kit (10, 11); miR-17-92 cluster regulates spermatogonial differentiation by target gene Stat3, Socs3, Bim, and c-Kit (12); miR-34b/c regulates meiosis of spermatocytes by target gene FoxJ2 (13); miR-34 and miR-122 regulate sperm development by target gene GSK3a and TNP2 (14, 15). However, there are no reports about miRNAs regulating spermatogenesis in deer. With the continuous in-depth study of miRNAs regulating spermatogenesis, it is important to understand the mechanism of deer miRNAs regulating spermatogenesis through target genes, which in turn affects male deer reproduction.

The expression of miRNA in the testis is species-specific and stage-specific. So far, many miRNAs have been identified in different species, but there are obvious differences in these miRNAs. For example, Yang et al. used miRNA microarray to analyze the testicular tissues of rhesus monkey and human. The results showed that 26.4% of miRNAs were differentially expressed in rhesus monkeys (such as mir-493-3p, mir-376b, miR-222, etc.), and 31.3% of miRNAs were differentially expressed in humans (such as miR-181c, let-7e, mir-219, etc.) (16). In addition, miRNA expression changes with testis development and spermatogenesis. Gao et al. found that 223 miRANs were differentially expressed in bovine testes at neonatal (3 days after birth) and mature (13 months) stages by RNA-seq (17). Bai et al. found that 137, 106, and 28 miRNAs were differentially expressed in sheep testes in 2 vs. 6, 6 vs. 12, and 2 vs. 12 months, respectively (18). Ran et al. found that 93, 104, and 122 miRNAs were differentially expressed in pig testes in 90-dpc (days post coitus) vs. 60-dpc, 30 days vs. 90-dpc, and 180 days vs. 30-day, respectively (19). However, there is still a lack of research on the expression patterns and mechanisms of miRNAs at different developmental stages in the testis of deer family.

There were no reports on types of germ cells in different stages in Cervidae, but Sertoli cells, primary spermatocytes, secondary spermatocytes, round spermatids and long spermatids were observed in the juvenile bovine testis closely related to Cervidae. All classes of germ cells were observed in the adolescent cattle testis, although the numbers of germ cells were small. Complete spermatogenesis was observed on adult stage and the number of sperm was large (20). Therefore, in this study, we selected the four developmental stages (juvenile, adolescent, adult, and aged) of the Sika Deer testis as the research object, and used Illumina sequencing technology to establish a comprehensive mRNA and miRNA expression profile of testis of sika deer in the whole life stage for the first time. We further constructed a miRNA–mRNA interaction network related to Sika Deer testis development and spermatogenesis. The results of this study will help to determine the molecular markers that affect the reproductive efficiency of male Sika Deer and provide a reference for finding molecular markers that regulate the reproductive ability of male Sika Deer.

MATERIALS AND METHODS

Tissues Collection

In this study, 12 Sika Deer were divided into four groups, namely the juvenile group: 1-year-old (Tst_1), the adolescence group: 3 years old (Tst_2), the adult group: 5 years old (Tst_3), and the aged group: 10 years old (Tst_4). After manual slaughter, testicular tissues were taken, frozen, and stored in liquid nitrogen until RNA extraction. All operations of Sika Deer in this study strictly followed the guidelines approved by the Ethics Committee of Jilin Agricultural University.

mRNA and miRNA Sequencing and Data Analysis

Total RNA was isolated from testis with TRIzol reagent. The Agilent 2100 bioanalyzer and NanoDrop 2000 were used to measure the quality, concentration, and integrity of RNA. Total RNA pool was collected from testes of three individuals to construct an mRNA library or a small RNA library for each growth period. According to the method we described earlier, mRNA library and small RNA library were generated and sequenced on an Illumina HiSeq2500 platform (21). The unigenes (the longest transcript of each gene) with $P_{adj} < 0.05$ and $|\log_2(\text{fold change})| > 0$ were taken as DE unigenes (22). The DE miRNAs were identified by threshold [$q < 0.005$ and $|\log_2(\text{fold change})| > 1$].

miRNA–mRNA Network Integration

miRanda and TargetScan were used to predict the target mRNAs of known and novel miRNAs. The putative target mRNAs were crossed with DE miRNAs in Tst_2 vs. Tst_1, Tst_3 vs. Tst_2, Tst_4 vs. Tst_3, respectively. Then the Pearson correlation coefficient was used to determine the candidate target mRNA the expression level of which was negatively correlated with miRNA. Finally, the regulatory networks of DE miRNA and target mRNA were modeled in Cytoscape 3.5.1.

GO and KEGG Pathway Analyses

All the DE mRNAs and DE miRNA target mRNAs were analyzed using the GO (http://geneontology.org) and KEGG (www.genome.jp/kegg) databases. The GO enrichment was used to analyze the functions of mRNAs. The *p*-value of GO terms <0.05 was significantly enriched. Similarly, the KEGG enrichment was used to analyze the pathways in which the mRNAs were involved. The *p*-value of KEGG terms <0.05 was significantly enriched.

Real-Time Fluorescent Quantitative PCR

Nine DE mRNAs (PPP2R4, Calm1, SLC7A5, DST, GSTM1, TIMP2, USF2, ITPKB, and GDI2) and nine DE miRNAs (miR-7,

miR-124a, miR-145, let-7b, miR-214, miR-196a, miR-26a, miR-125a, and miR-574) were selected for analysis of differential expression levels. For each sample, mRNAs and miRNAs were reverse-transcribed using PrimeScript™ RT reagent Kit with gDNA Eraser (Takara, Shiga, Japan) and miScript II RT Kit (Qiagen, Hilden, Germany), respectively. Q-PCR analyses on the mRNAs and miRNAs were confirmed using TB Green® Premix Ex Taq™ II (Takara) and miScript SYBR Green PCR Kit (Qiagen) in the ABI Prism 7900 System (Ambion, Carlsbad, CA, USA). GAPDH and U6 snRNA were selected as internal control of mRNA and miRNA, respectively. The $2^{-\Delta\Delta}$CT method was used to evaluate relative expression levels between surveys.

Dual-Luciferase Reporter Assays

The 3′-UTR fragments of IGF1R containing the wild-type (WT-IGF1R) or mutant (Mut-IGF1R) were cloned into the psiCHECK-2 vector. The vectors were co-transfected with miR-140 mimic into HEK-293T cells by Lipofectamine 2000 transfection reagent (Invitrogen, Carlsbad, CA, USA). Luciferase activities were measured using a Dual-Luciferase Reporter Assay System (Promega Corporation, Madison, WI, USA) after transfection for 48 h.

Data Availability

All the sequencing data of this study have been submitted to the NCBI Gene Expression Omnibus. The accession number was GSE188370.

RESULTS

Overview of mRNA Library

A total of 34,792,106; 34,728,704; 27,299,920; and 29,437,362 raw reads were generated in the Tst_1, Tst_2, Tst_3, and Tst_4 libraries, respectively. Removing the adaptors and low-quality sequences, a total of 34,199,251 (98.30%), 34,183,418 (98.43%), 26,940,428 (98.68%), and 29,030,291 (98.62%) clean reads were obtained for further analysis (**Supplementary File 1**). A total of 56,698 (59.26%), 57,243 (57.91%), 58,169 (60.69%), 55,461 (58.72%) unigenes which FPKM >0.3 were obtained (**Supplementary File 2**). The results showed that as the testis matured, the number of unigenes increased significantly. On the contrary, for testicular aging, the number of unigenes decreases significantly.

DE Unigenes and Functional Annotation Analysis

In the present study, a total of 23,558 DE unigenes among 80,133 expressed unigenes existed in the testis of Tst_1, Tst_2, Tst_3, and Tst_4 groups by calculating the $|\log_2(\text{fold change})| > 0$ and $p_{Adj} < 0.05$ as the cut off. Among them, 8,413 up- and 6,505 downregulated, 2,453 up- and 2,535 downregulated, 8,544 up- and 6,752 downregulated, 2,929 up- and 2,752 downregulated, 2,638 up- and 2,619 downregulated, and 9,015 up- and 7,872 downregulated unigenes were detected in Tst_2 vs. Tst_1, Tst_3 vs. Tst_2, Tst_3 vs. Tst_1, Tst_4 vs. Tst_3, Tst_4 vs. Tst_2, and Tst_4 vs. Tst_1, respectively (**Figure 1A**, **Supplementary File 3**).

In GO enrichment analysis, 112, 263, and 205 GO BP terms were found from Tst_2 vs. Tst_1, Tst_3 vs. Tst_2, and Tst_4 vs. Tst_3, respectively ($p < 0.05$; **Supplementary File 4**). In Tst_2 vs. Tst_1, the most enriched GO BP terms were mainly involved in the synthesis and metabolism of sugar, protein, and lipids, such as: carbohydrate derivative biosynthetic process, cellular carbohydrate biosynthetic process, cellular carbohydrate metabolic process, cellular lipid metabolic process, cellular polysaccharide biosynthetic process, cellular polysaccharide metabolic process, and cellular protein metabolic process. In Tst_3 vs. Tst_2, the most enriched GO BP terms were mainly involved in the localization and transport of cellular and protein, such as cellular localization, intracellular transport, intracellular protein transport, and cellular protein localization. In Tst_4 vs. Tst_3, the most enriched GO BP terms were

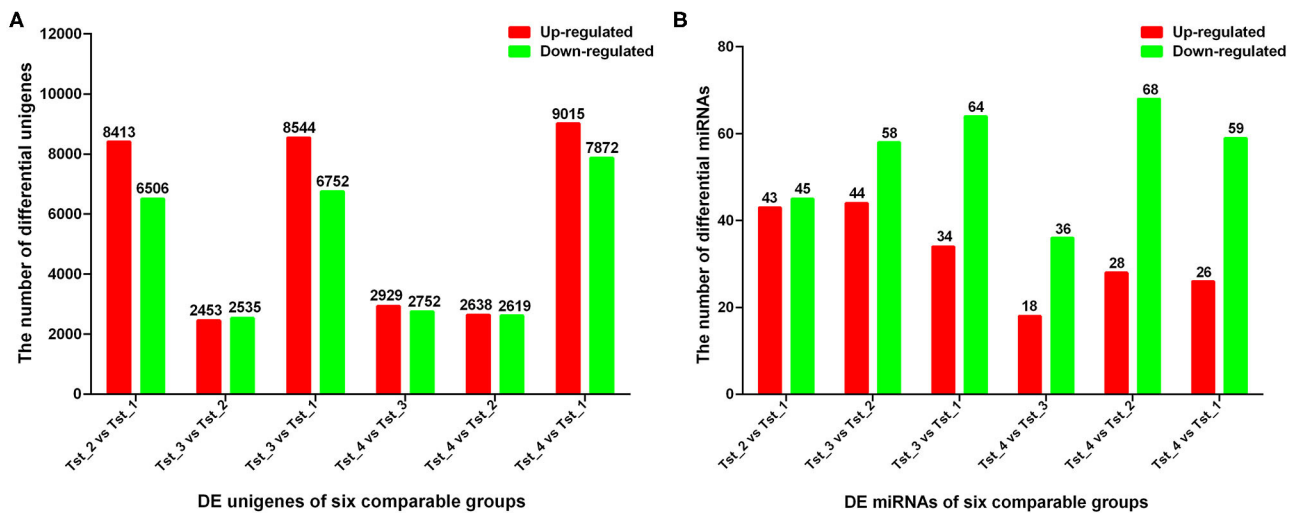

FIGURE 1 | Statistics for DE unigenes and miRNAs in each comparable group. **(A)** *q* value < 0.005 and | log 2 (*fold change*) | >1 were used as thresholds of significance for DE unigenes. **(B)** *q* value < 0.01 and |*log2* (*fold change*) | >1 were used as thresholds of significance for DE miRNAs.

mainly involved in the microtubule, such as microtubule-based process and microtubule-based movement. The top 20 enriched GO terms were shown in **Supplementary Figure 1**. In pathway analysis, 77, 61, and 75 enriched pathways were detected in Tst_2 vs. Tst_1, Tst_3 vs. Tst_2, and Tst_4 vs. Tst_3, respectively ($p < 0.05$; **Supplementary File 5**). In Tst_2 vs. Tst_1, the most significant pathway was enriched in the Hedgehog signaling pathway, Cell adhesion molecules (CAMs), MAPK signaling pathway, insulin signaling pathway, estrogen signaling pathway, and glycerophospholipid metabolism. In Tst_3 vs. Tst_2, the most significant pathway was enriched in the phagosome, hedgehog signaling pathway, and glycerophospholipid metabolism. In Tst_4 vs. Tst_3, the most significant pathway was enriched in the phagosome, thyroid hormone signaling pathway, and glycerophospholipid metabolism. The top 20 significantly enriched pathways are shown in **Supplementary Figure 2**.

Interaction Network Analysis of DE Unigenes

A total of 7,658, 1,533, and 1,599 mRNA–mRNA pairs in Tst_2 vs. Tst_1, Tst_3 vs. Tst_2, Tst_4 vs. Tst_3 contrasts were predicted in our study. In addition, DAVID was also used to examine which mRNA-mRNA interaction networks were enriched (**Supplementary File 6**). In Tst_2 vs. Tst_1, we detected that most interaction networks were involved in the MAPK signaling pathway, Wnt signaling pathway, oxytocin signaling pathway, hedgehog signaling pathway (**Figure 2A**, **Table 1**), and, especially, members of Wnt signaling pathway, the GSK3B, PRKACB, CTNNB1, and PLCB1, were the core of this network. In Tst_3 vs. Tst_2, we detected that most interaction networks were involved in the adherens junction, insulin signaling pathway, intracellular signal transduction, calcium (**Figure 2B**, **Table 1**), and especially, insulin signaling pathway, including SHC4, PTPN1, GSK3B, PDPK1, PRKCZ, PPP1CB, AKT2, and CALM1. In Tst_4 vs. Tst_3, we detected that most interaction networks were involved in arrhythmogenic right ventricular cardiomyopathy, adherens junction, calcium, and positive regulation of apoptotic process (**Figure 2C**, **Table 1**). The result indicated that the pathways of the adherens junction and calcium might play important roles both in Tst_3 vs. Tst_2 and Tst_4 vs. Tst_3. The members of the adherens junction pathway CTNNA1 and CTNNB1 were the core of these networks.

Overview of Small RNA Library

Sequencing of four libraries produced 11,297,281; 13,817,801; 12,142,852; and 10,566,461 raw reads, respectively. A total of 11,057,680 (97.88%), 13,457,309 (97.39%), 11,808,585 (97.25%), and 10,353,783 (97.99%) clean reads were obtained after removing the contaminant and adaptor reads (**Supplementary File 7**). These sequences were further mapped to the bovine reference genome (**Supplementary File 8**). In addition, an average of 1.7% of clean reads were mapped to miRNA, rRNA, tRNA, snRNA, and snoRNA (**Supplementary File 9**). A total of 183, 137, 120, and 100 known miRNAs and 45, 26, 32, and 27 novel miRNAs were identified from four development stages, respectively (**Supplementary File 10**). Among them, 92, 17, and 32 miRNAs were co-expressed in four stages, three stages, and two stages, respectively. It was worth noting that 43, 6, 6, and 2 miRNAs were specifically expressed only in the juvenile, adolescence, adult, and the aged group, respectively. The length distributions of small RNA are shown in **Supplementary Figure 3**. The ranges of 20–24 nt small RNAs were the main sizes and accounted for at least 89.5% of the population in Tst_1, while Tst_2, Tst_3, and Tst_4 were mainly 25–32 nt in size.

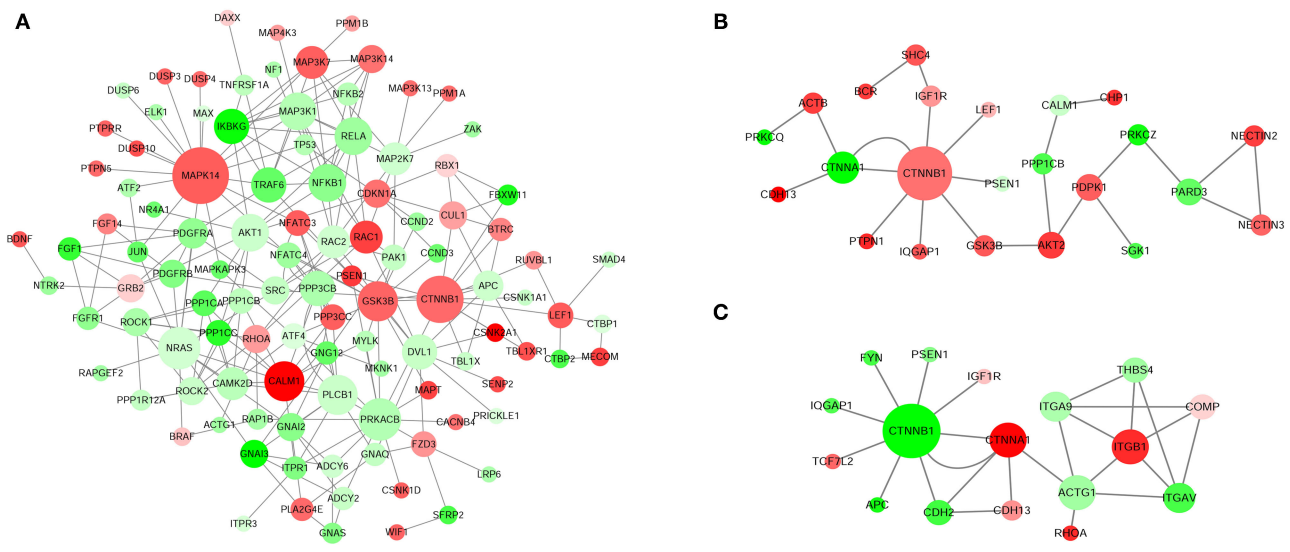

FIGURE 2 | Interaction networks of top DE unigenes in each comparable group. **(A)** Tst_2 vs. Tst_1. **(B)** Tst_3 vs. Tst_2. **(C)** Tst_4 vs. Tst_3. The up-regulated unigenes were displayed as red circles, and the down-regulated unigenes were displayed as green circles.

TABLE 1 | Summary of the represented networks generated by pathway analysis.

Data	Molecules in networks	Score	*p*-Value	Top functions
Tst_2 vs. Tst_1	AKT1, GRB2, ATF2, PTPRR, ZAK, FGF1, ELK1, PPP3CB, PPP3CC, DUSP10, MECOM, RAC2, RAC1, IKBKG, PRKACB, MAP3K7, PDGFRB, DUSP4, PDGFRA, DAXX, DUSP3, PLA2G4E, DUSP6, TNFRSF1A, PPM1A, PPM1B, CACNB4, MAPKAPK3, TRAF6, RAPGEF2, MAPT, TP53, ATF4, MAX, RELA, RAP1B, NRAS, PAK1, MKNK1, MAP2K7, MAP4K3, NTRK2, JUN, MAP3K1, BDNF, NFATC3, BRAF, GNG12, MAPK14, NFKB1, NFKB2, NR4A1, FGF14, NF1, MAP3K13, PTPN5, MAP3K14, FGFR1	108	0.003	MAPK signaling pathway
	SMAD4, GSK3B, CAMK2D, CTBP2, CTBP1, ROCK2, LEF1, CUL1, PRICKLE1, PSEN1, LRP6, CCND3, PPP3CB, PPP3CC, CCND2, WIF1, RUVBL1, DVL1, RAC2, TBL1X, RAC1, BTRC, PRKACB, MAP3K7, FZD3, JUN, CSNK2A1, FBXW11, CSNK1A1, NFATC3, SENP2, RHOA, NFATC4, RBX1, SFRP2, APC, TBL1XR1, CTNNB1, PLCB1, TP53		0.003	Wnt signaling pathway
	CDKN1A, CAMK2D, ROCK1, SRC, ROCK2, ITPR1, GNAI3, ITPR3, ADCY2, ELK1, ADCY6, ACTG1, MYLK, GNAI2, PPP1CB, PPP1CC, NRAS, PPP3CB, PPP3CC, PRKACB, JUN, PPP1R12A, PLA2G4E, NFATC3, RHOA, PPP1CA, NFATC4, CACNB4, GNAQ, GNAS, CALM1, PLCB1		0.023	Oxytocin signaling pathway
	GSK3B, CSNK1A1, FBXW11, CSNK1D, BTRC, PRKACB		0.003	Hedgehog signaling pathway
Tst_3 vs. Tst_2	PTPN1, PARD3, LEF1, CTNNA1, CTNNB1, IQGAP1, NECTIN3, ACTB, NECTIN2, IGF1R	23	0.003	Adherens junction
	SHC4, PTPN1, GSK3B, PDPK1, PRKCZ, PPP1CB, AKT2, CALM1		0.031	Insulin signaling pathway
	PDPK1, PSEN1, PRKCZ, BCR, AKT2, PRKCQ, SGK1		0.035	Intracellular signal transduction
	CDH13, CHP1, CALM1		0.033	Calcium
Tst_4 vs. Tst_3	ITGB1, TCF7L2, CDH2, CTNNA1, CTNNB1, ITGAV, ITGA9, ACTG1	17	0.044	Arrhythmogenic right ventricular cardiomyopathy
	TCF7L2, CTNNA1, CTNNB1, FYN, IQGAP1, RHOA, IGF1R, ACTG1		0.011	Adherens junction
	THBS4, COMP, CDH2, CDH13, ITGAV		0.008	Calcium
	APC, CTNNB1, PSEN1		0.028	Positive regulation of apoptotic process

DE miRNAs and Their Target Genes Functional Annotation Analysis

According to DESeq analysis between the four libraries by calculating the $\log_2$-ratio with $q < 0.005$ and $|\log_2(\text{fold change})| > 1$ as the threshold, 88, 102, 98, 54, 96, and 85 miRNAs were different in Tst_2 vs. Tst_1, Tst_3 vs. Tst_2, Tst_3 vs. Tst_1, Tst_4 vs. Tst_3, Tst_4 vs. Tst_2, and Tst_4 vs. Tst_1, respectively (**Supplementary File 11**). In Tst_2 vs. Tst_1, 43 miRNAs were upregulated, and 45 miRNAs were downregulated. In Tst_3 vs. Tst_2, 44 miRNAs were upregulated, and 58 miRNAs were downregulated. In Tst_3 vs. Tst_1, 34 miRNAs were upregulated, and 64 miRNAs were downregulated. In Tst_4 vs. Tst_3, 18 miRNAs were upregulated, and 36 miRNAs were downregulated. In Tst_4 vs. Tst_2, 28 miRNAs were upregulated, and 68 miRNAs were downregulated. In Tst_4 vs. Tst_1, 26 miRNAs were upregulated, and 59 miRNAs were downregulated (**Figure 1B**, **Supplementary File 11**). Moreover, the hierarchical clusters of DE miRNAs between four stages indicated there were a large number of DE miRNA in the development of Sika Deer testis (**Figure 3**).

In order to identify the potential functional of miRNAs, miRanda was used to predict the target gene of DE miRNAs. In total, 36,571; 19,504; and 13,808 target genes of DE miRNAs were predicted in Tst_2 vs. Tst_1, Tst_3 vs. Tst_2, and Tst_4 vs. Tst_3, respectively. We further analyzed the function of target genes during the development of Sika Deer testis according to GO and KEGG analysis. There was no significant difference in the GO enrichment among four comparisons, mainly including substance and energy synthesis, protein modification, metabolic process, cell mitosis, etc. (**Supplementary Figure 4**). Similarly, there was no significant difference in the KEGG pathway enrichment among four comparisons, mainly including, PI3K-Akt signaling pathway, Focal adhesion, protein digestion and absorption, ECM-receptor interaction, etc. (**Supplementary Figure 5**).

Identification of DE Unigenes Involved in Testis Development and Spermatogenesis and Their Interacting miRNAs

The interaction network of DE unigenes and DE miRNAs, which regulated the testis development and spermatogenesis of Sika Deer, was predicted by STRING website and visualized by Cytoscape 3.5.1. Integrating the miRNA-gene interaction network and previous reports, we found that there were

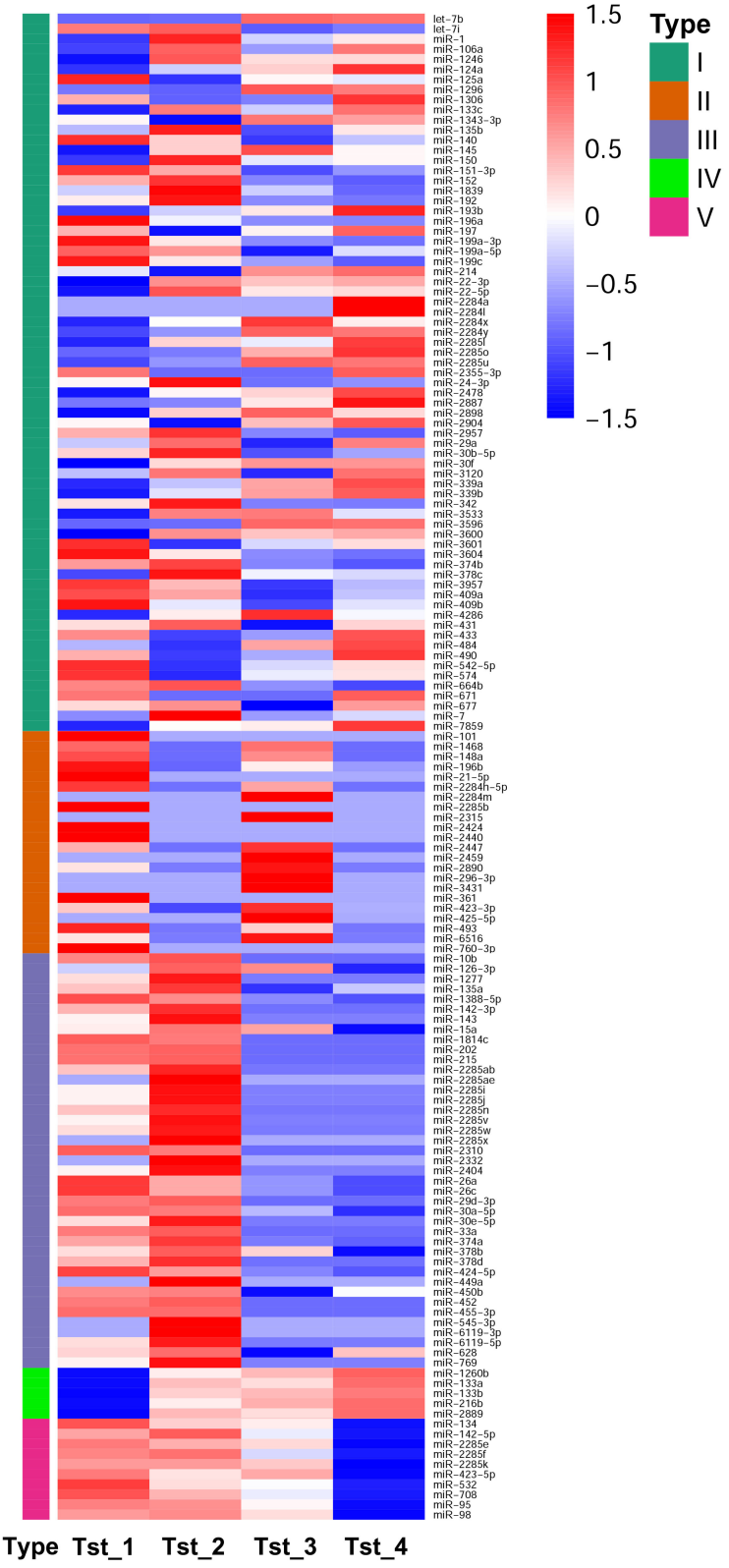

FIGURE 3 | Hierarchical clustering of DE miRNAs.

18 miRNAs involved in the regulation of testis development and spermatogenesis (**Table 2**). Among them, 189 pairs of miRNA-gene were negatively related to testis development, and 331 pairs of miRNA-gene were negatively related to spermatogenesis (**Figures 4**, **5**). **Figure 4A** shows that miR-7 and miR-145 were upregulated which targeted HMGB1, HSPA8, CYP11A1, ALKBH5, etc., associated with testis development. In contrast, **Figure 4B** shows that miR-26a, miR-574, miR-140, miR-125a, miR-202, and miR-215 were downregulated, which targeted IGF1R, Piwil, StAR, TSPYL1, etc., associated with testis development. Similarly, **Figure 5A** shows that let-7b, miR-214, miR-124a, miR-106a, miR-449a, and miR-7 were upregulated, which targeted HIF1A, CSF1, TCP11, SPAG17, PEBP1, AKAP3, CNOT7, PHB, etc., associated with spermatogenesis. On the contrary, **Figure 5B** shows that miR-135a, miR-196a, miR-10b, miR-21-5p, miR-15a, miR-26a, miR-140, and miR-202 were downregulated, which targeted DPY19L2, HSPA4L, PELO, Piwil1, TSGA10, IP6K1, MNS1, BRDT, CEP55, SMC6, etc., associated with spermatogenesis. The above miRNAs contributed significantly to the regulation of mRNA expression during the testis development and spermatogenesis of Sika Deer.

RNA-seq and miRNA-seq Data Validation

Nine mRNAs (PPP2R4, Calm1, SLC7A5, DST, GSTM1, TIMP2, USF2, ITPKB, and GDI2) and nine known miRNAs (miR-7, miR-124a, miR-145, let-7b, miR-214, miR-196a, miR-26a, miR-125a, and miR-574) were randomly selected to verify the RNA-seq and miRNA-seq data by Q-PCR. As shown in **Figures 6**, **7**, Q-PCR data were basically consistent with sequencing data in the four stages. The results indicated that our sequencing data were reliable, although the fold change was not completely consistent.

miR-145 Targets IGF1R

IGF1R was observed to be a major target of miR-140-5p based on bioinformatics databases. To verify their targeted regulatory relationship, we performed the Luciferase reporter assays and confirmed that, compared with the negative control, the luciferase activity of IGF1R receptor decreased by 75.6% after co-transfection of mir-140 mimics for 48 h. The results showed that miR-140 can directly target IGF1R-3′UTR (**Figure 8**).

DISCUSSION

The improvement of the reproductive efficiency of Sika Deer, especially in the male deer, was essential for livestock production. The testis development and spermatogenesis, which were mainly regulated by uniquely expressed genes at different developmental stages, were key factors affecting the reproductive efficiency of male deer. In this study, we analyzed mRNAs and miRNAs expression in the testes from 1-, 3-, 5-, and 10-year-old testis, which represent the juvenile, adolescence, adult, and aged stages,

TABLE 2 | miRNAs identified in testis associated with testis development and spermatogenesis.

miRNA ID	Testis development	miRNA ID	Spermatogenesis
miR-145	Regulating the tight junctions of the epididymis by targeting Cldn10 (23)	let-7b	Regulating the glycolysis in asthenozoospermia by targeting AURKB (24)
miR-7a	Regulating the FSH and LH synthesis and secretion by pituitary prostaglandin and BMP4 signaling (25)	miR-214	Regulating the meiosis by targeting WD and WDTC1 (26)
miR-26a	Regulating the testis steroidogenesis by targeting FGF9 (27)	miR-124a	Regulating the proliferation of immature sertoli cells by targeting AR (28)
miR-574	Regulating the testis development and reproduction by targeting AURKA (29)	miR-106a	Regulating the renewal and differentiation of spermatogonial stem cells by targeting STAT3 and Ccnd1 (30)
miR-140	testis differentiation (31)	miR-449a	Regulating the proliferation of spermatogonia by targeting CEP55 (32)
miR-125a	Regulating the testis degeneration by targeting SOD-1 (33)	miR-7	Regulating the differentiation of germ stem cells into primary spermatocytes by targeting Bam (34)
miR-202	male differentiation and development (35)	miR-135a	Regulating the proliferation and renewal of spermatogonial stem cells by targeting Foxo1 (36)
miR-215	Regulating the testis early developmental stage by targeting p53 (37)	miR-196a	Regulating the proliferation and apoptosis of immature sertoli cell by targeting RCC2 and ABCB9 (38)
		miR-10b	Regulating the proliferation of spermatogonial stem cells by targeting KLF4 (39)
		miR-21-5p	Regulating the renewal of spermatogonial stem cells by targeting ETV5 (40)
		miR-15a	Regulating the differentiation of spermatogonial stem cells by targeting Ccnt2 (41)
		miR-26a	Regulating the proliferation and promotes apoptosis of sertoli cells by targeting PAK2 (19)
		miR-140	Regulating the transformation from spermatogonia cells to primary spermatocytes (42)
		miR-202	(1) Regulating the proliferation, apoptosis, and synthesis of sertoli cells by targeting LRP6 and Cyclin D1 (43) (2) Regulating the renewal and differentiation of spermatogonial stem cells by targeting GDNF and RA (44)

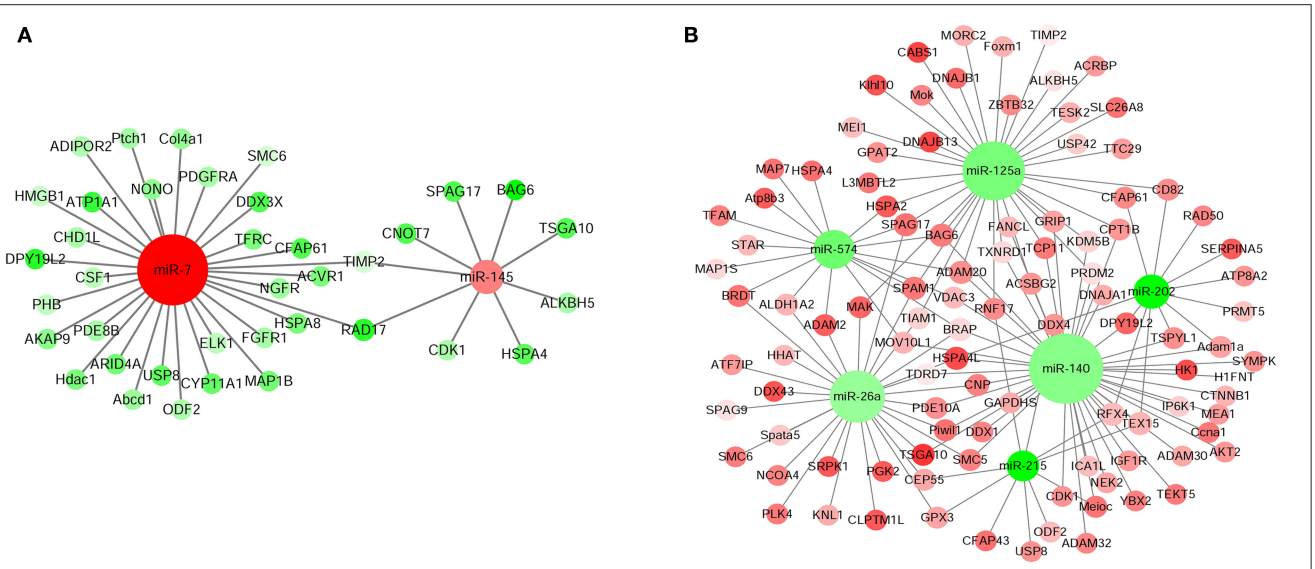

FIGURE 4 | miRNA-mRNA interaction network related to testis development of Sika Deer. **(A)** Up-regulated miRNAs and down-regulated target genes related to testis development. **(B)** Down-regulated miRNAs and up-regulated target genes related to testis development. The up-regulated miRNAs or genes were displayed as red circles, and the down-regulated miRNAs or genes were displayed as green circles.

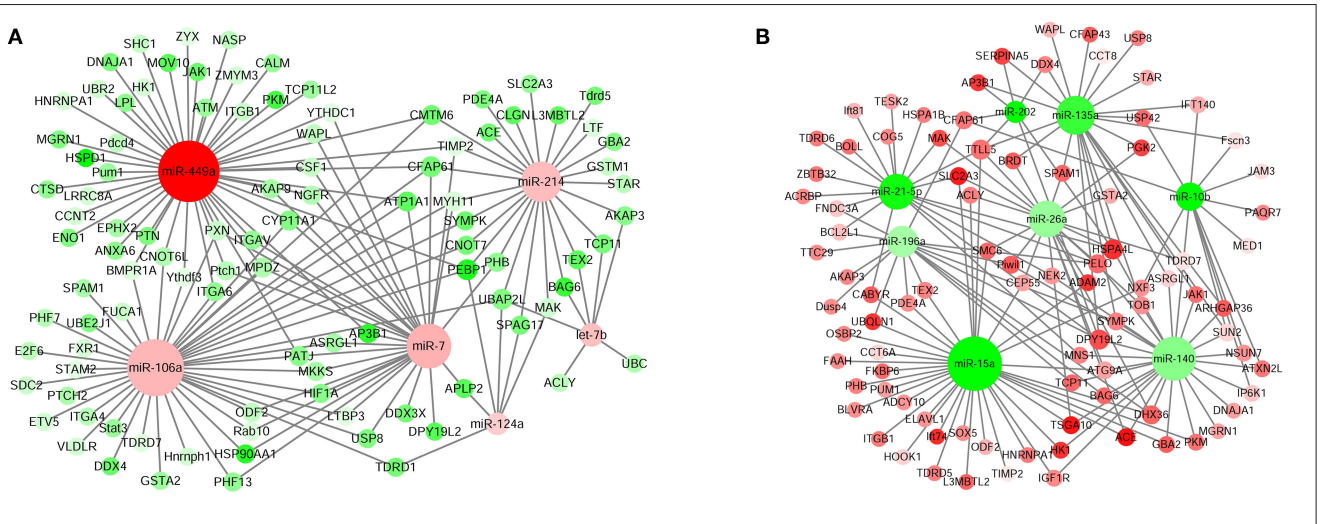

FIGURE 5 | miRNA-mRNA interaction network related to spermatogenesis of Sika Deer. **(A)** Up-regulated miRNAs and down-regulated target genes related to spermatogenesis. **(B)** Down-regulated miRNAs and up-regulated target genes related to spermatogenesis. The up-regulated miRNAs or genes were displayed as red circle, and the down-regulated miRNAs or genes were displayed as green circles.

using high throughput deep sequencing. The aim of this study was to identify crucial miRNAs and mRNAs in testis development and spermatogenesis of Sika Deer. This analysis will help reveal biomarkers related to the reproductive efficiency of male Sika Deer.

In this study, the DE unigenes in Sika Deer testes at four development stages were enriched by GO. It was found that testicular development at different stages was regulated by different genes and biological functions, which was a complex biological process. In pathway analysis, for Tst_2 vs. Tst_1 contrast, the most significant pathway was enriched in cell adhesion molecules (CAMs), MAPK signaling pathway, insulin signaling pathway, and estrogen signaling pathway. These signal pathways were closely related to testicular development and spermatogenesis. For example, the pathway of CAMs can control the sexual and asexual development (45). MAPK signaling pathways were involved in mediating the mitogenic effect of IL-1 on Sertoli cells *in vitro* (46). Insulin signaling pathway played the essential role in regulating the final number of Sertoli cells, testis size, and daily sperm output (47). Estrogen signaling pathway had an important influence on the proliferation, apoptosis, survival, and maturation of sperm (48). It could be seen that these signaling pathways play an important role in the early stages of sexual maturity. Furthermore, Hedgehog signaling pathway was an overlapping pathway in Tst_2 vs. Tst_1 and Tst_3 vs. Tst_2. The Hedgehog signaling pathway has been reported to

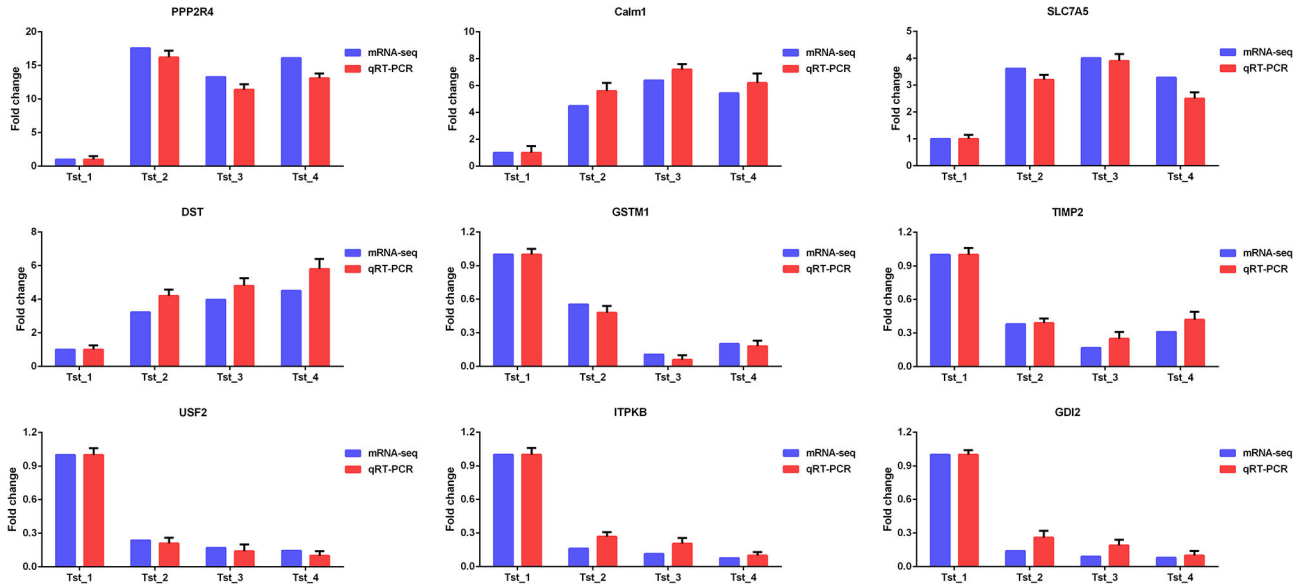

FIGURE 6 | Q-PCR validation of mRNA-seq data.

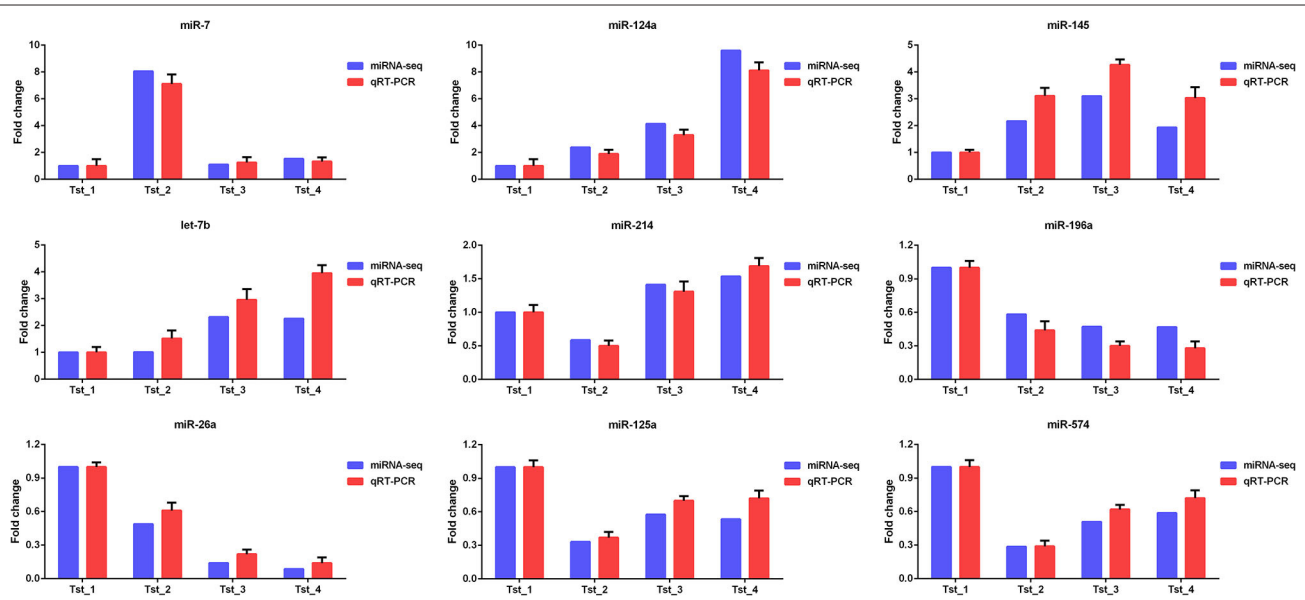

FIGURE 7 | Q-PCR validation of miRNA-seq data.

regulate the development of testicular cord and spermatogonial stem cells (49, 50). Phagosome was an overlapping pathway in Tst_3 vs. Tst_2 and Tst_4 vs. Tst_3. Phagosome was involved in the regulation of spermatogenesis (51). Glycerophospholipid metabolism was an overlapping pathway in three groups. It has been reported that glycerophospholipid metabolism was predicted to have dramatic effects on the male sexual differentiation and development (52). The results suggested that these pathways play a vital role in the testis development and spermatogenesis.

The core mRNA–mRNA network was constructed to reveal the regulatory relationship of testis development and spermatogenesis. In Tst_2 vs. Tst_1, the top DE unigenes interaction networks participated in MAPK signaling pathway, Wnt signaling pathway, oxytocin signaling pathway, and hedgehog signaling pathway. Among them, Wnt signaling pathway played a suppression role in mouse and human spermatogonia, which was a prerequisite for the normal development of primordial germ cells (53). The CTNNB1 and GSK3B were the core of this network. CTNNB1 could participate

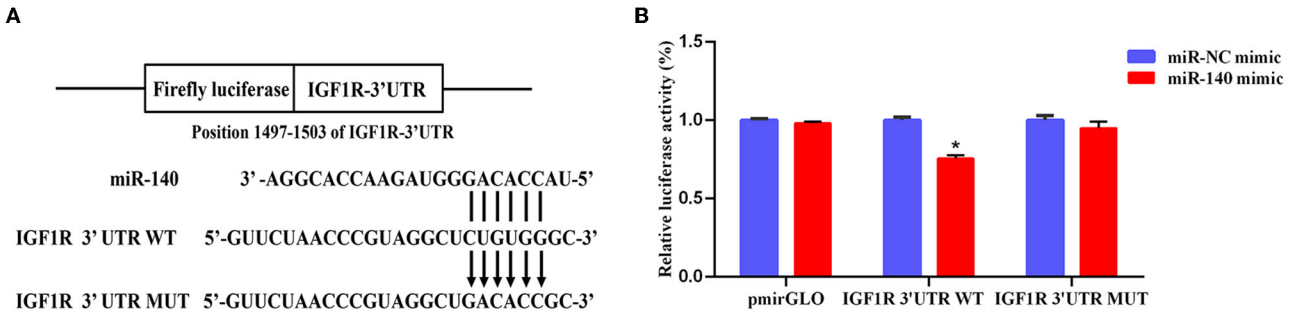

FIGURE 8 | Detection of interactions between miR-140 and IGF1R by dual luciferase reporter system. **(A)** Binding site sequence of miR-140 and target gene IGF1R. **(B)** miR-140 mimic was cotransfected with IGF1R 3 'UTR WT or IGF1R 3 'UTR MUT to detect the luciferase activity for 48 h. *$p < 0.05$.

in the Wnt signaling pathway by encoding the β-catenin gene. Overexpression of CTNNB1 led to gender reversal, which was essential for male reproduction (54). GSK3B could precisely control the testis development of tambaqui by regulating Wnt signaling pathway and/or sox9 expression (55). Furthermore, the top DE unigene interaction networks participated in the adherens junction signaling pathway and calcium signaling pathway both in Tst_3 vs. Tst_2 and Tst_4 vs. Tst_3. Adhesive junctions mainly occur at the seminiferous epithelium (Sertoli–Sertoli and Sertoli–germ cell interfaces), so that the developing germ cells can migrate from the basal compartment of the seminiferous epithelium toward the adluminal compartment for further development (56). CTNNA1 and CTNNB1 were the core members of the Adherens junction signaling pathway. As we all know, CTNNA1 was a member of the catenin protein family, which was crucial for cell adhesion. It was located on the plasma membrane and binds to cadherin (57). In addition, calcium signaling pathway was necessary for many physiological processes such as spermatogenesis, sperm motility, capacitation, acrosome reaction, and fertilization (58). CDH2 was an important member of calcium signaling pathway. The lack of Cdh2 in Sertoli cells caused damage to the blood–testis barrier, which in turn led to meiosis and spermatogenesis failure (59). Taken together, through interaction network analysis of DE unigenes, we have screened the core regulatory unigenes for Sika Deer testis development and spermatogenesis, such as CTNNA1, CTNNB1, GSK3B, and CDH2.

It was known that miRNA played an important regulatory role in testis development and spermatogenesis, but there was no related research on its regulation of Sika Deer testis. We integrated the changes of miRNA profiles in testis at four different developmental stages. The ranges of 20–24nt small RNAs were the main size of the population in Tst_1, while Tst_2, Tst_3, and Tst_4 were mainly 25–32 nt in size. This result suggested that reads longer than 25 nt were mainly from piRNA. As a newly discovered small regulatory RNA, piRNA was abundantly enriched in mature testis (60). In our research, the expression profile of miRNAs had obvious growth stage specificity, in which miRNAs associated with testis development and spermatogenesis were expressed at specific growth stages. For example, miR-106b, miR-19b, miR-27a-3p, miR-27b, miR-31, and miR-335 were expressed specifically on the juvenile stage (61–66); miR-449a was expressed specifically on the adolescence stage (32); miR-296-3p was expressed specifically on the adult stage (67). The results suggested that the growth period-specific miRNAs have an important influence on testis development and spermatogenesis.

This study tried for the first time to determine the key miRNA targets by integrated analysis and the expression profiles of miRNA and mRNA in the testes of Sika Deer. In **Figure 4A**, miR-7 and miR-145 related to testis development were upregulated. The target mRNAs of these miRNAs included HMGB1, HSPA8, CYP11A1, ALKBH5, etc., as the central node genes. Among them, HMGB1, as a paracrine host defense factor in the testis, was translocated from testicular cells and blocking its action by ethyl pyruvate regulated inflammatory reactions in testes and spermatogenic damage (68, 69). Testis-specific HSPA8 gene was confirmed to decrease with the development of goat testis, which may be due to dilution by the maturing germ cell population (70). Lower concentrations of HSPA8 were associated with subfertility in men (71). CYP11A1, as a steroidogenic enzyme gene, induced gonadal differentiation and development by regulating steroidogenesis (72). CYP11A1 was fetal Leydig cell marker genes (73). Kim et al. found that CYP11A1 was responsible for C21-steroid hormone metabolism and played an important role in the recovery of testicular aging in rats (74). Baker et al. found that there was a significant correlation between the rate of ALKBH5 protein-coding substitutions and the rate of testis size evolution. ALKBH5 drives the evolution of testis size in tetrapod vertebrates (75). In our study, with the development of Sika Deer testes, upregulation of miR-7 and miR-145 inhibited the expression of HMGB1, HSPA8, CYP11A1, and ALKBH5, respectively, thereby regulating testicular maturation.

In **Figure 4B**, miR-26a, miR-125a, miR-140, miR-202, miR-215, and miR-574 related to testis development were downregulated. The target mRNAs of these miRNAs included IGF1R, Piwil, StAR, TSPYL1, etc., as the central node genes. Among them, IGF1R was required for the appearance of male gonads and thus for male sexual differentiation (76). IGF1R has also been confirmed to decrease in expression with increasing age in goat testes, presumably due to maturation of cells and cessation of testis growth (70). Piwil mainly appeared in the early stage of gonadal development, and its expression in testis first increased and then decreased. It was an important regulatory gene of germ cell division during gonadal development (77).

StAR was mainly expressed in Leydig cells of mammalian testis and played an imperative role in testosterone biosynthesis and male fertility (78). The interstitial lipid deposits worsened considerably in StAR knockout mice testes, and the germ cells showed the histological characteristics of apoptosis, which was consistent with the unsatisfactory androgen secretion (79). TSPYL1 specifically recruited ZFP106 through amino acids 412–781, which was considered to be a key pathway involved in testes development (80). It was first reported in 2004 that the loss of function mutations of TSPYL1 gene caused Sudden Infant Death with Dysgenesis of the Testes syndrome (81). Taken together, it was speculated that the downregulation of miR-140 promoted the expression of the IGF1R, Piwil, and TSPYL1 during the development of Sika Deer testes, thereby promoting testicular maturation. In conclusion, these DE miRNAs might play an important role in the regulation of the development of Sika Deer testes through target genes.

In **Figure 5A**, let-7b, miR-214, miR-124a, miR-106a, miR-449a, and miR-7 related to spermatogenesis were upregulated. The target mRNAs of these miRNAs included HIF1A, CSF1, TCP11, SPAG17, PEBP1, AKAP3, CNOT7, PHB, etc., as the central node genes. Among them, the upregulation of miR-7 inhibited the expression of target genes HIF1A and CSF1. HIF1 was a highly specific nuclear transcription factor, which was closely related to the apoptosis of spermatogenic cells (82). After silencing the HIF1A gene in the testis of varicocele rats, the apoptosis of spermatogenic cells was reduced and the spermatogenic function of the testes was significantly improved (83). CSF1 was an extrinsic stimulator of spermatogonial stem cells self-renewal (84). The protein level of CSF1 was the highest in the testis of 1-week-old mice and decreased significantly with age (2–12 weeks). CSF1 was also involved in inducing the proliferation and differentiation of spermatogonial cells to meiotic and postmeiotic stages (85). Therefore, it was speculated that the upregulated miR-7 promoted spermatogenesis through target genes HIF1A and CSF1. Similarly, the upregulation of miR-214 inhibited the expression of target genes TCP11, SPAG17, PEBP1, AKAP3, CNOT7, and PHB. TCP11 was a testis-specific gene, which played a role in elongated spermatids to confer proper motility in mature sperm (86). In addition to affecting sperm motility, SPAG17-deficient mice were sterile due to prevention of the normal manchette structure, protein transport, and formation of the sperm head and flagellum (87). PEBP1 was specifically expressed in the head of the elongated spermatids and mature spermatozoa. PEBP1 could affect the function of mature sperm in pachytene primary spermatocytes and spermatids by activating the expression of ERK1/2 (88). AKAP3 was one of the main components of sperm tail fibrous sheath formed during spermatogenesis. In the elongating stage of mice spermiogenesis, the protein complexes of AKAP3, PKA, and RNA binding proteins can be synthesized under the regulation of PKA signaling to participate in the process of spermatogenesis (89). CNOT7 was a CCR4-related transcription cofactor, which is essential for spermatogenesis. The maturation of spermatids in seminiferous tubules of CNOT7 deficient mice was asynchronous and damaged (90). PHB was mainly located in mitochondria during spermatogenesis, which regulated the proliferation of spermatogonia, mitochondrial morphology, and function in spermatogenic cells (91). PHB-deficient mice resulted in infertility due to meiotic pachytene arrest, mitochondrial morphology, and function impairment (92). In conclusion, it was speculated that upregulated miR-214 was involved in spermatogenesis through target genes TCP11, SPAG17, PEBP1, AKAP3, CNOT7, and PHB.

In **Figure 5B**, miR-135a, miR-196a, miR-10b, miR-21-5p, miR-15a, miR-26a, miR-140, and miR-202 were downregulated. The target mRNAs of these miRNAs included DPY19L2, HSPA4L, PELO, Piwil1, TSGA10, IP6K1, MNS1, BRDT, CEP55, SMC6, etc., as the central node genes. Among them, Piwil1 was crucial for spermatogenesis because it used different domains to interact with several spermiogenic mRNAs after meiosis, and partially participated in translation regulation through 3′-UTRs (93). TSGA10-deficient mice had significantly reduced sperm motility due to the disorder of mitochondrial sheath formation during spermatogenesis (94). The spermatids of IP6K1-deficient mice express TNP2 and PRM2 prematurely, resulting in abnormal elongation of spermatid and inability to complete spermatid differentiation (95). MNS1 was located in the sperm flagella and played an important role in spermatogenesis, the assembly of sperm flagella, and ciliary movement (96). Thus, the downregulated miR-140 promoted spermatogenesis through target genes Piwil1, TSGA10, IP6K1, and MNS1. Similarly, BRDT was a key regulator of transcription in meiotic and post-meiotic cells. The loss of BRDT function destroyed the epigenetic state of meiotic sex chromosome inactivation in spermatocytes (97). CEP55 gene silencing could inhibit the proliferation of mouse spermatogonia and play a key role in spermatogenesis (98). SMC6 played a role in preventing aberrant recombination events between pericentromeric regions in the first meiotic prophase (99). These findings suggested that miR-26a low-expression partially regulated spermatogenesis by promoting the expression of BRDT, CEP55, and SMC6. In addition, the defect of DPY19L2 gene was the main genetic cause of human globozoospermia, which may be related to the defect of chromatin compaction during spermatogenesis and sperm DNA damage (100). HSPA4L was highly expressed from late pachytene spermatocytes to postmeiotic spermatids. The germ cells of HSPA4L deficient mice were apoptotic, resulting in a decrease in the number of sperm count (101). PELO gene mutation led to cell cycle arrest in the G2/M transition period before the first meiosis during spermatogenesis (102). DPY19L2 was the target gene for miR-135a, miR-202, miR-196a, miR-21-5p, and miR-140. HSPA4L was the target gene for miR-21-5p, miR-26a, miR-135a, miR-140, and miR-202. PELO was the target gene for miR-196a, miR-21-5p, miR-26a, and miR-140. It was speculated that these miRNAs might promote spermatogenesis by upregulating the target genes DPY19L2, HSPA4L, and PELO.

In addition, IGF1R was a widely expressed tyrosine kinase that regulated cell proliferation, differentiation, and survival (103). As one of the sex differentiation genes, IGF1R played an important role in regulating Sertoli cell number, testis size, and daily sperm output (47). Pintus et al. found that the Sertoli cell number affected testis size, sperm quantity, and sperm quality in red deer (104). It could be seen that IGF1R was crucial to regulate

testis development in Cervidae. Bioinformatics analysis and dual luciferase reporter analysis showed that the 3′UTR of IGF1R matched the seed sequence of miR-140. miR-140 could reduce the expression of IGF1R. However, the hypothesis that miR-140 is involved in Sika Deer testis development and spermatogenesis by targeting IGF1R needs to be further verified.

CONCLUSION

This study first reported the important miRNA–mRNA network derived by the global analysis and integration of the changes of miRNA and mRNA levels in Sika Deer testis. Some mRNAs and miRNAs were found to be common, which means that they could be necessary for testis development and spermatogenesis. At the same time, some differential expressions of mRNAs and miRNAs were found in testis at different developmental stages (1-, 3-, 5-, and 10-year-old), which means that they could play different but important roles in testis development and spermatogenesis. In particular, the binding sites of miR-140 with IGF1R was validated. In the future, we will focus on studying the role of individual miRNA in testicular development and exploring relevant pathways to reveal the mechanism of Sika Deer spermatogenesis.

DATA AVAILABILITY STATEMENT

The datasets presented in this study can be found in online repositories. The names of the repository/repositories and accession number(s) can be found in the article/**Supplementary Material**.

ETHICS STATEMENT

The animal study was reviewed and approved by Jilin Agricultural University Committee on the use of live animals. Written informed consent was obtained from the owners for the participation of their animals in this study.

AUTHOR CONTRIBUTIONS

BJ, RD, and ZC: conceptualization. BJ, LZ, FM, XW, and FY: methodology. BJ, JL, ND, XL, YZ, and QG: software. BJ, KS, and FZ: writing—original draft preparation. BJ, FL, and RC: writing—reviewing and editing. RD and ZC: supervision. All authors contributed to the article and approved the submitted version.

FUNDING

This study was funded by National Natural Science Foundation of China (Grant/Award Nos. 32002171 and 81802869) and Science and Technology Research Project of Jilin Province Education Department (Grant/Award No. JJKH20220364KJ).

SUPPLEMENTARY MATERIAL

The Supplementary Material for this article can be found online at: https://www.frontiersin.org/articles/10.3389/fvets.2022.854503/full#supplementary-material

Supplementary Figure 1 | The top 20 GO categories of DE unigenes in each comparable group.

Supplementary Figure 2 | The top 20 enriched KEGG pathways of DE unigenes in each comparable group.

Supplementary Figure 3 | Characterization of miRNA-seq mapped reads from the small RNA sequencing of testis.

Supplementary Figure 4 | The top 20 enriched GO terms for the potential genes targeted by DE miRNAs.

Supplementary Figure 5 | The top 20 enriched KEGG pathways for the potential genes targeted by DE miRNAs.

Supplementary File 1 | Summary of transcriptome data.

Supplementary File 2 | FPKM statistical of testis transcriptome in Sika Deer.

Supplementary File 3 | The lists of DE unigenes from RNA sequencing.

Supplementary File 4 | GO categories of differential unigenes in four growth periods.

Supplementary File 5 | KEGG pathways of differential unigenes in four growth periods.

Supplementary File 6 | Interaction networks of DE unigenes in each comparable group.

Supplementary File 7 | Summary of miRNAome data.

Supplementary File 8 | Statistical information of small RNAs mapping to reference sequence.

Supplementary File 9 | Small RNAs annotation.

Supplementary File 10 | Identification of known miRNAs and novel miRNAs.

Supplementary File 11 | The lists of DE known miRNAs.

REFERENCES

1. Li Y, Li J, Fang C, Shi L, Tan J, Xiong Y, et al. Genome-wide differential expression of genes and small RNAs in testis of two different porcine breeds and at two different ages. *Sci Rep.* (2016) 6:26852. doi: 10.1038/srep26852
2. de Kretser DM, Loveland KL, Meinhardt A, Simorangkir D, Wreford N. Spermatogenesis. *Hum Reprod.* (1998) 13 (Suppl. 1):1–8. doi: 10.1093/humrep/13.suppl_1.1
3. Hayakawa D, Sasaki M, Suzuki M, Tsubota T, Igota H, Kaji K, et al. Immunohistochemical localization of steroidogenic enzymes in the testis of the sika deer (Cervus nippon) during developmental and seasonal changes. *J Reprod Dev.* (2010) 56:117–23. doi: 10.1262/jrd.09-102T
4. Hombach-Klonisch S, Schon J, Kehlen A, Blottner S, Klonisch T. Seasonal expression of INSL3 and Lgr8/Insl3 receptor transcripts indicates variable differentiation of leydig cells in the roe deer testis. *Biol Reprod.* (2004) 71:1079–87. doi: 10.1095/biolreprod.103.024752
5. Koziol K, Broda D, Romerowicz-Misielak M, Nowak S, Koziorowski M. Melatonin concentration in peripheral blood and melatonin receptors (MT1 and MT2) in the testis and epididymis of male roe deer during active spermatogenesis. *Theriogenology.* (2020) 149:25–37. doi: 10.1016/j.theriogenology.2020.03.025
6. Wagener A, Blottner S, Goritz F, Streich WJ, Fickel J. Differential changes in expression of a and b FGF. IGF-1 and−2, and TGF-alpha during

seasonal growth and involution of roe deer testis. *Growth Fact.* (2003) 21:95–102. doi: 10.1080/0897719031000162102 3
7. Wagener A, Blottner S, Goritz F, Streich WJ, Fickel J. Circannual changes in the expression of vascular endothelial growth factor in the testis of roe deer (*Capreolus capreolus*). *Anim Reprod Sci.* (2010) 117:275–8. doi: 10.1016/j.anireprosci.2009.05.006
8. Bartel DP. MicroRNAs: genomics, biogenesis, mechanism, and function. *Cell.* (2004) 116:281–97. doi: 10.1016/S0092-8674(04)00045-5
9. Kotaja N. MicroRNAs and spermatogenesis. *Fertil Steril.* (2014) 101:1552–62. doi: 10.1016/j.fertnstert.2014.04.025
10. Yang QE, Racicot KE, Kaucher AV, Oatley MJ, Oatley JM. MicroRNAs 221 and 222 regulate the undifferentiated state in mammalian male germ cells. *Development.* (2013) 140:280–90. doi: 10.1242/dev.087403
11. Yu M, Mu H, Niu Z, Chu Z, Zhu H, Hua J. miR-34c enhances mouse spermatogonial stem cells differentiation by targeting Nanos2. *J Cell Biochem.* (2014) 115:232–42. doi: 10.1002/jcb.24655
12. Xie R, Lin X, Du T, Xu K, Shen H, Wei F, et al. Targeted disruption of mir-17-92 impairs mouse spermatogenesis by activating mTOR signaling pathway. *Medicine.* (2016) 95:e2713. doi: 10.1097/MD.0000000000002713
13. Comazzetto S, Di Giacomo M, Rasmussen KD, Much C, Azzi C, Perlas E, et al. Oligoasthenoteratozoospermia and infertility in mice deficient for miR-34b/c and miR-449 loci. *PLoS Genet.* (2014) 10:e1004597. doi: 10.1371/journal.pgen.1004597
14. Guo W, Xie B, Xiong S, Liang X, Gui JF, Mei J. miR-34a Regulates Sperm Motility in zebrafish. *Int J Mol Sci.* (2017) 18:2676. doi: 10.3390/ijms18122676
15. Liu T, Huang Y, Liu J, Zhao Y, Jiang L, Huang Q, et al. MicroRNA-122 influences the development of sperm abnormalities from human induced pluripotent stem cells by regulating TNP2 expression. *Stem Cells Dev.* (2013) 22:1839–50. doi: 10.1089/scd.2012.0653
16. Yan N, Lu Y, Sun H, Qiu W, Tao D, Liu Y, et al. Microarray profiling of microRNAs expressed in testis tissues of developing primates. *J Assist Reprod Genet.* (2009) 26:179–86. doi: 10.1007/s10815-009-9305-y
17. Gao Y, Wu F, Ren Y, Zhou Z, Chen N, Huang Y, et al. MiRNAs expression profiling of bovine (*Bos taurus*) testes and effect of bta-miR-146b on proliferation and apoptosis in bovine male germline stem cells. *Int J Mol Sci.* (2020) 21:3846. doi: 10.3390/ijms21113846
18. Bai M, Sun L, Jia C, Li J, Han Y, Liu H, et al. Integrated analysis of miRNA and mRNA expression profiles reveals functional miRNA-targets in development testes of small tail han sheEP. *G3.* (2019) 9:523–33. doi: 10.1534/g3.118.200947
19. Ran M, Weng B, Cao R, Li Z, Peng F, Luo H, et al. miR-26a inhibits proliferation and promotes apoptosis in porcine immature sertoli cells by targeting the PAK2 gene. *Reprod Domest Anim.* (2018) 53:1375–85. doi: 10.1111/rda.13254
20. Rawlings N, Evans AC, Chandolia RK, Bagu ET. Sexual maturation in the bull. *Reprod Domest Anim.* (2008) 43 (Suppl. 2):295–301. doi: 10.1111/j.1439-0531.2008.01177.x
21. Jia B, Liu Y, Li Q, Zhang J, Ge C, Wang G, et al. Altered miRNA and mRNA expression in sika deer skeletal muscle with age. *Genes.* (2020) 11:172. doi: 10.3390/genes11020172
22. Zhuo D, Zhao WD, Wright FA, Yang HY, Wang JP, Sears R, et al. Assembly, annotation, and integration of UNIGENE clusters into the human genome draft. *Genome Res.* (2001) 11:904–18. doi: 10.1101/gr.164501
23. Belleannee C, Calvo E, Thimon V, Cyr DG, Legare C, Garneau L, et al. Role of microRNAs in controlling gene expression in different segments of the human epididymis. *PLoS ONE.* (2012) 7:e34996. doi: 10.1371/journal.pone.0034996
24. Zhou R, Zhang Y, Du G, Han L, Zheng S, Liang J, et al. Down-regulated let-7b-5p represses glycolysis metabolism by targeting AURKB in asthenozoospermia. *Gene.* (2018) 663:83–7. doi: 10.1016/j.gene.2018.04.022
25. Ahmed K, LaPierre MP, Gasser E, Denzler R, Yang Y, Rulicke T, et al. Loss of microRNA-7a2 induces hypogonadotropic hypogonadism and infertility. *J Clin Invest.* (2017) 127:1061–74. doi: 10.1172/JCI90031
26. Marcon E, Babak T, Chua G, Hughes T, Moens PB. miRNA and piRNA localization in the male mammalian meiotic nucleus. *Chromosome Res.* (2008) 16:243–60. doi: 10.1007/s10577-007-1190-6
27. Gao X, Zhu M, An S, Liang Y, Yang H, Pang J, et al. Long non-coding RNA LOC105611671 modulates fibroblast growth factor 9 (FGF9) expression by targeting oar-miR-26a to promote testosterone biosynthesis in Hu sheep. *Reprod Fertil Dev.* (2020) 32:373–82. doi: 10.1071/RD19116
28. Yang X, Feng Y, Li Y, Chen D, Xia X, Li J, et al. AR regulates porcine immature sertoli cell growth via binding to RNF4 and miR-124a. *Reprod Domest Anim.* (2020) 56:416–26. doi: 10.1111/rda.13877
29. Zhang Q, Wang Q, Zhang Y, Cheng S, Hu J, Ma Y, et al. Comprehensive analysis of MicroRNA(-)Messenger RNA from white yak testis reveals the differentially expressed molecules involved in development and reproduction. *Int J Mol Sci.* (2018) 19:3083. doi: 10.3390/ijms19103083
30. He Z, Jiang J, Kokkinaki M, Tang L, Zeng W, Gallicano I, et al. MiRNA-20 and mirna-106a regulate spermatogonial stem cell renewal at the post-transcriptional level via targeting STAT3 and Ccnd1. *Stem Cells.* (2013) 31:2205–17. doi: 10.1002/stem.1474
31. Rakoczy J, Fernandez-Valverde SL, Glazov EA, Wainwright EN, Sato T, Takada S, et al. MicroRNAs-140-5p/140-3p modulate leydig cell numbers in the developing mouse testis. *Biol Reprod.* (2013) 88:143. doi: 10.1095/biolreprod.113.107607
32. Hua R, Chu QJ, Zhou Y, Zhou X, Huang DX, Zhu YT. MicroRNA-449a suppresses mouse spermatogonia proliferation via inhibition of CEP55. *Reprod Sci.* (2021) 28:595–602. doi: 10.1007/s43032-020-00354-9
33. Papaioannou MD, Lagarrigue M, Vejnar CE, Rolland AD, Kuhne F, Aubry F, et al. Loss of dicer in sertoli cells has a major impact on the testicular proteome of mice. *Mol Cell Proteomics.* (2011) 10:M900587MCP900200. doi: 10.1074/mcp.M900587-MCP200
34. Pek JW, Lim AK, Kai T. Drosophila maelstrom ensures proper germline stem cell lineage differentiation by repressing microRNA-7. *Dev Cell.* (2009) 17:417–24. doi: 10.1016/j.devcel.2009.07.017
35. Qiu W, Zhu Y, Wu Y, Yuan C, Chen K, Li M. Identification and expression analysis of microRNAs in medaka gonads. *Gene.* (2018) 646:210–6. doi: 10.1016/j.gene.2017.12.062
36. Moritoki Y, Hayashi Y, Mizuno K, Kamisawa H, Nishio H, Kurokawa S, et al. Expression profiling of microRNA in cryptorchid testes: miR-135a contributes to the maintenance of spermatogonial stem cells by regulating FoxO1. *J Urol.* (2014) 191:1174–80. doi: 10.1016/j.juro.2013.10.137
37. Xu XY, Wu, X.u SY, Che LQ, Fang ZF. Feng B, et al. Comparison of microRNA transcriptomes reveals differential regulation of microRNAs in different-aged boars. *Theriogenology.* (2018) 119:105–13. doi: 10.1016/j.theriogenology.2018.06.026
38. Zhang S, Guo J, Liang M, Qi J, Wang Z, Jian X, et al. miR-196a promotes proliferation and inhibits apoptosis of immature porcine sertoli cells. *DNA Cell Biol.* (2019) 38:41–8. doi: 10.1089/dna.2018.4387
39. Li J, Liu X, Hu X, Tian GG, Ma W, Pei X, et al. MicroRNA-10b regulates the renewal of spermatogonial stem cells through Kruppel-like factor 4. *Cell Biochem Funct.* (2017) 35:184–91. doi: 10.1002/cbf.3263
40. Niu Z, Goodyear SM, Rao S, Wu X, Tobias JW, Avarbock MR, et al. MicroRNA-21 regulates the self-renewal of mouse spermatogonial stem cells. *Proc Natl Acad Sci USA.* (2011) 108:12740–5. doi: 10.1073/pnas.1109987108
41. Teng Y, Wang Y, Fu J, Cheng X, Miao S, Wang L. Cyclin T2: a novel miR-15a target gene involved in early spermatogenesis. *FEBS Lett.* (2011) 585:2493–500. doi: 10.1016/j.febslet.2011.06.031
42. Luo M, Hao L, Hu F, Dong Y, Gou L, Zhang W, et al. MicroRNA profiles and potential regulatory pattern during the early stage of spermatogenesis in mice. *Sci China Life Sci.* (2015) 58:442–50. doi: 10.1007/s11427-014-4737-8
43. Yang C, Yao C, Tian R, Zhu Z, Zhao L, Li P, et al. miR-202-3p regulates sertoli cell proliferation, synthesis function, and apoptosis by targeting LRP6 and cyclin D1 of Wnt/beta-catenin signaling. *Mol Ther Nucleic Acids.* (2019) 14:1–19. doi: 10.1016/j.omtn.2018.10.012
44. Chen J, Cai T, Zheng C, Lin X, Wang G, Liao S, et al. MicroRNA-202 maintains spermatogonial stem cells by inhibiting cell cycle regulators and RNA binding proteins. *Nucleic Acids Res.* (2017) 45:4142–57. doi: 10.1093/nar/gkw1287
45. Muramoto T, Urushihara H. Small GTPase RacF2 affects sexual cell fusion and asexual development in *Dictyostelium discoideum* through the regulation of cell adhesion. *Dev Growth Differ.* (2006) 48:199–208. doi: 10.1111/j.1440-169X.2006.00857.x

46. Petersen C, Svechnikov K, Froysa B, Soder O. The p38 MAPK pathway mediates interleukin-1-induced sertoli cell proliferation. *Cytokine.* (2005) 32:51–9. doi: 10.1016/j.cyto.2005.07.014
47. Pitetti JL, Calvel P, Zimmermann C, Conne B, Papaioannou MD, Aubry F, et al. An essential role for insulin and IGF1 receptors in regulating sertoli cell proliferation, testis size, and FSH action in mice. *Mol Endocrinol.* (2013) 27:814–27. doi: 10.1210/me.2012-1258
48. Carreau S, Bouraima-Lelong H, Delalande C. Estrogen, a female hormone involved in spermatogenesis. *Adv Med Sci.* (2012) 57:31–6. doi: 10.2478/v10039-012-0005-y
49. Li S, Wang M, Chen Y, Wang W, Wu J, Yu C, et al. Role of the hedgehog signaling pathway in regulating the behavior of germline stem cells. *Stem Cells Int.* (2017) 2017:5714608. doi: 10.1155/2017/5714608
50. Sahin Z, Szczepny A, McLaughlin EA, Meistrich ML, Zhou W, Ustunel I, et al. Dynamic hedgehog signalling pathway activity in germline stem cells. *Andrology.* (2014) 2:267–74. doi: 10.1111/j.2047-2927.2014.00187.x
51. Tang EI, Lee WM, Cheng CY. Coordination of actin- and microtubule-based cytoskeletons supports transport of spermatids and residual bodies/phagosomes during spermatogenesis in the rat testis. *Endocrinology.* (2016) 157:1644–59. doi: 10.1210/en.2015-1962
52. Jin S, Hu Y, Fu H, Sun S, Jiang S, Xiong Y, et al. Analysis of testis metabolome and transcriptome from the oriental river prawn (Macrobrachium nipponense) in response to different temperatures and illumination times. *Comp Biochem Physiol Part D Genom Proteom.* (2020) 34:100662. doi: 10.1016/j.cbd.2020.100662
53. Golestaneh N, Beauchamp E, Fallen S, Kokkinaki M, Uren A, Dym M. Wnt signaling promotes proliferation and stemness regulation of spermatogonial stem/progenitor cells. *Reproduction.* (2009) 138:151–62. doi: 10.1530/REP-08-0510
54. Li Y, Zhang L, Hu Y, Chen M, Han F, Qin Y, et al. beta-Catenin directs the transformation of testis sertoli cells to ovarian granulosa-like cells by inducing Foxl2 expression. *J Biol Chem.* (2017) 292:17577–86. doi: 10.1074/jbc.M117.811349
55. Lobo IKC, Nascimento ARD, Yamagishi MEB, Guiguen Y, Silva GFD, Severac D, et al. Transcriptome of tambaqui *Colossoma macropomum* during gonad differentiation: different molecular signals leading to sex identity. *Genomics.* (2020) 112:2478–88. doi: 10.1016/j.ygeno.2020.01.022
56. Wong EW, Mruk DD, Cheng CY. Biology and regulation of ectoplasmic specialization, an atypical adherens junction type, in the testis. *Biochim Biophys Acta.* (2008) 1778:692–708. doi: 10.1016/j.bbamem.2007.11.006
57. Zhu X, Yang M, Zhao P, Li S, Zhang L, Huang L, et al. Catenin alpha 1 mutations cause familial exudative vitreoretinopathy by overactivating Norrin/beta-catenin signaling. *J Clin Invest.* (2021) 131:e139569. doi: 10.1172/JCI139869
58. Beigi Harchegani A, Irandoost A, Mirnamniha M, Rahmani H, Tahmasbpour E, Shahriary A. Possible mechanisms for the effects of calcium deficiency on male infertility. *Int J Fertil Steril.* (2019) 12:267–72. doi: 10.22074/ijfs.2019.5420
59. Jiang X, Ma T, Zhang Y, Zhang H, Yin S, Zheng W, et al. Specific deletion of Cdh2 in sertoli cells leads to altered meiotic progression and subfertility of mice. *Biol Reprod.* (2015) 92:79. doi: 10.1095/biolreprod.114.126334
60. Lian C, Sun B, Niu S, Yang R, Liu B, Lu C, et al. A comparative profile of the microRNA transcriptome in immature and mature porcine testes using solexa deep sequencing. *FEBS J.* (2012) 279:964–75. doi: 10.1111/j.1742-4658.2012.08480.x
61. Daguia Zambe JC, Zhai Y, Zhou Z, Du X, Wei Y, Ma F, et al. miR-19b-3p induces cell proliferation and reduces heterochromatin-mediated senescence through PLZF in goat male germline stem cells. *J Cell Physiol.* (2018) 233:4652–65. doi: 10.1002/jcp.26231
62. Hurtado A, Palomino R, Georg I, Lao M, Real FM, Carmona FD, et al. Deficiency of the onco-miRNA cluster, miR-106b approximately 25, causes oligozoospermia and the cooperative action of miR-106b approximately 25 and miR-17 approximately 92 is required to maintain male fertility. *Mol Hum Reprod.* (2020) 26:389–401. doi: 10.1093/molehr/gaaa027
63. Liang M, Wang H, He C, Zhang K, Hu K. LncRNA-Gm2044 is transcriptionally activated by A-MYB and regulates Sycp1 expression as a miR-335-3p sponge in mouse spermatocyte-derived GC-2spd(ts) cells. *Differentiation.* (2020) 114:49–57. doi: 10.1016/j.diff.2020.05.004
64. Norioun H, Motovali-Bashi M, Javadirad SM. Hsa-miR-27a-3p overexpression in men with nonobstructive azoospermia: a case-control study. *Int J Reprod Biomed.* (2020) 18:961–8. doi: 10.18502/ijrm.v13i11.7963
65. Wang Y, Zuo Q, Bi Y, Zhang W, Jin J, Zhang L, et al. miR-31 regulates spermatogonial stem cells meiosis via targeting Stra8. *J Cell Biochem.* (2017) 118:4844–53. doi: 10.1002/jcb.26159
66. Zhou JH, Zhou QZ, Lyu XM, Zhu T, Chen ZJ, Chen MK, et al. The expression of cysteine-rich secretory protein 2 (CRISP2) and its specific regulator miR-27b in the spermatozoa of patients with asthenozoospermia. *Biol Reprod.* (2015) 92:28. doi: 10.1095/biolreprod.114.124487
67. Shin JY, Gupta MK, Jung YH, Uhm SJ, Lee HT. Differential genomic imprinting and expression of imprinted microRNAs in testes-derived male germ-line stem cells in mouse. *PLoS ONE.* (2011) 6:e22481. doi: 10.1371/journal.pone.0022481
68. Aslani F, Schuppe HC, Guazzone VA, Bhushan S, Wahle E, Lochnit G, et al. Targeting high mobility group box protein 1 ameliorates testicular inflammation in experimental autoimmune orchitis. *Hum Reprod.* (2015) 30:417–31. doi: 10.1093/humrep/deu320
69. Zetterstrom CK, Strand ML, Soder O. The high mobility group box chromosomal protein 1 is expressed in the human and rat testis where it may function as an antibacterial factor. *Hum Reprod.* (2006) 21:2801–9. doi: 10.1093/humrep/del256
70. Faucette AN, Maher VA, Gutierrez MA, Jucker JM, Yates DC, Welsh H Jr, et al. Temporal changes in histomorphology and gene expression in goat testes during postnatal development. *J Anim Sci.* (2014) 92:4440–8. doi: 10.2527/jas.2014-7903
71. Garrido N, Martinez-Conejero JA, Jauregui J, Horcajadas JA, Simon C, Remohi J, et al. Microarray analysis in sperm from fertile and infertile men without basic sperm analysis abnormalities reveals a significantly different transcriptome. *Fertil Steril.* (2009) 91:1307–10. doi: 10.1016/j.fertnstert.2008.01.078
72. Rajakumar A, Senthilkumaran B. Expression analysis of cyp11a1 during gonadal development, recrudescence and after hCG induction and sex steroid analog treatment in the catfish, *Clarias batrachus*. *Comp Biochem Physiol B Biochem Mol Biol.* (2014) 176:42–7. doi: 10.1016/j.cbpb.2014.07.007
73. Wen Q, Wang Y, Tang J, Cheng CY, Liu YX. Sertoli cell wt1 regulates peritubular myoid cell and fetal leydig cell differentiation during fetal testis development. *PLoS ONE.* (2016) 11:e0167920. doi: 10.1371/journal.pone.0167920
74. Kim IH, Kim SK, Kim EH, Kim SW, Sohn SH, Lee SC, et al. Korean red ginseng up-regulates C21-steroid hormone metabolism via Cyp11a1 gene in senescent rat testes. *J Ginseng Res.* (2011) 35:272–82. doi: 10.5142/jgr.2011.35.3.272
75. Baker J, Meade A, Venditti C. Genes underlying the evolution of tetrapod testes size. *BMC Biol.* (2021) 19:162. doi: 10.1186/s12915-021-01107-z
76. Nef S, Verma-Kurvari S, Merenmies J, Vassalli JD, Efstratiadis A, Accili D, et al. Testis determination requires insulin receptor family function in mice. *Nature.* (2003) 426:291–5. doi: 10.1038/nature02059
77. Wen X, Wang D, Li X, Zhao C, Wang T, Qian X, et al. Differential expression of two piwil orthologs during embryonic and gonadal development in pufferfish, Takifugu fasciatus. *Comp Biochem Physiol B Biochem Mol Biol.* (2018) 219–20:44–51. doi: 10.1016/j.cbpb.2018.03.005
78. Zhang Y, Cui Y, Zhang X, Wang Y, Gao J, Yu T, et al. Pig StAR: mRNA expression and alternative splicing in testis and leydig cells, and association analyses with testicular morphology traits. *Theriogenology.* (2018) 118:46–56. doi: 10.1016/j.theriogenology.2018.05.031
79. Hasegawa T, Zhao L, Caron KM, Majdic G, Suzuki T, Shizawa S, et al. Developmental roles of the steroidogenic acute regulatory protein (StAR) as revealed by StAR knockout mice. *Mol Endocrinol.* (2000) 14:1462–71. doi: 10.1210/mend.14.9.0515
80. Grasberger H, Bell GI. Subcellular recruitment by TSG118 and TSPYL implicates a role for zinc finger protein 106 in a novel developmental pathway. *Int J Biochem Cell Biol.* (2005) 37:1421–37. doi: 10.1016/j.biocel.2005.01.013
81. Puffenberger EG, Hu-Lince D, Parod JM, Craig DW, Dobrin SE, Conway AR, et al. Mapping of sudden infant death with dysgenesis of the testes syndrome (SIDDT) by a SNP genome scan and identification of TSPYL loss of function.

Proc Natl Acad Sci USA. (2004) 101:11689–94. doi: 10.1073/pnas.0401194101
82. Cai X, Huang Y, Zhang X, Wang S, Zou Z, Wang G, et al. Cloning, characterization, hypoxia and heat shock response of hypoxia inducible factor-1 (HIF-1) from the small abalone haliotis diversicolor. *Gene.* (2014) 534:256–64. doi: 10.1016/j.gene.2013.10.048
83. Zhao W, Liu J, Wang D, Wang Y, Zhang F, Jin G, et al. Effect of silencing HIF-1alpha gene on testicle spermatogenesis function in varicocele rats. *Cell Tissue Res.* (2019) 378:543–54. doi: 10.1007/s00441-019-03064-0
84. Oatley JM, Oatley MJ, Avarbock MR, Tobias JW, Brinster RL. Colony stimulating factor 1 is an extrinsic stimulator of mouse spermatogonial stem cell self-renewal. *Development.* (2009) 136:1191–9. doi: 10.1242/dev.032243
85. Sawaied A, Arazi E, AbuElhija A, Lunenfeld E, Huleihel M. The presence of colony-stimulating factor-1 and its receptor in different cells of the testis; it involved in the development of spermatogenesis *in vitro*. *Int J Mol Sci.* (2021) 22:2325. doi: 10.3390/ijms22052325
86. Castaneda JM, Miyata H, Archambeault DR, Satouh Y, Yu Z, Ikawa M, et al. Mouse t-complex protein 11 is important for progressive motility in spermdagger. *Biol Reprod.* (2020) 102:852–62. doi: 10.1093/biolre/ioz226
87. Kazarian E, Son H, Sapao P, Li W, Zhang Z, Strauss JF, et al. SPAG17 is required for male germ cell differentiation and fertility. *Int J Mol Sci.* (2018) 19:1252. doi: 10.3390/ijms19041252
88. Xu W, Fang P, Zhu Z, Dai J, Nie D, Chen Z, et al. Cigarette smoking exposure alters pebp1 DNA methylation and protein profile involved in MAPK signaling pathway in mice testis. *Biol Reprod.* (2013) 89:142. doi: 10.1095/biolreprod.113.111245
89. Xu K, Yang L, Zhao D, Wu Y, Qi H. AKAP3 synthesis is mediated by RNA binding proteins and PKA signaling during mouse spermiogenesis. *Biol Reprod.* (2014) 90:119. doi: 10.1095/biolreprod.113.116111
90. Nakamura T, Yao R, Ogawa T, Suzuki T, Ito C, Tsunekawa N, et al. Oligo-astheno-teratozoospermia in mice lacking Cnot7, a regulator of retinoid X receptor beta. *Nat Genet.* (2004) 36:528–33. doi: 10.1038/ng1344
91. Gao X, Du C, Zheng X, Hou C, Wang Y, Xu S, et al. Characterisation, expression and possible functions of prohibitin during spermatogenesis in the silver pomfret *Pampus argenteus*. *Reprod Fertil Dev.* (2020) 32:1084–98. doi: 10.1071/RD19381
92. Zhang LF, Tan-Tai WJ, Li XH, Liu MF, Shi HJ, Martin-DeLeon PA, et al. PHB regulates meiotic recombination via JAK2-mediated histone modifications in spermatogenesis. *Nucleic Acids Res.* (2020) 48:4780–96. doi: 10.1093/nar/gkaa203
93. Wu Y, Xu K, Qi H. Domain-functional analyses of PIWIL1 and PABPC1 indicate their synergistic roles in protein translation via 3'-UTRs of meiotic mRNAs. *Biol Reprod.* (2018) 99:773–88. doi: 10.1093/biolre/ioy100
94. Luo G, Hou M, Wang B, Liu Z, Liu W, Han T, et al. Tsga10 is essential for arrangement of mitochondrial sheath and male fertility in mice. *Andrology.* (2021) 9:368–75. doi: 10.1111/andr.12889
95. Malla AB, Bhandari R. IP6K1 is essential for chromatoid body formation and temporal regulation of Tnp2 and Prm2 expression in mouse spermatids. *J Cell Sci.* (2017) 130:2854–66. doi: 10.1242/jcs.204966
96. Zhou J, Yang F, Leu NA, Wang PJ. MNS1 is essential for spermiogenesis and motile ciliary functions in mice. *PLoS Genet.* (2012) 8:e1002516. doi: 10.1371/journal.pgen.1002516
97. Manterola M, Brown TM, Oh MY, Garyn C, Gonzalez BJ, Wolgemuth DJ. BRDT is an essential epigenetic regulator for proper chromatin organization, silencing of sex chromosomes and crossover formation in male meiosis. *PLoS Genet.* (2018) 14:e1007209. doi: 10.1371/journal.pgen.1007209
98. Zhu Y, Liu J, Zhang W, Wu J, Li W, Li H, et al. CEP55 may be a potential therapeutic target for non-obstructive azoospermia with maturation arrest. *Nan Fang Yi Ke Da Xue Xue Bao.* (2019) 39:1059–64. doi: 10.12122/j.issn.1673-4254.2019.09.09
99. Verver DE, van Pelt AM, Repping S, Hamer G. Role for rodent Smc6 in pericentromeric heterochromatin domains during spermatogonial differentiation and meiosis. *Cell Death Dis.* (2013) 4:e749. doi: 10.1038/cddis.2013.269
100. Escoffier J, Yassine S, Lee HC, Martinez G, Delaroche J, Coutton C, et al. Subcellular localization of phospholipase Czeta in human sperm and its absence in DPY19L2-deficient sperm are consistent with its role in oocyte activation. *Mol Hum Reprod.* (2015) 21:157–68. doi: 10.1093/molehr/gau098
101. Held T, Paprotta I, Khulan J, Hemmerlein B, Binder L, Wolf S, et al. Hspa4l-deficient mice display increased incidence of male infertility and hydronephrosis development. *Mol Cell Biol.* (2006) 26:8099–108. doi: 10.1128/MCB.01332-06
102. Eberhart CG, Wasserman SA. The pelota locus encodes a protein required for meiotic cell division: an analysis of G2/M arrest in *Drosophila spermatogenesis*. *Development.* (1995) 121:3477–86. doi: 10.1242/dev.121.10.3477
103. Lopez IP, Rodriguez-de la Rosa L, Pais RS, Pineiro-Hermida S, Torrens R, Contreras J, et al. Differential organ phenotypes after postnatal Igf1r gene conditional deletion induced by tamoxifen in UBC-CreERT2; Igf1r fl/fl double transgenic mice. *Transgenic Res.* (2015) 24:279–94. doi: 10.1007/s11248-014-9837-5
104. Pintus E, Ros-Santaella JL, Garde JJ. Beyond testis size: links between spermatogenesis and sperm traits in a seasonal breeding mammal. *PLoS ONE.* (2015) 10:e0139240. doi: 10.1371/journal.pone.0139240

Conflict of Interest: The authors declare that the research was conducted in the absence of any commercial or financial relationships that could be construed as a potential conflict of interest.

Publisher's Note: All claims expressed in this article are solely those of the authors and do not necessarily represent those of their affiliated organizations, or those of the publisher, the editors and the reviewers. Any product that may be evaluated in this article, or claim that may be made by its manufacturer, is not guaranteed or endorsed by the publisher.

frontiers | Frontiers in Veterinary Science

ORIGINAL RESEARCH
published: 08 April 2022
doi: 10.3389/fvets.2022.795050

Procyanidin B2 Protects Aged Oocytes Against Meiotic Defects Through Cortical Tension Modulation

Qingrui Zhuan[1†], Jun Li[2†], Guizhen Zhou[1], Xingzhu Du[1], Hongyu Liu[1], Yunpeng Hou[3], Pengcheng Wan[4] and Xiangwei Fu[1,4]*

[1] Key Laboratory of Animal Genetics, Breeding and Reproduction of the Ministry of Agriculture and Rural Affairs, National Engineering Laboratory for Animal Breeding, Beijing Key Laboratory for Animal Genetic Improvement, College of Animal Science and Technology, China Agricultural University, Beijing, China, [2] Department of Reproductive Medicine, Reproductive Medical Center, The First Hospital of Hebei Medical University, Shijiazhuang, China, [3] State Key Laboratories of Agrobiotechnology, College of Biological Sciences, China Agricultural University, Beijing, China, [4] State Key Laboratory of Sheep Genetic Improvement and Healthy Breeding, Institute of Animal Husbandry and Veterinary Sciences, Xinjiang Academy of Agricultural and Reclamation Sciences, Shihhotze, China

OPEN ACCESS

Edited by:
Kangfeng Jiang,
Yunnan Agricultural University, China

Reviewed by:
Huanyu Qiao,
University of Illinois at Urbana-Champaign, United States
Mallikarjun Bidarimath,
United States Food and Drug Administration, United States

***Correspondence:**
Xiangwei Fu
xiangweifu@126.com

[†]These authors have contributed equally to this work and share first authorship

Specialty section:
This article was submitted to Animal Reproduction - Theriogenology, a section of the journal Frontiers in Veterinary Science

Received: *14 October 2021*
Accepted: *20 January 2022*
Published: *08 April 2022*

Citation:
Zhuan Q, Li J, Zhou G, Du X, Liu H, Hou Y, Wan P and Fu X (2022) Procyanidin B2 Protects Aged Oocytes Against Meiotic Defects Through Cortical Tension Modulation. Front. Vet. Sci. 9:795050. doi: 10.3389/fvets.2022.795050

Defects in meiotic process are the main factors responsible for the decreased developmental competence in aged oocytes. Our recent research indicated that natural antioxidant procyanidin B2 (PCB2) promoted maturation progress in oocytes from diabetic mice. However, the effect of PCB2 on aging-induced chromosome abnormalities and the underlying mechanism have not been explored. Here, we found that PCB2 recovered aging-caused developmental arrest during meiotic maturation, germinal vesicle breakdown (GVBD) rate was significantly higher in aged oocytes treated with PCB2 ($P < 0.05$). Furthermore, we discovered that cortical mechanics were altered during aging process, cortical tension-related proteins were aberrantly expressed in aged oocytes ($P < 0.001$). PCB2 supplementation efficaciously antagonized aging-induced decreased cortical tension ($P < 0.001$). Moreover, PCB2 restored spindle morphology ($P < 0.01$), maintained proper chromosome alignment ($P < 0.05$), and dramatically reduced reactive oxygen species (ROS) level ($P < 0.05$) in aged oocytes. Collectively, our results reveal that PCB2 supplementation is a feasible approach to protect oocytes from reproductive aging, contributing to the improvement of oocytes quality.

Keywords: PCB2, reproductive aging, oocyte, cortical tension, meiotic maturation

INTRODUCTION

There is a global tendency that women delay conception until late 30's, by which time the chance of pregnancy is compromised as the reproductive capacity in women declines beyond their mid-30's (1). Reproductive aging deteriorates oocyte quality (2). It is known that maternal aging is associated with meiotic defects, and in addition to this, increased vulnerability of aged oocytes to reactive oxygen species (3) leads to mitochondrial dysfunction, since mitochondria are the most significant targets of oxidative stress (1, 4).

Cortical tension and stiffness experience dynamic changes through meiotic maturation and fertilization progression to facilitate and/or direct cellular remodeling in the mammalian oocyte (5). This cortex remodeling is part of the creation of cellular asymmetry and mediates the progression of the prophase I, germinal vesicle-intact (GVI) oocyte to the MII stage (6).

The biochemical and structural features of the cortex are regulated by actin assembly, non-muscle myosin-II expression, and Ezrin/Radixin/Moesin (ERM) protein activity (5). A previous study indicated that abnormal cortical mechanics and myosin-II activity were associated with post-ovulatory aging (7), but changes in cortical tension during reproductive aging remain unclear.

Recently, antioxidants such as melatonin and resveratrol have received increasing attention in the development of therapeutic strategies against oocytes quality deterioration caused by reproductive aging (8, 9). Procyanidins, a group of plant polyphenols with powerful anti-oxidative properties, have been found effective in treating metabolic and inflammatory diseases (10, 11). Dimer procyanidin B2 [4,8′-BI- [4,8′-BI- [(+)-epicatechin]] (PCB2) is a member of oligomeric anthocyanins precursors, which can improve oocyte maturation and subsequent embryo development in diabetic mice (12, 13). In alcoholic liver disease model, dimer procyanidincan reduce hepatic lipid disposition and ROS over production, thereby activate hepatic autophagy to eliminate lipid droplets and damaged mitochondria (14). Furthermore, procyanidins also play a role in alleviation endoplasmic reticulum stress and metabolic disorders associated with endothelial dysfunction (15). However, the effect of PCB2 on the aged oocytes under oxidative stress and the mechanism underlying are not determined yet.

In light of this, the goal of the present study was to investigate the effect of reproductive aging on cortical tension in oocytes, and elucidate the role and the mechanism underlying PCB2 treatment in protecting oocytes from aging-caused quality declines.

MATERIALS AND METHODS

Animals and Housing

All studies were performed using 8-week-old and 42–45-week-old CD-1® (ICR) female mice (Vital River Laboratory Animal Technology Co., Ltd. Beijing, China). Mice were housed in ventilated cages on a 12 h light/12 h dark cycle (lights on from 08: 00 to 20: 00) under controlled temperature (22 ± 2°C) with freely available food and water. The mice were allowed to adapt to conditions for 7 days before the initiation of experiments. In this experiment, 42–45-week-old female mice nearly at the end of their reproductive lifespan were used as a natural aging model.

Chemicals and Antibodies

All chemicals and drugs were purchased from Sigma (St. Louis, MO, USA) unless otherwise indicated. The anti-pERM antibody (#3726), anti-pMRLC antibody (#3675), and anti-rabbit IgG (H+L), F(ab')2 Fragment (Alexa Fluor® 594 Conjugate) secondary antibody (#8889) were purchased from Cell Signaling Technology (Cell Signaling, USA). The anti-alpha Tubulin antibody (62204) was purchased from Thermo Fisher (Thermo Fisher Scientific, USA). The Fluorescein (FITC)–conjugated Affinipure Goat Anti-Rabbit IgG (H+L) secondary antibody (SA00003-2) was purchased from Proteintech (Proteintech Group, Inc.).

Experimental Design

8-week-old young mouse oocytes were regarded as young group. 42–45-week-old aged mouse oocytes were randomly assigned to aged and PCB2-supplemented groups. Procyanidin B2 (PCB2) was dissolved in DMSO and diluted to a final concentration of 5 μg/mL with M16 or M2 medium, respectively. The youth group served as the control and received no treatment. The *in vitro* matured oocytes were randomly divided into three groups as follows: (1) young group: oocytes obtained from 8-week-old mice matured *in vitro*; (2) aged group: oocytes obtained from 42 to 45-week-old mice matured *in vitro*; (3) aged+PCB2 group: oocytes obtained from 42 to 45-week-old mice matured *in vitro* and treated with 5 μg/mL PCB2.

Oocyte Collection

The mice were sacrificed by cervical dislocation 46–48 h after intraperitoneal injection of 10 IU pregnant mare serum gonadotropin (PMSG, Ningbo Hormone Product Co. Ningbo, Zhejiang Province, China). Fully-grown GV oocytes were collected by removing cumulus cells in a drop of M2 medium supplemented with dbcAMP (100 ng/mL) through repeatedly pipetting. Fully-grown GV oocytes were cultured in M16 medium under mineral oil at 37°C in 5% CO_2 incubator.

Immunofluorescence Staining (IF) and Confocal Microscopy

Oocytes were fixed with 4% (w/v) paraformaldehyde (PFA) for 40 min at room temperature, followed by permeabilization with 0.5% Triton X-100 at room temperature for 1h. After being blocked in 3% BSA for 1h at room temperature, oocytes/embryos were incubated with different primary antibodies (anti-pERM, 1:600; anti-pMRLC, 1:300; anti-α-tubulin, 1:8000; anti-β-tubulin, 1:100) overnight at 4°C. The oocytes were further incubated with FITC–conjugated Affinipure Goat Anti-Rabbit IgG (H+L) or Alexa Fluor 594-conjugated goat anti-rabbit antibody for 1 h at room temperature. Finally, all oocytes were stained with 4′,6-diamidino-2-phenylindole (DAPI) for 5 min at room temperature, then oocytes were mounted on glass slides and the fluorescent images were taken with a laser scanning confocal microscopy (A1 Cell Imaging System; Nikon) under the same staining procedure and confocal microscopy parameters. Mean fluorescence intensity per unit area within the region of interest was used to quantify the fluorescence intensity of each oocyte.

Intracellular ROS Level Assay

Denuded oocytes were added to the medium which contains 1 mmol/L 2′, 7′-dichlorodihydrofluoresceindiacetate (DCFHDA) for measuring ROS at 37°C in 5% CO_2 for 20 min. Then oocytes were washed by M2 three times. The fluorescence was examined under an epifluorescence microscope with a filter at 460-nm excitation for ROS (IX73; Olympus). The fluorescence of each oocyte was analyzed by EZ-C1Free-Viewer (Nikon).

Statistical Analysis

In all experiments, data were analyzed using SPSS software v.21.0 (SPSS Inc., Chicago, IL, USA). Student's *t*-test was performed for statistical analysis. For abnormal spindle and chromosome

alignment, chi-square test was performed for statistical analysis. Unless otherwise stated, * = $P < 0.05$, ** = $P < 0.01$, *** = $P < 0.001$, ns = non-significant difference ($P > 0.05$).

RESULTS

PCB2 Promotes Meiotic Resumption in Aged Oocytes

Meiotic resumption during *in vitro* maturation progress was examined. As shown in **Figure 1A**, a large majority of oocytes in the young group underwent germinal vesicle breakdown (GVBD) stage, then developed to the metaphase II (MII) stage with the extrusion of first polar body. However, oocytes in the aged group exhibited decreased GVBD rate at the same developmental time points (young: 89.67 ± 3.28%, $n = 70$; aged: 75.96 ± 2.33%, $n = 67$, $P < 0.05$). To determine the protective effect of PCB2 on meiotic recovery, fully-grown GV oocytes were cultured in M16 medium supplemented with 5 μg/mL PCB2. The quantitative analysis indicated that the oocytes treated with PCB2 exhibited significantly increased GVBD rate compared with the aged group (aged: 75.96 ± 2.33%, $n = 67$; aged+PCB2: 89.87 ± 2.13%, $n = 58$, $P < 0.05$, **Figure 1B**). However, after 12 h culture, there was no significant difference in the occurrence of polar body extrusion (PBE) among different groups (**Figure 1C**).

PCB2 Recovers Aging-Related Sharp Decrease in PERM Expression

Previous study shown that post-ovulatory aged MII-stage oocytes exhibited abnormal cortical tension (7), which drives us to investigate whether reproductive aging can affect the cortical tension in MII-stage oocytes. We, therefore, conducted immunostaining assay to evaluate the expression of active phospo-ERMs (pERM), which play a crucial role in regulating cortical tension (**Figure 2A**). As shown in **Figure 2B**, quantitative analysis indicated that the fluorescence intensity of pERM was significantly reduced in aged oocytes (young: 189.14 ± 18.86, $n = 17$; aged: 43.02 ± 11.24 pixels, $n = 16$, $P < 0.001$), while PCB2 treatment rescued this abnormal phenomenon (aged: 43.02 ± 11.24, $n = 16$; aged+PCB2: 150.58 ± 28.28 pixels, $n = 12$, $P < 0.001$). In addition, DNA (DAPI staining) was used as internal reference to normalize the immunofluorescent staining results, and the ratio of pERM to DNA fluorescence further validated that PCB2 significantly increased pERM level in aged oocytes (**Figure 2C**).

PCB2 Restores Abnormal Cytoplasmic Distribution of PMRLC in Aged Oocytes

In addition to ERMs, non-muscle myosin-II is also a key factor regulating the cortical tension in oocytes (5). Reduced level of the active form of the myosin-II regulatory light chain [phosphorylated MRLC, pMRLC] was found in post-ovulatory oocytes (7). In the present study, normal localization of pMRLC in the amicrovillar domain (the region overlying the spindle, indicated with arrow in **Figure 3A**) was observed in most young oocytes. However, the amicrovillar domain distribution of pMRLC was disturbed in aged oocytes, and exhibited clustered distribution in the cytoplasm (**Figure 3A**). As expected, PCB2 treatment rescued this abnormal distribution. As shown in **Figure 3B**, the corresponding quantitative data showed a significantly increased pMRLC intensity in the cytoplasm of aged oocytes (young: 179.81 ± 10.67, $n = 27$; aged: 263.44 ± 15.54 pixels, $n = 18$, $P < 0.001$) and PCB2 rescued this phenomenon (aged: 263.44 ± 15.54, $n = 18$; aged+PCB2: 165.84 ± 23.20 pixels, $n = 11$, $P < 0.001$). Moreover, the ratio of pMRLC to DNA fluorescence further verified the above results (**Figure 3C**).

PCB2 Maintains Normal Spindle Assembly and Protects Aged Oocytes From Chromosome Defects

Normal spindle assembly is prerequisite for proper chromosome segregation. To delineate age-related changes in spindle architecture and chromosome aberrations, oocytes were immunostained with anti-α-tubulin antibody to observe the spindle morphology and counterstained with DAPI to analyze the chromosome alignment. As shown in **Figure 4A**, normal spindle displayed a typical barrel-shaped apparatus. Meanwhile, a well-aligned chromosome on the equatorial plate next to the cortical region was also fond of the oocyte membrane. However, disruptions in spindle organization and chromosomes alignment were observed in aged oocytes. PCB2 treatment not only rescued disorganized spindle assembly, but also recovered the misaligned chromosomes. As shown in **Figure 4B**, the corresponding quantitative data confirmed the protective role of PCB2 on spindle formation in aged oocytes ($P < 0.01$). Moreover, the quantitative data showed that PCB2 supplementation also rescued the chromosome abnormalities ($P < 0.05$, **Figure 4C**) in aged oocytes treated with PCB2.

PCB2 Supplementation Attenuates ROS Levels in Aged Oocytes

Our previous study indicated that reproductive aging can impair mitochondrial function and further induce increased ROS levels in oocytes (16). Therefore, we further investigated whether PCB2 treatment could alleviate the oxidative stress in aged oocytes. We used 2′7′-DCFHDA to measure the intracellular ROS level (**Figure 5A**). PCB2 treatment significantly decreased the ROS level of aged oocyte caused by reproductive aging (young: 34.59 ± 6.33, $n = 15$; aged: 120.76 ± 17.16, $n = 12$; aged+PCB2: 58.33 ± 10.92 pixels, $n = 15$, $P < 0.05$) (**Figure 5B**).

DISCUSSION

Decreased oocyte quality is one of the irreversible damages due to aging (17). Oocyte quality can be influenced by reproductive aging through nuclear and cytoplasmic maturation during oocyte development (18). In addition to the nuclear and cytoplasmic dynamics, other changes occurred in the cortex of the aged oocyte also attribute to the declined developmental capacity (19). It was reported that abnormal distribution and decreased amount of cortical granules (CGs), which are golgi apparatus-derived

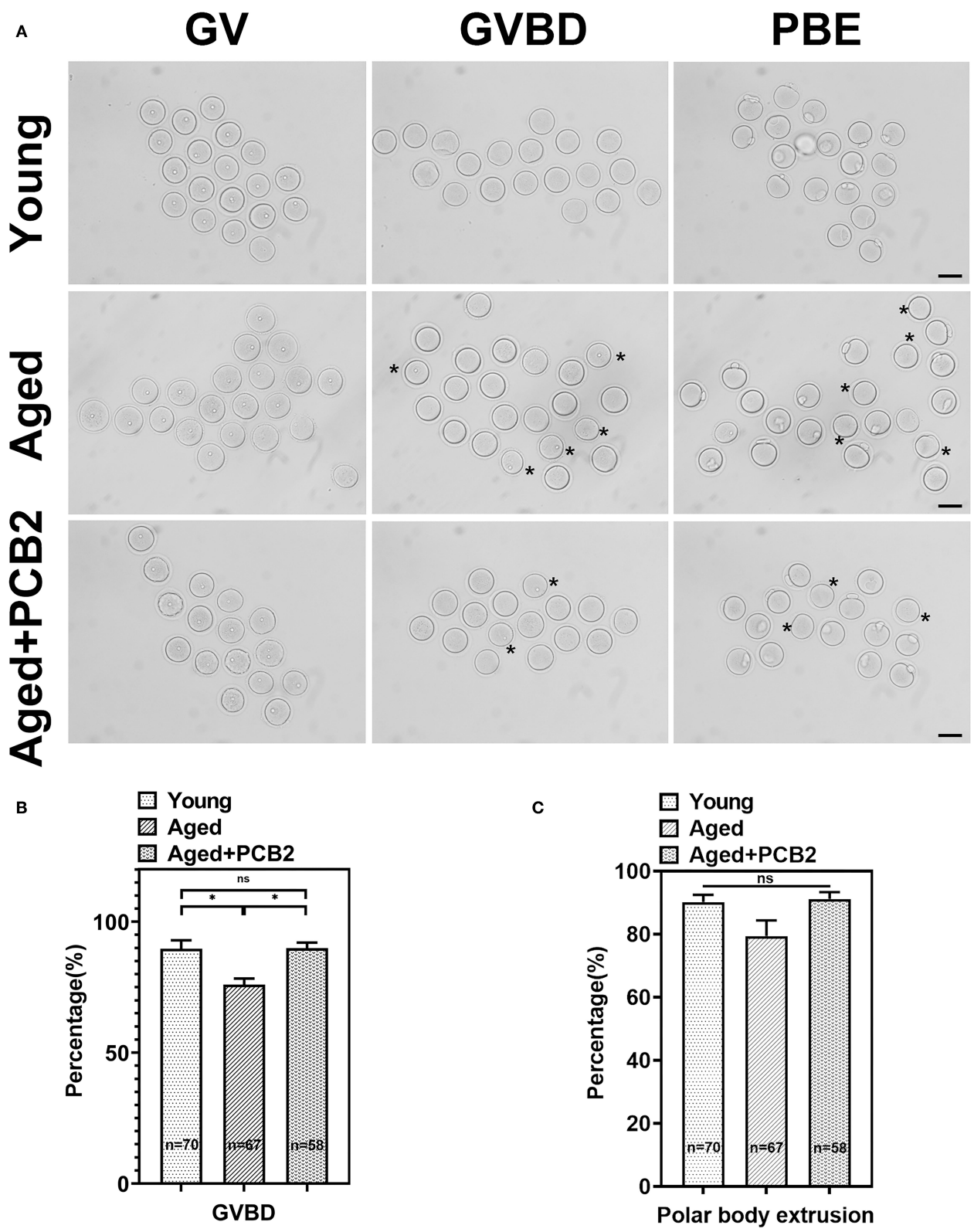

FIGURE 1 | PCB2 supplementation can improve germinal vesicle breakdown (GVBD) rate of aged oocytes. **(A)** Oocytes were cultured *in vitro* with or without PCB2 supplementation to analyze GVBD and polar body extrusion (PBE) rates. Scale bar, 50 μm. **(B,C)** The GVBD and PBE rates of oocytes were recorded in different groups. Data are presented as mean percentage (mean ± SEM) of at least three independent experiments. *$P < 0.05$.

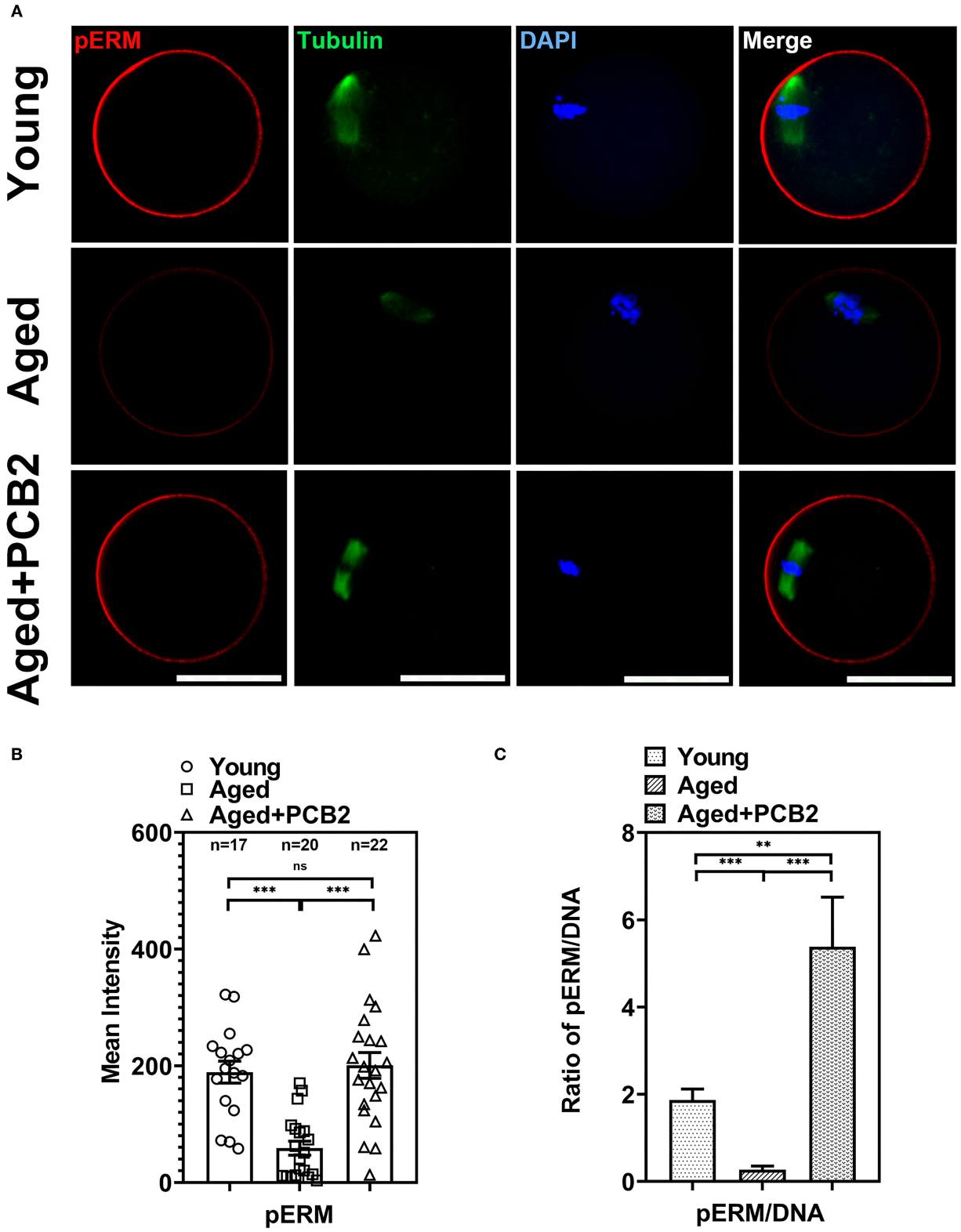

FIGURE 2 | Effects of PCB2 on pERM expression and spindle formation during *in vitro* culture of aged oocytes. **(A)** IF staining of *in vitro* matured oocytes for pERM and tubulin. DNA was counterstained with DAPI (blue). Scale bar, 50 μm. **(B)** Fluorescence intensity of pERM signals was recorded in different groups. **(C)** The ratio of pERM to DNA fluorescence. Data are presented as mean percentage (mean ± SEM) of at least three independent experiments. $^{**}P < 0.01$, $^{***}P < 0.001$. ns, non-significant difference, $P > 0.05$.

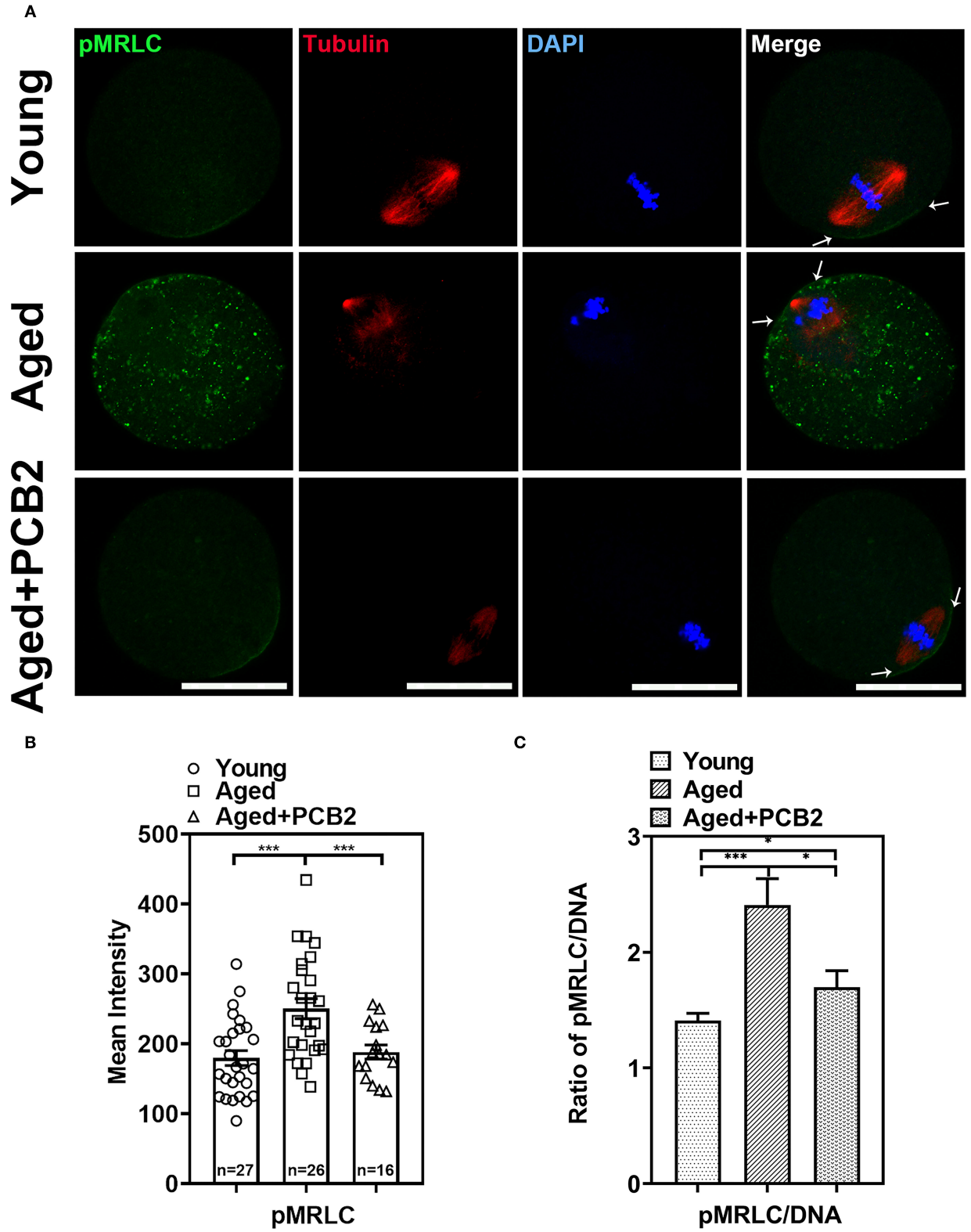

FIGURE 3 | Effects of PCB2 on pMRLC expression and spindle formation during *in vitro* culture of aged oocytes. **(A)** IF staining of *in vitro* matured oocytes for pMRLC and tubulin. DNA was counterstained with DAPI (blue). Scale bar, 50 μm. **(B)** Fluorescence intensity of pMRLC signals was recorded in different groups. **(C)** The ratio of pMRLC to DNA fluorescence. Data are presented as mean percentage (mean ± SEM) of at least three independent experiments. $^{*}P < 0.05$, $^{***}P < 0.001$. ns, non-significant difference, $P > 0.05$.

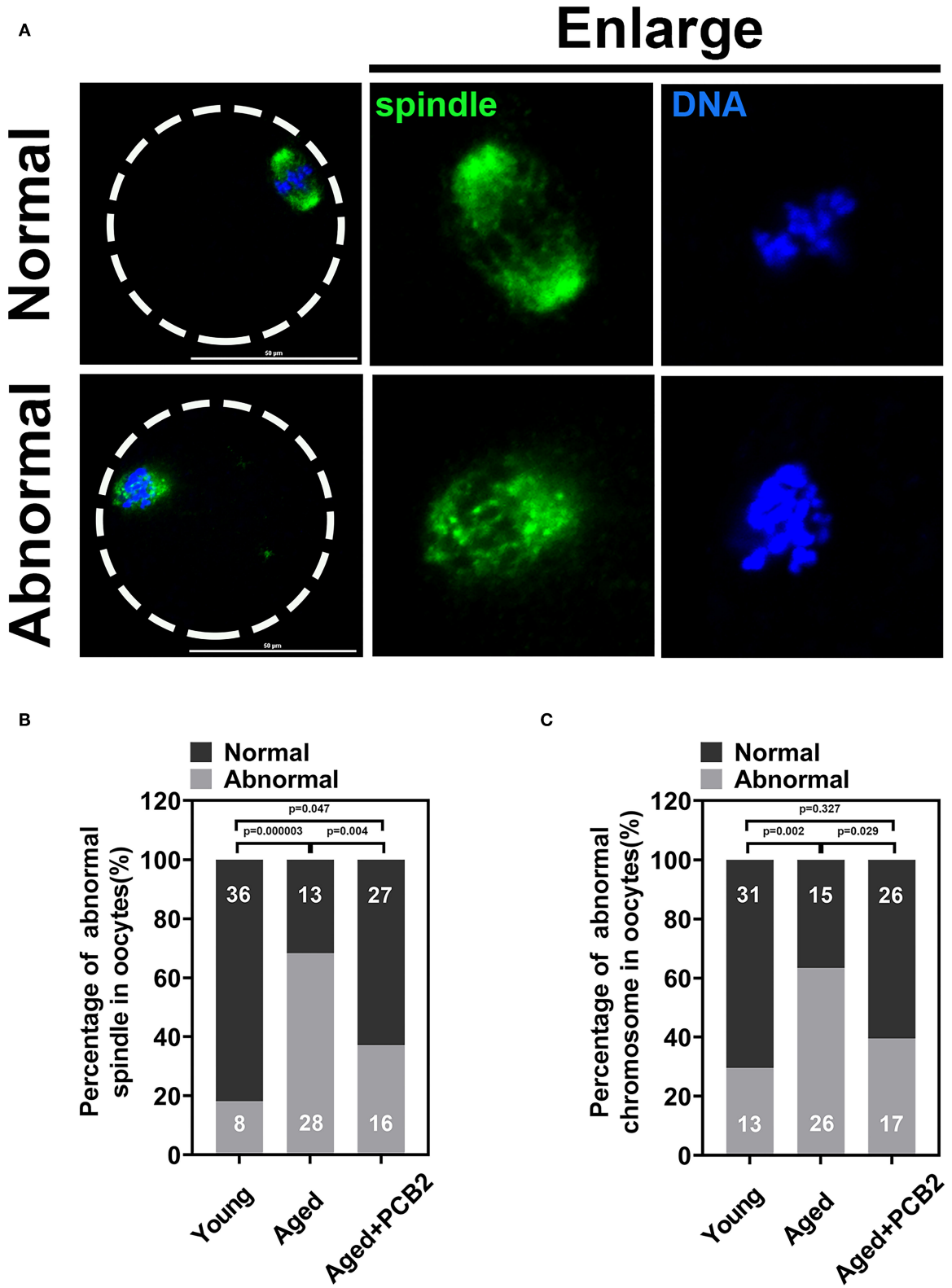

FIGURE 4 | PCB2 alleviates abnormal spindle formation and misalignment of chromosome in aged oocytes. **(A)** Representative images of normal and abnormal spindle formation as well as chromosome alignment. Scale bar, 50 μm. **(B)** Quantification of normal and aberrant spindles was recorded in different groups. **(C)** Quantification of normal and misalignment chromosome was recorded in different groups. Chi-square test was performed for statistical analysis.

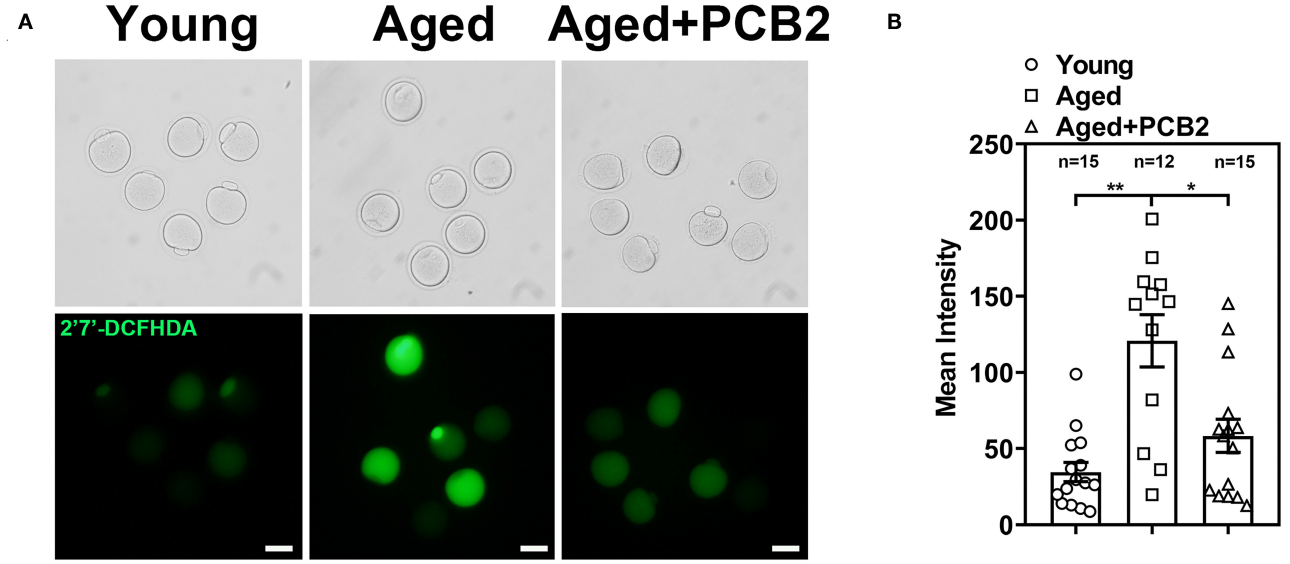

FIGURE 5 | Effect of PCB2 supplementation on oxidative stress levels in aged oocytes. **(A)** Representative images of ROS levels in different groups. Scale bar, 50 μm. **(B)** Quantification of ROS fluorescence intensity was recorded in different groups. Data are presented as mean percentage (mean ± SEM) of at least three independent experiments. $^{*}P < 0.05$, $^{**}P < 0.01$.

vesicles that localize under the oocyte subcortex, were induced by reproductive aging in mouse oocytes (20).

Exogenous antioxidants can alleviate the decrease in oocyte quality caused by reproductive aging (8, 20). Procyanidins are a class of natural plant polyphenols, which have strong antioxidant properties (11, 21). We previously found that 5 μg/mLPCB2 supplementation during *in vitro* maturation progress could attenuate meiosis defects, improve the subsequent developmental potential after parthenogenetic activation of diabetic mouse oocytes (12). In agreement with our previous findings, the GVBD rate was significantly decreased in the aged oocytes, while the PBE rate was similar (16). As we pointed out in our previous report, aged oocytes underwent both GVBD and PBE more slowly than young oocytes, this indicated that the meiotic process in the aged oocytes was disrupted to a certain extent (16). In the present study, we found PCB2 supplementation can significantly improve the GVBD rate in aged oocytes (**Figure 1**). As the most numerous organelles in the cytoplasm, mitochondria supply the ATP needed for the oocyte to support critical events including maturation and spindle formation (22, 23). Previous study showed that improved mitochondria function alleviated meiotic defects (20). Our research indicated that PCB2 could improve the viability and restore mitochondrial function of vitrified-thawed oocytes (unpublished data). The present finding proved that PCB2 played a pivotal role in oocytes meiosis resumption, suggested that PCB2 might also contribute to maintain mitochondrial function in aged oocytes under oxidative stress.

Apart from the antioxidant property, we also discovered that PCB2 served as a cortical tension enhancer in aged oocytes. It has been reported that the aged oocytes are related to the changes in actin cytoskeleton integrity, loss of dynamic activity, and clump formation in actin (24, 25). The polarity of the cortex is mediated by the polarization of the oocyte, including the translocation of the spindle to the cortex in an actin-dependent manner, the enrichment of microfilaments to form the actin cap, the redistribution of cortical granules (CGs) to form a CGs-free domain, and microvilli loss in the region overlying the spindle (26, 27). During reproductive aging, aged mouse oocytes exhibited cortical polarity degradation (28). Similarly, aberrant cortical mechanics and actomyosin cytoskeleton functions were also found in post-ovulatory aged oocytes (7). Actin, myosin-II, and the ERM (Ezrin/Radixin/Moesin) family of proteins are enriched in complementary cortical domains and mediate cellular mechanics in mammalian oocytes (5). ERM is active through its phosphorylated form (pERM) and myosin-II contractility works with actin to mediate cortical tension and is regulated by phosphorylation of the myosin-II regulatory light chain (pMRLC) (7). In the present study, we found decreased cortical tension in reproductive aged oocytes. pERM activity was significantly decreased in cortical area in reproductive aged oocytes, which was consistent with post-ovulatory aged oocytes. By using a cVCA construct to decrease cortical tension in mouse oocytes, the newly established extra-soft mouse oocytes show impaired chromosome alignment, mainly due to a cytoplasmic increase in myosin-II activity (29). This was also consistent with our findings that the distribution of cytoplasmic pMRLC increased sharply and cortical pMRLC decreased significantly in aged oocytes (**Figure 3**). In post-ovulatory aged oocytes, anti-pMRLC signals were reduced in amicrovillar localization (subcortical spindle region), and showed aberrant amicrovillar morphology, such as a protruding amicrovillar domain, uneven

pMRLC distribution around the boundary of the amicrovillar domain, and patchy pMRLC over the amicrovillar domain (7). But in our findings, reproductive aged oocytes mostly exhibited reduced pMRLC signals in amicrovillar domain, and clustered distribution in the cytoplasm (**Figure 3A**). The results demonstrated that the cortical tension was altered during aging process, and the discrepancies in pMRLC distribution pattern implied that different mechanisms underlying reproductive and post-ovulatory aging. This phenomenon was one of the abnormal distribution of post-ovulatory aged oocytes. Through immunofluorescence co-staining, we found that aberrant spindle formation and abnormal chromosome alignment were also increased in aged oocytes (**Figure 4**). Cheng et al. have pointed out that aged oocytes underwent GVBD and PBE with similar efficiencies and kinetics as young oocytes, but aging can cause an increase in chromosome aneuploidy of MII oocytes (30). Indeed, our results also suggest that aging induced meiosis defect does not necessarily affect the rate of the PBE. Cohesion forces on the centromere and hold the sister chromatids together (31). However, the activity of cohesion decreases with age and makes recombinant chromosomes prone to mis-segregation (2). Reports also indicated that intracellular pH (pHi) was elevated in aged oocytes, the elevated oocyte pHi might be related to the loss of cohesion and the increased aneuploidy in aged mouse (30). This indicated that aging can induce abnormal chromosome alignment and eventually lead to aneuploidy. However, the extrusion of first polar body is a dynamic process, variations in the PBE rate is largely dependent on the observation time points. Although the proportion of PBE was similar to that of young oocytes, the increased proportion of chromosome misalignment in old oocytes suggested that there was a defect in the monitoring mechanism during chromosome separation. This may explain our results that reproductive aging induces decreased cortical tension, increased cytoplasmic myosin-II activity, and further disrupts normal spindle morphology and chromosome alignment. These results are consistent with the findings in post-ovulatory aged oocytes, both reveal the relevance of cortical tension to normal oocyte function (5, 7). Furthermore, PCB2 supplementation restores decreased expression of pERM and pMRLC, alleviates abnormal spindle formation as well as chromosome misalignment. It was reported that cell mechanics changes affected the shape and function of the mitotic spindle (32). Our result also indicated that spindles exhibited morphological differences in response to cortical tension variations.

Reproductive aging not only impair oocytes meiosis resumption, but also affect the mitochondrial Ca^{2+} homeostasis and mitochondria function (16). The proper distribution of mitochondria plays a key role in the regulation of redox homeostasis and is necessary for cell survival (33, 34). We previously demonstrated that maternal age could disturb mitochondrial distribution, accompanied by overload mitochondrial Ca^{2+} level and decreased mitochondrial heat production (16). Alterations in mitochondrial function permit aging cells to regulate senescence phenotypes induced by DNA damage, which include the overproduction of ROS via mitochondrial dysfunction (34, 35). Since the robust interplay between increased ROS level and mitochondrial dysfunction, the observed reduced ROS level after PCB2 treatment proved our assumption that PCB2 could improve mitochondrial function in aged oocytes. In the present study, we found that the decreased cortical tension and increased ROS level in oocytes from maternally aged mice was associated with meiotic defects, which was consistent with previous findings that increased ROS level and reduced cortical tension in post-ovulatory aged oocytes further induce oocyte cortex and spindle abnormalities (3). To divide, cells dramatically change shape and round up against extracellular confinement (36). It was discovered that the mechanical characteristic of extracellular matrix could be perceived and its variation was associated with mitochondrial function alterations (34). In the present study, abnormal spindle formation and chromosome arrangement induced by cortical tension and oxidative stress in aged oocytes were corrected by PCB2, probably attributed to the ameliorated mitochondrial function. Other antioxidants such as melatonin, resveratrol and mogroside V, have been reported to improve oocytes quality through ameliorating mitochondrial function, but the effect of antioxidants on cortical tension has not been reported. Our results implied that there was an intricate relationship between mitochondrial function and cortical tension in aged oocytes. To our knowledge, this is the first report identified the additional role of PCB2 played in cortical tension regulation in aged oocytes.

CONCLUSION

In conclusion, our results indicated that PCB2 could protect reproductive aged oocytes from meiotic abnormalities by increasing cortical tension, which correlates with restored redox homeostasis under maternal age-induced oxidative stress. Overall, our work provides insights into the mechanism underlying age-related increase in oocyte meiotic defects, and expounds the theoretical basis for application of PCB2 to improve oocyte quality in aged women.

DATA AVAILABILITY STATEMENT

The original contributions presented in the study are included in the article/supplementary material, further inquiries can be directed to the corresponding author.

ETHICS STATEMENT

The animal study was reviewed and approved by Institutional Animal Care and Use Committee of China Agricultural University.

AUTHOR CONTRIBUTIONS

QZ, JL, and XF conceived and designed the study. QZ, GZ, XD, and HL performed experiments, collected data, and analyzed data. QZ, XF, and JL wrote the initial manuscript. YH and PW

revised the manuscript. All authors have read and agreed to the published version of the manuscript.

FUNDING

This work was funded by Chinese Universities Scientific Fund, Grant/Award Number: 2021TC061; Natural Science Foundation of Hebei Province, Grant/Award Number: H2020206254; Special Program for Training and Guiding Outstanding Young and Middle-Aged Talents, Grant/Award Number: SKLSGIHP2021A01; National Natural Science Foundation of China, Grant/Award Number: 81901562 and 31372307; Key Research and Development Projects in Hebei Province, Grant/Award Number: 18226604D; Xinghuo Program of the First Hospital of Hebei Medical University, Grant/Award Number: XH202005.

REFERENCES

1. Sasaki H, Hamatani T, Kamijo S, Iwai M, Kobanawa M, Ogawa S, et al. Impact of oxidative stress on age-associated decline in oocyte developmental competence. *Front Endocrinol.* (2019) 10:811. doi: 10.3389/fendo.2019.00811
2. Qiao J, Wang ZB, Feng HL, Miao YL, Wang Q, Yu Y, et al. The root of reduced fertility in aged women and possible therapentic options: current status and future perspects. *Mol Aspects Med.* (2014) 38:54–85. doi: 10.1016/j.mam.2013.06.001
3. Cecconi S, Rossi G, Deldar H, Cellini V, Patacchiola F, Carta G, et al. Post-ovulatory ageing of mouse oocytes affects the distribution of specific spindle-associated proteins and Akt expression levels. *Reprod Fertil Dev.* (2014) 26:562–9. doi: 10.1071/RD13010
4. Kasapoglu I, Seli E. Mitochondrial dysfunction and ovarian aging. *Endocrinology*. (2020) 161:bqaa001. doi: 10.1210/endocr/bqaa001
5. Larson SM, Lee HJ, Hung PH, Matthews LM, Robinson DN, Evans JP. Cortical mechanics and meiosis II completion in mammalian oocytes are mediated by myosin-II and Ezrin-Radixin-Moesin (ERM) proteins. *Mol Biol Cell.* (2010) 21:3182–92. doi: 10.1091/mbc.e10-01-0066
6. Brunet S, Maro B. Cytoskeleton and cell cycle control during meiotic maturation of the mouse oocyte: integrating time and space. *Reproduction.* (2005) 130:801–11. doi: 10.1530/rep.1.00364
7. Mackenzie AC, Kyle DD, McGinnis LA, Lee HJ, Aldana N, Robinson DN, et al. Cortical mechanics and myosin-II abnormalities associated with post-ovulatory aging: implications for functional defects in aged eggs. *Mol Hum Reprod.* (2016) 22:397–409. doi: 10.1093/molehr/gaw019
8. Li C, He X, Huang Z, Han L, Wu X, Li L, et al. Melatonin ameliorates the advanced maternal age-associated meiotic defects in oocytes through the SIRT2-dependent H4K16 deacetylation pathway. *Aging.* (2020) 12:1610–23. doi: 10.18632/aging.102703
9. Yoon J, Juhn KM, Jung EH, Park HJ, Yoon SH, Ko Y, et al. Effects of resveratrol, granulocyte-macrophage colony-stimulating factor or dichloroacetic acid in the culture media on embryonic development and pregnancy rates in aged mice. *Aging.* (2020) 12:2659–69. doi: 10.18632/aging.102768
10. Jung M, Triebel S, Anke T, Richling E, Erkel G. Influence of apple polyphenols on inflammatory gene expression. *Mol Nutr Food Res.* (2009) 53:1263–80. doi: 10.1002/mnfr.200800575
11. Yin M, Zhang P, Yu F, Zhang Z, Cai Q, Lu W, et al. Grape seed procyanidin B2 ameliorates hepatic lipid metabolism disorders in db/db mice. *Mol Med Rep.* (2017) 16:2844–50. doi: 10.3892/mmr.2017.6900
12. Luo Y, Zhuan Q, Li J, Du X, Huang Z, Hou Y, et al. Procyanidin B2 improves oocyte maturation and subsequent development in type 1 diabetic mice by promoting mitochondrial function. *Reprod Sci.* (2020) 27:2211–22. doi: 10.1007/s43032-020-00241-3
13. Zhang JQ, Gao BW, Wang J, Ren QL, Chen JF, Ma Q, et al. Critical role of FoxO1 in granulosa cell apoptosis caused by oxidative stress and protective effects of grape seed procyanidin B2. *Oxid Med Cell Longev.* (2016) 2016:6147345. doi: 10.1155/2016/6147345
14. Cao P, Zhang Y, Huang Z, Sullivan MA, He Z, Wang J, et al. The preventative effects of procyanidin on binge ethanol-induced lipid accumulation and ROS overproduction via the promotion of hepatic autophagy. *Mol Nutr Food Res.* (2019) 63:e1801255. doi: 10.1002/mnfr.201801255
15. Nie X, Tang W, Zhang Z, Yang C, Qian L, Xie X, et al. Procyanidin B2 mitigates endothelial endoplasmic reticulum stress through a PPARδ-dependent mechanism. *Redox Biol.* (2020) 37:101728. doi: 10.1016/j.redox.2020.101728
16. Zhuan Q, Li J, Du X, Zhang L, Meng L, Cheng K, et al. Nampt affects mitochondrial function in aged oocytes by mediating the downstream effector FoxO3a. *J Cell Physiol.* (2022) 237:647–659. doi: 10.1002/jcp.30532
17. Li M, Ren C, Zhou S, He Y, Guo Y, Zhang H, et al. Integrative proteome analysis implicates aberrant RNA splicing in impaired developmental potential of aged mouse oocytes. *Aging cell.* (2021) 20:e13482. doi: 10.1111/acel.13482
18. Conti M, Franciosi F. Acquisition of oocyte competence to develop as an embryo: integrated nuclear and cytoplasmic events. *Hum Reprod Update.* (2018) 24:245–66. doi: 10.1093/humupd/dmx040
19. Trapphoff T, Heiligentag M, Dankert D, Demond H, Deutsch D, Fröhlich T, et al. Postovulatory aging affects dynamics of mRNA, expression and localization of maternal effect proteins, spindle integrity and pericentromeric proteins in mouse oocytes. *Hum Reprod.* (2016) 31:133–49. doi: 10.1093/humrep/dev279
20. Miao Y, Cui Z, Gao Q, Rui R, Xiong B. Nicotinamide mononucleotide supplementation reverses the declining quality of maternally aged oocytes. *Cell Rep.* (2020) 32:107987. doi: 10.1016/j.celrep.2020.107987
21. Heidker RM, Caiozzi GC, Ricketts ML. Dietary procyanidins selectively modulate intestinal farnesoid X receptor-regulated gene expression to alter enterohepatic bile acid recirculation: elucidation of a novel mechanism to reduce triglyceridemia. *Mol Nutr Food Res.* (2016) 60:727–36. doi: 10.1002/mnfr.201500795
22. May-Panloup P, Chretien MF, Malthiery Y, Reynier P. Mitochondrial DNA in the oocyte and the developing embryo. *Curr Top Dev Biol.* (2007) 77:51–83. doi: 10.1016/S0070-2153(06)77003-X
23. Chappel S. The role of mitochondria from mature oocyte to viable blastocyst. *Obstet Gynecol Int.* (2013) 2013:183024. doi: 10.1155/2013/183024
24. Gourlay CW, Carpp LN, Timpson P, Winder SJ, Ayscough KR. A role for the actin cytoskeleton in cell death and aging in yeast. *J Cell Biol.* (2004) 164:803–9. doi: 10.1083/jcb.200310148
25. Kim MJ, Choi KH, Seo DW, Lee HR, Kong HS, Lee CH, et al. Association Between functional activity of mitochondria and actin cytoskeleton instability in oocytes from advanced age mice. *Reprod Sci.* (2020) 27:1037–46. doi: 10.1007/s43032-020-00145-2
26. Longo FJ, Chen DY. Development of cortical polarity in mouse eggs: involvement of the meiotic apparatus. *Dev Biol.* (1985) 107:382–94. doi: 10.1016/0012-1606(85)90320-3
27. Deng M, Kishikawa H, Yanagimachi R, Kopf GS, Schultz RM, Williams CJ. Chromatin-mediated cortical granule redistribution is responsible for the formation of the cortical granule-free domain in mouse eggs. *Dev Biol.* (2003) 257:166–76. doi: 10.1016/S0012-1606(03)00045-9
28. Sun SC, Gao WW, Xu YN, Jin YX, Wang QL, Yin XJ, et al. Degradation of actin nucleators affects cortical polarity of aged mouse oocytes. *Fertil Steril.* (2012) 97:984–90. doi: 10.1016/j.fertnstert.2012.01.101
29. Bennabi I, Crozet F, Nikalayevich E, Chaigne A, Letort G, Manil-Ségalen M, et al. Artificially decreasing cortical tension generates aneuploidy in mouse oocytes. *Nat Commun.* (2020) 11:1649. doi: 10.1038/s41467-020-15470-y
30. Cheng JM, Li J, Tang JX, Chen SR, Deng SL, Jin C, et al. Elevated intracellular pH appears in aged oocytes and causes oocyte aneuploidy associated with the loss of cohesion in mice. *Cell Cycle.* (2016) 15:2454–63. doi: 10.1080/15384101.2016.1201255

31. Prieto I, Tease C, Pezzi N, Buesa JM, Ortega S, Kremer L, et al. Cohesin component dynamics during meiotic prophase I in mammalian oocytes. *Chromosome Res.* (2004) 12:197–213. doi: 10.1023/B:CHRO.0000021945.83198.0e
32. Evans JP, Robinson DN. The spatial and mechanical challenges of female meiosis. *Mol Reprod Dev.* (2011) 78:769–77. doi: 10.1002/mrd.21358
33. Frederick RL, Shaw JM. Moving mitochondria: establishing distribution of an essential organelle. *Traffic.* (2007) 8:1668–75. doi: 10.1111/j.1600-0854.2007.00644.x
34. Tharp KM, Higuchi-Sanabria R, Timblin GA, Ford B, Garzon-Coral C, Schneider C, et al. Adhesion-mediated mechanosignaling forces mitohormesis. *Cell Metab.* (2021) 33:1322–41.e13. doi: 10.1016/j.cmet.2021.04.017
35. Sun N, Youle RJ, Finkel T. The mitochondrial basis of aging. *Mol Cell.* (2016) 61:654–66. doi: 10.1016/j.molcel.2016.01.028
36. Toyoda Y, Cattin CJ, Stewart MP, Poser I, Theis M, Kurzchalia TV, et al. Genome-scale single-cell mechanical phenotyping reveals disease-related genes involved in mitotic rounding. *Nat Commun.* (2017) 8:1266. doi: 10.1038/s41467-017-01147-6

Conflict of Interest: The authors declare that the research was conducted in the absence of any commercial or financial relationships that could be construed as a potential conflict of interest.

frontiers | Frontiers in Veterinary Science

ORIGINAL RESEARCH
published: 06 May 2022
doi: 10.3389/fvets.2022.867405

Exploration of the Shared Gene and Molecular Mechanisms Between Endometriosis and Recurrent Pregnancy Loss

Zhuang Ye[1], Qingxue Meng[2], Weiwen Zhang[3], Junli He[2], Huanyi Zhao[4], Chengwei Yu[5], Weizheng Liang[2]*, Xiushen Li[3,6,7]* and Hao Wang[3,6,7]**

[1] Department of Rheumatology, The First Hospital of Jilin University, Changchun, China, [2] Department of Pediatrics, Shenzhen University General Hospital, Shenzhen, China, [3] Department of Obstetrics and Gynecology, Shenzhen University General Hospital, Shenzhen, China, [4] Guangzhou University of Chinese Medicine, Guangzhou, China, [5] School of Future Technology, University of Chinese Academy of Sciences, Beijing, China, [6] Guangdong Key Laboratory for Biomedical Measurements and Ultrasound Imaging, School of Biomedical Engineering, Shenzhen University Health Science Center, Shenzhen, China, [7] Shenzhen Key Laboratory, Shenzhen University General Hospital, Shenzhen, China

OPEN ACCESS

Edited by:
Shou-Long Deng,
Chinese Academy of Medical Sciences and Peking Union Medical College, China

Reviewed by:
Tingting Sun,
The First Affiliated Hospital of Sun Yat-sen University, China
Wenting Li,
Henan Agricultural University, China

***Correspondence:**
Chengwei Yu
sustcyucw@gmail.com
Weizheng Liang
jmbb1203@126.com
Xiushen Li
lixiushenzplby@163.com
Hao Wang
haowang0806@gmail.com

Specialty section:
This article was submitted to Animal Reproduction - Theriogenology, a section of the journal Frontiers in Veterinary Science

Received: 01 February 2022
Accepted: 14 March 2022
Published: 06 May 2022

Citation:
Ye Z, Meng Q, Zhang W, He J, Zhao H, Yu C, Liang W, Li X and Wang H (2022) Exploration of the Shared Gene and Molecular Mechanisms Between Endometriosis and Recurrent Pregnancy Loss. Front. Vet. Sci. 9:867405. doi: 10.3389/fvets.2022.867405

Endometriosis (EMs) is a common benign gynecological disease in women of childbearing age, which usually causes pelvic pain, secondary dysmenorrhea, and infertility. EMs has been linked to recurrent pregnancy loss (RPL) in epidemiological data. The relationship of both, however, remains unknown. The purpose of this study is to explore the underlying pathological mechanisms between EMs and RPL. We searched Gene Expression Omnibus (GEO) database to obtain omics data of EMs and RPL. Co-expression modules for EMs and RPL were investigated by using weighted gene co-expression network analysis (WGCNA). The intersections of gene modules with the strong correlation to EMs or RPL obtained by WGCNA analysis were considered as shared genes. MicroRNAs (miRNAs) and their corresponding target genes linked to EMs and RPL were found though the Human MicroRNA Disease Database (HMDD) and the miRTarbase database. Finally, we constructed miRNAs-mRNAs regulatory networks associated with the two disorders by using the intersection of previously obtained target genes and shared genes. We discovered as significant modules for EMs and RPL, respectively, by WGCNA. The energy metabolism might be the common pathogenic mechanism of EMs and RPL, according to the findings of a Kyoto Encyclopedia of Genes and Genomes (KEGG) enrichment analysis. We discovered several target genes that might be linked to these two disorders, as well as the potential mechanisms. RAB8B, GNAQ, H2AFZ, SUGT1, and LEO1 could be therapeutic candidates for RPL and EMs. The PI3K-Akt signaling pathway and platelet activation were potentially involved in the mechanisms of EM-induced RPL. Our findings for the first time revealed the underlying pathological mechanisms of EM-induced RPL and identified several useful biomarkers and potential therapeutic targets.

Keywords: endometriosis, recurrent pregnancy loss, WGCNA, PI3K-Akt signaling pathway, platelet activation, miRNAs-mRNAs

INTRODUCTION

Endometriosis (EMs) is a chronic, inflammatory, estrogen-dependent gynecological disease, the most typical symptom of which is the appearance of endometrial tissue in the non-uterine cavity (1). Retrograde menstruation, in which endometrial tissue flows back into the pelvis and subsequently scatters to various areas, producing the local inflammatory response and causing local tissue adhesions, is currently the most widely accepted pathologic explanation (2). Worldwide, approximately 8% of women of reproductive age suffer from EMs, which are accompanied by common clinical symptoms such as dysmenorrhea, pelvic pain, and infertility. Specific diagnostic markers, on the other hand, have yet to emerge, leading to delayed diagnosis of EMs (3). Although surgery is currently the gold standard for diagnosing EMs, patients should be aware of the risk of diminished ovarian reserve and recurrence of EMs as the results of surgical treatment. Oral medicine therapy, which is the most commonly recommended in the clinic, can only help with the symptoms of EMs. When pharmacological treatment is interrupted, the chances of recurrence are significant (4). Although EMs is a benign gynecological disease, they also have the risk of malignant transformation. In clinical practice, there is currently no satisfactory treatment approach.

The disorder having more than two miscarriages before 20–24 weeks of gestation is called recurrent pregnancy loss (RPL) (5). The lack of standardized early miscarriage diagnostic guidelines and the variable miscarriage symptoms of early miscarriage patients hinder the diagnosis and treatment of RPL. Patients with RPL have the better prognosis, but it is dependent on their age, mental health, and the number of losses (6). Even though aberrant uterine morphology, chromosomal structural abnormalities, and autoimmune disorders are all linked to the development of RPL, the underlying mechanisms of miscarriage in most RPL patients remain unknown (7). The therapy of RPL patients has been complicated by the lack of the recognized mechanisms of occurrence. EMs are associated with up to 50% of infertility patients and often lead to failure of assisted reproductive treatments (8). The mechanisms of EMs-induced RPL could be that inflammatory alterations in the endometrium of EMs patients impact predecidual transformation, eventually leading to placental abnormalities (9). However, the mechanisms through which EMs cause RPL are far from flawless.

With the widespread adoption of high-throughput transcriptome sequencing technology, we can now easily find differentially expressed genes in diseases, allowing us to gain the better understanding of disease onset and progression, as well as provide guidance for clinical disease treatment. In this study, We used different bioinformatic analysis approaches, including weighted gene co-expression network analysis (WGCNA), to analyze datasets linked to EMs and RPLs in the Gene Expression Omnibus (GEO) database. Finally, we found that the underlying mechanisms of EM-induced RPL were discovered to be connected to the PI3K/AKT signaling pathway and platelet activation.

Abbreviations: EMs, endometriosis; RPL, recurrent pregnancy loss; GEO, gene expression omnibus; WGCNA, weighted gene co-expression network analysis; miRNA, microRNA; HMDD, human microRNA disease database; TOM, topological overlap matrix; PPI, protein-protein interaction; GO, gene ontology; KEGG, kyoto encyclopedia of genes and genomes.

METHODS

Research Process

Figure 1 depicted the flowchart of this study. Transcriptome sequencing data for EMs and RPL were obtained from the GEO database. WGCNA was used to investigate gene modules linked to EMs and RPL, respectively. Shared genes were defined as intersection of gene modules with high correlation to EMs and RPL obtained by WGCNA. Find the related microRNAs (miRNAs) of EMs and RPL. Shared genes and miRNAs were subjected to bioinformatics analysis. Finally, genes and molecular mechanisms linked to EMs and RPL had been discovered.

Screening of the GEO Dataset

We searched the GEO database with the keywords "endometriosis" and "recurrent pregnancy loss" respectively. The screening conditions of the dataset were as follows: (1) mRNA mRNA sequencing data from healthy people and diseased (EMs or RPL) patients, each with a population of more than 10, must be included in datasets; (2) The tissue used for sequencing should be the endometrium; (3) The sample's expression matrix file should be included in the dataset for further analysis.

WGCNA

WGCNA, which uses phenotypic weight parameters, scale-free clustering, and dynamic shear trees to evaluate data, is frequently employed to investigate disease-related gene modules. The GSE51981 and GSE165004 datasets, respectively, contained transcriptome sequencing data for about 20,000 and 30,000 genes. Since the number of genes in the datasets was different, we took the intersection of the genes in the two datasets. Most of the genes in the GEO datasets had no difference in expression among the healthy and disease groups, so we selected the top 5,000 genes with significant differences for subsequent WGCNA analysis according to the *p*-value calculated by the R language "limma" package. We used the R language "WGCNA" package to uncover gene modules linked to EMs and RPL in this study. The "Hclust" function in the R language was used to eliminate outliers in the GSE51981 and GSE165004 datasets before starting the WGCNA analysis. Then, the "pickSoftThreshold" function in the R language was used to filter the soft threshold from 1 to 30. By modifying the adjacency matrix according to the selected soft threshold, we obtained the topological overlap matrix (TOM) and the corresponding dissimilarity (1-TOM). Then, we set the minimum number of genes in the module to 50 and utilized the cut line (mergeCutHeight = 0.25) to merge comparable gene modules. Finally, we assessed the relationship between gene modules and disease.

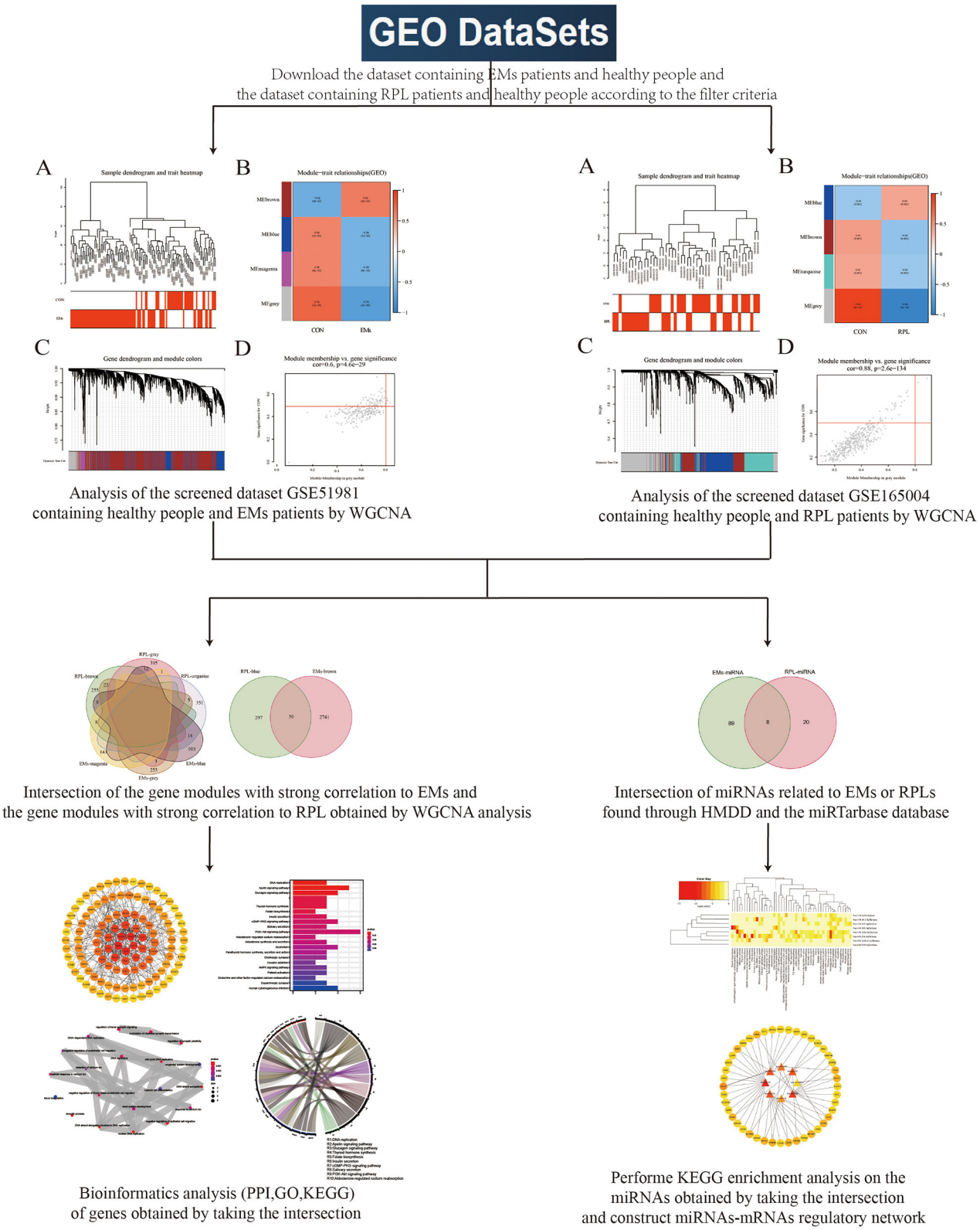

FIGURE 1 | Flowchart. This figure depicted the process of using bioinformatics methods such as WGCNA analysis to look for shared genes and biological processes between EMs and RPL.

Identification the Shared Genes of EMs and RPL

We used absolute value of the correlation more than 0.4 as the screening threshold to obtain gene modules that were strongly associated with EMs and RPL, respectively. The gene modules positively and negatively correlated with EMs and RPL were intersected and visualized through the R language "Venn" package, respectively. We defined the genes obtained from the intersection as shared genes.

Construction of Protein-Protein Interaction Network

As a main method in bioinformatics, protein-protein interaction (PPI) network can comprehensively analyze the relationship and function of multiple proteins in organisms. The STRING database could be used to study and predict numerous protein interactions. To investigate gene interactions, we entered shared genes into STRING data. The "Homo sapiens" species was chosen, and PPI analysis was carried out with the "Multiple proteins" analysis module. The PPI network was constructed with the minimum required interaction score greater than 0.15 as the screening condition. Then, We downloaded the protein interaction information of the PPI network and optimized it though Cytoscape software.

GO Term and KEGG Pathway Enrichment Analysis

The Gene Ontology (GO) database is composed of three sub-databases: molecular function, biological process, and cellular composition, which are used to define and describe gene functions. Kyoto Encyclopedia of Genes and Genomes (KEGG) database is a comprehensive database including system information, genome information, and chemical information, among which the KEGG pathway database is the most commonly used bioinformatics database. Both GO term and KEGG pathway enrichment analysis was performed on shared genes by using the R language "cluster Profiler" package and visualized the results of the enrichment analysis by the R language "ggplot" package.

Exploration of Shared miRNAs for EMs and RPL

As non-coding RNAs, miRNAs play the vital function in gene regulation. As a result, we searched for miRNAs linked to EMs and RPL to build a miRNAs-mRNAs regulatory network. Experimentally validated miRNAs associated with human diseases could be found in the Human MicroRNA Disease Database (HMDD). In this study, we took the intersection of EMs-related and RPL-related miRNAs from the HMDD database. The intersection of EM-related and RPL- related miRNAs were defined as shared miRNAs.

Bioinformatics Analysis of Shared miRNAs

The miRtarbase database has been continuously updated as a repository for miRNAs-mRNAs targeting relationships since its inception in 2011. We searched the miRtarbase database for target genes of shared miRNAs and took intersections with shared genes. Then, the miRNAs-mRNAs regulatory network was constructed by Cytoscape software. The DIANA Tools website aggregates miRNAs and lncRNAs research data and provides a variety of non-coding RNA research tools. Therefore, we used the DIANA tools website's mirPath v3.0 program to conduct the KEGG pathway enrichment analysis of miRNAs.

RESULTS

Information From the Filtered GEO Dataset

According to our screening criteria, datasets with the GEO numbers GSE51981 and GES165004 were obtained. We exclusively used the data of GSE51981 dataset, which contained 77 EMs patients and 34 healthy people. For the GSE165004 dataset, we only used the transcriptome sequencing data of 24 healthy people and 24 patients with RPL. The platform annotation file corresponding to the dataset was used to convert gene probes into gene names.

WGCNA Results of EMs and RPL Datasets

By clustering samples on the EMs dataset (GSE51981) and the RPL dataset (GSE165004), we found no abnormal samples. For these two datasets, **Figures 2A**, **3A** showed sample clustering dendrograms and clinical feature heatmaps, respectively. We obtained 4 gene modules from the EMs dataset and the RPL dataset by clustering similar gene modules, respectively. Based on the correlation of gene modules with EMs and RPL, we created heatmaps of gene modules and the relationship between EMs and RPL (**Figures 2B**, **3B**). The "brown," "blue," "magenta," and "gray" gene modules had the high connection with EMs (brown gene module: $r = 0.62$, $p = 3e\text{-}13$; blue gene module: $r = -0.56$, $p = 1e\text{-}10$; magenta gene module: $r = -0.59$, $p = 6e\text{-}12$; gray gene module: $r = -0.74$, $p = 1e\text{-}20$). EMs was negatively linked with the blue, magenta, and gray gene modules, which contained 953, 150, and 283 genes (**Supplementary Table 1**), respectively. The brown gene module was positively correlated with EMs and contained 2,791 genes (**Supplementary Table 1**). Similarly, the gene modules "brown," "turquoise," and "gray," which contain 293, 370, and 411 genes (**Supplementary Table 2**), were negatively connected with RPL (brown gene module: $r = -0.44$, $p = 0.002$; turquoise gene module: $r = -0.43$, $p = 0.002$; gray gene modules: $r = -0.96$, $p = 6e\text{-}26$). The "blue" gene module, which included 347 genes (**Supplementary Table 2**), was positively linked with RPL (blue gene module: $r = 0.44$, $p = 0.002$). Gene clustering dendrograms based on the top 5,000 differential genes were shown in **Figures 2C**, **3C**. We identified the gene modules most linked with EMs and RPL by examining the correlation between gene modules and clinical characteristics (**Figures 2D**, **3D**).

Shared Genes of EMs and RPL

We obtained 73 and 50 genes (**Figures 4A,B**, **Supplementary Table 3**) by intersecting gene modules positively and negatively correlated with EM and RPL (gene module with

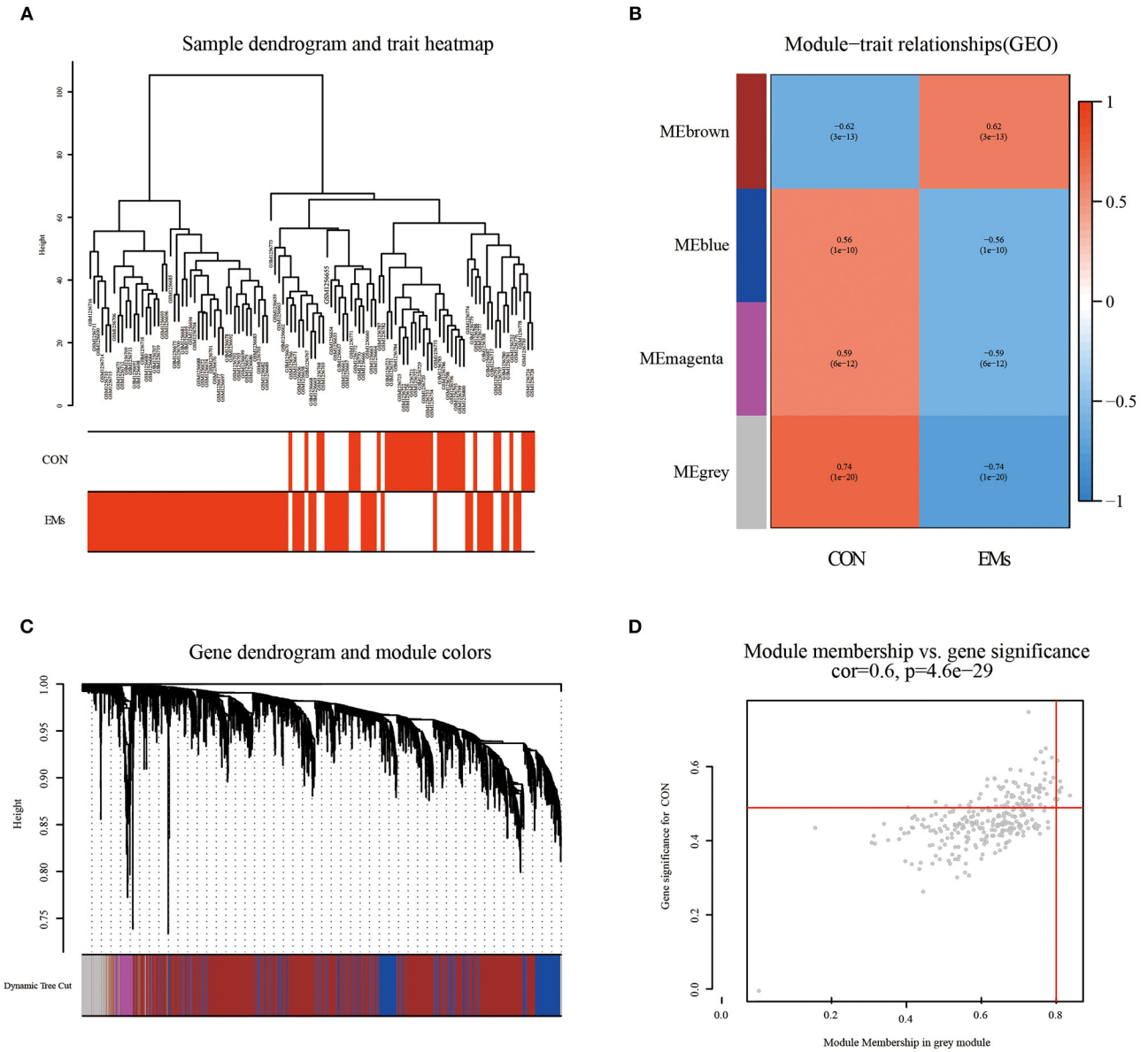

FIGURE 2 | The results of WGCNA on the EMs dataset (GSE51981). **(A)** Dendrograms and corresponding feature heatmaps of the healthy and EMs samples. **(B)** Heatmap of correlations between gene modules and clinical features, with each grid showing the correlation between gene modules and clinical features. **(C)** Cluster dendrogram of co-expressed genes in EMs. **(D)** Correlation analysis results of gray gene modules and EMs.

disease correlation > 0.4), respectively. These 123 genes were identified as shared genes since they were closely associated with EMs and RPL.

Construction of PPI Network

From the STRING database, we obtained the PPI network with 114 nodes and 738 edges (**Supplementary Table 4**). To further find the core genes of the PPI network, we imported the obtained PPI network into the Cytoscape software. Then, the degree value of each node in the PPI network was calculated through the CytoHubba plug-in. **Figure 4C** showed the PPI network containing node degree information. The node color was positively related to the degree value. The darker the color, the higher the degree value. RAB8B, GNAQ, H2AFZ, SUGT1, and LEO1 were the 5 nodes with the highest degree value (**Figure 4D**), which might be closely related to the occurrence, development, treatment and prognosis of EMs and RPL.

Annotation of Shared Genes

The R language "Venn" package was used to perform GO term and KEGG pathway enrichment analysis on 123 shared genes (**Figures 5A–D**, **Supplementary Tables 5, 6**). GO biological process analysis found that the top 20 analysis results

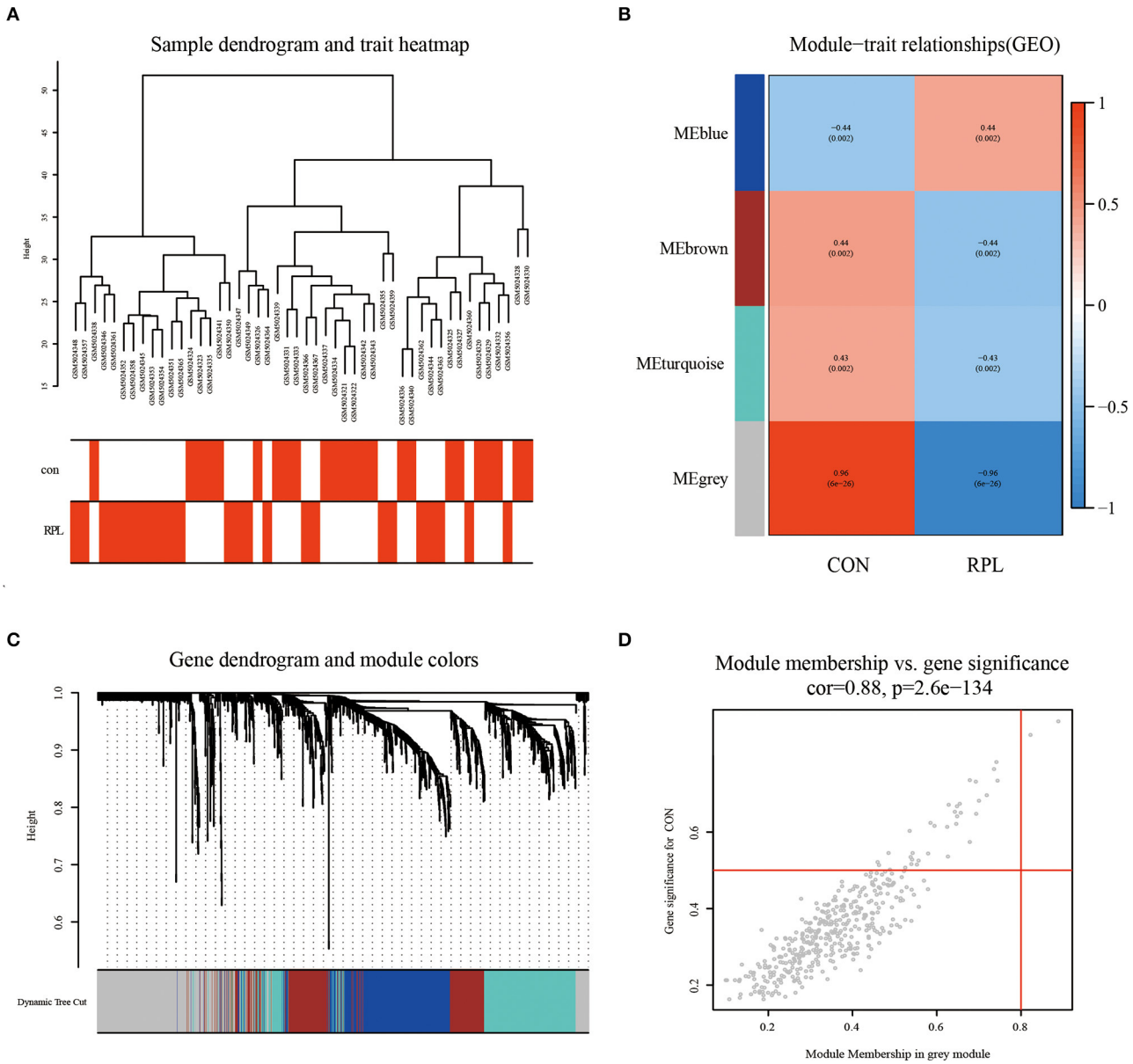

FIGURE 3 | The results of WGCNA on the RPL dataset (GSE165004). **(A)** Dendrograms and corresponding feature heatmaps of the healthy and RPL samples. **(B)** Heatmap of correlations between gene modules and clinical features. **(C)** Cluster dendrogram of co-expressed genes in EMs. **(D)** Correlation analysis results of gray gene modules and EMs.

included 6 DNA-related results, namely DNA strand elongation involved in DNA replication, nuclear DNA replication, DNA strand elongation, cell cycle DNA replication, and DNA replication. KEGG pathway enrichment analysis showed that DNA replication, Apelin signaling pathway, Glucagon signaling pathway, cGMP-PKG signaling pathway, PI3K-Akt signaling pathway, AMPK signaling pathway, Alcoholism, and Cocaine addiction might be involved in the pathological process of EMs and RPL. We used the R language "enrichplot" package to perform correlation analysis on the results to further investigate the link between these enrichment results of EMs and RPL (**Figures 5E,F**). We exhibited the top ten results of GO biological process enrichment analysis and KEGG pathway enrichment analysis with their corresponding genes in **Figures 5G,H**.

Shared miRNAs of EMs and RPL

Through the HMDD database, we searched with EMs and abortion as keywords, respectively, and obtained 150 and 28 related miRNAs (**Supplementary Table 7**). After taking the intersection (**Figure 6A**), a total of 8 miRNAs were retrieved,

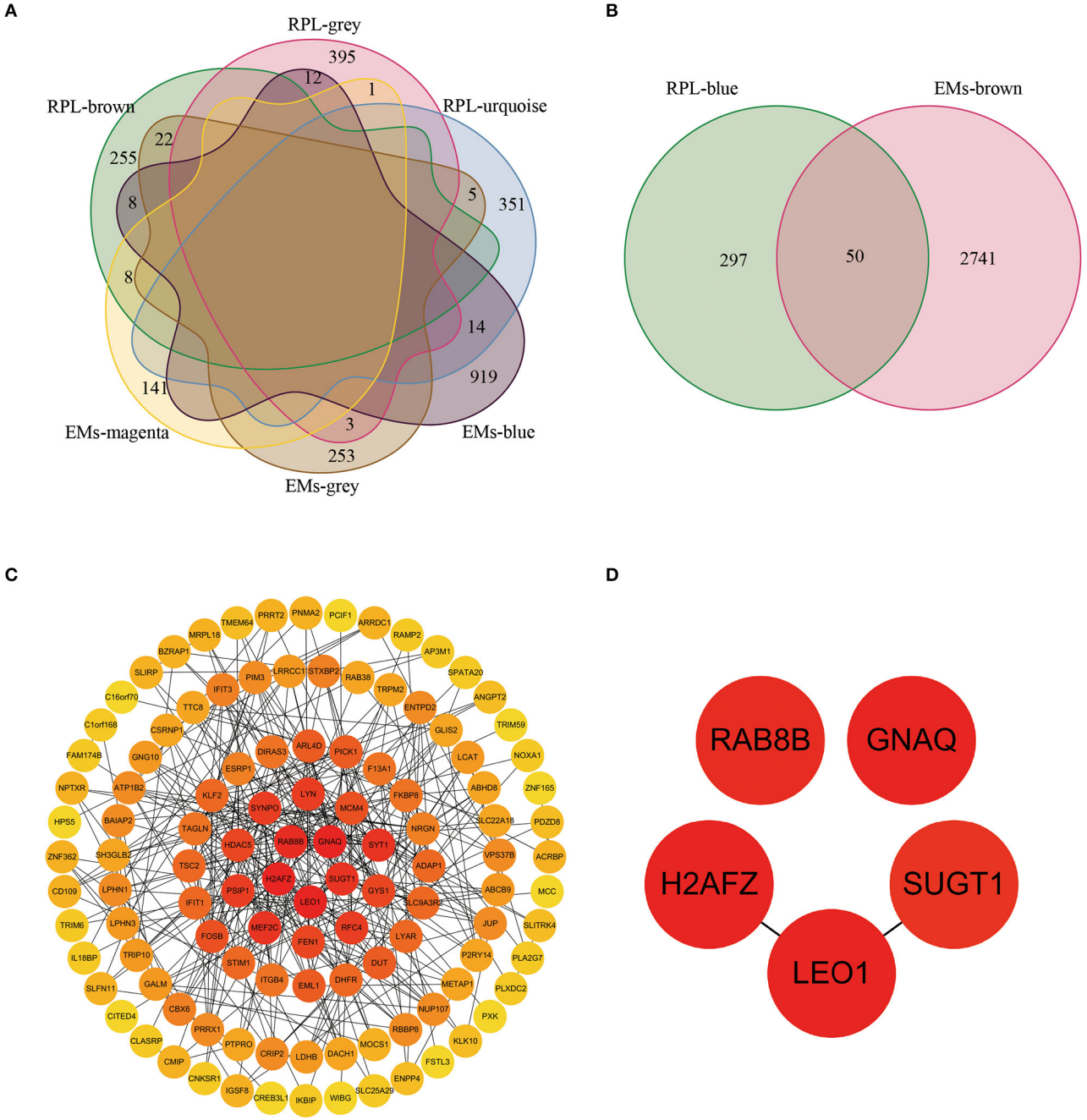

FIGURE 4 | The shared genes and PPI network between the EMs-related gene modules and the RPL-related gene modules. **(A)** Shared genes between gene modules negatively correlated with EMs and gene modules negatively correlated with RPL (module correlation greater than 0.4). **(B)** Shared genes between gene modules positively correlated with EMs and gene modules positively correlated with RPL (module correlation greater than 0.4). **(C)** PPI network constructed by EMs and RPL shared genes. **(D)** Core shared genes for EMs and RPLs.

including hsa-mir-100, hsa-mir-125a, hsa-mir-125b-2, hsa-mir-16, and hsa-mir-223, which were classified as shared miRNAs. We found target genes for 8 common miRNAs by searching the miRtarbase database (**Supplementary Table 8**). To establish the miRNAs-mRNAs regulation interaction related to EMs and RPL, the target genes of each shared miRNAs were intersected with the shared genes. Cytoscape software was used to visualize the regulatory connection between miRNAs and mRNAs (**Figure 6B**,

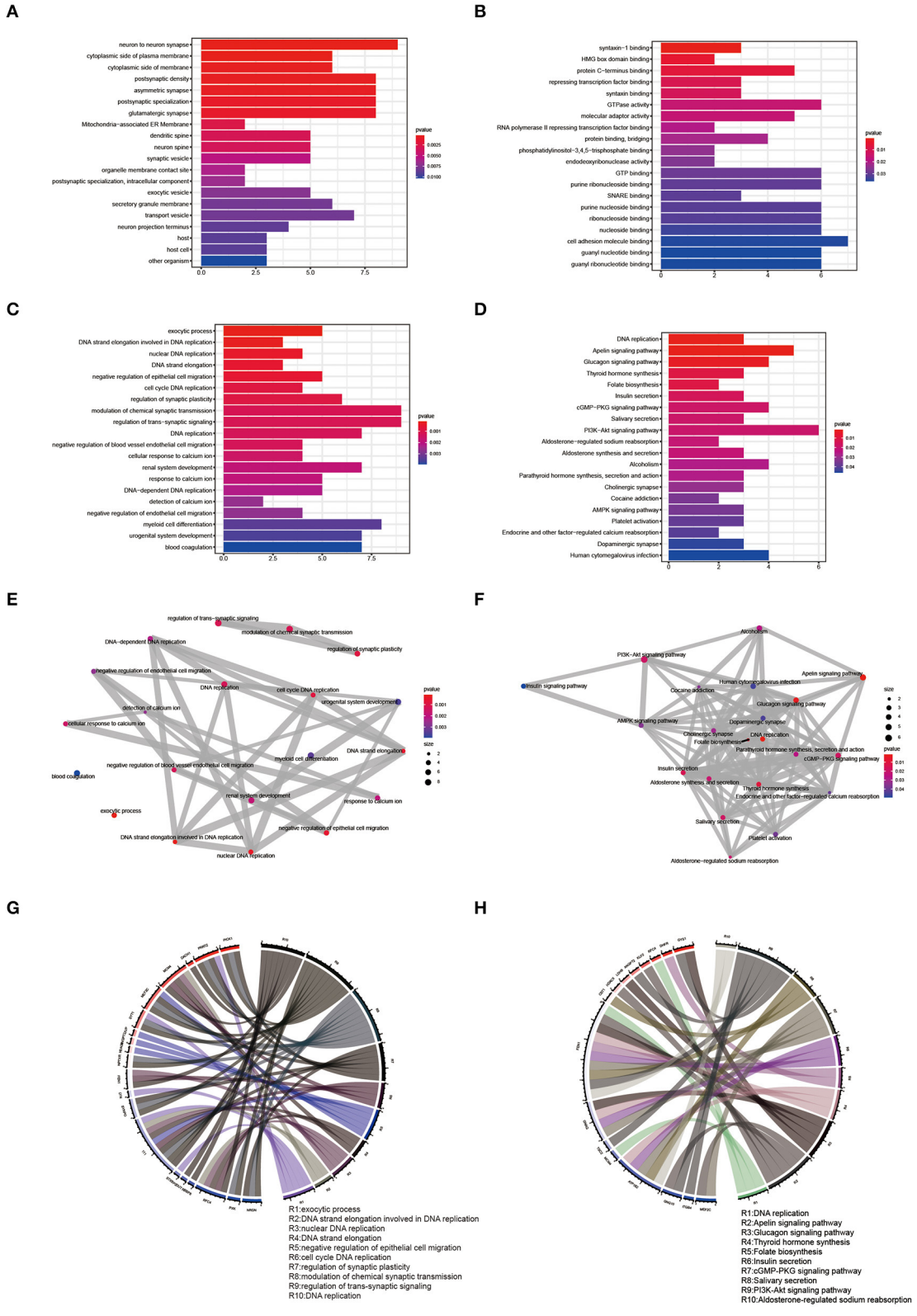

FIGURE 5 | GO term and KEGG pathway enrichment analysis of shared genes. **(A–C)** Results of CC, MF, and BP of the GO term enrichment analysis of shared genes, respectively. **(D)** Results of KEGG pathway enrichment analysis of shared genes. **(E,F)** Correlation analysis of the GO BP term and KEGG pathway enrichment analysis results of shared genes. **(G,H)** Top ten GO BP term enrichment analysis results and the top ten KEGG pathway enrichment analysis results and their corresponding shared genes.

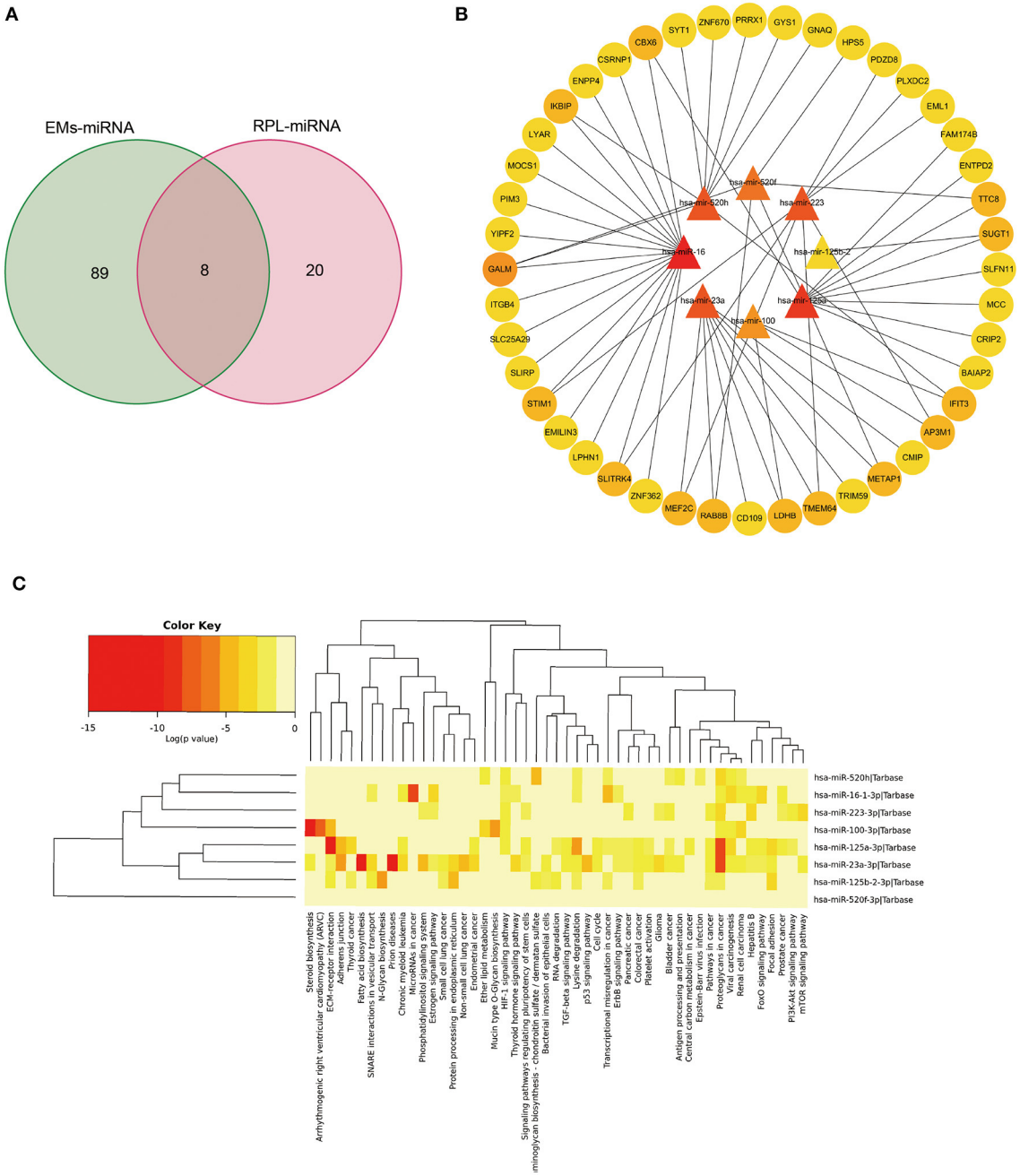

FIGURE 6 | Bioinformatics analysis of genes and miRNAs shared by EMs and RPL. **(A)** Venn diagram of the intersection of EMs-related and RPL-related miRNAs. **(B)** Regulatory network of shared miRNAs and corresponding shared genes for EMs and RPL. **(C)** KEGG pathway enrichment analysis of shared miRNAs of EMs and RPL.

Supplementary Table 9). MiRNAs were shown by triangles, while mRNAs were represented by circles. The higher the degree value, the darker the color. By using the mirPath v3.0 tool, we performed KEGG pathway enrichment analysis on 8 common miRNAs (**Figure 6C**, **Supplementary Table 10**). There were two overlapping pathways in the KEGG enrichment results of shared miRNAs and shared genes, namely the PI3K-Akt signaling pathway and platelet activation.

DISCUSSION

EMs is a chronic estrogen-dependent condition that can produce symptoms like dysmenorrhea, pelvic discomfort, and infertility, all of which have a negative impact on patients' physical and emotional health (10). EMs affects roughly 10% of women globally, yet the majority of them do not receive meaningful relief from the symptoms produced by EMs (11). EMs is the

leading cause of infertility, with about two-fifths of infertile women suffering from EMs (12). Although hormone therapy and surgical therapy have been used to help EMs patients with infertility, the results are always disappointing (13). It is necessary to develop innovative and effective medical treatments. EMs, chronic endometritis, and other diseases that produce persistent endometrial inflammation disrupt the function of endometrium function, leading to early miscarriage and the development of RPL (9). However, the specific molecular process by which EMs leads to RPL is unknown. Bioinformatics is now widely used in the life sciences by integrating biology, computing, information engineering, mathematics and other disciplines to analyze massive amounts of data.

WGCNA is often used to find potential biomarkers and therapeutic targets by clustering highly related genes and performing correlation analysis between the clustered gene modules and clinical characteristics (14). In this study, we searched gene modules related to EMs and RPL by WGCNA, and obtained 123 shared genes. Among them, RAB8B, GNAQ, H2AFZ, SUGT1, and LEO1 may serve as potential therapeutic targets for patients with EM-induced RPL. As one of the most abundant protein families in the human body, the Rab family participates in the regulation of cell functions and is closely related to the transport of various components within cells (15). Multiple members of the Rab family can participate in different stages of autophagy, and RAB8B is mainly involved in regulating autophagosome maturation (16). RAB8B regulates the Wnt/β-catenin signaling pathway by affecting the activity and function of LRP6 (17). GNAQ, a member of the alpha subunit of the G protein, is mutated in approximately 80% of melanoma patients (18). By influencing the MAPK signaling pathway and the epithelial-mesenchymal transition, GNAQ enhances lung cancer cell proliferation and invasion (19). However, GNAQ activates the antioxidant properties of the Nrf2 protein and prevents cell damage (20). Placental oxidative stress has been linked to the development of RPL (21). The histone variant encoded by H2AFZ is an essential component of the nucleosome and affects the structure and function of eukaryotic chromatin (22). A recent prospective clinical study detected oocytes from EMs patients and healthy individuals by single-cell sequencing technology and found that H2AFZ was highly expressed in EMs patients' oocytes (23). As a co-chaperone of multiple proteins, SUGT1 participates in multiple cellular biological processes (24). The ability of SUGT1 to inhibit the proliferation of gastric cancer cells by regulating AKT phosphorylation makes it a potential therapeutic target for gastric cancer (25). The RNA polymerase-associated factor 1 complex contains LEO1, which is involved in chromatin remodeling and transcriptional elongation (26). LEO1 may be critical in zebrafish heart differentiation and neural crest cell population development (27). In summary, these 5 core genes are highly diverse in function and they may be involved in various stages of EM-induced RPL.

We used GO term enrichment analysis on shared genes to learn more about the molecular mechanisms of EMs-induced RPL. DNA replication appears to be implicated in the process of EMs-induced RPL, according to the results. Cell division happens constantly in the human body and is involved in different processes of human growth, development, and reproduction. Before cell division, various cellular components, including DNA replication, are frequently replicated (28). Several investigations have discovered that several epigenetic changes, including DNA methylation, are involved in the incidence and development of RPL at various stages through controlling the expression of critical genes in cell biological processes. Among them, DNA methylation-induced gene expression disorders and immunological imbalances affect all phases of embryonic development, which may be linked to RPL pathobiology (29). In addition, clinical studies have found that DNA damage induced by heavy metals may be related to the occurrence and development of RPL (30). Multiple modification mechanisms of epigenetics may be involved in the pathophysiology of EMs (31). Clinical studies have found that DNA methylation regulates genes related to endometrial function, which in turn affects the occurrence of many biological processes including cell proliferation and steroid hormone response (32). Furthermore, circulating cell-free nuclear DNA contained in human plasma and serum has been shown to be the biomarker for EMs (33).

We found 22 and 49 signaling pathways by using KEGG pathway enrichment analysis on shared genes and shared miRNAs, respectively. Two signaling pathways associated with EMs and RPL were discovered by intersecting the two analytical results, namely the PI3K-Akt signaling pathway and Platelet activation. By receiving signals from outside the cell, the PI3K-Akt signaling pathway is primarily engaged in the control of numerous cellular activities in the human body. The up-regulation of AXL and SHC1 could be related to the participation of the PI3K-Akt signaling pathway in the pathogenesis of EMs (34). As the pivotal pathway is closely associated with the progression of EMs, the PI3K/AKT signaling pathway is strongly linked to the regulation of functions such as proliferation, epithelial-mesenchymal transition, and invasion of ectopic endometrial stromal cells (35). The development of new drugs based on the PI3K/AKT signalling pathway for the treatment of EMs has great potential. Through the downstream matrix metalloproteinase 2, the PI3K/AKT signaling pathway is implicated in the migration of female trophoblast cells, which is linked to the incidence of RPL (36). PI3K/AKT signaling pathway is closely related to macrophage polarization. At the maternal-fetal interface, decidual macrophages govern immunological responses, and aberrant macrophage polarization is frequently linked to poor pregnancy timing, including RPL (37). Platelets are anucleated cells rich in many types of organelles. Through the regulation of the PI3K/AKT signaling pathway, platelets reduce the immune response of the microenvironment at the lesion site of EMs patients and then slow the progression of EMs (38). Platelets agglomerate in the lesions of patients with EMs, according to clinical investigations, may play a role in the advancement of EMs by causing microangiogenesis (39). Anti-platelet therapy can block epithelial-mesenchymal transition and fibrosis in EMs mice (40). Patients with RPL had the higher sensitivity to arachidonic acid, which promotes platelet aggregation (41). Platelet factor 4 and other blood biomarkers may be used to identify women at risk for RPL (42). In conclusion, the PI3K/AKT signaling pathway and platelet activation were both involved in the pathological process of EMs and RPL, so we speculated that these

two pathways might be the potential mechanisms of EMs-induced RPL.

CONCLUSION

In this study, the transcriptome sequencing data of EMs and RPL were analyzed by bioinformatics methods. For the first time, we investigated the underlying mechanisms (PI3K-Akt signaling pathway and platelet activation) and potential therapeutic targets (RAB8B, GNAQ, H2AFZ, SUGT1, and LEO1) of EMs-induced RPL by using multiple bioinformatics approaches, including WGCNA, to aid basic research, clinical diagnosis, and treatment of this disease.

DATA AVAILABILITY STATEMENT

The original contributions presented in the study are included in the article/**Supplementary Material**, further inquiries can be directed to the corresponding author/s.

AUTHOR CONTRIBUTIONS

HW, XL, WL, and CY developed the concept of the project. ZY collected and analyzed the data with the help of QM, JH, WZ, and HZ. HW, XL, WL, CY, and ZY wrote the manuscript. All authors have read and approved the final manuscript, reviewed and discussed the results, and contributed to the paper preparation.

FUNDING

This study was supported by Shenzhen Key Laboratory Foundation (ZDSYS20200811143757022), Shenzhen Science and Technology Innovation Commission Project (Grant No. JCYJ20180302174235893), and Research funding for post-doctoral research in Shenzhen.

SUPPLEMENTARY MATERIAL

The Supplementary Material for this article can be found online at: https://www.frontiersin.org/articles/10.3389/fvets.2022.867405/full#supplementary-material

Supplementary Table 1 | Four gene modules associated with EMs.

Supplementary Table 2 | Four gene modules associated with RPL.

Supplementary Table 3 | Shared genes for EMs and RPL.

Supplementary Table 4 | PPI network analysis results of shared genes.

Supplementary Table 5 | GO term enrichment analysis results of shared genes.

Supplementary Table 6 | KEGG pathway enrichment analysis results of shared genes.

Supplementary Table 7 | MiRNAs associated with EMs and RPL.

Supplementary Table 8 | Target genes corresponding to shared miRNAs.

Supplementary Table 9 | MiRNAs-mRNAs regulatory network.

Supplementary Table 10 | KEGG pathway enrichment analysis results of shared miRNAs.

REFERENCES

1. Chapron C, Marcellin L, Borghese B, Santulli P. Rethinking mechanisms, diagnosis and management of endometriosis. *Nature reviews Endocrinol.* (2019) 15:666–82. doi: 10.1038/s41574-019-0245-z
2. Lin LL, Makwana S, Chen M, Wang CM, Gillette LH, Huang TH, et al. Cellular junction and mesenchymal factors delineate an endometriosis-specific response of endometrial stromal cells to the mesothelium. *Mol Cell Endocrinol.* (2022) 539:111481. doi: 10.1016/j.mce.2021.111481
3. Taylor HS, Kotlyar AM, Flores VA. Endometriosis is a chronic systemic disease: clinical challenges and novel innovations. *Lancet.* (2021) 397:839–52. doi: 10.1016/S0140-6736(21)00389-5
4. Falcone T, Flyckt R. Clinical management of endometriosis. *Obstet Gynecol.* (2018) 131:557–71. doi: 10.1097/AOG.0000000000002469
5. Hong Li Y, Marren A. Recurrent pregnancy loss: a summary of international evidence-based guidelines and practice. *Australian journal of general practice.* (2018) 47:432–6. doi: 10.31128/AJGP-01-18-4459
6. Dimitriadis E, Menkhorst E, Saito S, Kutteh WH, Brosens JJ. Recurrent pregnancy loss. *Nature reviews Disease primers.* (2020) 6:98. doi: 10.1038/s41572-020-00228-z
7. Habets DHJ, Schiffer V, Kraneburg LPA, de Krom FJW, Gürtekin I, van Bree BE, et al. Preconceptional evaluation of women with recurrent pregnancy loss: the additional value of assessing vascular and metabolic status. *BMC Pregnancy Childbirth.* (2022) 22:75. doi: 10.1186/s12884-021-04365-5
8. de Ziegler D, Pirtea P, Carbonnel M, Poulain M, Cicinelli E, Bulletti C, et al. Assisted reproduction in endometriosis. *Best Prac Res Clin Endocrinol Metabol.* (2019) 33:47–59. doi: 10.1016/j.beem.2018.10.001
9. Pirtea P, Cicinelli E, De Nola R, de Ziegler D, Ayoubi JM. Endometrial causes of recurrent pregnancy losses: endometriosis, adenomyosis, and chronic endometritis. *Fertil Steril.* (2021) 115:546–60. doi: 10.1016/j.fertnstert.2020.12.010
10. Giudice LC, Kao LC. Endometriosis. *Lancet.* (2004) 364:1789–99. doi: 10.1016/S0140-6736(04)17403-5
11. Armour M, Sinclair J, Cheng J, Davis P, Hameed A, Meegahapola H, et al. Endometriosis and cannabis consumption during the covid-19 pandemic: an international cross-sectional survey. *Cannabis Cannabinoid Res.* (2022). doi: 10.1089/can.2021.0162
12. Ozkan S, Murk W, Arici A. Endometriosis and infertility: epidemiology and evidence-based treatments. *Ann N Y Acad Sci.* (2008) 1127:92–100. doi: 10.1196/annals.1434.007
13. Macer ML, Taylor HS. Endometriosis and infertility: a review of the pathogenesis and treatment of endometriosis-associated Infertility. *Obstet Gynecol Clin North Am.* (2012) 39:535–49. doi: 10.1016/j.ogc.2012.10.002
14. Langfelder P, Horvath S. Wgcna: an r package for weighted correlation network analysis. *BMC Bioinformatics.* (2008) 9:559. doi: 10.1186/1471-2105-9-559
15. Kumar R, Donakonda S, Müller SA, Bötzel K, Höglinger GU, Koeglsperger T. Fgf2 affects Parkinson's disease-associated molecular networks through exosomal Rab8b/Rab31. *Front Genet.* (2020) 11:572058. doi: 10.3389/fgene.2020.572058
16. Ao X, Zou L, Wu Y. Regulation of autophagy by the rab gtpase network. *Cell Death Differ.* (2014) 21:348–58. doi: 10.1038/cdd.2013.187
17. Demir K, Kirsch N, Beretta CA, Erdmann G, Ingelfinger D, Moro E, et al. rab8b is required for activity and caveolar endocytosis of Lrp6. *Cell Rep.* (2013) 4:1224–34. doi: 10.1016/j.celrep.2013.08.008
18. Scholz SL, Möller I, Reis H, Süßkind D, van de Nes JAP, Leonardelli S, et al. Frequent Gnaq, Gna11, and Eif1ax mutations in iris melanoma. *Invest Ophthalmol Vis Sci.* (2017) 58:3464–70. doi: 10.1167/iovs.17-21838
19. Choi JY, Lee YS, Shim DM, Lee YK, Seo SW. Gnaq Knockdown promotes bone metastasis through epithelial-mesenchymal

transition in lung cancer cells. *Bone Joint Res.* (2021) 10:310–20. doi: 10.1302/2046-3758.105.BJR-2020-0262.R3
20. Sun X, Li GP, Huang P, Wei LG, Guo JZ, Ao LJ, et al. Gnaq Protects Pc12 Cells from oxidative damage by activation of Nrf2 and inhibition of Nf-Kb. *Neuromolecular Med.* (2020) 22:401–10. doi: 10.1007/s12017-020-08598-z
21. Zejnullahu VA, Zejnullahu VA, Kosumi E. The role of oxidative stress in patients with recurrent pregnancy loss: a review. *Reprod Health.* (2021) 18:207. doi: 10.1186/s12978-021-01257-x
22. Dong M, Chen J, Deng Y, Zhang D, Dong L, Sun D. H2afz Is a prognostic biomarker correlated to Tp53 mutation and immune infiltration in hepatocellular carcinoma. *Front Oncol.* (2021) 11:701736. doi: 10.3389/fonc.2021.701736
23. Ferrero H, Corachán A, Aguilar A, Quiñonero A, Carbajo-García MC, Alamá P, et al. Single-cell rna sequencing of oocytes from ovarian endometriosis patients reveals a differential transcriptomic profile associated with lower quality. *Human Rep.* (2019) 34:1302–12. doi: 10.1093/humrep/dez053
24. Ogi H, Sakuraba Y, Kitagawa R, Xiao L, Shen C, Cynthia MA, et al. The Oncogenic role of the cochaperone Sgt1. *Oncogenesis.* (2015) 4:e149. doi: 10.1038/oncsis.2015.12
25. Gao G, Kun T, Sheng Y, Qian M, Kong F, Liu X, et al. Sgt1 Regulates Akt signaling by promoting beta-Trcp-dependent Phlpp1 degradation in gastric cancer cells. *Mol Biol Rep.* (2013) 40:2947–53. doi: 10.1007/s11033-012-2363-8
26. Tiwari V, Kulikowicz T, Wilson DM III, Bohr VA. Leo1 is a partner for cockayne syndrome protein B (Csb) in response to transcription-blocking DNA damage. *Nuc Acids Res.* (2021) 49:6331–46. doi: 10.1093/nar/gkab458
27. Nguyen CT, Langenbacher A, Hsieh M, Chen JN. The Paf1 Complex component Leo1 is essential for cardiac and neural crest development in zebrafish. *Dev Biol.* (2010) 341:167–75. doi: 10.1016/j.ydbio.2010.02.020
28. Alberts B, DNA. Replication and Recombination. *Nature.* (2003) 421:431–5. doi: 10.1038/nature01407
29. Zhou Q, Xiong Y, Qu B, Bao A, Zhang Y, DNA. Methylation and recurrent pregnancy loss: a mysterious compass? *Front Immunol.* (2021) 12:738962. doi: 10.3389/fimmu.2021.738962
30. Alrashed M, Tabassum H, Almuhareb N, Almutlaq N, Alamro W, Alanazi ST, et al. Assessment of DNA damage in relation to heavy metal induced oxidative stress in females with recurrent pregnancy loss (Rpl). *Saudi J Biol Sci.* (2021) 28:5403–7. doi: 10.1016/j.sjbs.2021.05.068
31. Koukoura O, Sifakis S, Spandidos DA, DNA. Methylation in endometriosis (review). *Mol Med Rep.* (2016) 13:2939–48. doi: 10.3892/mmr.2016.4925
32. Houshdaran S, Nezhat CR, Vo KC, Zelenko Z, Irwin JC, Giudice LC. Aberrant endometrial DNA methylome and associated gene expression in women with endometriosis. *Biol Reprod.* (2016) 95:93. doi: 10.1095/biolreprod.116.140434
33. Zachariah R, Schmid S, Radpour R, Buerki N, Fan AX, Hahn S, et al. Circulating cell-free DNA as a potential biomarker for minimal and mild endometriosis. *Reprod Biomed Online.* (2009) 18:407–11. doi: 10.1016/S1472-6483(10)60100-9
34. Honda H, Barrueto FF, Gogusev J, Im DD, Morin PJ. Serial analysis of gene expression reveals differential expression between endometriosis and normal endometrium. Possible Roles for Axl and Shc1 in the pathogenesis of endometriosis. *Reprod Biol Endocrinol: RB&E.* (2008) 6:59. doi: 10.1186/1477-7827-6-59
35. Wang H, Ni C, Xiao W, Wang S. Role of Lncrna Ftx in invasion, metastasis, and epithelial-mesenchymal transition of endometrial stromal cells caused by endometriosis by regulating the Pi3k/Akt signaling pathway. *Annals Translat Med.* (2020) 8:1504. doi: 10.21037/atm-20-6810
36. Ye Y, Jiang S, Du T, Ding M, Hou M, Mi C, et al. Environmental pollutant benzo[a]pyrene upregulated long non-Coding RNA Hz07 inhibits trophoblast cell migration by inactivating Pi3k/Akt/Mmp2 signaling pathway in recurrent pregnancy loss. *Reproductive Sci.* (2021) 28:3085–93. doi: 10.1007/s43032-021-00630-2
37. Cui L, Jin X, Xu F, Wang S, Liu L, Li X, et al. Circadian rhythm-associated rev-erbα modulates polarization of decidual macrophage via the Pi3k/Akt signaling pathway. *Am J Rep Immunol.* (2021) 86:e13436. doi: 10.1111/aji.13436
38. Xiao F, Liu X, Guo SW. Platelets and regulatory T cells may induce a type 2 immunity that is conducive to the progression and fibrogenesis of endometriosis. *Front Immunol.* (2020) 11:610963. doi: 10.3389/fimmu.2020.610963
39. Ding D, Liu X, Duan J, Guo SW. Platelets are an unindicted culprit in the development of endometriosis: clinical and experimental evidence. *Human Reproduction.* (2015) 30:812–32. doi: 10.1093/humrep/dev025
40. Zhang Q, Liu X, Guo SW. Progressive development of endometriosis and its hindrance by anti-platelet treatment in mice with induced endometriosis. *Reprod Biomed Online.* (2017) 34:124–36. doi: 10.1016/j.rbmo.2016.11.006
41. Flood K, Peace A, Kent E, Tedesco T, Dicker P, Geary M, et al. Platelet reactivity and pregnancy loss. *Am J Obst Gynecol.* (2010) 203:281. doi: 10.1016/j.ajog.2010.06.023
42. Kotani S, Kamada Y, Shimizu K, Sakamoto A, Nakatsuka M, Hiramatsu Y, et al. Increased plasma levels of platelet factor 4 and β-thromboglobulin in women with recurrent pregnancy loss. *Acta Med Okayama.* (2020) 74:115–22. doi: 10.18926/amo/58269

Conflict of Interest: The authors declare that the research was conducted in the absence of any commercial or financial relationships that could be construed as a potential conflict of interest.

Publisher's Note: All claims expressed in this article are solely those of the authors and do not necessarily represent those of their affiliated organizations, or those of the publisher, the editors and the reviewers. Any product that may be evaluated in this article, or claim that may be made by its manufacturer, is not guaranteed or endorsed by the publisher.

frontiers | Frontiers in Veterinary Science

ORIGINAL RESEARCH
published: 13 June 2022
doi: 10.3389/fvets.2022.846981

The Mechanism of Heat Stress Resistance During Spermatogenesis in Turpan Black Sheep

Yukun Song[1†], Xi Zhao[1†], Aikebaier Aihemaiti[1], Aerman Haire[1], Yu Gao[1], Chao Niu[1], Peng Yang[2], Guoshi Liu[3], Gongxue Jia[4] and Abulizi Wusiman[1*]*

[1] Department of Animal Science, College of Animal Science, Xinjiang Agricultural University, Urumqi, China, [2] Tuokexun County Huishang Ecological Animal Husbandry Co., Ltd., Turpan, China, [3] National Engineering Laboratory for Animal Breeding, Beijing Key Laboratory for Animal Genetic Improvement, College of Animal Science and Technology, China Agricultural University, Beijing, China, [4] Key Laboratory of Adaptation and Evolution of Plateau Biota, Northwest Institute of Plateau Biology, Chinese Academy of Sciences, Xining, China

OPEN ACCESS

Edited by:
Shou-Long Deng,
Chinese Academy of Medical Sciences and Peking Union Medical College, China

Reviewed by:
Lei Gao,
Northwest A&F University, China
Ji-Xin Tang,
Guangdong Medical University, China

***Correspondence:**
Gongxue Jia
jiagongxue@nwipb.cas.cn
Abulizi Wusiman
abulizi68@126.com

[†] These authors have contributed equally to this work

Specialty section:
This article was submitted to Animal Reproduction - Theriogenology, a section of the journal Frontiers in Veterinary Science

Received: 31 December 2021
Accepted: 29 April 2022
Published: 13 June 2022

Citation:
Song Y, Zhao X, Aihemaiti A, Haire A, Gao Y, Niu C, Yang P, Liu G, Jia G and Wusiman A (2022) The Mechanism of Heat Stress Resistance During Spermatogenesis in Turpan Black Sheep. Front. Vet. Sci. 9:846981. doi: 10.3389/fvets.2022.846981

Heat stress can affect the reproductive function of livestock and cause harm to animal production, which can seriously damage the economic interests of livestock producers. Therefore, it is important to explore the effect of heat stress on reproductive function to improve livestock production. In this study, the experimental animals Turpan black sheep and Suffolk sheep were selected as controls, each with 10 sheep, and the reproductive physiological performance was measured in Turpan, China from April to August when there was no heat stress to strong heat stress. The results showed that the sperm density, vitality, and kinematic parameters of Suffolk sheep were significantly lower than that in Turpan black sheep ($p < 0.01$) after heat stress, while the sperm acrosome malfunctions and DNA damage were significantly higher in Suffolk sheep ($p < 0.01$). In addition, the endogenous levels of reproductive hormones and oxidative stress indicators in the blood of Turpan black sheep were stable before and after heat stress treatment, while Suffolk sheep showed different degrees of fluctuations. There was no significant difference in testicular histomorphology between the two after heat stress treatment. However, Suffolk sheep showed a significantly decreased number of spermatocytes after heat stress treatment ($p < 0.05$). It was found that during meiosis, the proportion of cells in the meiotic zygotene stage of Suffolk sheep was significantly higher than that of Turpan black sheep. To investigate the mechanism of normal spermatogenesis in Turpan black sheep under heat stress, we performed RNA-Seq analysis on the testis. The results showed that there were 3,559 differential genes in Turpan black sheep before and after heat stress, with 2,118 up-regulated genes and 1,441 down-regulated genes. The enrichment analysis of GO and KEGG showed that the differential genes are mainly involved in cellular component organization or biogenesis, cell cycle process, mitotic cell cycle process, meiotic cell cycle process, double-strand break repair and Rap1 signaling pathway, Ras signaling pathway, Cell cycle, signaling pathways regulating pluripotency of stem cells Oocyte meiosis. Genes related to spermatogenesis, *SYCP2*, *TDRD9*, *BRDT*, *CEP120*, *BRCA1*, etc. were significantly up-regulated in Turpan black sheep after heat stress. In summary, our results showed that the up-regulation of genes involved in spermatogenesis protects the normal production of

sperm in Turpan black sheep under HS, thereby achieving normal reproductive function.Our research systematically elucidated the mechanism of heat stress resistance during spermatogenesis in Turpan black sheep and provided potential possibilities for the subsequent breeding of new heat-resistant breeds.

Keywords: heat stress, spermatogenesis, meiosis, Turpan black sheep, RNA-seq

INTRODUCTION

Heat stress (HS) is the sum of the body's non-specific physiological responses to a high-temperature environment (1). Almost all animals would suffer from HS in a high-temperature environment (2). In recent years, with the industrialization and intensification of animal husbandry, the research on the stress of livestock and poultry has become a hot topic in the field of animal research (3, 4). HS can cause a series of body's sub-health or functional disorders, mainly including heat wheezing, increased tension of the cardiovascular system, accelerated heart rate, reduced secretion of digestive juices, increased oxidative metabolism, and decreased immunity (5), which results in a decline in production and reproductive performance. Therefore, studying the mechanism of HS resistance is very important to improve the livestock and poultry industry.

Testicular temperature below core body temperature is one of the necessary conditions for sheep to produce normal and highly viable sperm. However, when the testis is exposed to a high-temperature environment, it is extremely prone to induce irreversible damage. Previous studies have illustrated that the abnormal rate of sperm would be increased obviously and the viability of sperm would be decreased after HS (6). Additionally, HS can also induce germ cell apoptosis, DNA damage, and abnormal maturation of sperm (7). This is most likely due to the influence of HS on the concentration of amino acids, fatty acids, minerals, enzymes, antioxidants, growth factors in the spermatogenesis environment, or the activity of enzymes related to spermatogenesis (8). For example, Merino rams exposed to a high temperature of around 35°C for 3 days showed a significant decrease in sperm motility during the following 15 to 35 days (9). In addition, abnormal sperm motility, morphology, and quantity of sperm will also significantly decrease. The pachytene spermatocytes and round sperm cells were considered to be susceptible to HS (10), increasing the apoptosis, thus inhibiting the spermatogenesis. The increase in ambient temperature leads to the production of intracellular reactive oxygen species (ROS) (11), which damage DNA, inhibit cell proliferation, and induce apoptosis (7).

Turpan region belongs to the typical continental warm temperate desert climate, with abundant sunshine, abundant heat, and extremely dry. In summer, the maximum air temperature can reach 49.6°C, the surface temperature can reach more than 70°C. However, in this extreme environment, there is special livestock in the Turpan region – Turpan black sheep. Turpan black sheep is formed under long-term breeding by farmers and herdsmen in Toksun County of the Turpan region. It is one of the excellent local sheep breeds in China and is bred by Bayanbulak sheep, Kazak sheep, Karakul sheep, and other breeds. Turpan black sheep can not only adapt to the natural climatic conditions of cold and windy winter, but also adapt to the arid and hot climate in the Turpan area, and grow fast in the soil with strong lignification and arid saline-alkali. Even under extreme heat condition, Turpan black sheep still produce healthy sperm. However, when Suffolk sheep (12) were brought in Turpan, male Suffolk sheep showed severe reproductive dysfunction during the summer, failing to produce sperm normally. Hence, we thought that Turpan black sheep may have strong resistance to HS. To prove this hypothesis, we compared hormone levels, sperm production, and germ cell development of Turpan black sheep and Suffolk sheep before and after natural HS treatment. Combining the testicular transcriptome analysis, we identified HS signaling pathways and related molecular mechanisms and illustrated the mechanism of Turpan black sheep testicular resistance to HS. These results provide a new direction for sheep breeding to deal with the negative effects of HS on sheep reproduction.

MATERIALS AND METHODS

Ethics Statement

All experiments were performed following the approved guidelines. All procedures were reviewed and approved by the Ethics Committee of Xinjiang Agricultural University (Protocol Permit Number: 2020032, 7 May 2020).

Animals

The experiment was carried out in Toksun County, Turpan Region, Xinjiang, China from April to August 2021. The ambient temperature (AT) and relative humidity (RH) were continuously measured using a digital thermometer (Xiaomi Technology Co., Ltd.) for 104 days from April 28. Temperature and heat index (THI) was calculated as follow: THI = (1.8*AT+32)–(0.55–0.55*RH*0.01)*(1.8*AT-26). THI $\leq$ 72, no HS; 73 $\leq$ THI $\leq$ 77, mild HS; 78 $\leq$ THI $\leq$ 89, moderate HS; THI $\geq$ 90, severe HS.

At the beginning of the experiment, 1.5-year-old rams were chosen with healthy body conditions and normal reproductive function. Six Turpan black sheep and six Suffolk sheep were kept under the same conditions of breeding and management. The external or internal body temperature of animals was measured using an infrared digital thermometer or a mercury thermometer.

Detection of Hormone Levels and Antioxidant Indicators

Blood samples were collected and centrifuged to separate the serum, and stored at−80°C. The radioimmunoassay was used

to determine follicle-stimulating hormone (FSH), luteinizing hormone (LH), cortisol (COR), testosterone (T), cholesterol (CHOL), catalase (CAT), superoxide dismutase (SOD), malondialdehyde (MDA), and glutathione peroxidase (GSH-Px).

Determination of Sperm DNA Fragmentation Index

Sperm chromatin dispersion (SCD) test was carried out on 500 sperm per group, and the ratio of sperm head diameter to halo size: the statistics of large halo sperm, medium halo sperm, small halo sperm, no halo sperm, and degenerative sperm. Sperm DNA fragmentation index (DFI) = (small halo sperm + no halo sperm + degenerated sperm)/500 × 100%.DFI parameter values: (1) DFI < 15%, sperm with good DNA integrity. (2) 15% ≤ DFI ≤ 30%, sperm with average DNA integrity. (3) DFI > 30%, sperm with poor DNA integrity.

Testis Sample and Immunostaining

Testis fixed in 4% paraformaldehyde (PFA) at 4°C was dehydrated stepwise through an ethanol series and embedded in paraffin. About 5 μm sections were cut using Leica RM2235 Slicing Machine. After dewaxing and rehydration, sections were stained with H&E. For immunostaining, sections were boiled in 10 mM sodium citrate buffer (pH 6.0) for 20 min. On cooling to room temperature, samples were washed in PBS and blocked with 10% donkey serum in PBS for 1 h. Then sections were incubated with primary antibodies diluted in PBS containing 3% bovine serum albumin (BSA) at 4°C overnight and washed in PBS before incubating with secondary antibodies for 2 h at room temperature. After washing in PBS thoroughly, sections were incubated with DAPI and mounted on slides for immunofluorescence analysis in Leica DMR Fluorescence Microscope.

The antibodies used are as follows: anti-UCLH1 (Abcam, USA, Ms mAb; 1:400 dilution, 0.5 μg/ml), anti-SYCP1 (Santa Cruze, USA, Rb pAb; 1:100 dilution, 0.5 μg/ml), anti-SOX9 (Abcam, USA, Rb pAb; 1:400 dilution, 0.5 μg/ml), anti-PNA (Vector Labs, 1:500 dilution), Alexa-Fluor-488 Affinipure Goat Anti-Mouse IgG (Abcam, USA, 1:500, 4 μg/ml), Alexa-Fluor-555- Dnk pAb to Rb IgG (Abcam, USA, 1:500, 4 μg/ml).

Chromosome Spreading

Refer to the method for meiotic cell plating and make some modifications based on it. Tissue samples frozen in liquid nitrogen were thawed and thawed in a 37°C water bath. The tissue was minced in a centrifuge tube to prepare a single cell suspension, the supernatant was discarded and left for 20 min, and then 100 mM sucrose solution was added. Spread the suspension evenly on the glass slide, place it in a heat and humidity box for more than 2 h, and dry the prepared slides after 30 min. Prepared slides were placed in antibody dilution buffer (ADB) to seal for 1 h, and 50 μl of the primary antibody was added dropwise to the slides, sealed with rubber glue, and incubated a 37°C incubator for 24 h. Then add 50 μl secondary antibody and place in a 37°C incubator for 2 h. After washing with PBS, the specimens were stained with DAPI for 30 min and mounted with glycerol for microscopic examination.

RNA Extraction, Library Construction, and Sequencing

For each group, tissues from three animals were used for RNA extraction, library construction, and sequencing. Briefly, the total cellular RNA of testis was isolated using the Trizol kit (Promega, USA) following the manufacturer's instructions. RNA quality and concentration were measured by using Agilent 2100 Bio-analyzer (Agilent Technologies, Santa Clara, CA) and by RNase-free agarose gel electrophoresis after removing the genomic DNA. Next, Poly (A) mRNA was isolated using oligo-dT beads (Qiagen). All mRNA was broken into short fragments by adding a fragmentation buffer. First-strand cDNA was generated using random hexamer-primed reverse transcription, followed by the synthesis of the second-strand cDNA using RNase H and DNA polymerase I. The cDNA fragments were purified using a QIA quick PCR extraction kit. These purified fragments were then washed with EB buffer for end reparation poly (A) addition and ligated to sequencing adaptors. Following agarose gel electrophoresis and extraction of cDNA from gels, the cDNA fragments were purified and enriched by PCR to construct the final cDNA library. The cDNA library was sequenced on the Illumina sequencing platform (Illumina HiSeq^{TM} 2500) using the paired-end technology by Gene Denovo Co. (Guangzhou, China). A Perl program was written to select clean reads by removing low-quality sequences (there were more than 50% bases with quality lower than 20 in one sequence), reads with more than 5% N bases (bases unknown), and reads containing adaptor sequences.

Transcript Assembly and Expression Value Estimation

BosGRu_v2.0 was used for the alignment of RNA sequencing reads. Sequencing reads in FASTQ format were mapped to the reference genome, as well as splice junctions were identified using TopHat (13). Cufflinks package (14) was used for genome-guided transcript assembly and expression abundance estimated. First, Cufflinks was used to reconstruct transcripts based on genome annotation, then the transcripts from each sample were merged by cuffmerge. Novel transcripts were extracted from the result with the threshold of "length ≥200 bp and exon number ≥," and they were compared with three protein databases to obtain function annotation using blastx (15) with E-value cut-off of 1e-5. The databases contained NCBI non-redundant protein database (Nr) (http://www.ncbi.nlm.nih.gov/), KEGG (http://www.kegg.jp/), and GO (http://geneontology. org/). Next, the novel transcripts were integrated with the existing transcript in genome annotation to construct a new gft file. Finally, cuffquant and cuffnorm were used to estimate transcript expression value as FPKM with parameter library normalization methods: classic-fpkm, library types: fr-unstranded.

Cluster Analysis

DAVID database was used for functional annotation (https://david.ncifcrf.gov/). The significantly changed gene IDs of the RNA-seq data were converted to the IDs consistent with DAVID.

Converted IDs were loaded to DAVID listing KEGG pathways and functional clusters.

Data and Code Availability

The raw sequence data reported in this paper have been deposited in the Genome Sequence Archive (Genomics, Proteomics & Bioinformatics 2021) in National Genomics Data Center (Nucleic Acids Res 2021), China National Center for Bioinformation / Beijing Institute of Genomics, Chinese Academy of Sciences (GSA: CRA005723) that are publicly accessible at https://ngdc.cncb.ac.cn/gsa.

Statistical Analysis

SPSS version 22.0 software (SPSS Inc, Chicago, US) was used for the analysis of variance for Student's *t*-test and the values were expressed as mean ± SEM. $p < 0.05$ was regarded as a significant difference.

RESULTS

The Effect of High Ambient Temperature on the Body Temperature of Sheep

The results show that after May 26, the temperature increased significantly until the experiment was completed (**Figure 1A**). THI showed that sheep were under normal or mild HS before May 8. After June 23, the sheep were subjected to intense HS until the experiment was completed (**Figure 1B**). The temperature of the sheep was measured by infrared thermometers, including the head, ears, abdomen, rectum, and testicles once a week. From May 5th, the temperature of each part of the sheep decreased. With the increase in the ambient temperature, the temperature of the sheep increased significantly. The head temperature of Suffolk sheep was significantly higher than that of Turpan black sheep from June 2 to July 7. The highest temperature of 39.73°C appeared at the same time between them and then decreased to the normal temperature (**Supplementary Figure 1A**). The temperature of the ear in the two groups varied significantly. In the middle stage of HS, the temperature of Suffolk sheep was always at a high level, which was significantly higher than that of Turpan black sheep, and decreased to the normal temperature after July 28 (**Supplementary Figure 1B**). There was no significant difference in abdominal temperature between the two groups in the early stage of HS. After June 2, the temperature of Turpan black sheep was stable, while the abdominal temperature of Suffolk sheep was above 38.5°C, and began to decrease on July 21 (**Supplementary Figure 1C**). The rectal temperature of Suffolk sheep was significantly higher than that of Turpan black sheep before heat stress ($p < 0.05$). With the increase in HS intensity, the rectal temperature of sheep in both groups began to increase, and after June 2, the rectal temperature was in the range of 39–40.5°C (**Supplementary Figure 1D**). The testicle's temperature is lower than other parts of the body, which is conducive to sperm production. The temperature of the two groups increased after May 5. During heat stress, there was no significant difference in testicular temperature between the two groups ($p > 0.05$) (**Figure 1C**). Through continuous monitoring of environmental conditions, we found that sheep are under heat stress and that their body has changed.

HS Alters Sheep Sperm Quality

From May 26, the sperm density of both sheep showed a decreasing trend, and the decrease of Suffolk sheep was more significant than Turpan black sheep ($p < 0.05$). On August 11, the sperm density of Suffolk sheep reached the lowest value of 4.29×10^8/ml, which was significantly lower than that of Turpan black sheep ($p < 0.01$) (**Figure 1D**).

Meanwhile, the sperm motility of Suffolk sheep decreased significantly ($p < 0.05$) and was significantly lower than that of Turpan black sheep on August 4 and August 11, respectively ($p < 0.01$) (**Figure 1E**). Subsequently, the values of VCL, VSL, LIN, VAP, ALH, and WOB during HS were analyzed. It was found that the values of Suffolk sheep were significantly lower than those of Turpan black sheep ($p < 0.05$) (**Figures 1F–K**). These results suggest that HS adversely affects sperm production in Suffolk sheep. After HS, we also found that the semen of Suffolk sheep showed solid form, while the semen of Turpan black sheep showed normal liquid form (**Figure 4C**).

Changes in Serum Hormone and Antioxidant Indexes in Animals After Heat Stress

After HS, COR, a hormone that responds to stress, was increased in both groups of sheep. Between May 19 and May 26, the COR value in Suffolk sheep decreased significantly ($p < 0.05$), and then gradually returned to the initial level in both groups (**Figure 2A**). The concentrations of LH and FSH were determined. Before June 30, there were no significant differences in serum LH and FSH concentrations between the two groups ($p > 0.05$). The LH concentration of Turpan black sheep decreased on June 30 and was significantly lower than that of Suffolk sheep on July 28 and August 11 ($p < 0.05$) (**Figure 2B**). From July 14 to August 4, the FSH content of Turpan black sheep was significantly lower than that of Suffolk sheep ($p < 0.05$) (**Figure 2C**). T levels did not change significantly from May 12 to July 14. After July 14, the T levels in both groups gradually increased as the temperature increased. On July 21 and 28, the T content of Turpan black sheep was significantly lower than that of Suffolk sheep, and then reached the highest of 5.59 ng/ml on August 11 (**Figure 2D**). Interestingly, we found that the concentration of total cholesterol of Turpan black sheep during HS treatment was higher than that of Suffolk sheep. From June 23 to 30, the total cholesterol content of Turpan black sheep was significantly higher than that of Suffolk sheep ($p < 0.05$), and then the concentration of the two groups returned to the normal level (**Figure 2E**). Then, the levels of CAT, SOD, MDA, and GSH-Px were determined. With the increase in THI index, the concentrations of CAT, SOD, and MDA of Suffolk sheep gradually increased, and the concentrations of CAT, SOD, and MDA of Suffolk sheep were significantly higher than those of Turpan Black sheep from June 2 to 9 ($p < 0.05$). However, the changes in Turpan black sheep were not obvious (**Figures 2F–H**). After May 26, the GSH-Px change trend of Turpan black sheep was stable, while Suffolk

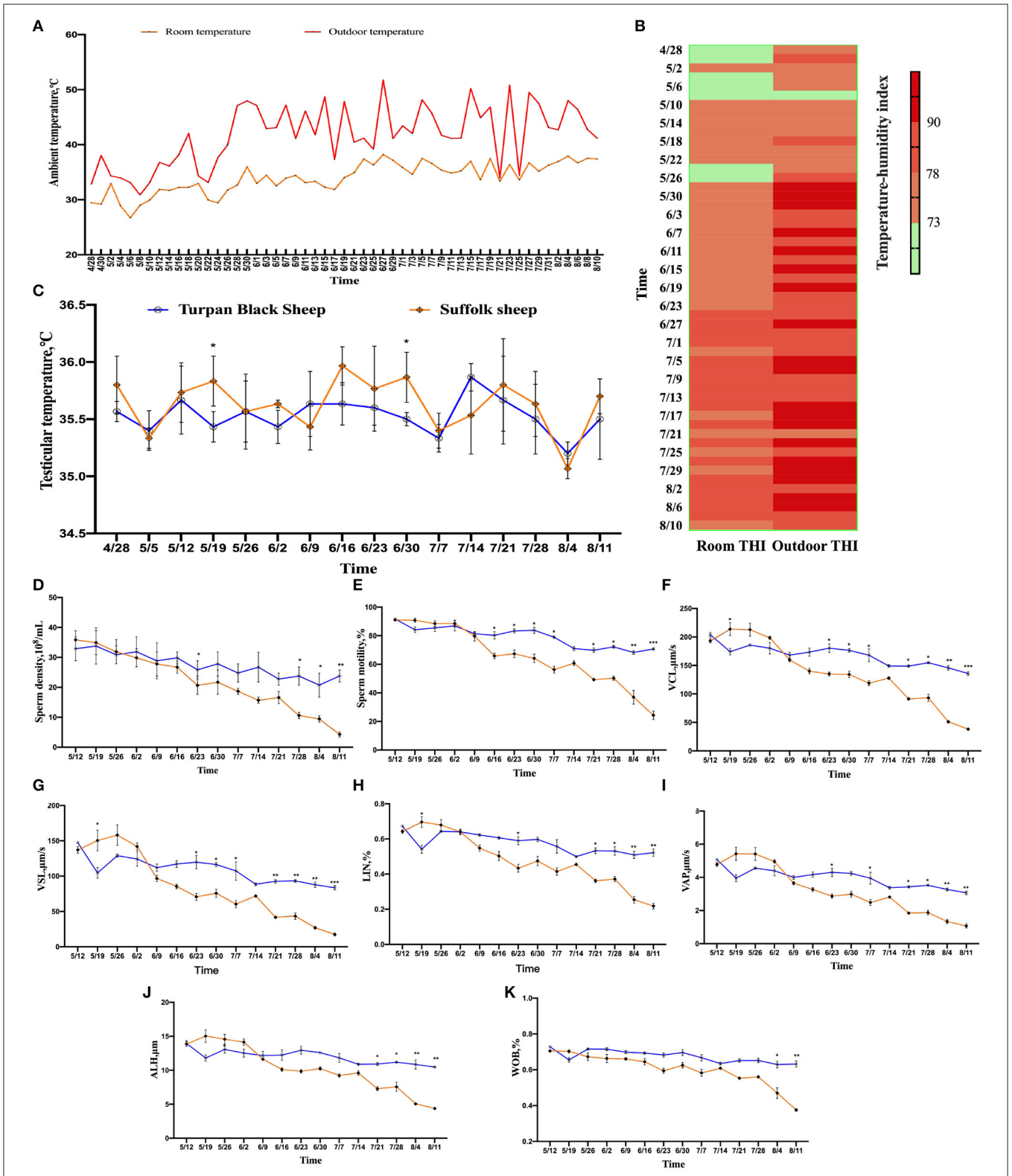

FIGURE 1 | Changes in environmental temperature and THI under heat stress. **(A)** Temperature changes inside and outside the shed from April 28 to August 10. **(B)** Temperature and humidity index change, the darker the color, the more serious the heat stress stimulation. Data were displayed through four measurements per day. **(C)** Testicular temperature changes during heat stress. **(D–K)** Continuous sampling of ram, and sperm motility parameters [**(D)** density, **(E)** vitality, **(F)** Curve line velocity, **(G)** straight line velocity, **(H)** Sperm movement linearity, **(I)** Velocity of the average path, **(J)** Mean side swing amplitude of sperm, **(K)** Sperm wobble].

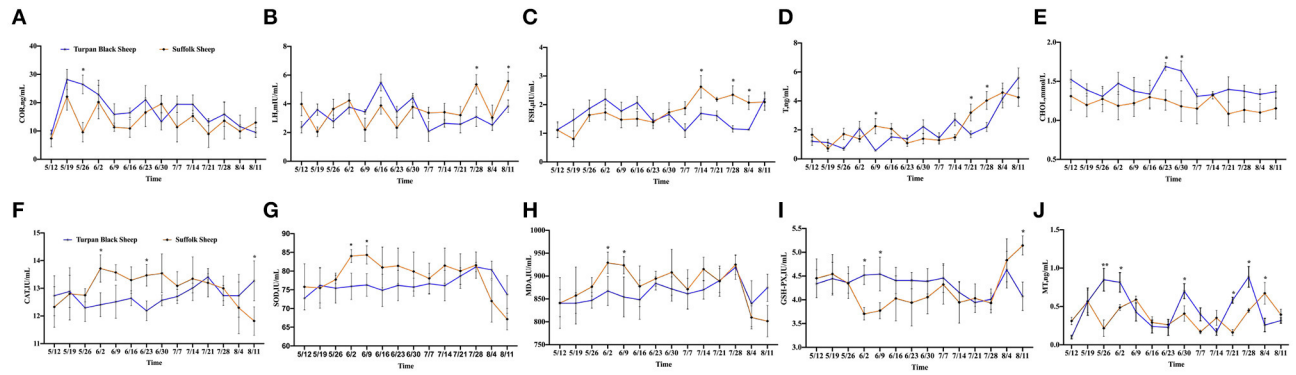

FIGURE 2 | Changes of reproductive hormones and antioxidant indices during HS. **(A)** Hydrocortisone. **(B)** Luteinizing hormone. **(C)** Follicle-stimulating hormone. **(D)** Testosterone. **(E)** Total cholesterol. **(F)** Catalase. **(G)** Superoxide dismutase. **(H)** Malonaldehyde. **(I)** Glutathione synthetase. **(J)** Melatonin. Significance was calculated by *T*-test, *means $P < 0.05$, ** means $P < 0.01$.

sheep decreased. From June 2 to June 9, the content of GSH-Px of Turpan black sheep was significantly higher than that of Suffolk sheep ($p < 0.05$). On August 11, the content of GSH-Px in Turpan black sheep was significantly lower than that in Suffolk sheep ($p < 0.05$) (**Figure 2I**). It was found that during HS, MT of Turpan black sheep changed significantly, and peaked on May 26, June 2, June 30, and July 28, respectively, which was significantly higher than that of Suffolk sheep ($p < 0.05$) (**Figure 2J**). Our results show changes in reproductive hormones and antioxidants in sheep before and after HS.

Changes in Sperm DFI and Acrosome Morphology After HS

PNA staining showed that there was no significant difference in acrosome morphology of Turpan black sheep, while Suffolk sheep showed a very significant decrease after HS ($p < 0.01$) (**Figures 3A,C**). On the other hand, DFI staining showed that the proportion of degraded sperm in Suffolk sheep was extremely significantly increased after HS ($p < 0.01$), the DFI index was 65.2%, which was extremely significantly increased, and sperm DNA was severely damaged (**Figures 3B,D,E**). Statistical results show severe sperm damage in Suffolk sheep after heat stress.

Morphological Change of Testis

The sheep were anesthetized and the testes and epididymis were removed. There was no significant difference in testicular weight between Turpan black sheep and Suffolk sheep before and after HS ($p < 0.05$) (**Figures 4A,B**). The results of H&E staining of testis showed that testis morphology was intact, and all types of germ cells including spermatogonial cells, spermatogamous cells, round sperm, and long sperm developed normally without significant differences (**Figure 4D**).

Immunofluorescence Analysis of Sertoli Cells and Spermatogonial Cells in Testis After HS

Next, the testis germ cells were analyzed. Immunofluorescence staining was performed on sheep testis before and after HS treatment using the antibody SOX9 of supporting cells (**Figure 4E**). After HS, there was no significant difference in the number of positive cells of Sertoli cells in each spermatogenic tubule between Turpan black sheep and Suffolk sheep, indicating that HS did not affect the number of Sertoli cells (**Figure 4F**). Testis was then immunofluorescent stained with spermatogonial antibodies UCLH1 and SOX9. The proportion of spermatogonial cells in 500 Sertoli cells was counted to analyze whether spermatogonial cells were reduced in spermatogenic tubules (**Figure 4E**). There were no significant differences in spermatogonial cells between the two groups (**Figure 4G**), indicating that HS did not affect the development of Sertoli cells and spermatogonial cells.

Meiotic Progression Is Blocked in Suffolk Sheep After HS

To find out the cause of reduced sperm count, immunofluorescence staining was performed with spermatocyte antibody SCP1, and spermatocyte statistics were performed (**Figure 5A**). The spermatocyte number in spermatogenic tubules of Suffolk sheep testis was significantly decreased (16.4 $\pm$ 2.8 vs. 33.2 $\pm$ 4.6) after HS ($p < 0.01$). However, there was no significant change in spermatocyte number (35.4 $\pm$ 3.6 vs. 30.2 $\pm$ 4.2) in spermatogenesis tubules of Turpan black sheep (**Figure 5B**). The results showed that HS had no significant effect on spermatocyte number in the testis of Turpan black sheep, but had a significant effect on Suffolk sheep. To determine the period of meiosis interruption in Suffolk sheep, we analyzed the entire meiotic phase I using meiotic plates. SYCP1 antibody staining was performed on the cells of linea, diplotene, pachytene, and diplotene of Turpan black sheep and Suffolk sheep after HS (**Figure 5C**). Both groups of sheep could complete the first meiosis. However, the cell proportion of Suffolk sheep was higher than that of Turpan black sheep (64.1 $\pm$ 3.4 vs. 18.0% $\pm$ 1.5%) (**Figure 5D**). Therefore, it was speculated that not all spermatocytes of Suffolk sheep could complete meiosis under HS, and a large number of spermatocytes were blocked in the zygotene and pachytene, followed by apoptosis. SOX9 and PNA

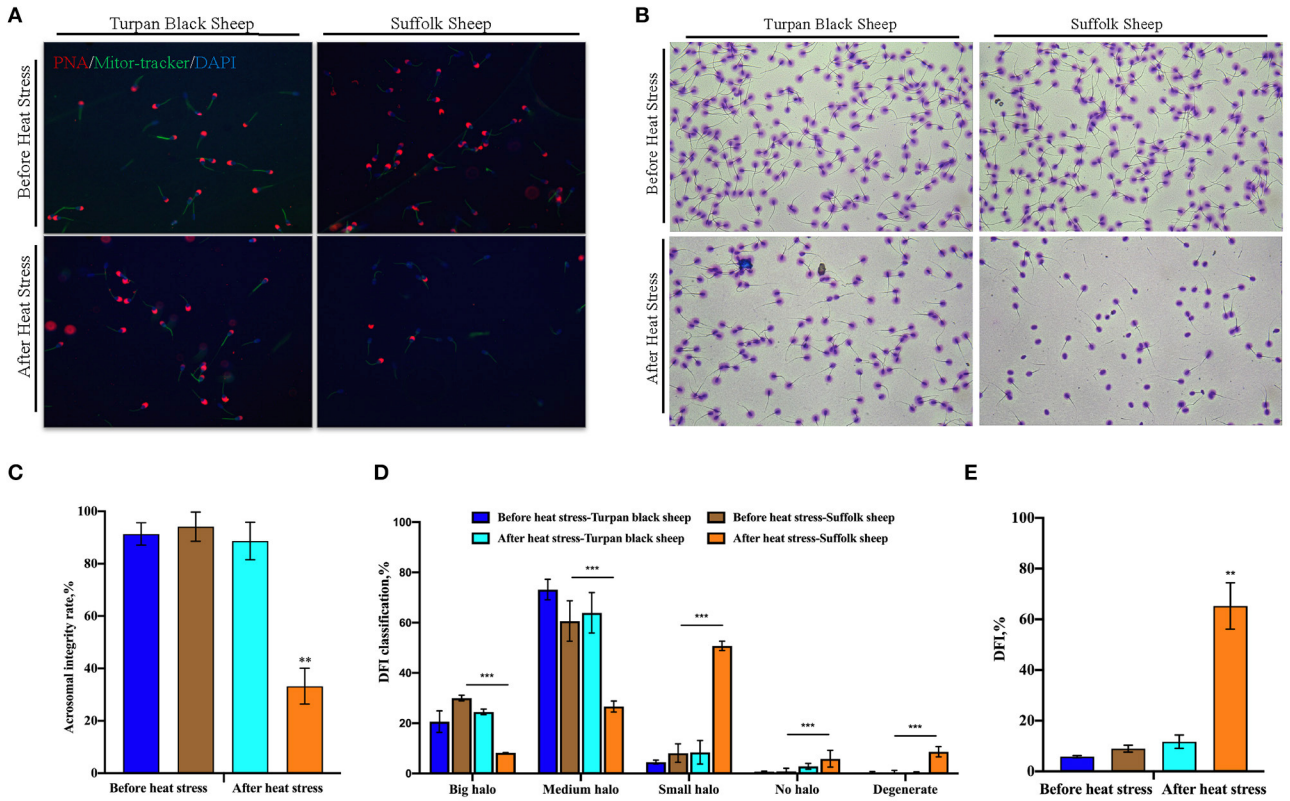

FIGURE 3 | Changes of sperm acrosome morphology and DNA damage after HS **(A)** 200× confocal laser microscopy: PNA (red fluorescence) labeled sperm acrosome; Mitor Tracker labeled mitochondria; DAPI (blue fluorescence) marks the nucleus. **(B)** SCD sperm DFI images. **(C)** Sperm acrosome morphological statistics. **(D)** SCD results showed the percentage of large halo, medium halo, small halo, non-halo and degenerate sperm. **(E)** DFI statistics. Significance was calculated by *T*-test, ** means $p < 0.01$, *** means $p < 0.001$.

reagents were used to stain sperm in spermatogenic tubules, and the number of spermatogenic tubules in 500 Sertoli cells was counted (**Supplementary Figure 2**). The results showed that the number of sperm in the spermatogenesis tubule of Suffolk sheep was significantly decreased after HS compared with that of Turpan black sheep (1,081.2 ± 103.1 vs. 2,642.3 ± 86.2) (**Figure 3B**). In conclusion, the reduction of spermatocytes and meiosis arrest ultimately lead to a decrease in sperm production.

Transcriptome Characteristics of Sheep Testis Before and After HS Treatment

Transcriptome sequencing of 12 representative testes was performed through a detailed description of testicular histology before and after HS treatment to determine which genes were altered during specific stages of spermatogenesis. We obtained 71333670, 76629072, 134221432, and 125842522 clean reads from transcriptome sequencing of testis tissues of Turpan black sheep and Suffolk sheep before and after HS treatment. A total of 95.14, 95.12, 94.64, and 95.00% clean reads were compared to the sheep genome. The overall gene expression analysis showed that there were 390 differentially expressed genes in Turpan black sheep compared to Suffolk sheep before HS, containing 200 up-regulated and 190 down-regulated genes (**Supplementary Figure 3A**). After HS, there were 311 differentially expressed genes in Turpan black sheep compared to Suffolk sheep, containing 211 up-regulated and 100 down-regulated genes (**Supplementary Figure 3G**). There were 1,562 differentially expressed genes before and after HS compared to Suffolk sheep, containing 1,032 up-regulated and 540 down-regulated genes (**Figure 6B**). There were 3,559 differentially expressed genes in Turpan black sheep and Suffolk sheep before and after HS, with 2,118 up-regulated and 1,441 down-regulated (**Figure 6A**). The differentially expressed genes among the groups were analyzed by clustering, and those clustered together where those with similar expression patterns. The differentially expressed genes between the groups were clustered, and the genes with similar expression patterns were clustered together. The colors in the heat map are compared horizontally. It can be seen from the heat map that all the differential gene sets of the repeat groups are clustered together, indicating that the same sheep gene expression pattern is the same under the same conditions, which is consistent with the heat map of the cluster analysis (**Figures 6D,E**) (**Supplementary Figures 3B**,**H**).

We randomly selected 10 differentially expressed genes in RNA-Seq for verification. After the analysis of RT-qPCR experimental data, it was consistent with the high and low gene

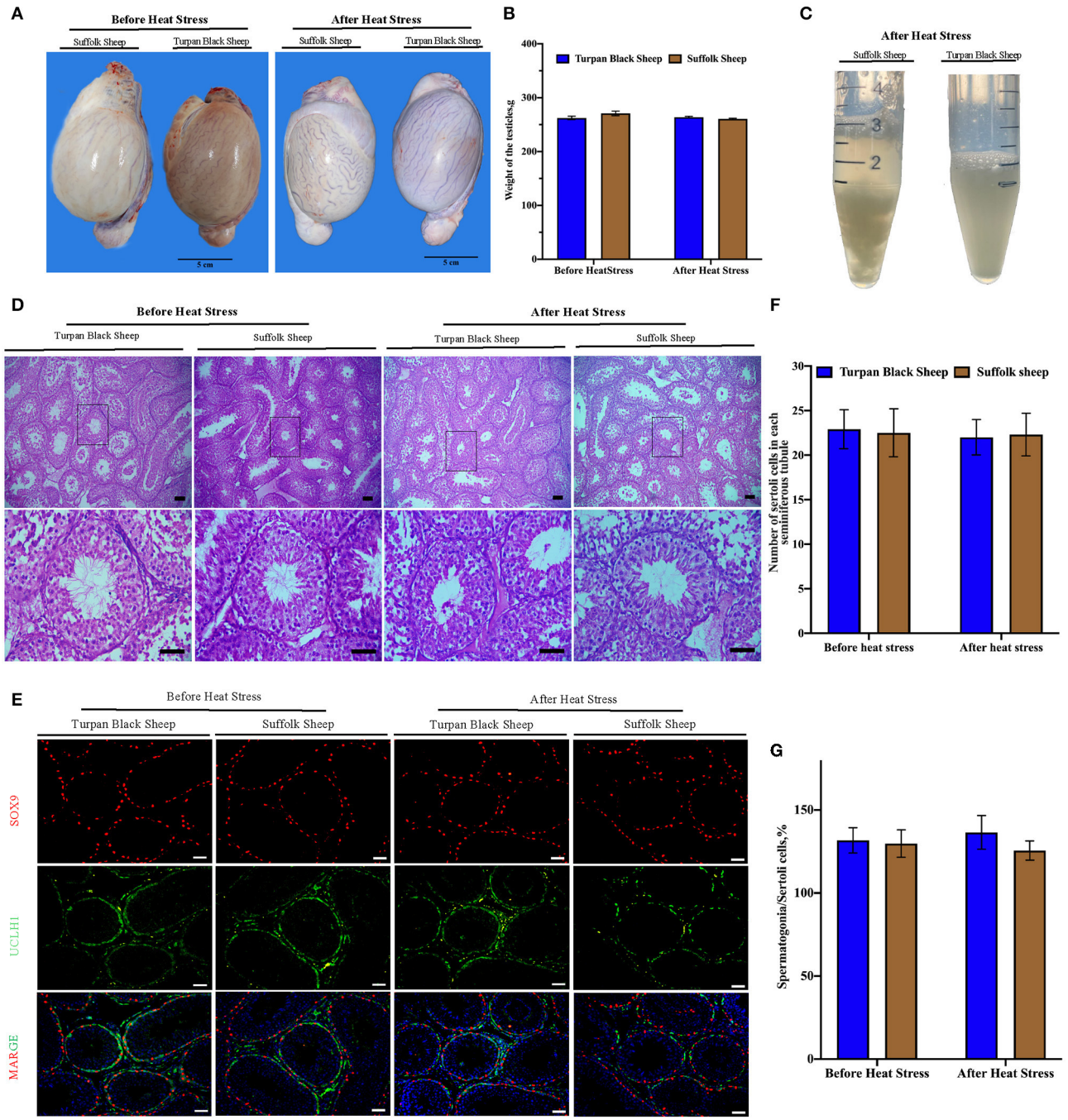

FIGURE 4 | Morphological characteristics of testis and semen after HS. **(A,B)** Typical testicular images and weight comparison after HS. **(C)** Semen morphology after HS. **(D)** Morphological analysis after H&E staining showed that spermatogonial cells, Sertoli cells, spermatocytes, and spermatozoa were arranged orderly in the convoluted tubules of the testis. **(E)** SOX9 (red fluorescence)-labeled Sertoli cells and UCLH1 (green fluorescence)-labeled spermatogonial cells. **(F)** Quantitative analysis of Sertoli cells in spermatogenic tubules. **(G)** The proportion of spermatogonia in 500 Sertoli cells in spermatogenic tubules. Scale = 50 μm, significance was calculated by *T*-test.

expression trends obtained by the RNA-seq transcript sequencing results (**Figure 6C**), which shows that the transcriptome sequencing data is more reliable, and the differentially expressed genes between different groups can be more accurately detected and selected.

Effect of HS Treatment on the Gene Expression Pattern of Sheep

Subsequently, GO enrichment and KEGG pathway analysis were performed on the differential genes of Turpan black sheep and Suffolk sheep before HS treatment. The genes

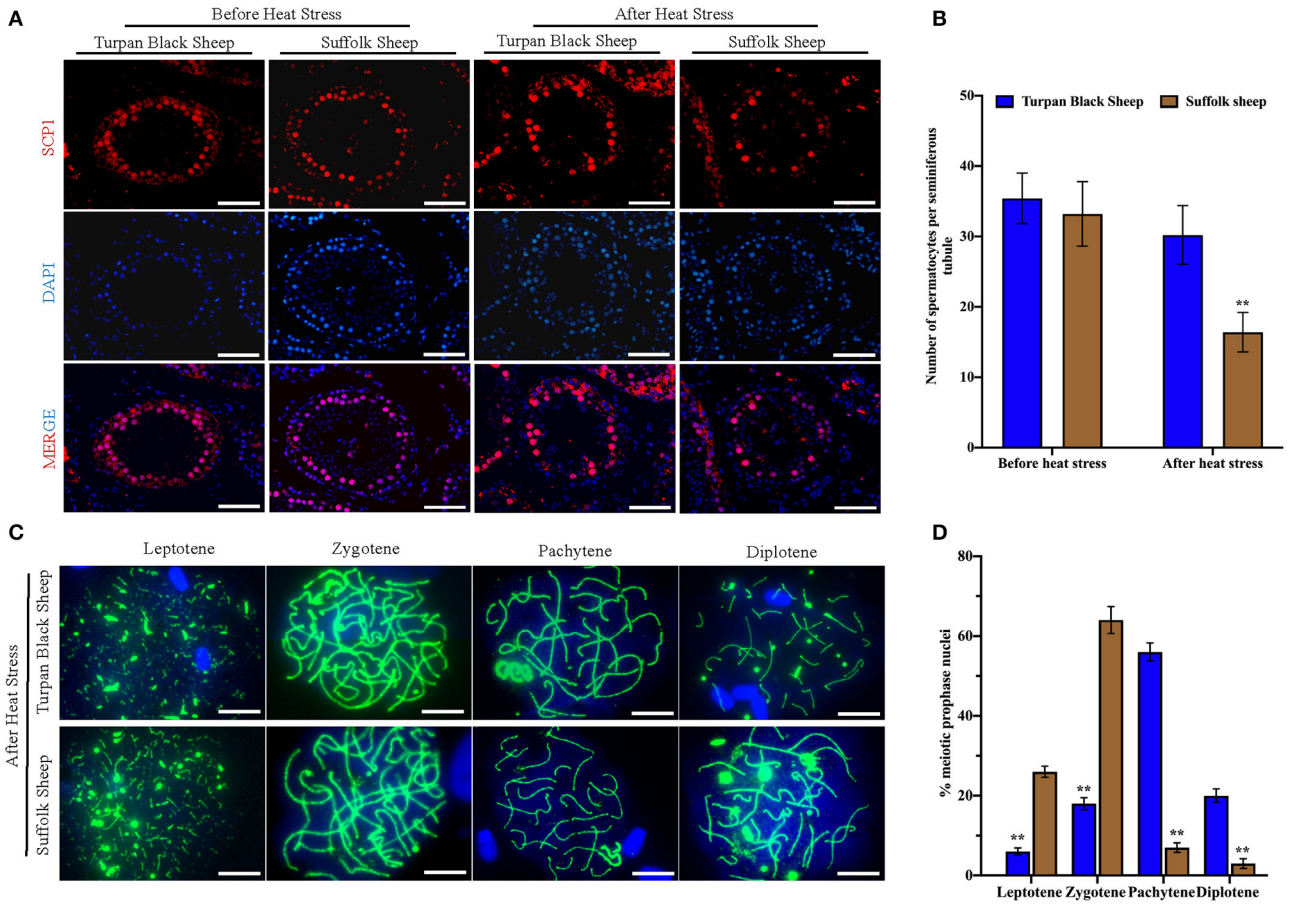

FIGURE 5 | Comparison of spermatocytes and meiosis slices after HS. **(A)** Spermatocyte labeled with SCP1 (red fluorescence) and nucleus labeled with DAPI (blue fluorescence), Scale = 50 μm. **(B)** Number of spermatocyte positive cells in spermatogenic tubules. **(C)** The process of meiosis was analyzed by the method of meiotic splicing and the synaptic complex is labeled by SYCP1 (green fluorescence), Scale = 5 μm. **(D)** The proportion of cells at different stages of meiosis. Significance was calculated by *T*-test, ** means $p < 0.01$.

with significant BP enrichment are immune response, regulation of the multi-organism process, regulation of defense response, cellular response to lipid, gland development, regulation of smooth muscle cell proliferation, etc. In CC, genes with significant enrichment are plasma membrane, extracellular exosome, receptor complex, synaptic membrane; MF includes receptor activity, heparin-binding, glutathione transferase activity, protein-lipid complex binding, etc. KEGG was enriched in Malaria, Metabolism of xenobiotics by cytochrome P450, *Staphylococcus aureus* infection, Cell adhesion molecules (CAMs), and Complement and coagulation cascades (**Supplementary Figures 3C–F**).

Next, we analyzed the differential genes of the two sheep before and after HS treatment and found that there were 961 differential genes in common (**Figure 6F**). First, GO enrichment and KEGG pathway analysis were performed on the differential genes of Turpan black sheep before and after HS treatment. The genes with significant GO enrichment are centrosome, dynein complex, synaptonemal complex assembly, cilium assembly, base-excision repair, male meiosis, fertilization, double-strand break repair via homologous recombination, positive regulation of histone H3-K4 methylation, G2/M transition of the mitotic cell cycle, negative regulation of cell death, positive regulation of JNK cascade, etc. (**Figure 7B**). KEGG is enriched in PI3K-Akt signaling pathway, cAMP signaling pathway, Rap1 signaling pathway, Ras signaling pathway, Cell cycle, Signaling pathways regulating pluripotency of stem cells, FoxO signaling pathway, mTOR signaling pathway, Notch signaling pathway, etc. (**Figure 7E**). Then, GO enrichment of differential genes in Suffolk sheep before and after HS treatment significantly showed: positive regulation of I-kappaB kinase/NF-kappaB signaling, cellular (**Figures 7C,F**). Then, we carried out GO enrichment for the common differential genes of Turpan black sheep and Suffolk sheep before and after HS treatment. The significant pathways are mitochondrial respiratory chain complex I, histone acetyltransferase activity, ATPase activity, transcription coactivator activity, histone demethylase activity (H3-K27 specific), positive regulation of canonical Wnt signaling pathway, bicellular tight junction, regulation of cell adhesion, negative regulation of retinoic acid receptor signaling pathway,

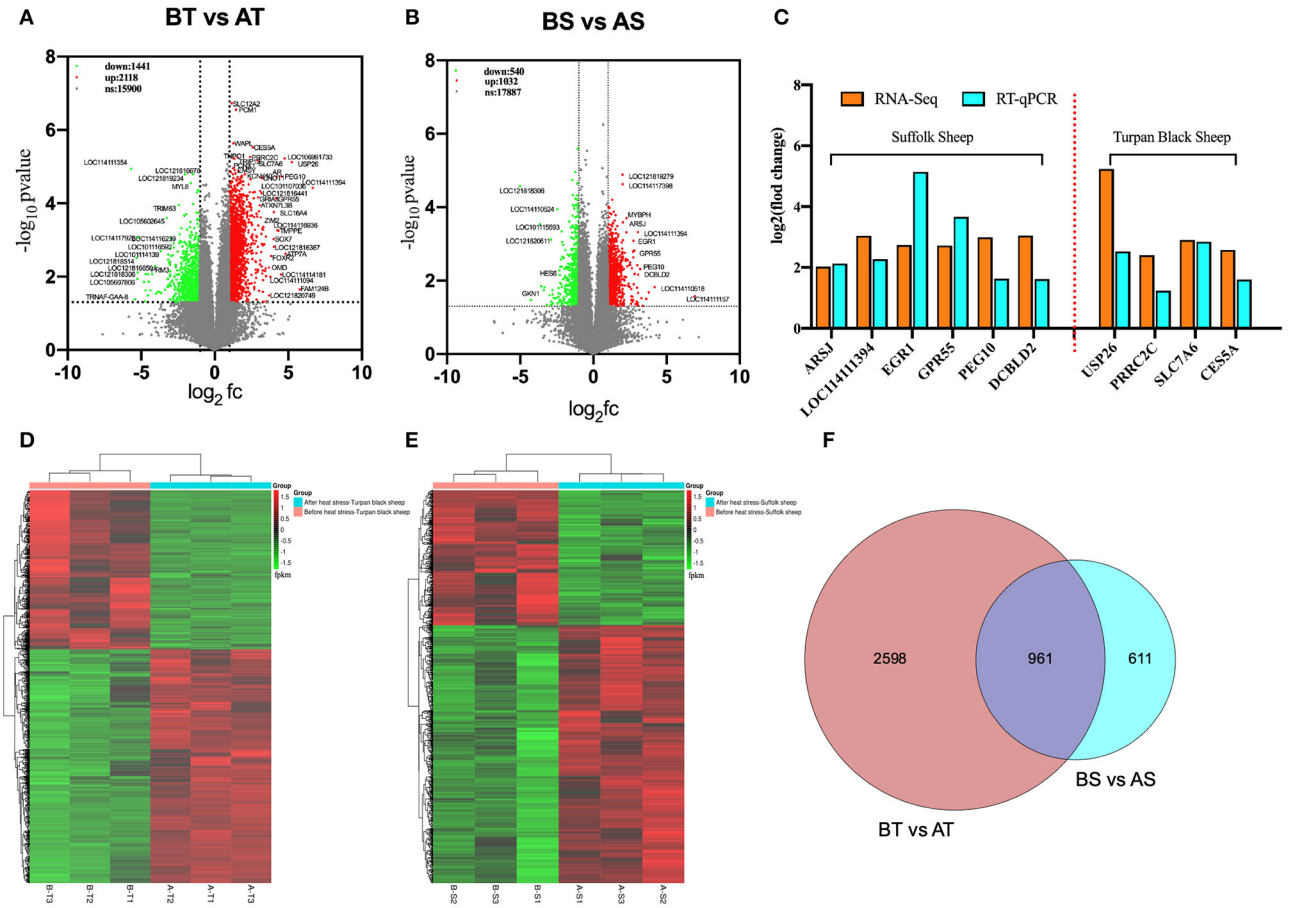

FIGURE 6 | Cluster analysis of differentially expressed genes in the testis transcriptome of Turpan black sheep before and after HS treatment. **(A,D)** Volcano map and heat map of testicular transcriptome differential genes in Turpan black sheep before and after HS. **(B–E)** Volcano plots and heat maps of differential genes in the testis transcriptome of Suffolk sheep before and after HS. **(C)** The trends of differentially expressed genes in RNA-seq and q-PCR. **(F)** Venn diagram representing the common differentially expressed gene distribution. In the volcano plot, red represents up-regulated genes, green represents down-regulated genes, and gray represents genes with no significant difference. The volcano plot showed that the differentially expressed genes satisfy the correction condition $p < 0.05$.

spermatogenesis, the stem cell population maintenance, etc. (**Figure 7A**). The KEGG pathway enrichment includes PI3K-Akt signaling pathway, Rap1 signaling pathway, cAMP signaling pathway, Ras signaling pathway, AMPK signaling pathway, ABC transporters, TGF-beta signaling pathway, Thyroid hormone synthesis, Ribosome, Oxidative phosphorylation, Metabolic pathways, Proteasome Wait (**Figure 7D**). By comparing the GO enrichment of differential genes and the KEGG pathway, it is found that the pathways between groups are mainly divided into three categories: (1) In Turpan black sheep, it is related to the regulation of spermatogenesis and meiosis; (2) In Suffolk sheep, it is cell Apoptosis related to inflammatory response and adaptability; (3) Among the shared differential genes are related to oxidative stress adaptive capacity. At the same time, after we selected the landmark genes, we found that they were all up-regulated, such as meiosis-related genes *SYCP2*, *BRCA1*, *TEX15*, *SMC4*, *SMC3*, *SETX*, *RAD54L*, *MEIOC*, *MCM8*, *MCM6*, *CENPF*, *TEX11*, *SMC5*, *RPA1,* etc. (**Figure 7H**), apoptosis-related genes *CASP8*, *TBK1*, *CFLAR*, *FOXO1*, *ADORA1*, *CASP8*, *MAP3K1*, etc. (**Figure 7I**), oxidative stress-related genes *NDUFB3*, *NDUFA8*, *NDUFA6*, *NDUFB7*, *HLTF*, *MYO9B*, *TFAP2A*, *MED13*, *MYSM1*, *STAT3*, etc. (**Figure 7G**).

DISCUSSION

High temperature is an important environmental stress factor that affects livestock production, reproduction, and welfare (16). HS occurs when the body temperature of livestock exceeds the thermoneutral zone, resulting in more heat production than heat loss. Under HS conditions, the heat exchange between livestock and the environment is likely to be blocked, which in turn leads to physical dysfunction in the body (17). Sheep are warm-blooded animals. To ensure their health, survival, and reproduction needs, their body temperature is usually kept within a narrow physiological range (18). The skin is an important way of heat exchange between the environment and the surface of the body. The temperature of the skin is the result of the adjustment of the blood flow of the skin, and the blood flow stops with

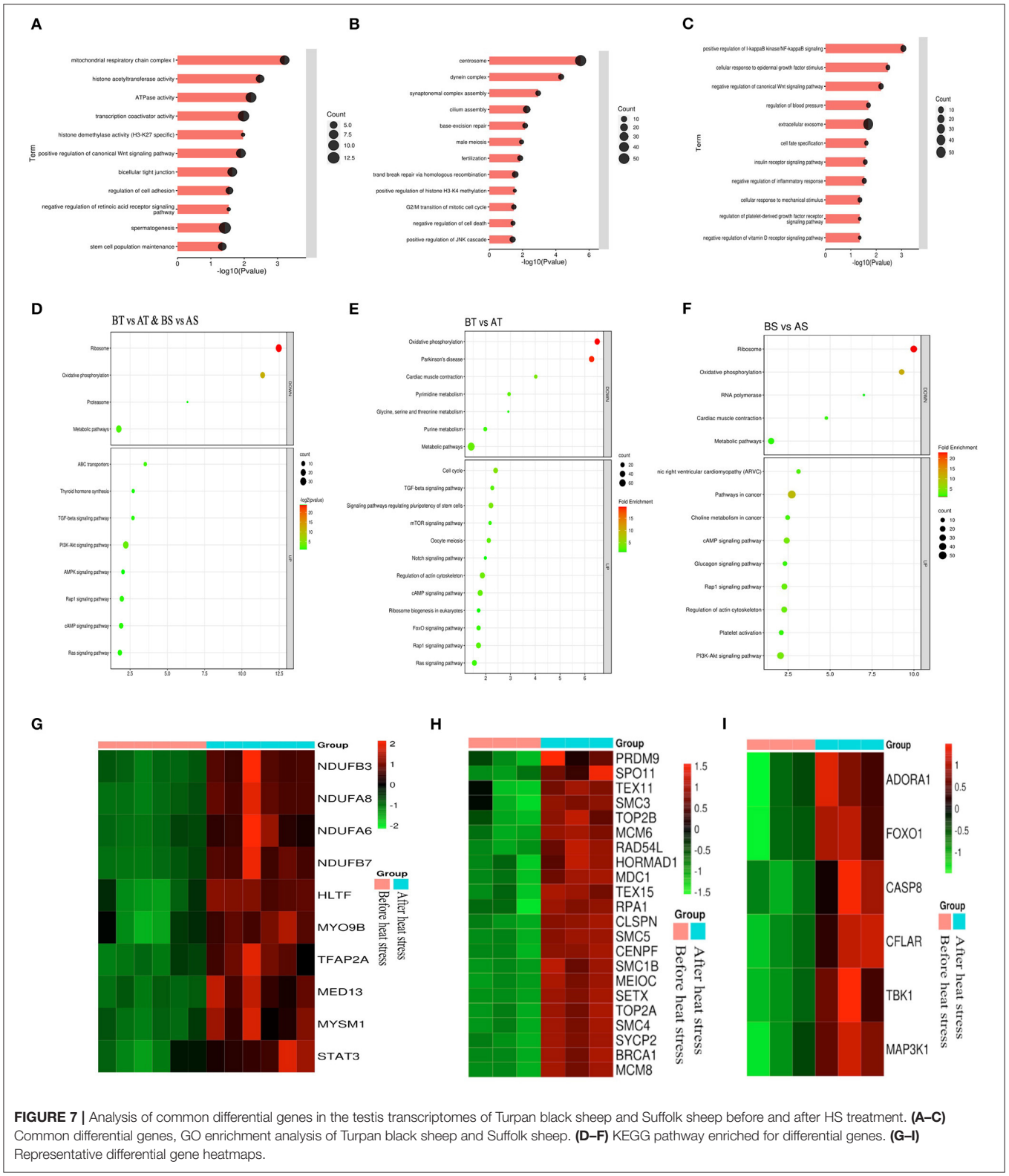

FIGURE 7 | Analysis of common differential genes in the testis transcriptomes of Turpan black sheep and Suffolk sheep before and after HS treatment. **(A–C)** Common differential genes, GO enrichment analysis of Turpan black sheep and Suffolk sheep. **(D–F)** KEGG pathway enriched for differential genes. **(G–I)** Representative differential gene heatmaps.

the adjustment of the heat between the core of the body and the skin (19). It is observed that the temperature of the sheep's skin surface is the highest in summer and the lowest in winter (20). Under HS, the average skin surface temperature of cattle will increase (21). This is similar to the results of this study. We counted the sheep's body temperature during the period

from no HS to strong HS and found that the temperature of different parts of the two groups of sheep began to rise when the HS started and then remained at high fever. level, especially in Suffolk sheep (22).

In this study, we found significantly enhanced resistance to male reproductive damage in Turpan black sheep than in Suffolk sheep under HS treatment. Through semen quality testing, we found that there was no significant difference between Turpan black sheep before and after HS, but Suffolk sheep after HS showed the amount of incomplete acrosome and a high proportion of DNA fragmentation. Sperm from mice treated at 35°C for 24 h showed significantly increased mitochondrial ROS production and oxidative DNA damage (23). Similarly, human sperm incubated at 42°C for 3 h can induce negative results in sperm motility, oxidative stress parameters, DNA damage, and cell apoptosis. In cattle, studies have shown that HS can increase the secretion of ACTH and cortisol (24), inhibit the secretion of GnRH and LH, and affect the hypothalamus-pituitary-ovarian axis (25). However, there is no significant difference in Turpan black sheep from the start to the end of HS treatment, although Turpan black sheep showed relatively higher levels of FSH, LH, and T than Suffolk sheep in the late of HS.

Sexually reproducing organisms use meiosis to produce haploid gametes and deliver their genomes to the next generation (26). Our results showed that the number of spermatogonia and Sertoli cells in the seminiferous tubules of Turpan black sheep and Suffolk sheep did not decrease before and after HS, while the spermatocytes of Suffolk sheep showed a significant decrease after HS. Although both groups of sheep could complete the first meiotic division, the proportion of cells in the meiotic zygotene of Suffolk sheep was significantly higher than that of Turpan black sheep. Studies showed that spermatogenesis is particularly sensitive to small temperature fluctuations, and spermatocytes must develop within very narrow isotherms (23, 27–29). Failure of testis thermoregulation and prolonged exposure to high temperatures can lead to male sterility (30). Meiotic prophase spermatocytes and postmeiotic sperm are particularly vulnerable to the effect of HS (10, 31). Furthermore, dysregulation of DNA damage and repair pathways during meiosis has been suggested as a potential mechanism between HS and spermatocyte DNA damage (32). Therefore, we speculate that a large number of cells are blocked in the zygotene and pachytene, followed by apoptosis in SS.

Transcriptome analysis provided more information about the mechanism of HS resistance in the testis of TBS. Our data found some enriched pathways involved in apoptosis, immune response, and oxidative stress. The main enriched pathways are Rap1, AMPK, TGF-β, etc. Rap1 is regulated by a wide range of external stimuli as a molecular switch when stress occurs (33). MAPK is one of the main signaling pathways in mammals and can also be activated by external stimuli, but the activity of the MAPK signaling pathway is stimulated by Rap1 in multiple cells (34, 35). Particularly, the pathways identified in the differential gene enrichment analysis of Turpan black sheep before and after HS are PI3K-Akt, Mtor, Notch, etc. Studies showed that the PI3K-Akt-mTOR signaling pathway can regulate cell growth, proliferation, differentiation, and survival (36), and can regulate the expression of p70S6K and 4EBP1 in testis tissue to regulate spermatogonia proliferation (37). mTOR signaling activates protein translation, participates in the regulation of protein synthesis and energy metabolism, and it is a central regulator of cell proliferation, differentiation, and growth (38). Therefore, we believe that the Turpan black sheep up-regulated meiosis-related genes when they were subjected to HS, causing a cascade of multiple pathways to maintain normal spermatogenesis, thereby reducing the harm caused by HS.

Our study reveals that the hormonal regulation changes and spermatogonia transition, meiotic cell, and haploid germ cell development in Turpan black sheep under HS are regulated by a large number of genetic changes. Transcriptome analysis plays an important role in the screening of candidate genes provided by spermatocytes and spermatogenesis. The up-regulation of related genes involved in spermatogenesis protected the normal production of sperm in the Turpan black sheep after HS treatment further proving that Turpan black sheep have evolved an ability to resist HS in a long-term HS environment.

DATA AVAILABILITY STATEMENT

The datasets presented in this study can be found in online repositories. The names of the repository/repositories and accession number(s) can be found in the article/**Supplementary Material**.

ETHICS STATEMENT

The animal study was reviewed and approved by The Ethics Committee of Xinjiang Agricultural University (Protocol Permit Number: 2020032, 7 May 2020).

AUTHOR CONTRIBUTIONS

YS: conceptualization, investigation, writing-original draft, and preparation. XZ: conceptualization, data curation, writing-original draft, and preparation. AA: validation, formal analysis, and visualization. AH, YG, and AD: validation. PY and GL: writing-review and editing. GJ and AW: project administration, funding acquisition, and conceptualization. All authors listed have made a substantial, direct, and intellectual contribution to the work and approved it for publication.

FUNDING

This work was granted by National Key Research and Development Project (2021YFD1200400) and Strategic Priority Research Program of CAS (XDA26040302). GJ was supported by Qinghai Kunlun Talents programs and Youth Innovation Promotion Association CAS.

SUPPLEMENTARY MATERIAL

The Supplementary Material for this article can be found online at: https://www.frontiersin.org/articles/10.3389/fvets.2022.846981/full#supplementary-material

Supplementary Figure 1 | Changes in temperature in different parts of the body during heat stress. **(A)** Head, **(B)** ear, **(C)** abdomen, and **(D)** rectum.

Supplementary Figure 2 | Analysis of spermatozoa number in spermatogenic tubules after HS. **(A)** SOX9 (green fluorescence) labeled supporting cells, PNA (red fluorescence) labeled sperm, and DAPI (blue fluorescence) labeled nucleus. **(B)** Spermatozoa in 500 sertoli cells. Scale = 50 μm, significance was calculated by *T*-test, ** means $P < 0.01$.

Supplementary Figure 3 | Testis transcriptional profile characteristics and differential gene clustering analysis. **(A,B)** Volcano and heat map of testis transcriptome differential genes in Turpan black sheep and Suffolk sheep before HS. **(C–F)** KEGG pathway and cluster analysis of the biological process (BP), cellular component (CC), and molecular function (MF) of differential gene enrichment in Turpan black sheep and Suffolk sheep before HS. **(G,H)** Volcano and heat maps of differentially gene genes in the testicular transcriptomes of Turpan black sheep and Suffolk sheep after HS. **(I)** Cluster analysis of differential genes BP, CC, and MF in Turpan black sheep and Suffolk sheep after HS. In the volcano plot, red represents up-regulated genes, green represents down-regulated genes, and gray represents genes with no significant difference. The volcano plot showed that the differentially expressed genes satisfy the correction condition $P < 0.05$.

REFERENCES

1. Bernabucci U, Lacetera N, Baumgard LH, Rhoads RP, Ronchi B, Nardone A. Metabolic and hormonal acclimation to heat stress in domesticated ruminants. *Animal.* (2010) 4:1167–83. doi: 10.1017/S175173111000090X
2. Rangel DE. Stress induced cross-protection against environmental challenges on prokaryotic and eukaryotic microbes. *World J Microbiol Biotechnol.* (2011) 27:1281–96. doi: 10.1007/s11274-010-0584-3
3. W. van Wettere Kind KL, Gatford KL, Swinbourne AM, Leu ST, Hayman PT, et al. Review of the impact of heat stress on reproductive performance of sheep. *J Anim Sci Biotechnol.* (2021) 12:26. doi: 10.1186/s40104-020-00537-z
4. Vandana GD, Sejian V, Lees AM, Pragna P, Silpa MV, Maloney SK. Heat stress and poultry production: impact and amelioration. *Int J Biometeorol.* (2021) 65:163–79. doi: 10.1007/s00484-020-02023-7
5. Wang J, Li J, Wang F, Xiao J, Wang Y, Yang H, et al. Heat stress on calves and heifers: a review. *J Anim Sci Biotechnol.* (2020) 11:79. doi: 10.1186/s40104-020-00485-8
6. Khan A, Dou J, Wang Y, Jiang X, Khan MZ, Luo H, et al. Evaluation of heat stress effects on cellular and transcriptional adaptation of bovine granulosa cells. *J Anim Sci Biotechnol.* (2020) 11:25. doi: 10.1186/s40104-019-0408-8
7. Hamilton T, Siqueira AFP, de Castro LS, Mendes CM, Delgado JC, de Assis PM, et al. Effect of heat stress on sperm DNA: protamine assessment in ram spermatozoa and testicle. *Oxid Med Cell Longev.* (2018) 2018:5413056. doi: 10.1155/2018/5413056
8. Ngoula F, Lontio FA, Tchoffo H, Manfo Tsague FP, Djeunang RM, Vemo BN, et al. Heat induces oxidative stress: reproductive organ weights and serum metabolite profile, testes structure, and function impairment in male cavy (*Cavia porcellus*). *Front Vet Sci.* (2020) 7:37. doi: 10.3389/fvets.2020.00037
9. Mieusset R, Quintana Casares P, Sanchez Partida LG, Sowerbutts SF, Zupp JL, Setchell BP. Effects of heating the testes and epididymides of rams by scrotal insulation on fertility and embryonic mortality in ewes inseminated with frozen semen. *J Reprod Fertil.* (1992) 94:337–43. doi: 10.1530/jrf.0.0940337
10. Perez-Crespo M, Pintado B, Gutierrez-Adan A. Scrotal heat stress effects on sperm viability, sperm DNA integrity, and the offspring sex ratio in mice. *Mol Reprod Dev.* (2008) 75:40–7. doi: 10.1002/mrd.20759
11. Slimen IB, Najar T, Ghram A, Dabbebi H, Ben Mrad M, Abdrabbah M. Reactive oxygen species, heat stress and oxidative-induced mitochondrial damage. A review. *Int J Hyperthermia.* (2014) 30:513–23. doi: 10.3109/02656736.2014.971446
12. Wolfova M, Wolf J, Milerski M. Calculating economic weights for sheep sire breeds used in different breeding systems. *J Anim Sci.* (2011) 89:1698–711. doi: 10.2527/jas.2010-3237
13. Kim D, Pertea G, Trapnell C, Pimentel H, Kelley R, Salzberg SL. TopHat2: accurate alignment of transcriptomes in the presence of insertions, deletions and gene fusions. *Genome Biol.* (2013) 14 R36. doi: 10.1186/gb-2013-14-4-r36
14. Trapnell C, Roberts A, Goff L, Pertea G, Kim D, Kelley DR, et al. Differential gene and transcript expression analysis of RNA-seq experiments with TopHat and Cufflinks. *Nat Protoc.* (2012) 7:562–78. doi: 10.1038/nprot.2012.016
15. Altschul SF, Madden TL, Schaffer AA, Zhang J, Zhang Z, Miller W, et al. Gapped BLAST and PSI-BLAST: a new generation of protein database search programs. *Nucleic Acids Res.* (1997) 25:3389–402. doi: 10.1093/nar/25.17.3389
16. Curtis SE. *Environmental Management in Animal Agriculture*. Ames: Iowa State University Press (1983).
17. Al-Haidary AA. Physiological responses of Naimey sheep to heat stress challenge under semi-arid environments. *Int J Agric Biol.* (2004) 2:307–9. Available online at: https://agris.fao.org/agris-search/search.do?recordID=PK2004000880
18. Marai I, El-Darawany A, Fadiel A, Abdel-Hafez M. Physiological traits as affected by heat stress in sheep—a review. *Small Ruminant Res.* (2007) 71:1–12. doi: 10.1016/j.smallrumres.2006.10.003
19. Piggins D, Phillips C. *Farm Animals and the Environment*. AFRC Institute for Grassland and Environmental Research (1992).
20. Fahmy S. *Effect of crossing Romanov with Rahmani sheep on some physiological productive performance* [M. Sc. Thesis]. Faculty of Agriculture, Al-Azhar University, Cairo, Egypt (1994).
21. Kuman N, Koknaroglu H. Developing an early warning system for heat stress in cattle. *J Anim Behav Biometeorol.* (2020) 4:89–92. doi: 10.14269/2318-1265/jabb.v4n3p89-92
22. Balić IM, Milinković-Tur S, SamardŽija M, Vince S. Effect of age and environmental factors on semen quality, glutathione peroxidase activity and oxidative parameters in simmental bulls. *Theriogenology.* (2012) 78:423–31. doi: 10.1016/j.theriogenology.2012.02.022
23. Houston BJ, Nixon B, Martin JH, De Iuliis GN, Trigg NA, Bromfield EG, et al. Heat exposure induces oxidative stress and DNA damage in the male germ line. *Biol Reprod.* (2018) 98:593–606. doi: 10.1093/biolre/ioy009
24. Hein K, Allrich R. Influence of exogenous adrenocorticotropic hormone on estrous behavior in cattle. *J Anim Sci.* (1992) 70:243–7. doi: 10.2527/1992.701243x
25. Khodaei-Motlagh M, Shahneh AZ, Masoumi R, Derensis F. Alterations in reproductive hormones during heat stress in dairy cattle. *Afr J Biotechnol.* (2011) 10:5552–8. Available online at: https://www.ajol.info/index.php/ajb/article/view/94340
26. Widlak W, Vydra N. The role of heat shock factors in mammalian spermatogenesis. The role of heat shock proteins in reproductive system development and function. *Adv Anat Embryol Cell Biol.* (2017) 222:45–65. doi: 10.1007/978-3-319-51409-3_3
27. Rohmer C, David JR, Moreteau B, Joly D. Heat induced male sterility in Drosophila melanogaster: adaptive genetic variations among geographic populations and role of the Y chromosome. *J Exp Biol.* (2004) 207:2735–43. doi: 10.1242/jeb.01087
28. Kim B, Park K, Rhee K. Heat stress response of male germ cells. *Cell Mol Life Sci.* (2013) 70:2623–36. doi: 10.1007/s00018-012-1165-4
29. Sage TL, Bagha S, Lundsgaard-Nielsen V, Branch HA, Sultmanis S, Sage RF. The effect of high temperature stress on male and female reproduction in plants. *Field Crops Res.* (2015) 182:30–42. doi: 10.1016/j.fcr.2015.06.011
30. Durairajanayagam D, Agarwal A, Ong C. Causes, effects and molecular mechanisms of testicular heat stress. *Reprod Biomed Online.* (2015) 30:14–27. doi: 10.1016/j.rbmo.2014.09.018
31. Chowdhury A, Steinberger E. Early changes in the germinal epithelium of rat testes following exposure to heat. *Reproduction.* (1970) 22:205–12. doi: 10.1530/jrf.0.0220205

32. Paul C, Melton DW, Saunders PT. Do heat stress and deficits in DNA repair pathways have a negative impact on male fertility? *MHR Basic Sci Reprod Med.* (2008) 14:1–8. doi: 10.1093/molehr/gam089
33. Frische E, Zwartkruis F. Rap1, a mercenary among the Ras-like GTPases. *Dev Biol.* (2010) 340:1–9. doi: 10.1016/j.ydbio.2009.12.043
34. Wu C, Ramirez A, Cui B, Ding J, Delcroix JDM, Valletta JS, et al. A functional dynein–microtubule network is required for NGF signaling through the Rap1/MAPK pathway. *Traffic.* (2007) 8:1503–20. doi: 10.1111/j.1600-0854.2007.00636.x
35. Kam CY, Dubash AD, Magistrati E, Polo S, Satchell KJ. Sheikh F, et al. Desmoplakin maintains gap junctions by inhibiting Ras/MAPK and lysosomal degradation of connexin-43. *J Cell Biol.* (2018) 217:3219–35. doi: 10.1083/jcb.201710161
36. Dibble CC, Cantley LC. Regulation of mTORC1 by PI3K signaling. *Trends Cell Biol.* (2015) 25:545–55. doi: 10.1016/j.tcb.2015.06.002
37. Xu H, Shen L, Chen X, Ding Y, He J. Zhu J, et al. mTOR/P70S6K promotes spermatogonia proliferation and spermatogenesis in Sprague Dawley rats. *Reprod Biomed Online.* (2016) 32:207–17. doi: 10.1016/j.rbmo.2015.11.007
38. Moreira BP, Oliveira PF, Alves MG. Molecular mechanisms controlled by mTOR in male reproductive system. *Int J Mol Sci.* (2019) 20:1633. doi: 10.3390/ijms20071633

Conflict of Interest: PY was employed by the company Tuokexun County Huishang Ecological Animal Husbandry Co., Ltd.

The remaining authors declare that the research was conducted in the absence of any commercial or financial relationships that could be construed as a potential conflict of interest.

Advantages of publishing in Frontiers

OPEN ACCESS
Articles are free to read for greatest visibility and readership

FAST PUBLICATION
Around 90 days from submission to decision

HIGH QUALITY PEER-REVIEW
Rigorous, collaborative, and constructive peer-review

TRANSPARENT PEER-REVIEW
Editors and reviewers acknowledged by name on published articles

Frontiers
Avenue du Tribunal-Fédéral 34
1005 Lausanne | Switzerland

Visit us: www.frontiersin.org
Contact us: frontiersin.org/about/contact

REPRODUCIBILITY OF RESEARCH
Support open data and methods to enhance research reproducibility

DIGITAL PUBLISHING
Articles designed for optimal readership across devices

FOLLOW US
@frontiersin

IMPACT METRICS
Advanced article metrics track visibility across digital media

EXTENSIVE PROMOTION
Marketing and promotion of impactful research

LOOP RESEARCH NETWORK
Our network increases your article's readership